

Use of transaminase enzymes for the synthesis of pharmaceutical intermediates

A thesis submitted to
University College London



By

Alexander Kweku Boateng Bour

for the degree of

Doctor of Philosophy

Declaration

I, Alexander Kweku Bour, confirm that the work presented in this thesis is my own.
Where information has been derived from other sources, I confirm that this has been
indicated in the thesis.

.....

Alexander Kweku Bour

Abstract

Chiral amines are highly valuable chemical species found in a broad spectrum of pharmaceutical, agrochemical and fine chemical products. The synthesis of some of these amines is often low yielding and convoluted (due to the use of protecting groups and chiral auxiliaries) or they have poor selectivities. The need for cleaner, more efficient and highly selective preparations of chiral amines therefore makes transaminases an attractive alternative to the classical chemical routes.

Transaminases (TAMs) are a group of enzymes that catalyse the conversion of aldehydes and prochiral ketones to primary amines and chiral secondary amines. Most TAMs typically catalyse the conversion of α -ketoacids to α -amino acids. There is however one class of TAMs (ω -TAMs) that shows broad selectivity beyond ketoacids.

The work in this thesis can be split in two halves:

The first half is a discussion on the discovery, cloning and characterization of novel ω -TAMs. Through BLAST sequence searches and phylogenetic matching to cloning, over-expressing and high through-put screening, a panel of 10 novel ω -TAMs were discovered.

The second half of this thesis discusses a novel transaminase-mediated chemoenzymatic intramolecular aza-Michael reaction. Three unsaturated ketoester substrates were screened against four of the 10 novel ω -TAMs alongside three previously discovered ones. This reaction can potentially provide access to a myriad of natural product alkaloids containing a 2,6-piperidine or a 2,5-pyrrolidine core.

Acknowledgements

First and foremost I would like to express my most sincere thanks and gratitude to my primary supervisor Prof. Helen C. Hailes for her assistance, guidance and overwhelming patience throughout this project.

I would also like to thank my secondary supervisor Prof. John Ward for his guidance and for access to his laboratory and cell culture library.

Many thanks to Dr Ian Taylor and my collaborating company Dr Reddy's UK for their financial support. Thanks also to Dr. Matthew Bycroft, Dr Toni Fleming, and Dr. Emma Rackham for their help, guidance, and for making my time in Cambridge an enjoyable one.

I would also like to thank the BBSRC for funding this project without which none of this could have been achieved.

Thanks to Dr. Kersti Krau for all her assistance with the GC-MS and ion-trap LC-MS analyses, without which a lot of the results in this project would not have been realised.

To past and present members of the Hailes and Tabor groups, especially to Zoe Wright, Dr. David Steadman, Dr. Robin Bowfinger and to Jack Jeffries and Benjamin Lichman of the Ward group. Thank you for your support and friendships.

I would indeed like to thank all my friends for their words of encouragement and exhortation. Thanks to Jason Okyere and his family, to Ibrahim Rahman, and to David Blake and the original members of Quince de Battishill.

Finally, I would like to thank my parents and sisters for their love and understanding throughout this project and above all to my dear aunt for her direction and guidance in the early years.

Abbreviations

Abbreviation	Definition
Aa	Amino acid
AABA	α -aminobutyric acid
AAO	Amino acid oxidase
Ac	Acetyl
ADH	Alcohol dehydrogenase
Ala, A	Alanine
Ar	Aromatic
Arg, R	Arginine
Asn, N	Asparagine
Asp, D	Aspartic acid
ATA	Aminotransferase
<i>B. subtilis</i> , BSU	<i>Bacillus subtilis</i>
<i>B.licheniformis</i> , BLi	<i>Bacillus licheniformis</i>
BCAa	Branched chain amino acid
BLAST	Basical Local Alignment Search Tool
Boc	<i>tert</i> -Butoxycarbonyl
bp	base pair
BSA	Bovine serum albumin
Bz	Benzyl
<i>C. atox</i>	<i>Crotallus atox</i>
<i>C. violaceum</i>	<i>Chromobacterium violaceum</i>
Cbz	Carboxybenzyl
Cys, C	Cysteine
d	Doublet

dd	double-doublet
DIBAL	Diisobutylaluminium hydride
DIPEA	<i>N,N'</i> -diisopropylethylamine
DMF	Dimethylformamide
DMPA	1,2-dimethyl propylamine
DMSO	Dimethyl sulfoxide
DNA	Deoxyribonucleic acid
DoE	Design of Experiment
DOS	Dissolved Oxygen Saturation
<i>E. coli</i>	<i>Escherichia coli</i>
e.e.	Enantiomeric excess
EDTA	Ethylenediaminetetraacetic acid
Et	Ethyl
FDH	Formate dehydrogenase
GABA	γ -aminobutanoic acid
GC	Gas chromatography
GDH	Glucose dehydrogenase
Gln, Q	Glutamine
Glu, E	Glutamate
Gly, G	Glycine
h	Hours
H₂O₂	Hydrogen peroxide
HEPES	2[4-(2-Hydroxyethyl)piperazin-1-yl]ethanesulfonic acid
His, H	Histidine
HPLC	High-performance liquid chromatography
HRP	Horse radish peroxidase

Ile, I	Isoleucine
<i>i</i>-Pr	<i>iso</i> -Propyl
<i>i</i>-PrNH₂	Isopropylamine
IPTG	Isopropyl β-D-1-thiogalactopyranoside
<i>K. pneumoniae</i>, KpN	<i>Klebsiella pneumoniae</i>
kDa	Kilodalton
KEGG	Kyoto Encyclopedia of Genes and Genomes
KPi	Potassium phosphate buffer
LC-MS	Liquid chromatography-mass spectrometry
LDA	Lithium diisopropylamide
LDH	Lactate dehydrogenase
Leu, L	Leucine
LOD	Limit of detection
Lys, K	Lysine
m	multiplet
MBA	(α)-methylbenzylamine
Me	Methyl
MeCN	Acetonitrile
MEGA	Molecular Evolutionary Genetics Analysis
Met, M	Methionine
min	minutes
NAD⁺	Nicotinamide adenine dinucleotide (oxidised)
NADH	Nicotinamide adenine dinucleotide (reduced)
NiSO₄	Nickel Sulfate
NMR	Nuclear magnetic resonance

OD₆₀₀	Optical density at 600 nm
<i>P. aeruginosa</i>, PA	<i>Pseudomonas aeruginosa</i>
<i>P. putida</i>, PP, Pput	<i>Pseudomonas putida</i>
PAGE	Polyacrylamide gel electrophoresis
PCC	Pyridinium chlorochromate
PCR	Polymarase chain reaction
PDB	Protein Data Bank
PGR	Pyrogallol red
Ph	Phenyl
Phe, F	Phenylalanine
PLES	<i>Pseudomonas aeruginosa</i> LESB58
PLP	Pyridoxal-5'-phosphate
PMP	Pyridoxamine-5'-phosphate
Pro, P	Proline
q	quartet
quint	quintet
<i>R. rubrum</i>, Rru	<i>Rhodospirillum rubrum</i>
<i>R. sphaeroides</i>, Rsph	<i>Rhodobacter sphaeroides</i>
<i>rac-</i>	racemic
s	singlet
SDS	Sodium dodecyl sulphate
sec	seconds
Ser, S	Serine
t	triplet
TAm	Transaminase

TDP	Thiamine diphosphate
TFA	Trifluoroacetic acid
THF	Tetrahydrofuran
Thr, T	Threonine
TLC	Thin layer chromatography
Trp, W	Tryptophan
Tyr, Y	Tyrosine
U	Units (of enzyme)
UniProt	Univeral Protein Resource
UPLC	Ultra-performance liquid chromatography
UV	Ultraviolet
<i>V. fluvialis</i>	<i>Vibrio fluvialis</i>
Val, V	Valine
YADH	Yeast alcohol dehydrogenase
λ_{\max}	Wavelength of maximum UV absorption

Table of Contents

DECLARATION	0
ABSTRACT	2
ACKNOWLEDGEMENTS.....	3
ABBREVIATIONS	4
TABLE OF CONTENTS	9
FIGURES	ERROR! BOOKMARK NOT DEFINED.
SCHEMES.....	13
TABLES.....	21
CHAPTER 1. INTRODUCTION.....	23
1.1. Overview of Transaminases	24
1.2. Enzyme Mechanism.....	24
1.3. Classes of Transaminases	27
1.3.1. Classes I and II	27
1.3.2. Class III	29
1.3.3. Class IV.....	30
1.3.4. Classes V and VI.....	30
1.4. Types of Transaminases	32
1.4.1. Amino Acid Transaminases.....	32
Amine Transaminases	33
1.5. Transaminase Structure	36
1.5.1. The Role of PLP.....	36
1.5.2. Transaminase Active Site	39
1.5.2.1. (S)-Selective Transaminase	40
1.5.2.2. (R)-Selective Transaminases	42

1.6.	Transaminase Assays.....	45
1.6.1.	Kinetic Resolution Assays	45
1.6.2.	Screening Assays	46
1.6.2.1.	pH-Based Colorimetric Assay	47
1.6.2.2.	Amino Acid Oxidase-Based Assay	48
1.6.2.3.	TTC-Based Screening Assay	50
1.6.3.	Equilibrium Displacement Assays	51
1.6.3.1.	Excess Isopropylamine.....	51
1.6.3.2.	LDH/GDH-Coupled enzyme reaction	52
1.6.3.4.	Diene Displacement Assay	54
1.7.	Transaminases in Asymmetric Synthesis	55
1.7.1.	(<i>S</i>)-Rivastigmine	55
1.7.2.	(<i>R</i>)-Sitagliptin	56
1.8.	Aims	58
CHAPTER 2. RESULTS AND DISCUSSION.....		60
2.1.	Cloning of Novel Transaminases.....	60
2.1.1.	(<i>S</i>)-Selective Transaminases	60
2.1.2.	(<i>R</i>)-Selective Transaminase	67
2.2.	Initial Use of CV2025 ω -TAm	69
2.3.	Method Development for Product Isolation	70
2.4.	Method Development for the Determination of the <i>e.e.</i> of α -MBA.....	73
2.5.	Direct chiral HPLC analysis of α -MBA.....	75
2.6.	Assessment and Optimisation of Conversion Yields For the Formation of (<i>S</i>)- α -MBA.....	77
2.7.	Enantioference Reactions Using CV2025 with Acetone and α -MBA	83
2.8.	LDH/GDH Coupled enzyme reaction.....	84
CHAPTER 3. SCALE-UP/FERMENTATION OF TAM RECOMBINANT <i>E. COLI</i>		87
3.1.	Acquiring Biomass	88
3.2.	Colorimetric Enzyme Activity Assay Screen of CV2025 ω -TAm	93

3.3.	Protein Purification	96
3.4.	Fermentation of (S)-Specific omega-Transaminases	100
CHAPTER 4. AAO-BASED SCREENING OF NOVEL ENZYMES AND AMINE DONORS		105
4.1.	Screening of Novel TAm Enzymes.....	106
4.2.	Screening of Amine Donors using CV2025 and VF_JS17	107
4.3.	Substrate Docking Studies	110
CHAPTER 5. TRANSAMINASE-MEDIATED SYNTHESIS OF CYCLIC AMINES.....		117
5.1.	Introduction	118
5.2.	Synthetic Plan For Transaminase-Mediated Aza-Michael Reaction	121
5.3.	Synthesis of Methyl-7-oxooct-2-enoate	124
5.3.1.	Michaelis-Arbuzov Reaction Approach	124
5.3.2.	Optimisation of Alkylation Step	125
5.3.3.	Optimisation of Wittig Step.....	127
5.4.	Chemical Synthesis of Methylpiperidine 44a	128
5.5.	Analytical Methods	129
5.6.	Biocatalytic Synthesis of Methylpiperidine 44a	134
5.7.	Design of Experiment (DoE) Studies	141
5.8.	Screening of Ketoester 42a Against Novel TAmS	148
5.9.	Synthesis of Phenylpiperidine 44b	155
5.10.	Synthesis of Methylpyrrolidine 47	158
5.11.	Screening of Ketoester Substrates 42b and 45 Against Novel TAmS	161
CHAPTER 6. CONCLUSIONS AND FUTURE DIRECTIONS		165
6.1.	Conclusions	166
6.2.	Future Directions.....	168
CHAPTER 7. EXPERIMENTAL.....		170
7.1.	General Instrumentation.....	171
7.2.	Synthesis of Ethyl 2-(2-(1,3-dioxolan-2-yl)ethyl)-3-oxobutanoate [55] (Grigg, Markandu et al. 1992)172	

7.3.	Synthesis of 5-oxohexanal [53] (Guthrie and Guo 1996)	173
7.4.	Synthesis of Methyl (<i>E</i>)-7-oxooct-2-enoate <i>trans</i> -[42a](Grigg, Markandu et al. 1992)	174
7.5.	Methyl (<i>Z</i>)-7-oxooct-2-enoate <i>cis</i> -[42a] (Grigg, Markandu et al. 1992)	174
7.6.	Synthesis of Methyl (\pm)-(cis-6'-methylpiperidin-2'-yl)acetate <i>cis</i> -[44a] (Banwell, Bissett et al. 1998)175	
7.7.	Methyl (\pm)-(trans-6'-methylpiperidin-2'-yl)acetate <i>trans</i> -[44a] (Banwell, Bissett et al. 1998) 175	
7.8.	Synthesis of 4-oxo-pentanal [73] (Padwa, Kulkarni et al. 1990)	177
7.9.	Synthesis of Methyl (<i>E</i>)-6-oxohept-2-enoate <i>trans</i> -[45] (Lory, Jones et al. 2006).....	178
7.10.	Synthesis of 1-phenylpentane-1,5-diol [65] (Ghobril, Sabot et al. 2008)	179
7.11.	Synthesis of 5-oxo-5-phenylpentanal [64] (Padwa, Kulkarni et al. 1990; Ghobril, Sabot et al. 2008) 180	
7.12.	Synthesis of Methyl (<i>E</i>)-7-oxo-7-phenylhept-2-enoate <i>trans</i> -[42b] (Grigg, Markandu et al. 1992; Tarantino, Liu et al. 2013).....	181
7.13.	Synthesis of Methyl 2-((2 <i>R</i> ,6 <i>S</i>)-6-phenylpiperidin-2-yl)acetate <i>cis</i> -[44b] (Cuthbertson and Taylor 2013).....	182
7.14.	Synthesis of Methyl 2-(5-methylpyrrolidin-2-yl)acetate <i>cis</i> -[47] (Thanh, Celerier et al. 1996) 183	
7.2.	Biological and Biochemical Methods	184
7.2.1.	Strains and Chemicals	184
7.2.1.1.	Chiral HPLC analysis of α -methylbenzylamine (1) to determine e.e.'s.....	185
7.2.1.2.	Biotransformation of Methyl (\pm)-(cis-6'-methylpiperidin-2'-yl)acetate <i>cis</i> -[44a] with (5)- α -methylbenzylamine [1].....	186
7.2.1.3.	Biotransformation of Methyl (\pm)-(cis-6'-methylpiperidin-2'-yl)acetate <i>cis</i> -[44a] with isopropylamine [11].....	187
7.2.1.4.	LDH/GDH Coupled enzyme reaction	187
7.2.1.5.	Design of experiment (DoE) study	189
7.2.1.6.	Cloning of the selected transaminases.....	192
7.2.1.7.	<i>Vibrio fluvialis</i> transaminase synthetic gene	196
7.2.2.	Fermentation of the Transaminase Gene Recombinant <i>E. coli</i>	197
7.2.2.1.	Purification of recombinant transaminases	198
7.2.2.2.	Amino Acid Oxidase Colorimetric Assay	199
	REFERENCES	201

Figures

- Figure 1:** -Stabilisation of the pyridinium nitrogen ion in aspartate TAm compared to alanine racemase.....40
- Figure 2:** – (A): Schematic of the first half-reaction depicting the orientation of an amino acid with the carboxylic acid and R groups situated in the L and S binding pockets respectively. (B): A substrate docking model of *P.put* ω -TAm showing the phenyl ring and methyl groups of (*S*)- α -MBA within the L and S binding pockets respectively.42
- Figure 3:** (A): Full structure of the (*R*)-selective TAm dyad from *A. fumigatus* showing PLP (stick model) bound to the two active sites via Lys179 at the domain interfaces. (B): Superimposed overall monomer folds of the (*R*)-selective TAm from *A. fumigatus* (green), a D-amino-acid TAm (PDB entry 31qs; cyan) and a branched-chain TAm (PDB entry 1wrv, violet) showing a novel N-terminal helix only found in the (*R*)-selective TAm.44
- Figure 4:** Active site residues and their interactions with the PLP internal aldimine in the *A. fumigatus* and *N. haematococca* (*R*)-selective TAm.45
- Figure 5:** Procedure for discovering and cloning novel transaminases.....62
- Figure 6:** Phylogenetic diagram of all 12 omega-TAm sequences.....65
- Figure 7:** 12% SDS-PAGE gels of all ten novel transaminases.....67
- Figure 8:** An unrooted phylogenetic tree of *A. aurescence*; the ω -TAm branch.....69
- Figure 9:** PCR of the 915bp DNA fragment BLi00607.....69
- Figure 10:** PCR products of PLES_54021, PA14_66260 and PA_5013

Figure 11: (A) – Calibration curve SDS-PAGE gel of purified CV2025 enzymes.....	71
Figure 12: Non-chiral HPLC trace showing isolated product of CV2025 biotransformation with IPA (blue) and an acetophenone standard (black).....	72
Figure 13: Chiral HPLC trace of commercially available benzoylated (\pm)- α -MBA (Blue) and (<i>S</i>)- α -MBA (Black).....	75
Figure 14: Separation of (\pm)- α -MBA on a ChiralPak AD-H column; (<i>R</i>)-MBA (Blue) (<i>S</i>)-MBA (Red)	76
Figure 15: Separation of (\pm)- α -MBA on the CrownPak CR+ column; (<i>S</i>)-MBA (Green) (<i>R</i>)-MBA (Blue)	77
Figure 16: Acetophenone production using (<i>R</i>)- and (<i>S</i>)- α -MBA with pyruvate.	79
Figure 17: Enantio-preference time-course experiment of 5 ω -TAMs monitoring acetophenone production in (A): (<i>S</i>)- α -MBA/pyruvate reaction and (B): (<i>R</i>)- α -MBA/pyruvate reaction.....	80
Figure 18: CV2025 biotransformation using (<i>S</i>)- and (<i>R</i>)-MBA with acetone	81
Figure 19: Time-course reaction - Acetophenone production using (<i>R</i>)- and (<i>S</i>)-MBA with acetone at pH 7.5 and CV2025 ω -TAM	84
Figure 20: Biostat® B-CDU II fermentor showing the overhead stirrer, cooling jacket, and feed bottle.	91
Figure 21: SDS-PAGE gel of samples taken during the fermentation process	93
Figure 22: Control colorimetric assay using ATA-113.....	94
Figure 23: Colorimetric assay using CV2025 from the three fermentations...	96

Figure 24: Chromatogram of CV2025 crude lysate purification by nickel affinity chromatography showing the UV peaks (blue) that denote protein concentration.	97
Figure 25: SDS-PAGE analysis of peaks isolated from the flow-through during His-tag purification of CV2025.	98
Figure 26: Bovine Serum Albumin (BSA) standard curve to determine protein concentration of CV2025 transaminases.	99
Figure 27: SDS-PAGE gel of samples taken during the fermentation process	101
Figure 28: Screening of amine donors against CV2025 – (A): after 1 min and (B): after 180 min.....	109
Figure 29: <i>In silico</i> docking image of PLP in the active site	111
Figure 30: Amino acid sequence alignment of the novel TAmS and CV2025 showing the residues of the R _L and R _S binding domains.....	112
Figure 31: <i>In silico</i> docking image of (S)-MBA in the R _L	113
Figure 32: Pyruvate in the R _S H-bonding to the highly conserved residue Tyr153.....	116
Figure 33: ¹ H NMR spectrum of mixed <i>cis</i> - and <i>trans</i> -44a showing the protons at the C _α position.....	129
Figure 34: Non-chiral HPLC traces of <i>cis</i> - and <i>trans</i> -42a (Blue) and methylpiperidine 44a (Red)	130
Figure 35: GC-MS traces of (A): chromatogram of <i>cis</i> - and <i>trans</i> -42a, (B): chromatogram of piperidine 44a, (C) mass peak of piperidine 44a and (D) mass peak of 42a.....	132

Figure 36: Linear ion trap LC-MS traces showing (A): Chromatogram of ketoester 42a. (B): Mass peak of ketoester 42a. (C): Chromatogram of piperidine 44a. (D): Mass peak of piperidine 44a	134
Figure 37: Optimised ion trap LC-MS method for the detection of all components of transaminase reaction in scheme 29.....	136
Figure 38: Calibration curve of methylpiperidine 44a on the ion trap LC-MS	136
Figure 39: Ion trap LC-MS results from comparative time-course TAm-mediated synthesis of 44a using (S)- α -MBA (Blue) and isopropylamine (Red)	137
Figure 40: Ion trap LC-MS results from comparative time-course TAm-mediated synthesis of 44a using (S)- α -MBA (Blue) and isopropylamine (Red) after overnight reaction.....	138
Figure 41: ¹ H NMR spectrum of the crude product from TAm-mediated synthesis of piperidine 44a showing the <i>cis</i> - and <i>trans</i> - protons at C α starting from a mixture of <i>cis</i> - and <i>trans</i> -42a	139
Figure 42: UPLC-MS trace chromatogram of methylpiperidine 44a chemical standard.....	140
Figure 43: UPLC-MS trace chromatogram of methylpiperidine 44a from a TAm-mediated synthesis.....	141
Figure 44: Calibration curve of methylpiperidine 44a on the UPLC-MS	142
Figure 45: Probability distribution plot of DoE results across 32 reactions...	144
Figure 46: Probability distribution plot of second round of DoE reactions	147
Figure 47: Calibration curve of piperidine 44a on a reverse phase HPLC ...	150

Figure 48: Screening of ketoester substrates <i>cis</i> - and <i>trans</i> -42a against a panel of ω -TAMs using non-chiral HPLC detection of piperidine 44a	152
Figure 49: (A): <i>In silico</i> docking studies on <i>trans</i> -42a	153
Figure 50: <i>In silico</i> docking studies on <i>cis</i> -42a.....	154
Figure 51: Calibration curve of <i>cis</i> -phenylpiperidine 44b by non-chiral HPLC	162
Figure 52: Calibration curve of <i>cis</i> -pyrrolidine 47 by non-chiral HPLC.....	162
Figure 53: Screening of ketoester substrates <i>trans</i> -42b and <i>trans</i> -45 against a panel of ω -TAMs using non-chiral HPLC detection of piperidine 44b and pyrrolidine 47.....	164

Schemes

Scheme 1: A model transaminase reaction.....	24
Scheme 2: The two half-reactions and mechanism of PLP-dependent transaminase enzymes.....	26
Scheme 3: Standard assay for the screening of ω -TAMs used by Shin and Kim <i>et al</i>	34
Scheme 4: Adapted from (Eliot and Kirsch 2004) – Dunathan’s stereoelectronic postulation showing the bond to C α that is to be broken is aligned with the π -orbitals of the PLP quinoid.	39
Scheme 5: Adapted from (Gutman, Meyer et al. 1992) - Enzymatic kinetic resolution of (<i>rac</i>)- 1-(naphthalen-1-yl)ethan-1-amine (5) using subtilisin and 2,2,2-trifluoroethyl butyrate (6).....	46
Scheme 6: Transaminase-mediated kinetic resolution of (<i>rac</i>)-alpha-methylbenzylamine (1) using an (<i>S</i>)-selective TAM and pyruvate (4).....	46
Scheme 7: pH-based colorimetric assay.	48
Scheme 8: Amino acid oxidase-based colorimetric assay using HRP and pyrogallol red to detect TAM activity in the form of alanine formation.....	49
Scheme 9: TTC-based colorimetric assay showing the potential colour changes when there is no conversion, moderate conversion, and complete conversion.	50
Scheme 10: Equilibrium displacement assay for transaminases using isopropylamine (11) in large excess (1 M) and evaporation of co-product acetone (12).	52
Scheme 11: Removal of pyruvate in transaminase reactions using the LDH/GDH system.	53
Scheme 12: Equilibrium displacement method for transaminases using YADH	54

Scheme 13: Equilibrium displacement using an aromatisation strategy	55
Scheme 14: Transaminase-catalysed synthesis of (S)-Rivastigmine.	56
Scheme 15: Adapted from (Savile, Janey et al. 2010) – (Red) Previous standard synthesis of sitagliptin. (Green) TAm-mediated biocatalytic synthesis of sitagliptin. .	57
Scheme 16: (A) - Stereospecific biotransformation reaction using L-alanine and subsequent chiral HPLC analysis. (B) - Stereospecific biotransformation using isopropylamine.....	71
Scheme 17: Reactions to assess the enantiopreference of CV2025 ω -TAm using (A) pyruvate as amine acceptor and (B) acetone as amine acceptor.....	78
Scheme 18: Screening of amine donors against transaminases using the amino acid oxidase colorimetric assay against a panel of 9 amine donors.....	108
Scheme 19: Examples of biologically active piperidine alkaloids.....	118
Scheme 20: Chemical synthesis of the piperidine and pyrrolidine cores of a selection of alkaloids.....	119
Scheme 21: Transaminase-catalysed synthesis of a 2,6-disubstituted piperidine by reductive amination of a diketone	121
Scheme 22: Proposed transaminase-mediated one-pot synthesis of disubstituted piperidines and pyrrolidines	122
Scheme 23: The role of double-bond geometry in the control of diastereoselectivity in an intramolecular aza-Michael reaction (Banwell, Bissett et al. 1998).....	123
Scheme 24: Transaminase-mediated synthesis of 2,6-disubstituted piperidine 44a may potentially access all four diastereomers	124
Scheme 25: (A) Initial plan for the synthesis of TAm substrate 42a and (B) Michaelis-Arbuzov reaction (C) Phosphorane synthesis for Wittig approach (D) Alkylation reaction in aldehyde synthesis for Wittig approach.....	125
Scheme 26: Alkylation of bromodioxolane 52	126
Scheme 27: Wittig olefination reaction	127
Scheme 28: Imine synthesis to facilitate trapping of amine precursor to piperidine 44a	128

Scheme 29: TAm-mediated synthesis of 2,6-disubstituted piperidine 44a.....	135
Scheme 30: Reaction scheme used in DoE	143
Scheme 31: Biocatalytic synthesis of <i>cis</i> - and <i>trans</i> -44a from their respective ketoester 42a isomers.....	149
Scheme 32: Rearrangement hydrogenation approach to the synthesis of phenylpiperidine 44b	156
Scheme 33: Unsuccessful alkylation attempt to prepare dioxolane 62.....	156
Scheme 34: Attempt at partial reduction of phenyl ketoacid.....	157
Scheme 35: Synthesis of unsaturated ester 42b and phenylpiperidine 44b	157
Scheme 36: Reductive amination of diketones to synthesise pyrrolidines - A: Jones' non-stereoselective approach with pyrrole intermediate. B: Boga's investigation into factors affecting diastereomeric ratio.....	159
Scheme 37: Ring-opening of butyrolactone to synthesise ketol 70	159
Scheme 38: Unsuccessful alkylation reaction in the synthesis of pyrrolidine 47	160
Scheme 39: Chemical synthesis of 2,5-disubstituted pyrrolidine 47.....	160
Scheme 40: Omega-TAm screen of <i>trans</i> -42b and <i>trans</i> -45 with isopropylamine (11)	161

Tables

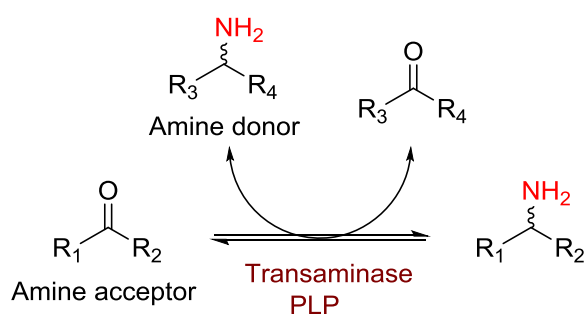
Table 1: Examples of Class I and II transaminases (Mehta, Hale et al. 1993; Hwang, Cho et al. 2005; Ward and Wohlgemuth 2010).....	28
Table 2: Examples of Class III transaminases (Hwang, Cho et al. 2005; Ward and Wohlgemuth 2010).....	29
Table 3: Examples of Class IV transaminases (Jansonius 1998; Eliot and Kirsch 2004).....	30
Table 4: Examples of Class V and VI transaminases (Jansonius 1998; Burgie, Thoden et al. 2007) (TDP = Thiamine-diphosphate).....	31
Table 5: Initial rates of reaction in CV2025 (Kaulmann, Smithies et al. 2007) and <i>V. fluvialis</i> (Shin and Kim 2001) ω -TAMs.....	35
Table 6: Non-transaminase PLP-dependent reactions and examples of their enzymes.....	37
Table 7: General Information on the Selected List of 12 Omega-Transaminases....	63
Table 8: Screening of Biotransformation Reaction pH.....	82
Table 9: Results from the LDH/GDH coupled-enzyme experiment.....	85
Table 10: Components of Seed, Production, and Feed Media used for <i>E. coli</i> fermentation.....	89
Table 11: Bradford Assay Results from all three CV2025 fermentation batches	99
Table 12: Total protein concentrations of fermentation batches from Figure 25	102
Table 13: OD ₆₀₀ values of the auto-induction screen of the six TAM <i>E. coli</i> cultures	103
Table 14: Colorimetric screening of transaminase enzymes against both enantiomers of α -MBA.....	107
Table 15: Volumetric enzyme activity of nine amine donors against CV2025 and VF_JS17	110

Table 16: Optimisation of Alkylation Reaction	126
Table 17: Optimisation of Wittig Reaction	127
Table 18: Reaction conditions non-cyclised primary amine 58	128
Table 19: First Round of DoE Studies	142
Table 20: “Best” and “Worst” Conditions from the First Round of DoE	144
Table 21: Second Round of DoE Studies	145
Table 22: The “Best” Conditions from the Second Round of DoE	147
Table 23: HPLC analysis of piperidine 44a in TAm screening of <i>cis-/trans-42a</i>	151
Table 24: HPLC analysis of phenylpiperidine 44b and pyrrolidine 47 in TAm screening of their respective precursors	163
Table 25: Components of the LDH/GDH-coupled enzyme reaction for the screening of novel TAmS	188
Table 26: Parameters and value ranges used in the first DoE study	189
Table 27: Design of experiment reaction list	190
Table 28: OD Values Recorded During Fermentation of All Six Cultures	197
Table 29: Components of AAO colorimetric assay screening of novel transaminases	199
Table 30: Layout of AAO colorimetric assay screen of novel TAmS	200

Chapter 1. Introduction

1.1. Overview of Transaminases

Transaminases (TAMs; aminotransferases; EC 2.6.1.) are a group of metabolic enzymes that reversibly convert ketones and aldehydes to chiral secondary amines and primary amines respectively. They belong to the pyridoxal-5'-phosphate (PLP) group of enzymes and are involved in the catabolism and synthesis of almost all 20 proteinogenic amino acids in nature. The reaction catalysed by transaminases involves the removal and transfer of the amine group from a donor compound (e.g. amino acid) to an acceptor ketone or aldehyde [Scheme 1].



Scheme 1: A model transaminase reaction

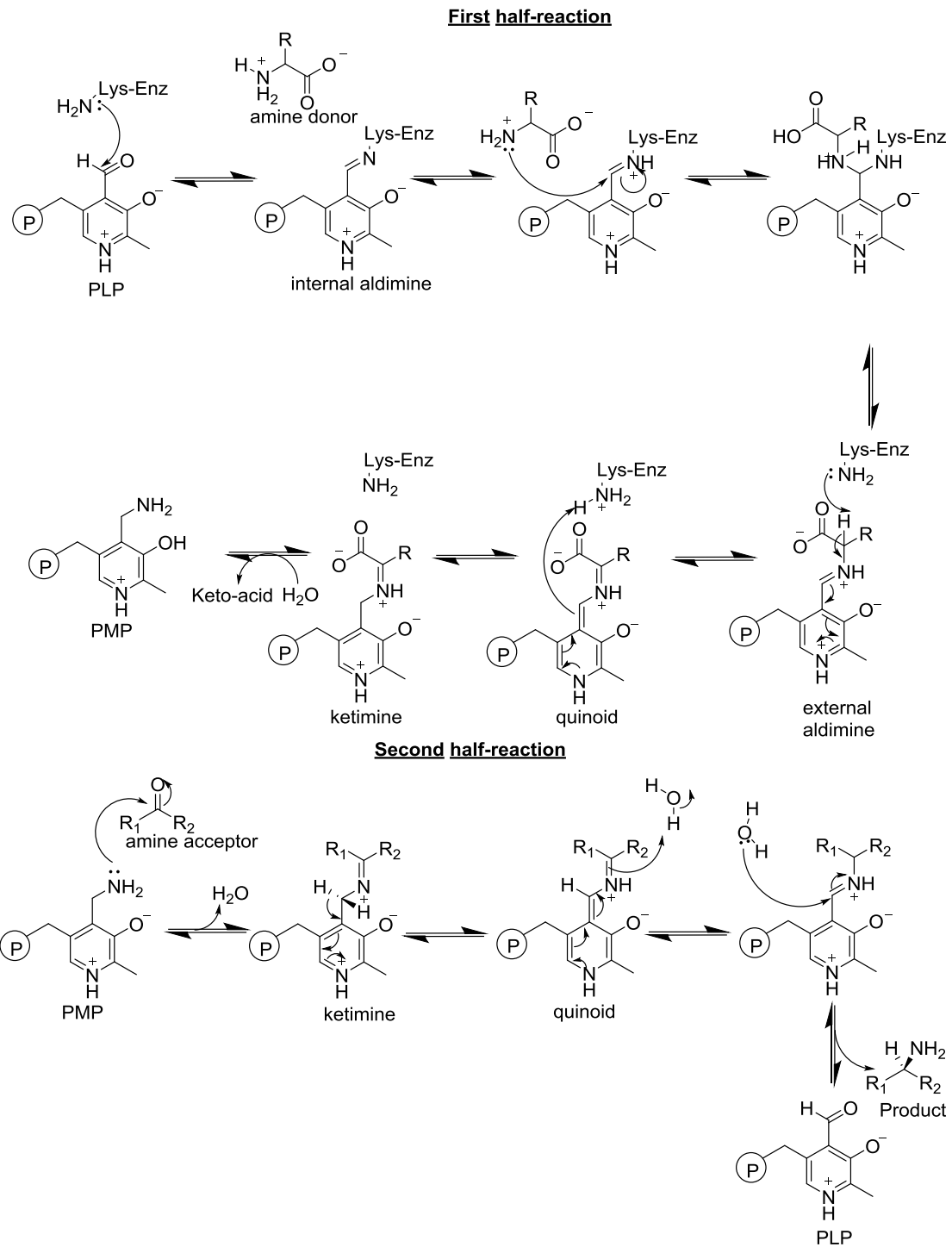
1.2. Enzyme Mechanism

The transaminase apoenzyme requires PLP (the biologically active form of vitamin B₆) to form its holoenzyme ^[1]. PLP is sequestered in the active site as a Schiff base via an imine linkage between its aldehyde group and the ε-amino group of a conserved lysine residue.

The reaction follows a classic ping-pong bi-bi or double displacement mechanism. This is a bireactant enzyme mechanism with the primary feature that the enzyme binds the first substrate and the resultant product has to dissociate before the second substrate can enter the active site to bind a modified enzyme cofactor ^[2]. The two

half-reactions of a one site ping-pong bi-bi mechanism are both reversible and the product from the second half-reaction can act as a substrate in the first half-reaction. Similar reactions include some transcarboxylase-catalysed reactions and some serine protease reactions ^[3].

In the first phase of the TAm catalytic cycle [Scheme 2] the internal aldimine of PLP and lysine undergo a transaldimination transformation forming an external aldimine with an amine donor (e.g. α -amino acid) ^[4]. The pyridoxal ring then acts as an electron sink that allows for transformation of the external aldimine to a ketimine via a 1,3-prototropic shift with a quinoid intermediate. Pyridoxamine-5'-phosphate (PMP), the crucial intermediate in this mechanism, is subsequently generated via hydrolysis of the ketimine and the concurrent release of an aldehyde or ketone side-product. The second half-reaction may only proceed upon the production of this PMP intermediate. It acts as the amine donor in the second half of the catalytic cycle following an exact reverse of the first half-reaction with a ketone or aldehyde acting as amine acceptor and ending in the regeneration of PLP. Unlike the covalently bound PLP, PMP remains in the enzyme active site by non-covalent interactions and therefore may be displaced using high concentrations of sulfate or phosphate ions ^[1b].



Scheme 2: The two half-reactions and mechanism of PLP in TAMs

PLP = pyridoxal 5'-phosphate; PMP = pyridoxamine 5'-phosphate; $\textcircled{\text{P}}$ = H_2PO_4

1.3. Classes of Transaminases

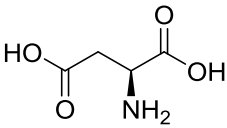
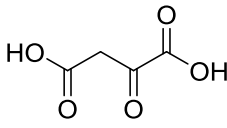
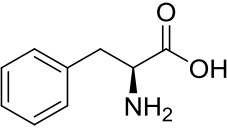
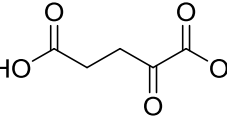
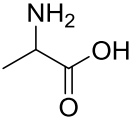
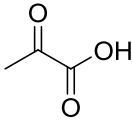
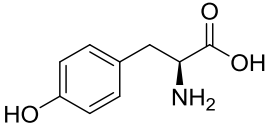
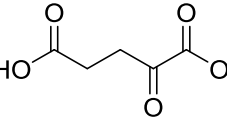
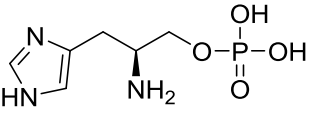
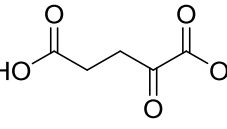
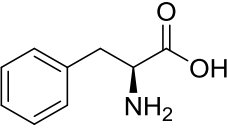
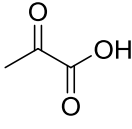
Transaminase enzymes are categorised under various different criteria. In 1989 Mehta and Christen began a bioinformatics-based characterisation of all known transaminase sequences at the time. Of the 16 transaminase amino acid sequences they aligned, only 12 amino acid residues (mainly those involved in interactions with the co-factor) were conserved out of approximately 400 residues ^[5]. Four years later, a larger set of 32 sequences were aligned as before, using algorithms for sequence comparison, hydropathy patterns, and secondary structure predictions ^[6].

These initial classifications were based solely on the evolutionary relatedness or phylogenetics of the sequences investigated and they gave rise to four subgroups of transaminases (class I, class II, class III, and class IV). The number of genome sequences increased dramatically after 1993 as whole genome sequences of various bacteria and other organisms were made available to search against. Searching the amino acid sequences of proteins against known transaminases of the 2005 Pfam database revealed there to be more than four classes of TAmS based on their evolutionary relatedness. Two more classes were therefore added to create classes I to V and a class VI or sugar aminotransferase (SAT). ^[7].

1.3.1. Classes I and II

Transaminase enzymes from classes I, and II [Table 1] catalyse the transfer of amines from α -amino acids to α -keto acids. Using family profile analysis of the amino acid sequences of transaminases, Hwang and co-workers proposed Class I TAmS to be sub-classified as aspartate-aminotransferases (AspATs) and Class II TAmS as aromatic-aminotransferases (AroATs). A direct link was found between the sequence similarity of transaminases (via BLAST screening) and their substrate specificity (via enzyme assay screens).

Table 1: Examples of Classes I and II transaminases ^[6-7]

Enzyme Name	EC Number	Main Donor	Main Acceptor
Aspartate TAm	2.6.1.1		
Aromatic TAm	2.6.1.57		
Alanine TAm	2.6.1.2		
Tyrosine TAm	2.6.1.5		
Histidinol-phosphate TAm	2.6.1.9		
Phenylalanine TAm	2.6.1.58		

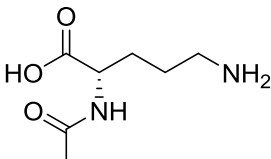
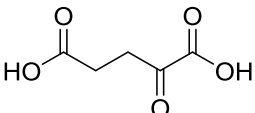
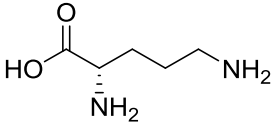
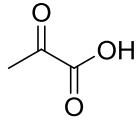
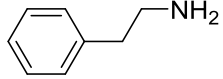
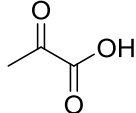
Although both subgroups have a specific affinity for the 2-ketocarboxylate group of α -amino acids, they differ in R-group preference as Class I TAmS prefer aliphatic R-groups whilst Class II TAmS have comparatively higher affinity towards aromatic α -

amino acids. They are therefore largely involved in amino acid synthesis, re-assortment and catabolism. The two subgroups were later expanded to include alanine-TAms, tyrosine-TAms, histidinol-phosphate-TAms, phenylalanine-TAms and aromatic-TAms (Ward and Wohlgemuth, 2010).

1.3.2. Class III

Unlike any of the other classes of transaminase enzymes, class III TAms do not normally require a 2-ketocarboxylate moiety on a substrate [Table 2]. Transaminases in this class therefore tolerate a wider range of substrates including aliphatic and aromatic ketones, ketoacids, hydroxyketones, and aldehydes.

Table 2: Examples of Class III transaminases ^[6b, 7]

Enzyme Name	EC Number	Main Donor	Main Acceptor
Acyl ornithine TAm	2.6.1.11		
Ornithine TAm	2.6.1.13		
Omega TAm	2.6.1.18		

Gamma aminobutyrate TAm	2.6.1.19		
Beta- aminocarboxylic acid TAm	-		

1.3.3. Class IV

In the past decade there has been a rapid increase in the isolation and characterisation of numerous class IV transaminases. The reason for this increase is the discovery that most (*R*)-selective transaminases are class IV transaminases [8].

Table 3: Examples of Class IV transaminases [8]

Enzyme Name	EC Number	Main Donor	Main Acceptor
D-Alanine TAm	2.6.1.21		
Branched-chain TAm	2.6.1.42		

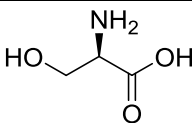
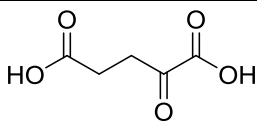
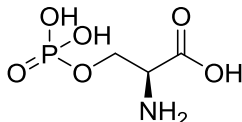
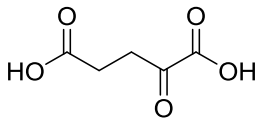
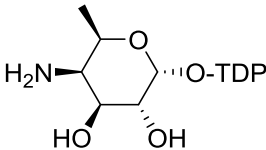
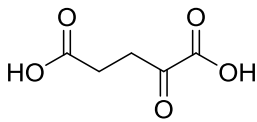
Groups of enzymes that make up the class IV sub-group are the D-alanine TAm and the branched-chain TAm [Table 3]. The amine donors of these two types of TAm are of opposite chirality although they share a preferred amine acceptor substrate (α -ketoglutarate) and a sequence homology of 31% [9].

1.3.4. Classes V and VI

The two members of the class V TAm subgroup (serine and phosphoserine TAm) have amine donor substrate preferences that are biosynthetically and structurally related (L-serine and 3-phospho-L-serine) [Table 4].

By contrast, class VI transaminases are a larger group of sugar aminotransferases (SATs) which are primarily involved in the synthesis of antibiotics (e.g. daunorubicin, streptomycin, erythromycin) and other secondary metabolites ^[10]. They are also present in the biosynthesis of O-antigens and the lipopolysaccharides and peptidoglycans found in the outer membrane of Gram –negative bacteria ^[11].

Table 4: Examples of Class V and VI transaminases ^[8a, 11] (TDP = Thiamine-diphosphate)

Enzyme Name	Class	EC Number	Main Donor	Main Acceptor
Serine TAm	V	2.6.1.51		
Phosphoserine TAm	V	2.6.1.52		
TDP-4-amino-4,6-dideoxy-D-glucose TAm	VI	2.6.1.33		

L-glutamine:2-deoxy-scylo-inosose TAm	VI	2.6.1.100	
TDP-3-keto-6-D-hexose TAm	VI	2.6.1.89	

1.4. Types of Transaminases

Transaminase enzymes can be further sub-divided into 2 groups based on their preference for the position of the amine moiety on a potential amine donor. TAm catalytic activity is dependent on the position of the amine functionality in the amine donor and that of the carbonyl group in the amine acceptor. There are two types of transaminases based on this criterion: amino acid transaminases and amine transaminases.

1.4.1. Amino Acid Transaminases

Amongst the 6 classes of transaminases based on sequence homology and evolutionary relatedness, enzymes from classes I, II, IV, and V are considered amino acid TAmS. This is due to their preference for the removal of amine groups to and from specific carbon positions relative to a carboxylic acid or phosphate ester group (in the case of the histidinol phosphate TAm) ^[12]. Within this sub-group however there are further differences in positional preferences. There are α -amino acid TAmS (e.g. aspartate-TAm and alanine-TAm), β -amino acid TAmS (e.g. β -alanine pyruvate TAm

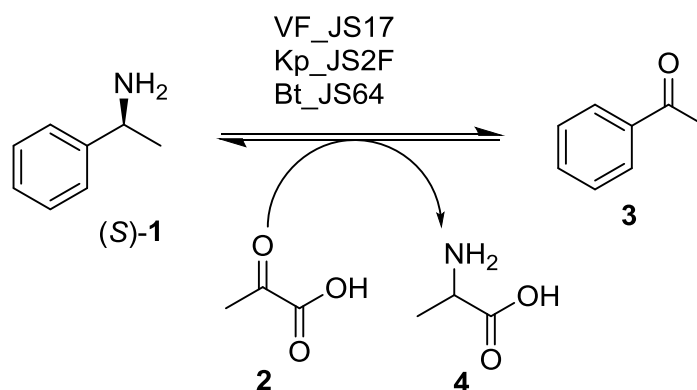
and β -aminocarboxylic acid TAm) and γ -amino acid TAm (e.g. GABA-TAm). Alpha-amino acid TAm are primarily responsible for amino acid metabolism in living cells. All except the α -amino acid transaminases have a broad spectrum of amine acceptor preference and have therefore proven to be ideal for industrial biocatalysis applications ^[13]. This classification criterion has little to do with the sequence homology and evolutionary relatedness of the various transaminases and more to do with the active site geometry of any given enzyme. This is exemplified by the TAm from *Mezorhizobium sp.* Strain LUK ^[14]. It is considered a class II transaminase (α -amino acid TAm) yet has the substrate specificity of a β -amino acid transaminase with a preference for β -aminocarboxylic acids. This indicates that the class groupings (based on sequence alignment of the enzymes) only reflects evolutionary relatedness of the whole enzyme and may not necessarily determine positional specificity ^[6b].

Amine Transaminases

Within the class III transaminase group there are various α - to γ -amino acid transaminases. Most importantly however there are ω -transaminases, a group with a preference for substrates that do not possess the carboxylate functionality. As a direct result of this, ω -TAm are considered “amine transaminases” and have a much broader substrate spectrum than all the other groups of TAm.

In 2001 Shin *et al* ^[15] published their findings on the comparison of ω -transaminases from the bacteria *Vibrio fluvialis* JS17 (VF_JS17), *Klebsiella pneumonia* JS2F (Kp_JS2F) and *Bacillus thuringiensis* JS64 (Bt_JS64). They identified the *V. fluvialis* enzyme as the most efficient for the kinetic resolution and asymmetric synthesis of enantiomerically pure chiral amines using (*S*)- α -MBA (**1**) as the amine donor [Scheme 3]. There were however problems with substrate and product inhibition of

the enzymes. Substrate inhibition by (S)- α -MBA was observed at a concentration of 100 mM and above for all three enzymes but *V. fluvialis* JS17 showed the lowest substrate inhibition as it had a higher reaction rate at above 50 mM.



Scheme 3: Standard assay for the screening of ω -TAMs used by Shin and Kim *et al*

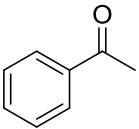
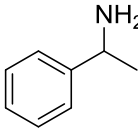
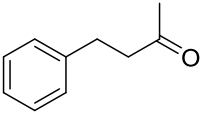
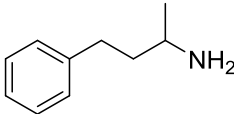
Inhibition by the amine acceptor (2), pyruvate, was most severe in *V. fluvialis* JS17. Initial rates began to drop at 10 mM compared to 100 mM in the other two enzymes. Product inhibition was found to be more severe with acetophenone (3) than (S)-alanine in all three enzymes. *B. thuringiensis* JS64 was strongly inhibited by acetophenone (61% relative initial rate at 3 mM acetophenone) and then by L-alanine (31% residual activity at 500 mM L-alanine).

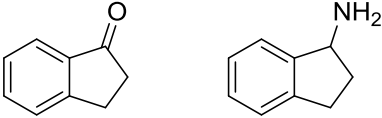
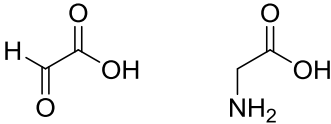



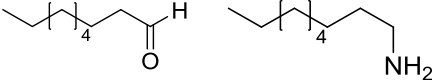
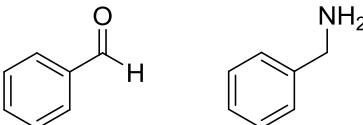
To address the issue of co-product inhibition the group used membrane reactors to remove volatile acetophenone from the reaction mixture ^[16]. They also employed the use of a biphasic reaction system to remove acetophenone from the aqueous phase. Using the biphasic method, substrate conversions were increased to 96% in 5 h compared to 36% without product extraction. The partition coefficient of acetophenone in organic/aqueous biphasic systems was measured in a number of organic solvents and hexane was found to have the highest value. This was therefore

the solvent of choice as it solvated acetophenone but not the substrates or the amino acid product (which remained in the aqueous phase).

Five years after this work, the ω -transaminase sequence from *V. fluvialis* JS17 [15, 17] was used to identify a new ω -TAm from *Chromobacterium violaceum* DSM30191 (CV2025) [18]. A BlastP™ search using the *V. fluvialis* JS17 amino acid sequence yielded a number of similar enzymes the most interesting of which was CV2025 with 38% sequence homology to Vf-JS17. As well as a higher over-expression (63% of the clarified lysate compared to 52% for Vf-JS17), CV2025 also exhibited a higher enzyme activity overall when screened against the same substrates as Vf-JS17 [Table 5].

Table 5: Initial rates of reaction in CV2025 [18] and *V. fluvialis* [15] ω -TAm

Name	Amine Acceptor	Amine Product	CV2025 Initial rate (%)	<i>V. fluvialis</i> Initial rate (%)
(±)- α -methylbenzylamine (MBA)			100(69.4)*	100(112.0)
(±)-1-methyl-3-phenylpropylamine			148.6	54.2 (61.4)

(±)-1-aminoindane		183.0 (157.9)	156.5 (161.7)
Glyoxylate		185.0	60.2
Propanal		132.3	36.4
Butanal		122.9	113.5
Hexanal		81.3	106.2
Nonanal		78.2	0.9
Benzaldehyde		91.2	72.8

*The values in brackets are the relative reactivities of the (S)-enantiomers determined via HPLC. Overall, the initial rates of reaction of the aromatic substrates were higher than that of the polar substrates when using both enzymes. This suggested a strong preference by both enzymes for aromatic compounds.

1.5. Transaminase Structure

1.5.1. The Role of PLP

Transaminases are part of a wider group of PLP-dependent enzymes with seven enzyme fold types ^[8], and transamination is not the only enzymatic transformation that PLP is able to catalyse. A list of the diverse range of non-transamination, PLP-catalysed transformations, at the alpha carbon position of its substrates include: elimination and replacement with electrophilic R groups, racemization, and

decarboxylation. Reactions at the β - and γ -positions include elimination or replacement reactions ^[8b]. Accordingly there are a wide variety of PLP-containing enzymes that carry out these different types of reactions from all seven fold types [Table 6].

In spite of the bewildering variety of transformations that PLP is able to mediate there is one common function of the co-factor in all these reactions. It is the ability of the pyridinium ring to act as an electron sink to stabilise the negative charge formed at C_{α} during the formation of the external aldimine Schiff base that makes all these reactions possible. PLP is able to catalyse many of these reactions, albeit very slowly, in the absence of a TAM ^[1b]. The functions of the various apoenzymes are therefore to stabilise and enhance the catalytic activity of the co-factor and perhaps more importantly, to confer and enforce reaction and substrate selectivity.

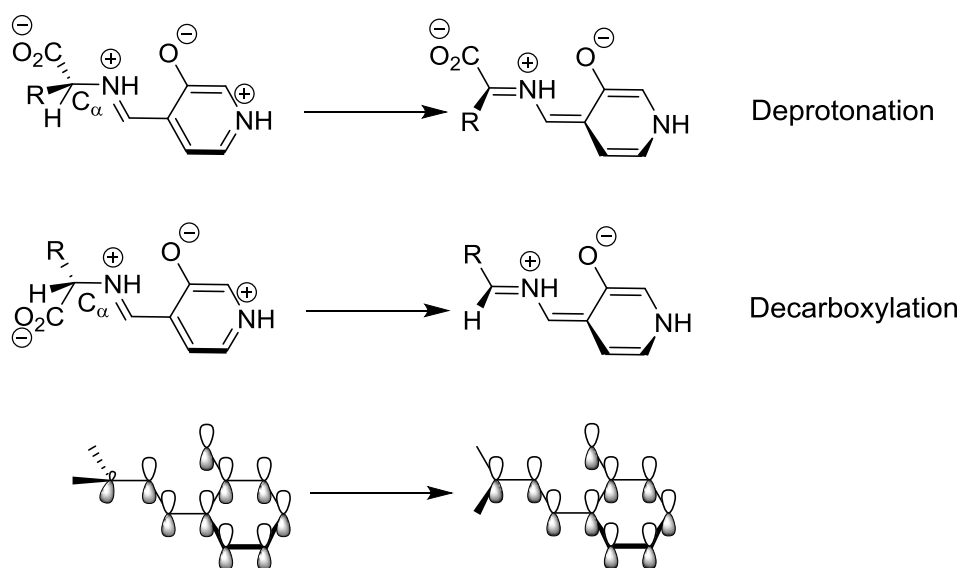
Table 6: Non-transaminase PLP-dependent reactions and examples of their enzymes

Enzyme	Reaction
Alanine racemase	Racemization
Ornithine decarboxylase	Decarboxylation
Dialkylglycine decarboxylase	
Serine hydroxymethyltransferase	α -Elimination and replacement
Tryptophan synthase	β -Replacement
Threonine deaminase	
O-acetylserine sulfhydrylase	
Serine dehydratase	β -Elimination
Tyrosine phenol lyase	

Cystathionine γ-synthase	γ -Replacement
Cystathionine γ-lyase	γ -Elimination
Tryptophan indole-lyase	

It is now known that the various fold types do not necessarily correspond to any particular PLP-dependent reaction. Each of the seven different structural classes have been found to contain representatives of a number of different reaction types [19]. What this implies therefore is that the different fold classes have evolved over time to replicate the active site geometry required to sequester PLP and conduct all these reactions independently.

It was postulated early in the research foray into PLP-dependent enzymes that the topology of the external aldimine would be the major determinant of which bond to C_{α} would be broken and therefore what type of reaction would take place in a given active site [20]. The theory was that the bond to be broken must be situated perpendicular to the pyridinium ring of the PLP quinoid intermediate so as to align with the π -orbitals of the co-factor [Scheme 4]. Control over substrate orientation by the apoenzyme is thus very crucial for determining what kind of reaction would take place in the active site (e.g. decarboxylation or deprotonation). The hypothesis was later confirmed through solving of the first aspartate transaminase structure by Jansonius and co-workers [21] and remains consistent with all transaminase structures solved subsequently.



Scheme 4: Dunathan's stereoelectronic postulation

Showing the bond to C_α that is to be broken is aligned with the π-orbitals of the PLP quinoid
Adapted from ^[8b].

1.5.2. Transaminase Active Site

There are 589 solved crystal structures of transaminases/aminotransferases available (via the PDB website) to date, spanning all classes, fold groups and types. The number of residues varies between 398 amino acids and 3324 amino acids, indicative of the wide variety within the transaminase family.

TAMs have been identified in Fold Types I and IV (of PLP-dependent enzymes) whose smallest catalytic subunits are homodimers. They comprise two domains (large and small) with the active site situated at the interface of the dimer ^[8b]. Amino acid residues from both monomers are present and crucial to activity in each other's active site. The two active sites of each homodimer are largely independent except for this. In addition, there are cases of asymmetry where the two functional active sites of a homodimer exhibit the same specific activity as a dimer with a single functional active site ^[22].

1.5.2.1. (S)-Selective Transaminase

The size and orientation of the two binding pockets also enforce stereoselectivity in the reactions catalysed by PLP. The catalytic activity of the co-factor and its role as an electron sink is enhanced in the active site of an (S)-selective transaminase by the interaction of the pyridinium nitrogen ion with various conserved residues depending on the type of transaminase. In the aspartate transaminase family a conserved aspartate residue (D223) interacts with the pyridinium nitrogen ion of PLP to keep the co-factor in the protonated state [Figure 1].

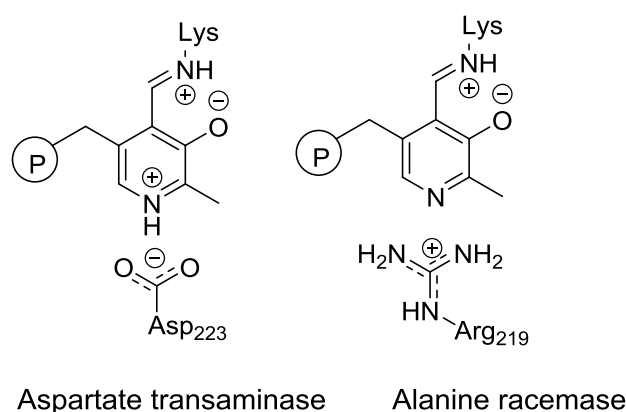


Figure 1: -Stabilisation of the pyridinium nitrogen ion in aspartate TAm compared to alanine racemase

Adapted from [8b]

Aspartic acid is conserved in that position in all known Fold Type I (S)-selective transaminase families including: alanine-TAm (D299), tyrosine-TAm (D216), GABA-TAm (D298), and ω -TAm (D259) [23]. In the absence of a stabilising counterion from a nearby amino acid the pyridinium cation does not form, giving rise to a different kind of reaction (e.g. racemization as seen in alanine racemases) [Figure 1]. In addition, the displaced lysine residue of the external aldimine (K288 in CV2025 ω -TAm) is positioned to transfer a proton to and from both the C _{α} and C_{4'} carbon atoms of the co-factor during catalysis [Figure 2].

In order to facilitate a stereoselective reaction in the active site, these (S)-selective Fold Type I enzymes have a closed active site conformation that obstructs the *re* face of the substrate-PLP intermediate from any solvent contact. Molecular water is therefore only able to access the *si* face of the quinoid intermediate to donate a proton thus allowing the near-exclusive synthesis of (S)-amines in high enantiomeric excess (e.e.) [24].

Stereoselectivity is further enhanced by anchorage of the co-factor within the active site via hydrogen bond interactions to the phosphate group. There are eight hydrogen bond interactions between the three non-ester phosphate oxygen atoms of PLP and the surrounding amino acid residues which form a so called “phosphate binding cup” [24]. The structure of the ω -transaminase from *Chromobacterium violaceum* (CV2025) was recently solved by Humble *et al*, shedding more light on the active site residues responsible for this anchorage. The R-groups of Ser121 and Tyr153 (from one monomer), the main chain amide nitrogen atoms of Thr321' and Tyr322', the side-chain hydroxyl group of Thr321' and the side-chain amide of Asn118' (from the other monomer) combine to form an intricate network of H-bonds that constitute the phosphate binding cup [23]. In addition, Asp226 was found to be involved in a water-bridged hydrogen bonding interaction with the hydroxyl group on PLP. The pyridine ring of PLP was also found in an edge-on interaction with Tyr153 on one edge and a hydrophobic interaction on the other edge of the ring with Val261. Although the most important interaction is the covalent bond that sequesters the co-factor in the active site, the combination of H-bonds and electrostatic interactions between PLP and the rest of the active site residues serve to enhance catalytic activity and crucially to confer stereoselectivity.

Through the size and orientation of the large (L) and small (S) binding pockets in the active site, the size and type of potential substrates are screened [Figure 2].

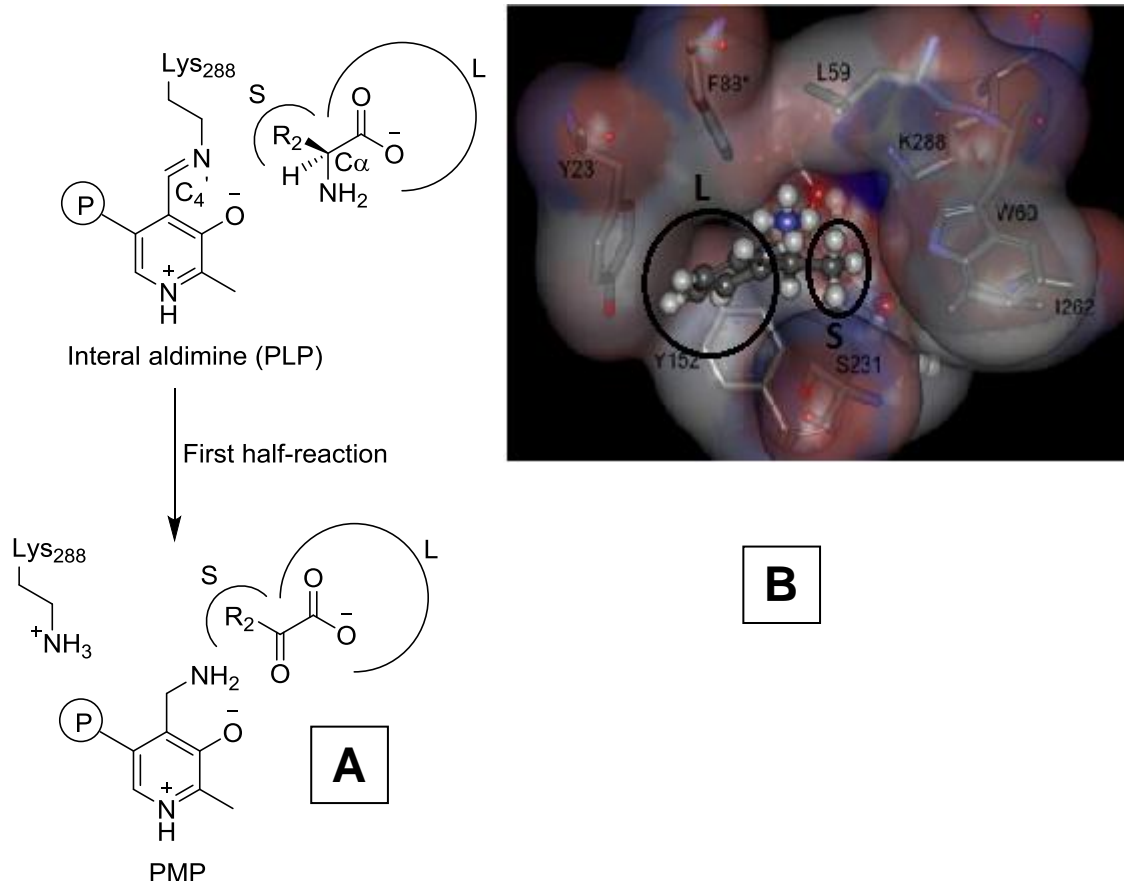


Figure 2: – (A): Schematic of the first half-reaction depicting the orientation of an amino acid with the carboxylic acid and R groups situated in the L and S binding pockets respectively. (B): A substrate docking model of *P.put* ω -TAM showing the phenyl ring and methyl groups of (S)- α -MBA within the L and S binding pockets respectively.

Adapted from [25]

The existence and variation in size of the large and small binding pocket in the active site of Fold Type I enzymes allow for the variety in transaminase classes within one fold family. TAm classes I, II, III and V are all Fold Type I enzymes whose difference in substrate preference [Tables 1.1, 1.2 and 1.4] exemplifies the important role played by binding pocket residues in determining substrate specificity.

1.5.2.2. (R)-Selective Transaminases

Fold Type I PLP-dependent enzymes ((S)-selective TAmS) have been found to be superficially similar to Fold Types II (tryptophan synthases) and IV (D-amino acid TAmS) in so far as they are all functional homodimers and are composed of a large and small binding pocket in their catalytic monomers. There is however one major difference between Fold Type IV and the other two. The active site of enzymes in this fold family is broadly a mirror image of the other fold families ^[8b]. As a direct result of this the *re* face of PLP in the active site is solvent exposed and obstructs molecular water access to its *si* face. The result is that Fold Type IV transaminases are (*R*)-selective ^[8b].

(*R*)-selective transaminases remain a small percentage of all known transaminases to date. Höhne *et al*, in 2010 identified a group of 17 (*R*)-selective TAmS using *in silico* methods ^[26]. Until then, only two (*R*)-selective TAmS were available in the literature: *Arthrobacter* sp. KNK168 ^[27] and the commercially available ATA117 (<http://www.codexis.com>). This scarcity is reflected in strain collection screenings that suggest that (*R*)-selective TAmS are quite rare in nature ^[28]. Discovery of the set of 17 putative enzymes started with an *in silico* search for the specific sequence motifs which underpin D-amino acid TAmS and branched-chain TAmS. The discovery of this pool of (*R*)-selective TAmS led to the first publication of an (*R*)-selective transaminase crystal structure from the fungus *Aspergillus fumigatus* ^[29].

This homodimer containing 639 amino acid residues and two PLP co-factors [Figure 3A] belongs to the Fold Type IV group of PLP-dependent enzymes. It has an overall structure similar to both a branched-chain TAm (from *Thermo thermophiles*) and a D-amino acid TAm (from *Bacillus* sp. YM-1) [Figure 3B]. There is however one characteristic difference in structure which pertains to the presence of a unique N-terminal helix which has been shown to play a significant role in protein stability.

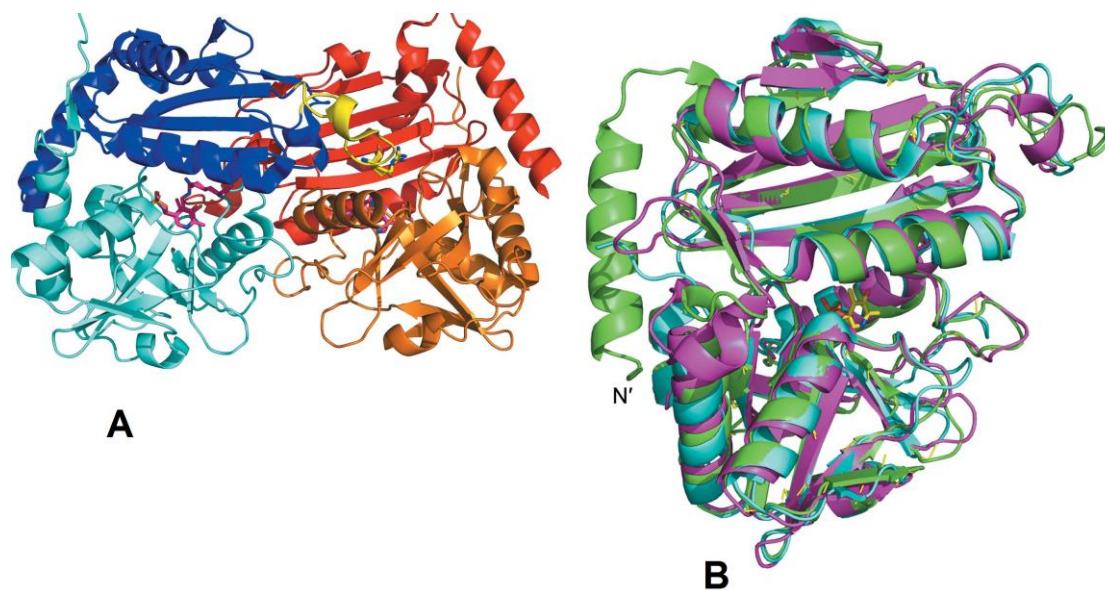


Figure 3: (A): Full structure of the (*R*)-selective TAM dyad from *A. fumigatus* showing PLP (stick model) bound to the two active sites via Lys179 at the domain interfaces. (B): Superimposed overall monomer folds of the (*R*)-selective TAM from *A. fumigatus* (green), a D-amino-acid TAM (PDB entry 31qs; cyan) and a branched-chain TAM (PDB entry 1wrv, violet) showing a novel N-terminal helix only found in the (*R*)-selective TAM.

Adapted from ^[29]

Most recently, Sayer and co-workers published the discovery of an (*R*)-selective transaminase co-crystallised with gabaculine. This (*R*)-selective TAM from the fungus *Nectria haematococca* was shown to have similar structural features as the *A. fumigatus* enzyme including the N-terminal helix for stability ^[30]. In both (*R*)-selective transaminases, the PLP co-factor is sequestered in the active site via a Schiff base internal aldimine with Lys179 whilst the pyridinium nitrogen cation forms a salt-bridge with the carboxylate ion of Glu212 in the active site of the enzymes [Figure 4]. The phosphate group is co-ordinated by three hydrogen bonds with threonine residues Thr238, Thr273, and Thr274 with the guanidinium ion of Arg77 forming a salt-bridge with the final non-ester oxygen. The active site residues Tyr58 and Trp183 were found to co-ordinate with the aldehyde group through a proximal water molecule to complete the active site interactions with PLP.

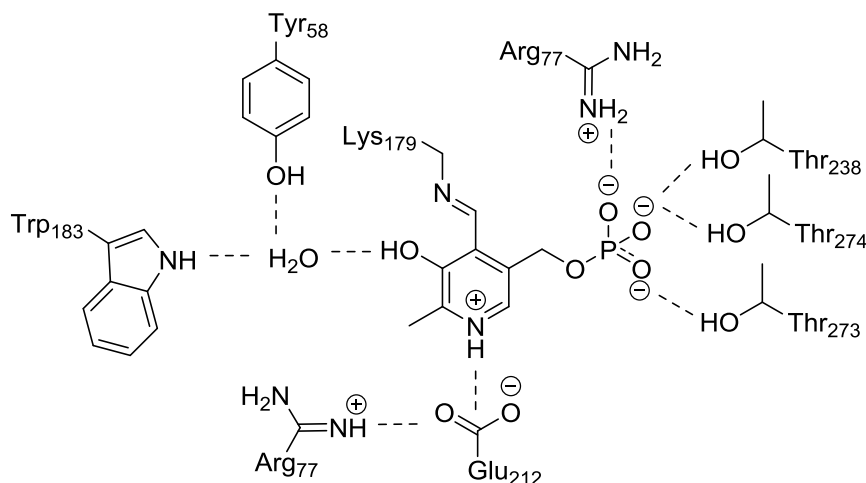


Figure 4: Active site residues and their interactions with the PLP internal aldimine in the *A. fumigatus* and *N. haematococca* (*R*)-selective TAmS.

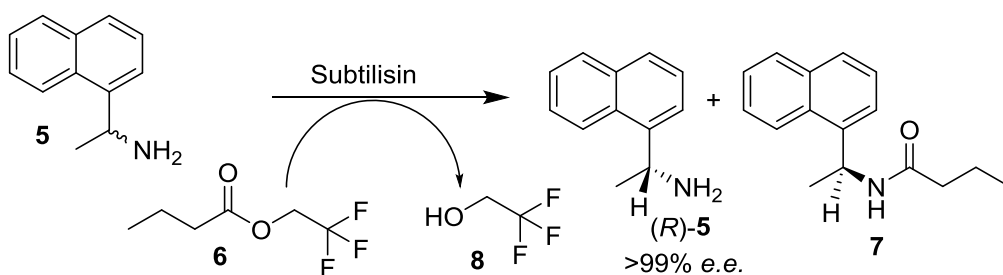
Adapted from [29]

1.6. Transaminase Assays

Over the past decade there has been a rapid increase in interest in transaminase enzymes and their properties in biocatalytic reactions. Due to their high stereoselectivity and atom efficiency, TAmS have been used in the synthesis and preparation of many chiral amines. These fall under two main types of reactions: kinetic resolution reactions and chiral amine synthesis reactions.

1.6.1. Kinetic Resolution Assays

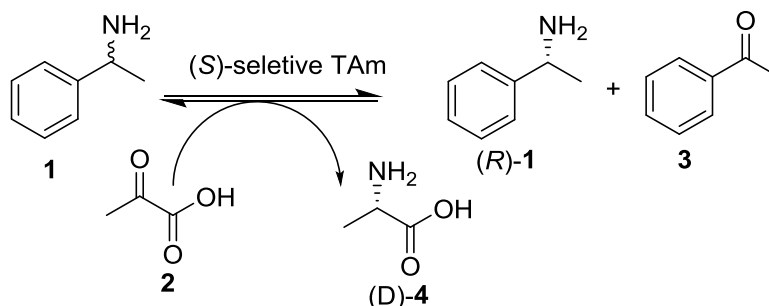
The biocatalytic preparation of enantiomerically pure chiral amines has been well documented over the years. This often involved the chemical synthesis of a racemic amine followed by its kinetic resolution using a range of methods including enzymes (e.g. lipases, hydrolases, and proteases) [31]. In the enzymatic resolution of 1-(naphthalen-1-yl)ethan-1-amine (**5**) using the protease subtilisin [Scheme 5], the (*S*)-enantiomer of compound **5** forms an amide with 2,2,2-trifluoroethyl butyrate (**6**) giving (*R*)-**5** (>99% e.e.) and the amide (**7**) [31b]



Scheme 5: Enzymatic kinetic resolution of (*rac*)-1-(naphthalen-1-yl)ethan-1-amine (5) using subtilisin and 2,2,2-trifluoroethyl butyrate (6)

Adapted from [31b]

Such kinetic resolution methods rely on the selective derivatisation of one enantiomer over another. A transaminase-catalysed kinetic resolution is by comparison more economical and has been shown to be superior in terms of productivity, yield and conversion as well as making product isolation easier (using changes in pH) [16, 32]. For example, in the transaminase-mediated kinetic resolution of racemic α -methylbenzylamine ((\pm)- α -MBA) (1), an (*S*)-selective TAM exclusively converted (*S*)- α -MBA to acetophenone (3), leaving (*R*)-1 [Scheme 6] [32a].



Scheme 6: Transaminase-mediated kinetic resolution of (*rac*)- α -methylbenzylamine (1) using an (*S*)-selective TAM and pyruvate (2).

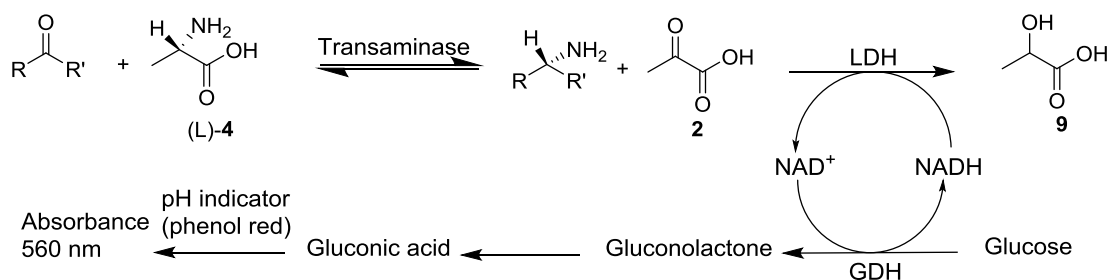
1.6.2. Screening Assays

Transaminases are more commonly used to facilitate the synthesis of amines from carbonyl groups [reverse reaction of Scheme 3]. They are of particular interest to the

pharmaceutical, agrochemical and fine chemicals industries for the synthesis of natural and unnatural amino acids and chiral amines ^[1b]. Methods for screening new transaminases are therefore a crucial part of the search for transaminases for any given substrate. A range of high-throughput screening methodologies used in transaminase-catalysed reactions have been developed in recent years ^[33]. The majority of screening approaches use high pressure liquid chromatography (HPLC) for analyte detection. Other innovative methods have been developed by many research groups using colorimetric, and gas chromatography (GC) analytical methods to monitor substrate consumption or product formation.

1.6.2.1. pH-Based Colorimetric Assay

One of the screening approaches involved the use of an enzyme coupled pH-based colorimetric assay [Scheme 7] ^[33b 2010, 33d]. Small scale reactions were performed with the substrate acetophenone and a pH indicator dye (phenol red). Automated additions of NaOH solution (2 M) allowed for the regulation of pH at its optimal value (7.5). A plate spectrophotometer was then used to measure reaction rate as a function of absorbance/pH change at 560 nm. The spectrophotometer-based micro-scale method (compared to a conventional HPLC-based assay) was found to be more efficient and more accurate. However, the main advantage of the pH dye assay over conventional HPLC was a reduced run-time (30 min) and the use of less substrate (5 mg). The pH indicator assay also enabled easy scale up of the reaction from 100 μ L to 25 mL.



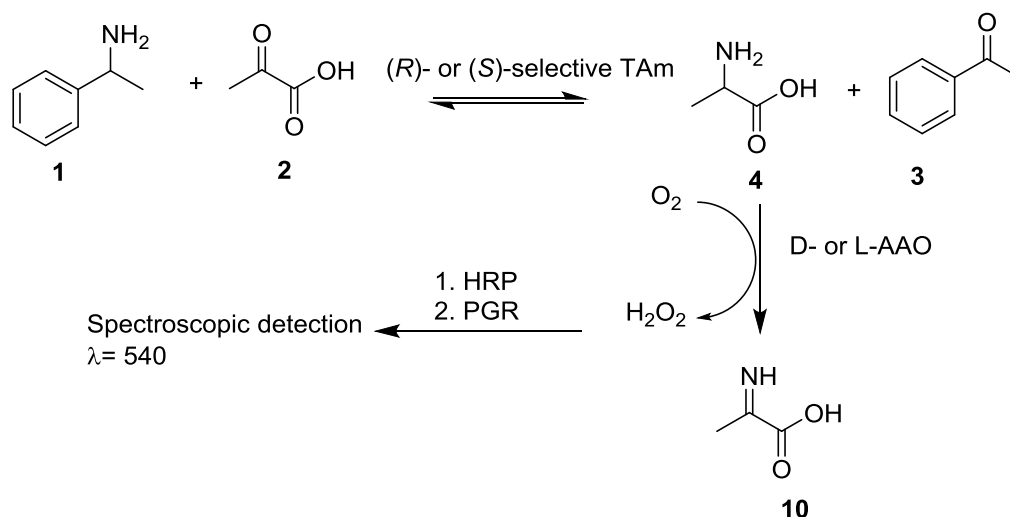
Scheme 7: pH-based colorimetric assay.

LDH = Lactate dehydrogenase; GDH = Glucose dehydrogenase

The production of gluconic acid at the end of the assay lowers the pH of the reaction mixture which allows for the rapid screening for TAm activity. It also offers an opportunity for *in situ* monitoring of progress of the reaction at a larger scale via an automated addition of base.

1.6.2.2. Amino Acid Oxidase-Based Assay

Another colorimetric assay in the literature uses a combination of amino acid oxidases (AAO), horse radish peroxidase (HRP) and the dye pyrogallol red (PGR) to detect the formation of alanine from pyruvate in a transaminase reaction [Scheme 8] [33c]. The transaminase step (one of three steps in this assay) can be a kinetic resolution of a racemic amine or a straightforward synthesis of a carbonyl compound using a chiral amine. The limiting aspect of the assay is that pyruvate has to be the amine acceptor in order for the second (amino acid oxidase) step to progress. The third step is the spectrophotometric detection step involving HRP and PGR.



Scheme 8: Amino acid oxidase-based colorimetric assay using HRP and pyrogallol red to detect TAm activity in the form of alanine formation.

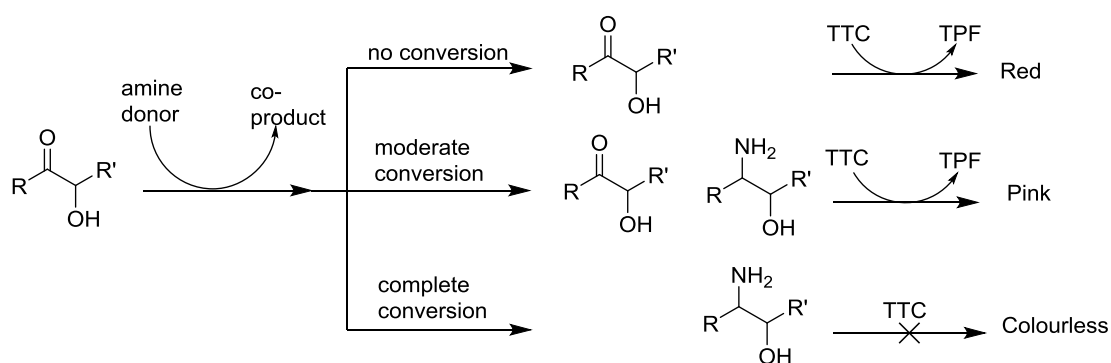
The assay can provide qualitative data on the enantio-preference of a transaminase by using either D- or L-AAO in the second reaction where the amine product of the transaminase reaction (D- or L-alanine (4)) is oxidised to its imine (10). The second reaction therefore relies on the correct enantiomer of alanine being produced from the first reaction. An (S)-selective transaminase will elicit a positive response when L-AAO is used in the second reaction whilst an (R)-selective TAm requires D-AAO. In addition to reducing molecular oxygen to hydrogen peroxide to be used in the third reaction in the assay, the amino acid oxidase step also creates an equilibrium displacement effect that results in a higher rate of reaction and turnover compared to a conventional TAm reaction where no equilibrium displacement method is used.

The final step in the assay involves the irreversible oxidation of pyrogallol red (a red dye) by hydrogen peroxide, to a yellow quinone derivative ^[34]. The colour change (from red to yellow) occurs in the visible wavelength range of light (540 nm) and a UV/Vis spectrophotometer can be used to quantify and correlate the rate of change of colour to a rate of reaction. Given that all other enzymes and reagents in the assay

are in excess, the TAM step becomes rate-limiting which allows for a direct correlation between colour change and transaminase enzyme activity to be deduced. One major disadvantage however, is the prohibitively high cost of L/D-AAO which makes this assay unsuitable for the screening of multiple transaminases. Based on the conditions reported, screening two transaminases (forty reactions) would require over £200 worth of L-AAO (90 U) and or £140 worth of D-AAO (90 U). The amino acid oxidase colorimetric assay can therefore be considered a fast and enantioselective screen for novel transaminases and amine donors. It is however very expensive (due to the high cost of AAO enzymes) and is not applicable with the screening of any other amine acceptors except pyruvate.

1.6.2.3. TTC-Based Screening Assay

A transaminase screening assay based on the oxidation of compounds with a 2-hydroxy ketone motif by colourless 2,3,5-triphenyltetrazolium chloride (TTC) has also been developed ^[35] [Scheme 9]. It was developed specifically as a hydroxyketone substrate-screening assay.



Scheme 9: TTC-based colorimetric assay

Showing the potential colour changes when there is no conversion, moderate conversion, and complete conversion.

In the presence of unreacted 2-hydroxy ketone substrates, TTC is reduced to 1,3,5-triphenylformazan (TFP), eliciting a colour change to red.

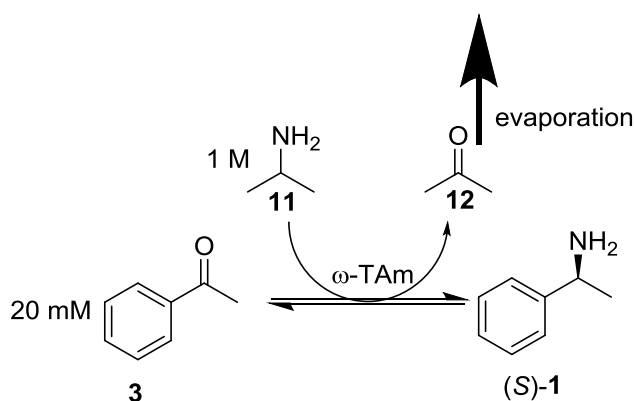
As with the amino acid oxidase assay, a UV/Vis spectrophotometer is then used to detect and quantify the intensity of colour which can then be converted to enzyme activity data. One of the limitations of the assay however, is that it requires amine acceptor substrates with a 2-hydroxy ketone motif and therefore is not as widely applicable.

1.6.3. Equilibrium Displacement Assays

One of the major disadvantages of transaminase-catalysed reactions is an unfavourable equilibrium in the amine synthesis direction. It has been found that the equilibrium constant in a transaminase reaction, more often than not favours production of the ketone starting material in the systems studied ^[36]. This coupled with product inhibition (by the ketone co-product), results in moderate to low yields in TAM-mediated chiral amine synthesis. There have been numerous innovative approaches developed to solve this unfavourable equilibrium problem and to improve the utility of transaminases in an industrial context.

1.6.3.1. Excess Isopropylamine

There have been a number of accounts of the use of isopropylamine as amine donor for the synthesis of chiral amines ^[33b, 37]. The advantages of isopropylamine (**11**) are its relative inexpensiveness, low molecular weight (little steric hindrance in the active site) and the production of a volatile co-product (acetone (**12**)) which can be removed under reduced pressure ^[33b] [Scheme 10].



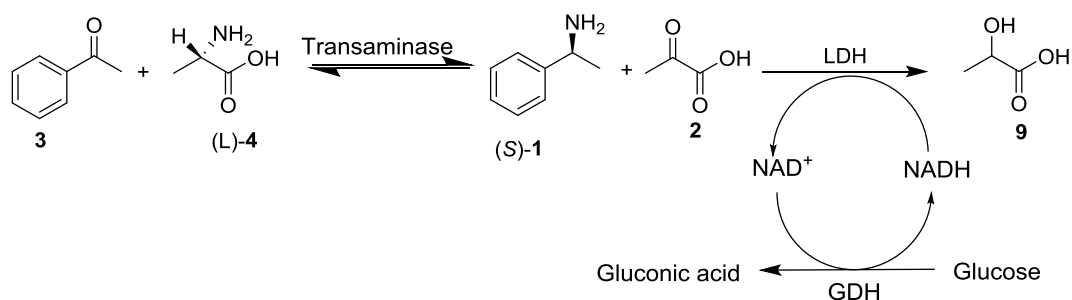
Scheme 10: Equilibrium displacement assay for transaminases

Using isopropylamine (**11**) in large excess (1 M) and evaporation of co-product acetone (**12**).

For example, using 1 M isopropylamine and 20 mM acetophenone, 95% conversion of (S)-**1** was attained with >99% *e.e* ^[33b]. This was in spite of a relatively low rate of reaction due to enzyme inactivation as a result of the extremely high concentration of **11**. There are further drawbacks in using this method however. The large scale distillation of the acetone is not feasible for water soluble compounds. This therefore limits the utility of such an approach to only a few reactions. In addition, the approach also requires the use of more thermostable transaminases to withstand the temperature increase required to drive off acetone. There is therefore the need for equilibrium displacement assays with much wider applicability.

1.6.3.2. LDH/GDH-Coupled Enzyme Reaction

Developed alongside the pH-based colorimetric assay, the LDH/GDH-coupled enzyme reaction is an equilibrium displacement assay that uses a secondary enzyme, lactate dehydrogenase (LDH), and glucose dehydrogenase (GDH) as a co-enzyme regeneration enzyme with glucose as its substrate. The assay requires alanine as an amine donor in the TAm reaction ^[33b] [Scheme 11].

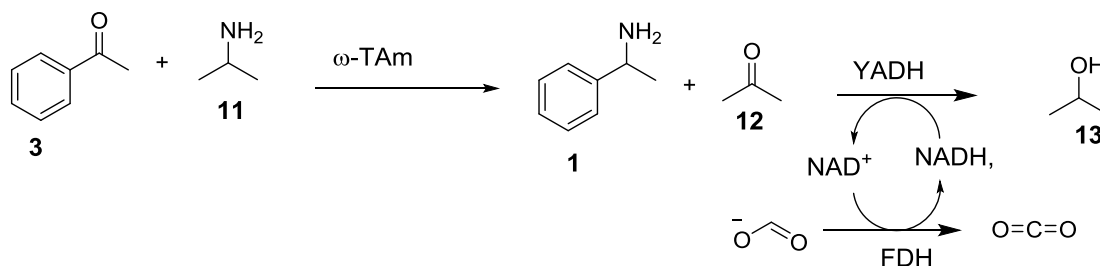


Scheme 11: Removal of pyruvate in transaminase reactions using the LDH/GDH system.

Lactate dehydrogenase (LDH) is used to reduce pyruvate (the product of alanine transamination) to lactic acid with β -nicotinamide adenine dinucleotide (NADH) as the hydride donor. This method serves the dual purpose of driving the reaction to completion via consumption of the co-product (**2**) and the elimination of product inhibition by reducing it to the acid (**9**). The co-enzyme (NADH) is then recycled by an oxidation reaction catalysed by glucose dehydrogenase (GDH) which converts glucose to gluconic acid. It was also observed that using the LDH/GDH system yielded over than 20 times more product (70% conversion) compared to without it (3% conversion) over a 24 h period.

1.6.3.3. YADH/FDH-Coupled enzyme reaction

Another iteration of the use of coupled enzyme systems has been developed involving yeast alcohol dehydrogenase (YADH) and formate dehydrogenase (FDH) [Scheme 12]. Unlike the LDH/GDH system [Scheme 11], the transaminase step in this assay uses isopropylamine as the amine donor [Scheme 12]. YADH is then used in the second reaction to remove acetone (**12**) by conversion to isopropanol (**13**). This is followed by *in situ* recycling of the co-enzyme NADH by formate dehydrogenase (FDH) ^[37a]



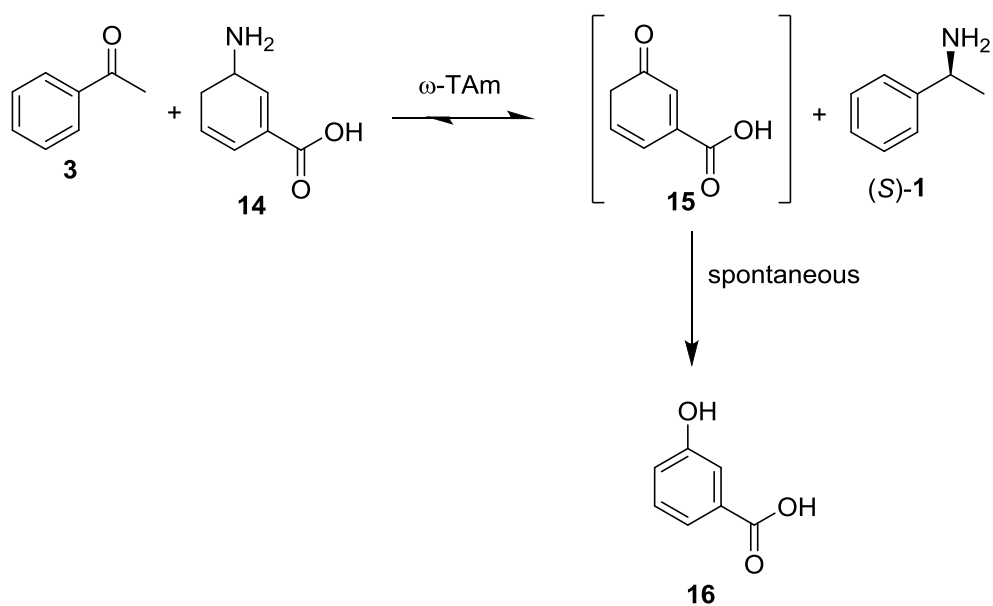
Scheme 12: Equilibrium displacement method for transaminases using YADH

YADH = Yeast alcohol dehydrogenase; FDH = Formate dehydrogenase

Yeast alcohol dehydrogenase is a very well-studied enzyme which has been shown to have a relatively narrow substrate range. The active site readily accommodates methanol/methanal and ethanol/ethanal but elicits low reaction rates when the chain length is increased. YADH is therefore effective with an isopropylamine/acetone substrate/product pairing.

1.6.3.4. Diene Displacement Assay

Using the amine donor 3-aminocyclohexa-1,5-dienecarboxylic acid (**14**), Wang and co-workers also recently developed a TAm enzymatic cascade for the asymmetric synthesis of chiral amines ^[38] [Scheme 13]. The spontaneous tautomerization/aromatization of the product ketone (**15**) to benzoic acid **16** allows for a displacement of equilibrium in favour of the formation of the chiral amine (*S*)-**1** up to a theoretical yield of 100%.



Scheme 13: Equilibrium displacement using an aromatisation strategy

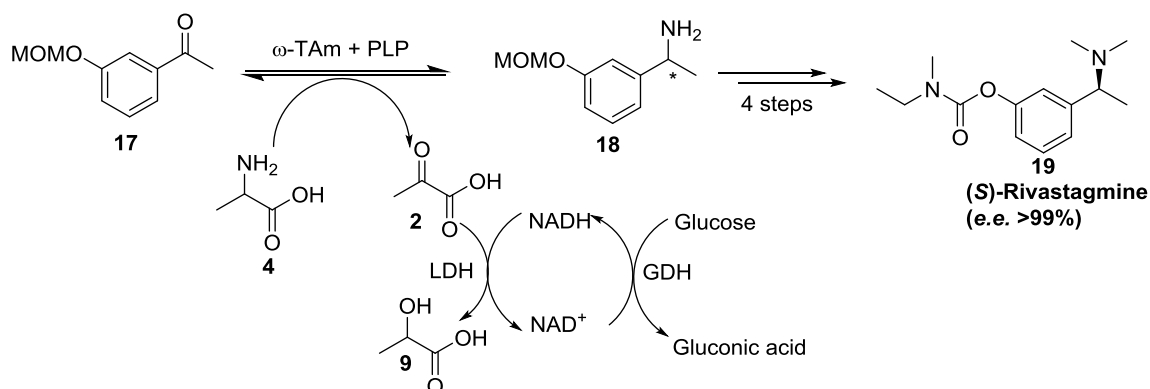
1.7. Transaminases in Asymmetric Synthesis

Perhaps the broadest and most research-intensive area on transaminases has been its use in asymmetric synthesis. Chiral amines account for about 40% of all pharmaceutical compounds and 20% of crop protection compounds used in the agrochemical industry. Transaminases can provide an atom efficient, clean and highly stereoselective route to chiral amines and a number of interesting reports demonstrate the utility of these enzymes as excellent chiral catalysts. Several industrial examples are highlighted below and in the following chapters.

1.7.1. (S)-Rivastigmine

(S)-Rivastigmine (**19**) is one of the most potent drug compounds available for the treatment of early-stage Alzheimer's disease. It is also known to curtail some of the effects of dementia in Parkinson's sufferers ^[39]. The chemocatalytic route to compound **19** involves the use of toxic transition metal catalysts, chiral acids, or a biocatalytic lipase-catalysed kinetic resolution of hydroxy-precursors ^[40]. The

transaminase-mediated biocatalytic synthesis however, as reported by Fuchs *et al*, is a four-step process with an overall 71% isolated yield and >99% e.e. [40] [Scheme 14]. The key building block required (**18**) is accessed via the asymmetric transamination of an acetophenone derivative (**17**).

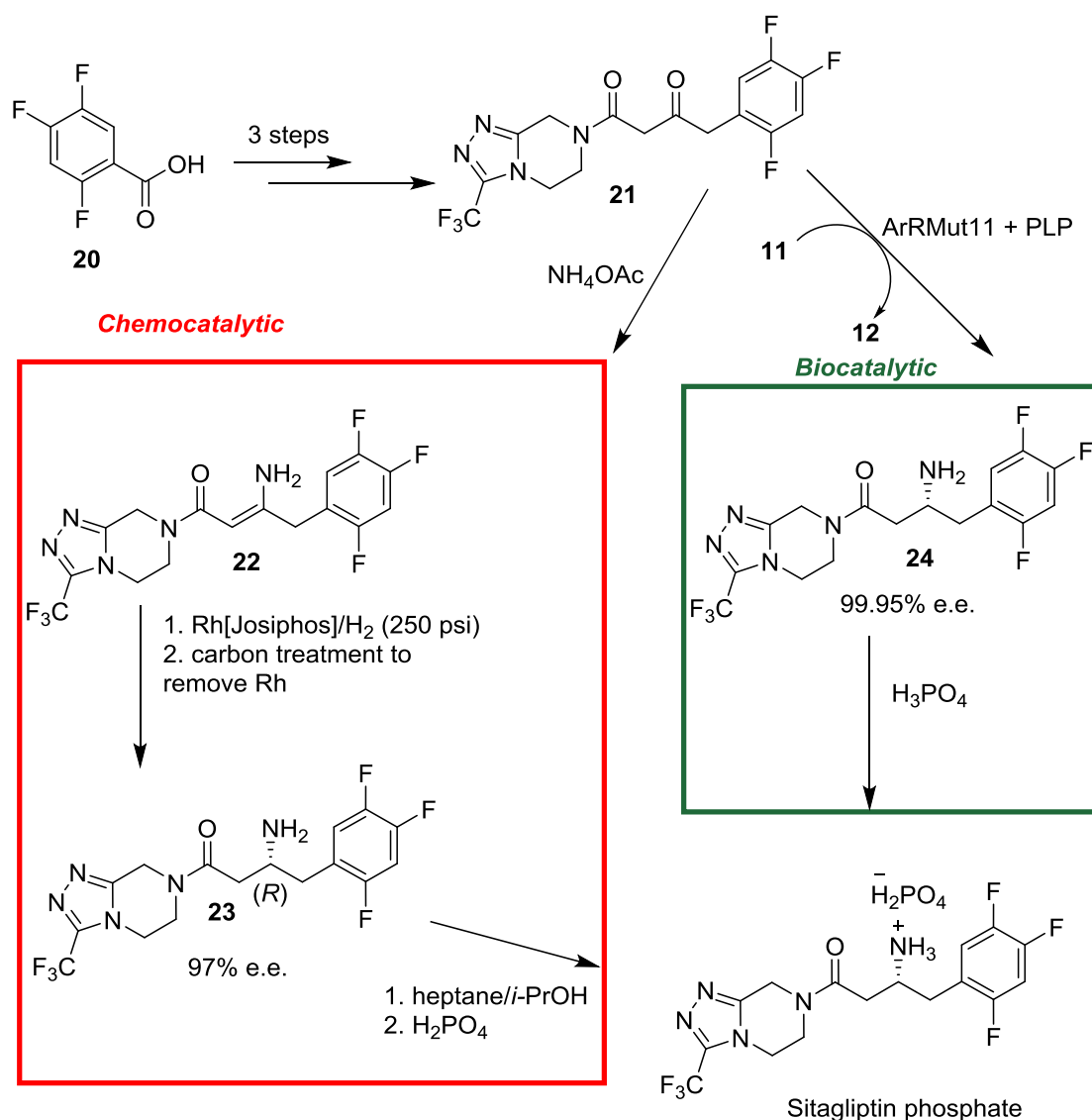


Scheme 14: Transaminase-catalysed synthesis of (S)-Rivastigmine.

Both (*R*)- and (*S*)-Rivastigmine were accessed: using *V. fluvialis* ω-TAm for (*S*)-Rivastigmine and the commercially available ATA-117 for (*R*)-Rivastigmine. The LDH/GDH coupled-enzyme system was employed in this synthesis for improved conversion yields.

1.7.2. (*R*)-Sitagliptin

(*R*)-sitagliptin is a peptidase inhibitor, an antidiabetic drug developed by Merck & Co. previously synthesised via a 3-step rhodium-catalysed enamine hydrogenation with 97% e.e [41]. The enzymatic route however is a one-step biotransformation using an engineered transaminase from *Arthrobacter* sp. (ArRMut11) with a large excess of isopropylamine (**11**) [Scheme 15] [37b].



Scheme 15: (Red) Previous standard synthesis of sitagliptin. (Green) TAM-mediated biocatalytic synthesis of sitagliptin.

Adapted from [37b]

This method was reported as giving up to a 92% conversion yield and 99.95% e.e. of the desired enantiomer (*R*)-**24**. In this work, the researchers specifically engineered a wild-type enzyme (an (*R*)-specific Codexis® TAM, ATA-117) via *in silico* design, mutagenesis and directed evolution. A mutant was developed with 11 mutations of amino acid residues in the binding pocket, to enlarge it and allow acceptance of large side-groups adjacent to the prochiral ketone. This was then subjected to several rounds of evolution to improve tolerance to the following industrial conditions: >25%

DMSO, >40 °C, 250 mM prositagliptin ketone and 1 M isopropylamine for 24 h, conditions that would inactivate any wild-type enzyme. This demonstrated the potential of engineered TAmS as industrial biocatalysts for the synthesis of highly valuable pharmaceutical targets.

1.8. Aims

At the start of this project the following set of aims were set out:

- To identify, clone and over-express novel TAmS in order to generate chiral amines.
- To investigate methods for the scale-up of *E. coli* fermentation and of transaminase reactions.
- To screen novel TAmS against a range of alternative amine donors.
- To develop the use of TAmS for the synthesis of chiral amines of industrial interest.

Results and Discussion

Chapter 2. Results and Discussion

2.1. Cloning of Novel Transaminases

2.1.1. (*S*)-Selective Transaminases

Ten novel TAmS were identified, cloned and over-expressed. The enzymes were selected based on their sequence homology to an omega-TAm discovered in-house (CV2025) [18]. The strategy employed [Figure 5] facilitated the discovery of novel omega-TAmS with high sequence homology to CV2025.

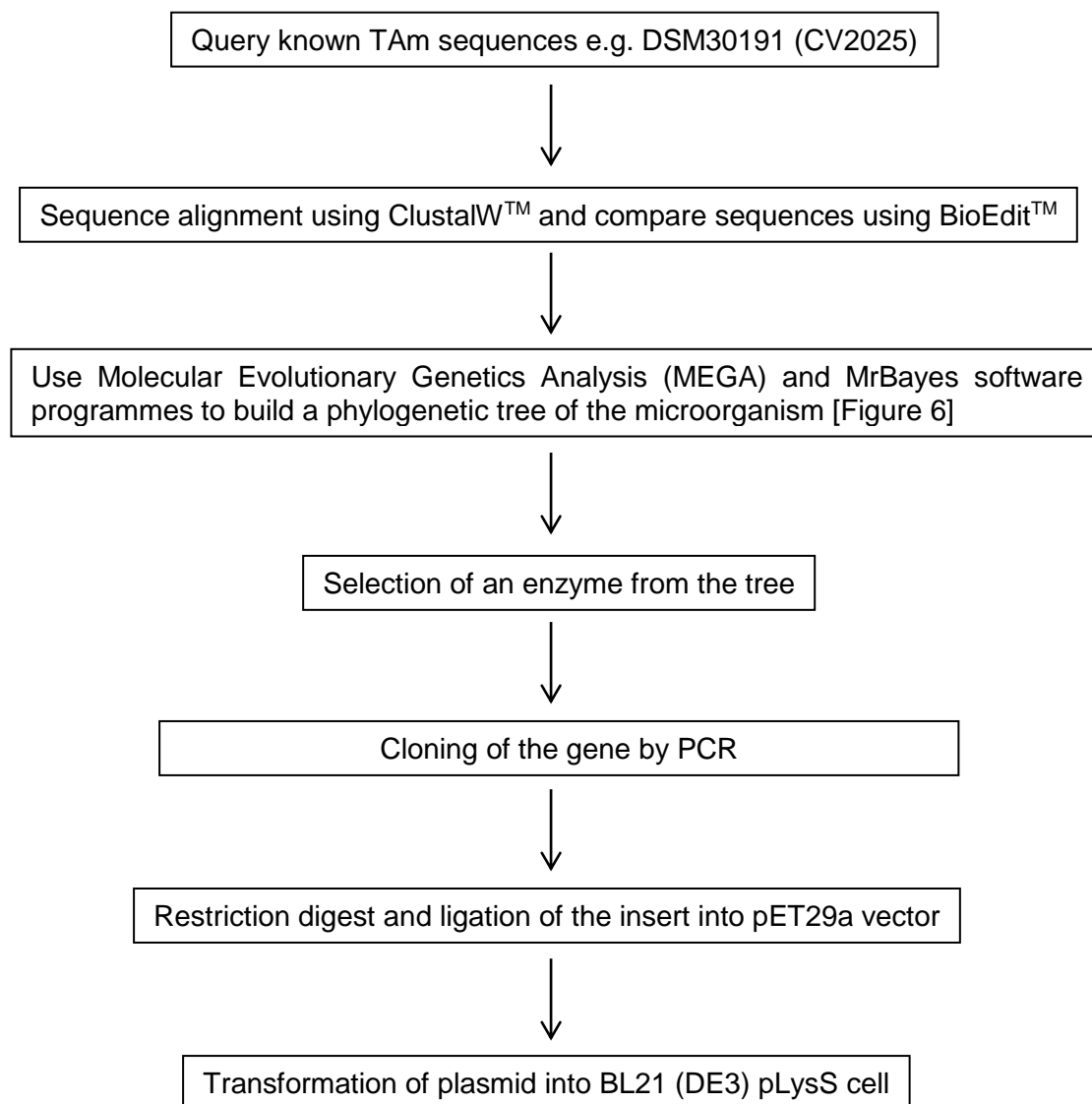


Figure 5: Procedure for discovering and cloning novel transaminases

This process has contributed to the majority of the active transaminases in an in-house library of over 100 novel transaminases. (*S*)-specific ω -TAmS form the bulk of these enzymes; however attempts were made in this project to also clone and over-express some (*R*)-specific enzymes from nature.

To begin with, a BlastPTM [42] search of the CV2025 ω -TAm amino acid sequence was conducted which resulted in the discovery of over 500 possible ω -TAm enzymes. The number of sequences was then reduced to a more manageable set. This was achieved following two sets of criteria: 1) a threshold for the level of identity was set to $\geq 30\%$ relative to CV2025, and 2) Only sequences from microorganisms already present in our in-house cell culture libraries would be selected. From this an initial list of ten ω -TAm sequences were selected. Following a previously established system of naming novel enzymes within the research group the newly cloned and transformed transaminases were assigned pQR codes [Table 7].

The list of 10 novel transaminases contained four examples of the flagellated, gram negative, rod-shaped *Pseudomonas putida*, used extensively in bioremediation. There are also, in addition, two examples of the heavily flagellated, sporulating, gram positive bacteria *Bacillus subtilis*; used in horticulture and agriculture [43]. A pair of enzymes from the photosynthetic, nitrogen-fixing bacteria *Rhodobacter sphaeroides* were also cloned [44]. *Klebsiella pneumoniae*, the non-motile, rod-shaped gram-negative bacteria (part of the ordinary human gut flora) and *Rhodospirillum rubrum*, the photosynthetic, nitrogen-fixing gram-negative bacteria formed the last two. A *Chromobacterium violaceum* TAm (CV2025) [18] and a *Vibrio fluvialis* TAm [15] were the two previously discovered enzymes on the total list of twelve transaminases involved in this study [Table 7].

Table 7: General Information on the Selected List of 12 Omega-Transaminases

Construct Name	Microorganism	KEGG Entry	Nucleotide Sequence Similarity to CV2025	Primers
pQR801	<i>C. violaceum</i>	CV 2025	100%	Previously cloned ^[18]
pQR958	<i>P. putida</i>	PP 3718	36%	<u>CATATGGCCACCCCAAGCAAAGCATTC</u> <u>CTCGAGTCGGCCTTGGTACAGGCCAAGCGC</u>
pQR1020	<i>P. putida</i>	Pput 2046	36%	<u>CATATGGCCACCCCAAGCACAGCATTC</u> <u>CTCGAGTCGGCCTTGGTACAGGCCAAG</u>
pQR959	<i>P. putida</i>	PP 2180	55%	<u>CATATGAGTGAACAGAATTCGCAGAC</u> <u>CTCGAGCCGAACAGCCTCATAGGTC</u>
pQR1018	<i>P. putida</i>	PputGB1 2189	36%	<u>CATATGGCCACCCCAAGCAAAGC</u> <u>CTCGAGTCGGCCCTGGTACAGGCC</u>
pQR960	<i>B. subtilis (1971)</i>	BSU09260	30%	<u>CATATGGAGATGATGGGGATGGAAAAC</u> <u>CTCGAGTATCGTTTGAAAGCTTTCTTTCAC</u>
pQR961	<i>B. subtilis (402)</i>	BSU09260	30%	<u>CATATGGAGATGATGGGGATGGAAAAC</u> <u>CTCGAGTATCGTTTGAAAGCTTTCTTTCAC</u>
pQR1006	<i>K. pneumoniae (00799)</i>	KPN 00799	22%	<u>CATATGACACTGGACGATCTCGC</u> <u>CTCGAGTTCGCTAAAAAATGTTTC</u>
pQR1017	<i>R. rubrum</i>	Rru A1254	58%	<u>CATATGACCGTCGTCGACCGCGGAAC</u> <u>CTCGAGTTTGGCCGTCTCGATCAGGG</u>
pQR1019	<i>R. sphaeroides 17025</i>	Rsph17025_2835	31%	<u>CATATGGCGCTGAATGACGCGGCG</u> <u>CTCGAGGACGGCGGCCGGTTCTTTCG</u>
pQR1021	<i>R. sphaeroides 17029</i>	Rsph17029_3177	32%	<u>CATATGACGCGGAATGACGCGACG</u> <u>AAGCTTGACGGCGGCCGGTTCTTTC</u>
pQR1003	<i>V. fluvialis</i>	Synthetic gene	38%	Synthetic gene ^[15]

A phylogenetic tree [Figure 6] created from the sequence alignment of CV2025 ω -TAm with the rest of the recruited sequences, including the pQR1003 synthetic gene from *V.fluvialis*, indicated that all twelve sequences belong to the same fold class of transaminase – Class III. The members of this class include acetyl ornithine-TAm, ornithine-TAm, omega-TAm, beta aminocarboxylic acid-TAm, gamma aminobutyrate-TAm, and diaminopelargonate-TAm [Table 2] [6a].

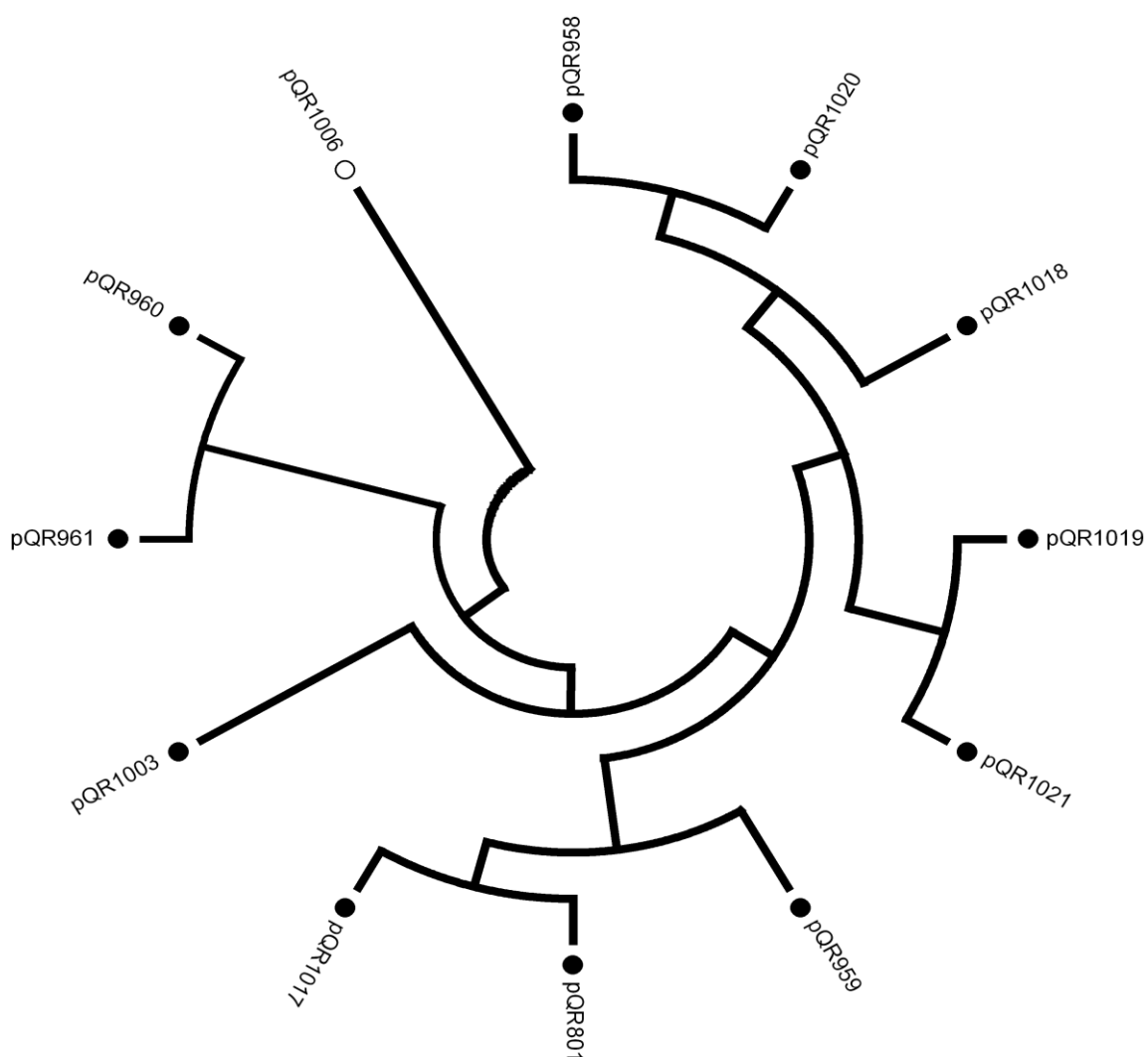


Figure 6: Phylogenetic diagram of all 12 omega-TAm sequences

The phylogenetic tree was inferred using the Neighbor-Joining method (Saitou and Nei 1987), and illustrates the relatedness of the recruited sequences to that from pQR801. Closed circles (●) represent sequences with a level of identity $\geq 30\%$, and open circles (○) represent a level of identity $< 30\%$. Phylogenetic analyses were conducted in MEGA4 [45].

Synthetic short oligonucleotide primers were designed for each of the ten novel transaminases based on the genome sequence of the microorganisms they came from [Table 7]. The extraction of genomic DNA from the five different bacterial strains involved in this work was conducted by a standard phenol-chloroform protocol. This was followed by amplification of the transaminase genes using the synthetic primers in a polymerase chain reaction (PCR). The PCR products were subsequently ligated into TOPO[®] cloning vectors and transformed into TOP10 competent *E. coli* cells. The cells were plated and positive clones picked for DNA mini-prep analyses. The isolated plasmid DNA were digested using the restriction enzymes *Xba I* and *Hind III* and analysed on 1.5% agarose gels. The appropriate DNA inserts were identified by size, excised, and isolated for ligation into expression vectors without sequencing.

The cloned transaminase genes were subsequently ligated into pET29a⁺ linearised vectors (using *Nde I* and *Hind III* for *R.rubrum* and *Nde I* and *Xho I* for the other genes) to produce the desired plasmid constructs. These new plasmids were then transformed into BL21 (DE3) pLysS *E. coli* cells for future overexpression. Sequencing of the gene inserts and diagnostic SDS-PAGE was used to confirm the right recombinant cells had been produced [Figure 7]. To facilitate nickel affinity protein purification at the latter stages, the choice of expression vector was pET29a⁺ which includes a C-terminal hexa histidine-tag (His-Tag[®]). Overexpression of the various recombinant cells was conducted using 2xTY media with kanamycin (0.05 mg/mL) and chloramphenicol (0.03 mg/mL). This enrichment broth comprises tryptone, yeast extract, and sodium chloride in the ratio 5:3:2. A final volume of 1 mM isopropyl β -D-1-thiogalactopyranoside (IPTG) was used to induce protein expression in 500 mL of media. An average of 3 g of wet pellet was generally expected from each of the cell cultures. The expected soluble protein content [Figure 7-B] ranged from 1 to 10 mg/mL for each overexpression.

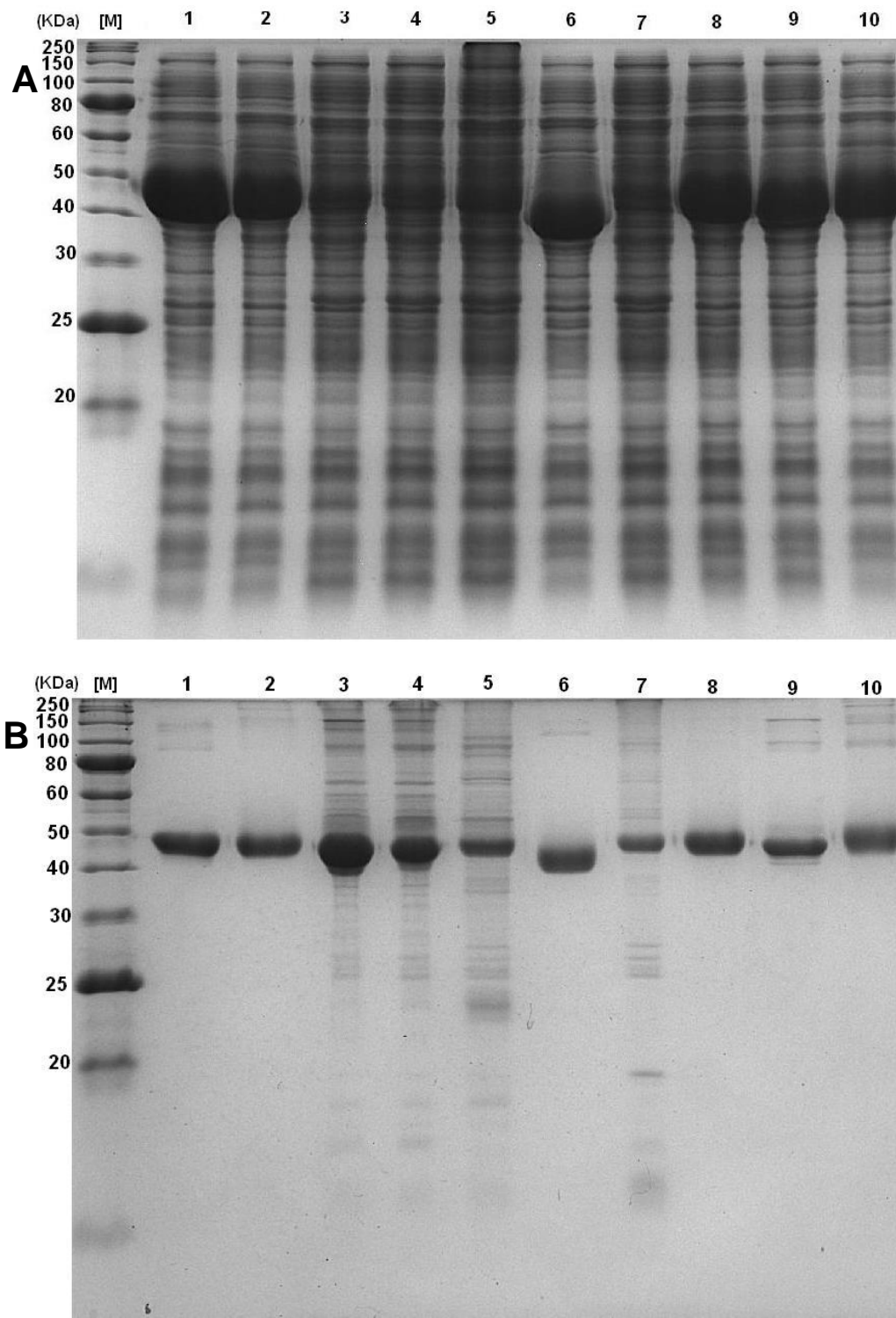


Figure 7: 12% SDS-PAGE gels of all ten novel transaminases

Showing the following: [M] Marker (KDa); 1) pQR801; 2) pQR958; 3) pQR960; 4) pQR961; 5) pQR1003; 6) pQR1006; 7) pQR1017; 8) pQR1018; 9) pQR959; 10) pQR1019. (A): Whole cell crude lysate. (B): Partially purified enzymes (using PD-10 desalting columns). The molecular weights were as follows: 51, 52, 50, 50, 50, 47, 50, 52, 50, 50 kDa respectively.

All the cells overexpressed sufficiently well with pQR960, pQR961, pQR1003 and pQR1017 (lanes 3, 4, 5 and 7 in Figure 7-A) showing levels of recombinant

transaminases >20% relative to the total protein content. The other cells showed levels of >60% of total protein obtained.

2.1.2. (*R*)-Selective Transaminase

In addition to the list of ten (*S*)-selective transaminases, the cloning and over-expression of some (*R*)-selective TAmS was also explored. At the beginning of this project the majority of TAmS characterised in the literature and in the in-house library were (*S*)-selective. However, in the search for enzymes for the stereoselective conversion of prochiral ketones to (*R*)-amines, more (*R*)-selective transaminases were required. There were two publications of known (*R*)-selective TAmS [46]. At the time, only one of the characterised (*R*)-TAmS was from an organism with known whole genome sequence (*Arthrobacter aurescence*) [27]. It was reasoned that enzymes from other microorganisms with high amino acid sequence homology to this (*R*)-selective TAm gene may also be (*R*)-selective. As a result of this, a search of the genome databases KEGG and UniProt was conducted which yielded three species of *Arthrobacter* sp, *Arthrobacter* sp. FB24, *Arthrobacter aurescence* and *Arthrobacter chlorophenolicus*. Seventy-eight putative TAm genes were recruited and aligned using the freeware ClustalW™ followed by comparison using BioEdit™. As with the search for the (*S*)-selective TAmS, a phylogenetic tree of all the putative (*R*)-selective TAmS was created using MEGA and MrBayes software programmes [Figure 8].

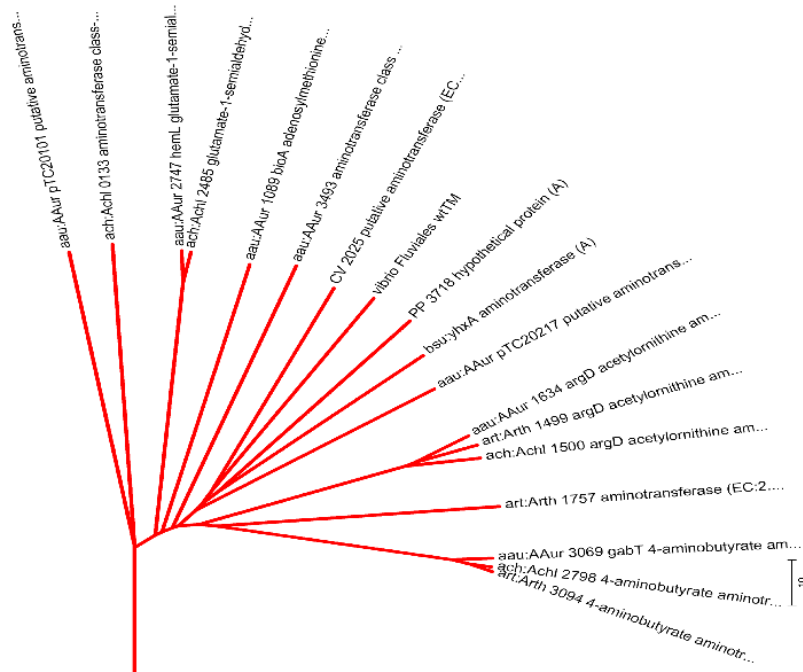


Figure 8: An unrooted phylogenetic tree of *A. aureus*; the ω -Tam branch

From this phylogenetic tree a branched-chain amino acid transaminase was identified from *Bacillus licheniformis*. This microorganism was already available in the in-house culture collection and so primers were designed for BLi00607 to be cloned following the same procedure as the previous ten. The search was expanded to include three other putative (*R*)-selective transaminases from *P. aeruginosa* (PLES_54021, PA14_66260, and PA_5013) [Figure 9]

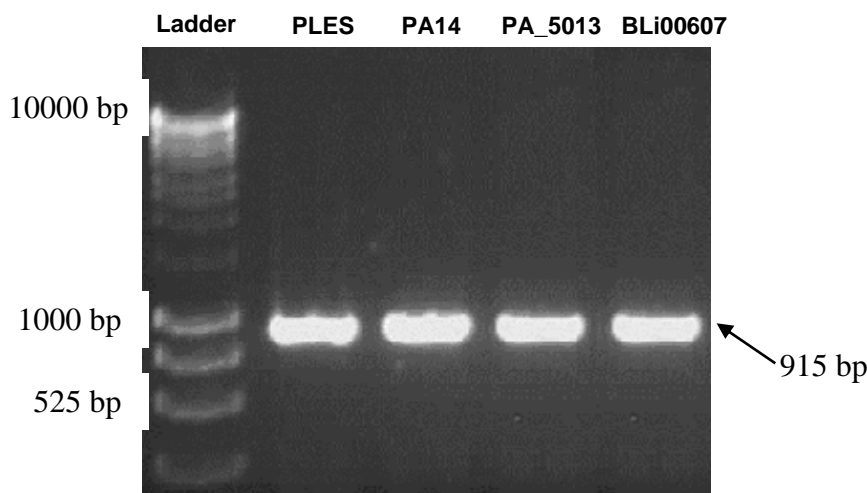


Figure 9: PCR products of PLES_54021, PA14_66260, PA_5013, and BLi00607

The fragments were subsequently ligated into pET29a⁺ vectors followed by transformation into BL21 (DE3) pLysS competent *E. coli* cells.

2.2. Initial Use of CV2025 ω -TAm

Throughout the period of this investigation the one transaminase which was employed as a benchmark against which all other transaminases were screened was CV2025 ω -TAm. It is an (S)-specific omega-transaminase and was cloned and characterised by Ward and Hailes ^[18]. It has a 36% homology to one of the earliest reported ω -transaminases, *V. fluvialis*_JS17 ω -TAm from Kim *et. al.* ^[15]. CV2025. The first assessment of CV2025 as part of this project was conducted on a small scale. A 20% glycerol stock of the *E. coli* containing CV2025 was cultured (100 mL 2xTY media) and the gene over-expressed for screening [Scheme 6]. The cells were harvested after over-expression and a 25 mg/mL crude lysate prepared in 100 mM HEPES buffer [Figure 10-B]. This was used for the initial screening of substrates to synthesise chiral amines detectable by chiral HPLC. The reason for choosing crude lysate over purified enzymes was due to the ease of scale-up. The conditions required to scale up a reaction with pure enzyme are significantly more problematic than one with crude lysate.

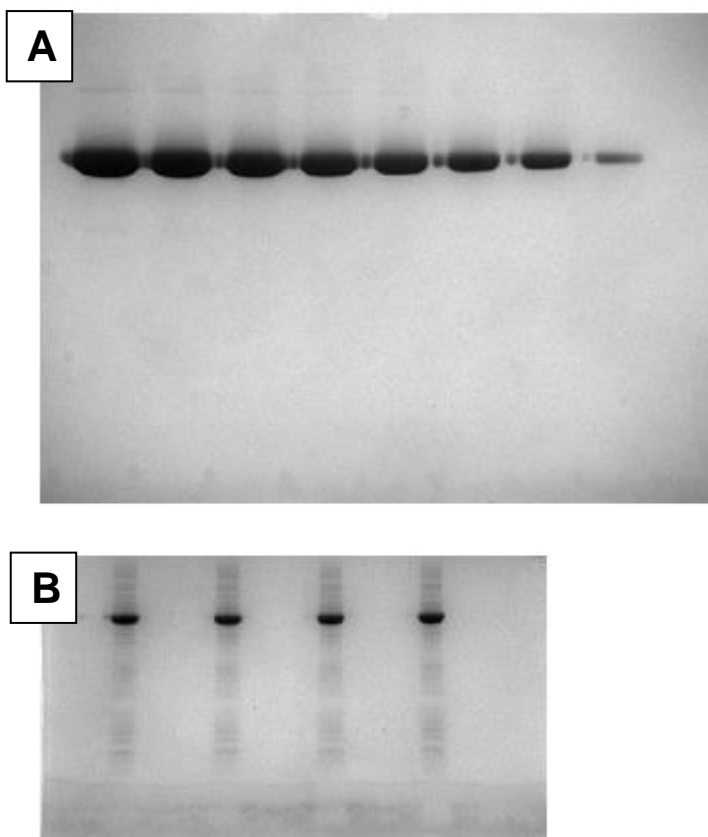


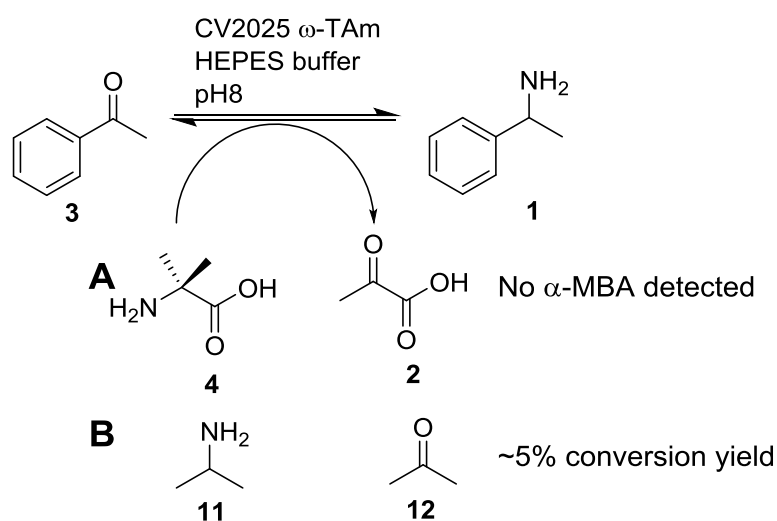
Figure 10: (A) – Calibration curve SDS-PAGE gel of purified CV2025 enzymes

(Lanes 1-8 = 70 mg/mL to 5 mg/mL). (B) - 25 mg/mL CV2025 crude lysate (all lanes). Based on the calibration curve it was calculated that the crude lysate contained 40 mg/mL pure CV2025 (based on band density).

2.3. Method Development for Product Isolation

Many reports have been published in recent years on the discovery of novel TAM enzymes [18, 30, 33a]. The enzymes are screened in assays to assess their substrate specificity profiles or their ability to synthesise interesting chiral amines. Detection and isolation of the amine product is often difficult to achieve and as a result TAM reactions are often monitored via detection of the ketone co-product. In this work, CV2025 was initially tested in an α -methylbenzylamine (α -MBA) synthesis assay, using reverse phase HPLC to detect the production of α -MBA [Scheme 16-A]. The rate of production of acetophenone using CV2025 and α -MBA (**1**) suggested that the reaction equilibrium was strongly in favour of acetophenone (**3**) formation and the

reverse reaction is less favoured. However, to probe this phenomenon and to establish α -MBA formation in assays with the new TAMs, the reaction in scheme 16-B was employed. In the reaction in scheme 16-A, no amine product was detected when an excess of the amine donor (**4**) (100 mM) and amine acceptor (**3**) (20 mM) was used, only the starting material acetophenone was detected by analytical HPLC on a standard C18 column.



Scheme 16: (A) - Biotransformation reaction using L-alanine and subsequent chiral HPLC analysis. (B) - Biotransformation using isopropylamine

It was rationalised that this was most likely due to the reaction equilibrium favouring acetophenone production. It is also possible that this was due to poor α -MBA product isolation. A number of extraction solvents and conditions were therefore briefly investigated. In this investigation the biotransformation reactions were carried out in a final volume of 10 mL (HEPES buffer, pH 7.5) using 30% v/v enzyme crude lysate. The reactions were then quenched after 24 h using 0.2% trifluoroacetic acid (TFA). The product isolation process first tested was a simple wash with ethyl acetate after basifying the filtered reaction mixture. This was followed by drying of the combined organic phase and evaporation of the solvent; only starting materials were observed.

Reaction monitoring by TLC was not possible as the amine substrate and product were inseparable on silica and alumina stationary phases. Following literature precedent for the use of methyl *tert*-butyl ether (MTBE) [47] and Amberlite® resin [48] were also unsuccessful as only starting material was isolated in both cases. The procedure for amine isolation using Amberlite® resin involves saturation of the quenched biotransformation mixture with the resin for 1 h. This is followed by filtration through a cation exchange column (Isolute® SCX-2 column) and elution with ammonia (4 N) in methanol to yield the reaction product. The lack of success under all these conditions suggested perhaps the enzyme was not accepting the substrate pair.

A number of other amine donors were therefore screened: γ -aminobutyric acid (GABA), *N*-methyl alanine, β -alanine and isopropylamine (IPA) against acetophenone. No α -MBA was detected in any of these reactions, however, using the three isolation methods described above. Only when isopropylamine (**11**) was used as an amine donor with the Amberlite® resin isolation protocol was α -MBA detected by HPLC (< 5% conversion yield) [Scheme 16 and Figure 11].

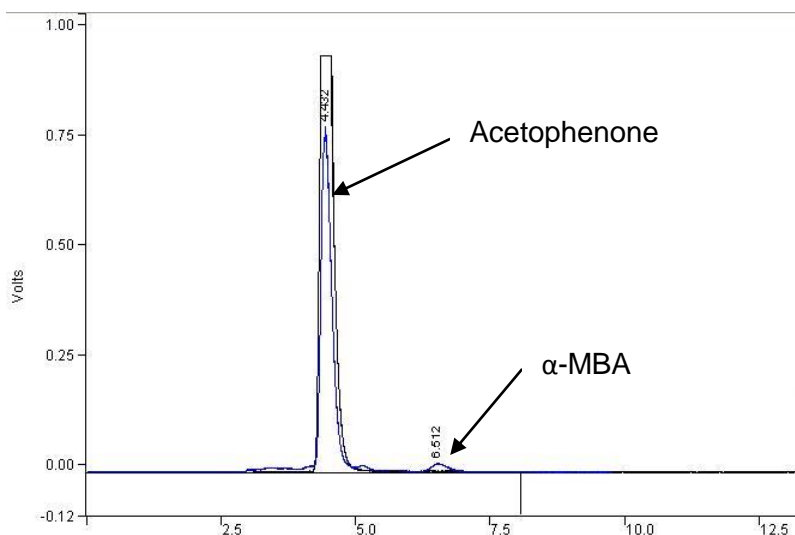


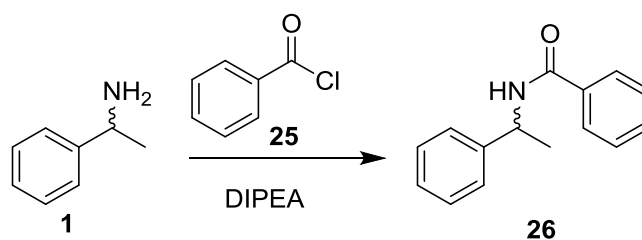
Figure 11: Non-chiral HPLC trace showing isolated product of CV2025 biotransformation with IPA (blue) and an acetophenone standard (black).

The HPLC data shows overall conversion of α -MBA (retention time: 6.5 min) to be <5%.

2.4. Method Development for the Determination of the *e.e.* of α -MBA

Direct chiral resolution of α -MBA (**1**) from the biotransformation reaction in scheme 16-B initially proved problematic as the chiral HPLC column available at the time did not show good baseline separation between the enantiomers. In spite of there being literature precedence for the use of ChiralPak[®] OD columns [33b] for the direct normal phase chiral analysis of α -MBA this was unsuccessful using our OD column. A switch to the higher resolution equivalent (the OD-H) under the same HPLC conditions also proved unsuccessful. This may have been due to the age and general wear and tear of the columns causing them to lose sensitivity to small analytes like α -MBA. The reverse phase equivalent of the ChiralPak[®] OD column (ChiralPak[®] IB) was also tested but again the α -MBA isomers did not give a clear baseline separation under all mobile phase conditions used.

Derivatisation of commercially available (\pm)- α -MBA as its benzoyl amide [Scheme 17] was subsequently run in order to establish a protocol for the chiral HPLC detection of benzoyl-derivatised α -MBA from a TAM reaction. This proved successful as a clear baseline was detected between the two enantiomers of (\pm)-**26** using a ChiralPak[®] AD column, a mobile phase mixture of isopropanol/hexane (20:80), and UV detection at 254 nm [Figure 12].



Scheme 17: Benzoyl derivatisation of (S)-MBA

Under these conditions and with a flow rate of 1 mL/min, (*S*)-**26** had a retention time of 5.8 minutes and (*R*)-**26** of 7.9 minutes. This was confirmed by co-injection with

benzoylated, purchased, enantiopure (*S*)- and (*R*)- α -MBA. Having established a method for the detection of (*R*)- and (*S*)- α -MBA using chiral HPLC, the biotransformation product, α -MBA (**1**), was isolated for derivatisation with benzoyl chloride and Hünig's base (DIPEA). The benzoyl-derivatised biotransformation product was then analysed under the same chiral HPLC conditions as the benzoylated commercially available standards. The results showed that a 22 h reaction with isopropylamine (**11**) as the amine donor and acetophenone as the amine acceptor using CV2025 ω -TAm produced (*S*)- α -MBA in 5% conversion yield and >99% enantiomeric excess.

The stereochemistry of the major isomer in this biotransformation was in agreement with previous selectivities reported for CV2025 ω -TAm which is an (*S*)-selective TAm as it preferred (*S*)- α -MBA as amine donor compared to the (*R*)-enantiomer ^[18].

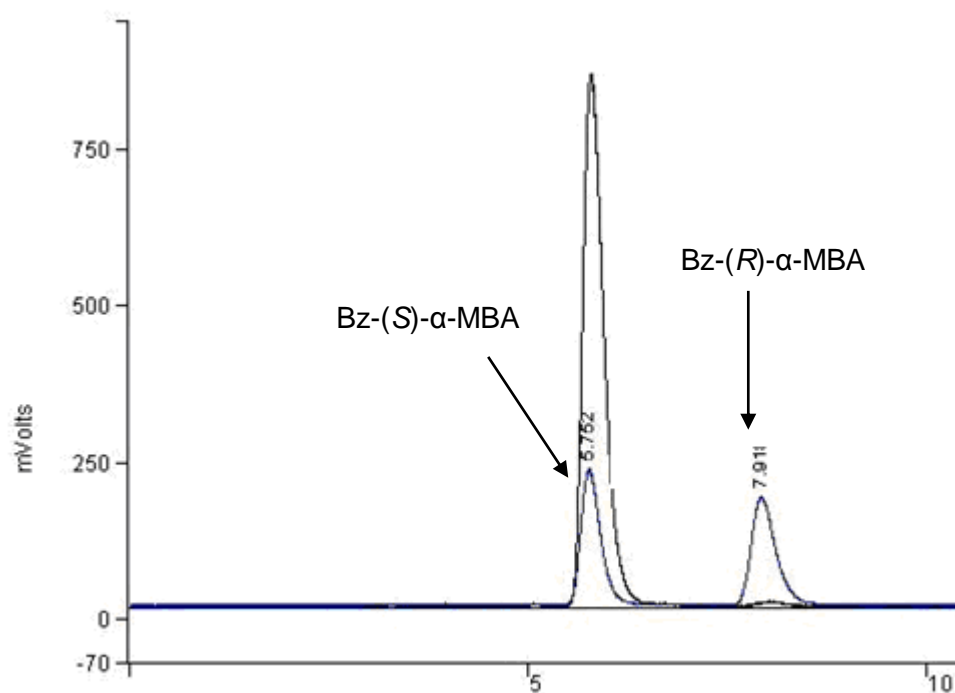


Figure 12: Chiral HPLC trace of commercially available benzoylated (\pm)- α -MBA (Blue) and commercially available (*S*)- α -MBA (Black)

2.5. Direct chiral HPLC analysis of α -MBA

In spite of the successful resolution of benzoyl-derivatised (\pm)- α -MBA on the ChiraPak AD column [Figure 12], further method development was carried out to find a suitable column for the direct chiral analysis of the underivatised compound to enhance reaction screening throughput. It would also alleviate the inevitable loss of material during the derivatisation step which can lead to errors in the final HPLC result. More recently purchased ChiralPak[®] AD and OD columns were re-tested using the same hexane/isopropanol mobile phase combinations without any positive results. Two other Astec Chirobiotic[®] columns were also screened as the manufacturers reported conditions for the chiral separation of α -MBA. These columns were also unable to separate the two enantiomers of α -MBA with a clear baseline.

Switching to the higher resolution version of the AD column (ChiralPak AD-H, 250 mm x 4.6 mm; 5 μ m), baseline separation was subsequently attained using a mobile phase mixture of heptane/ethanol/formic acid (95:5:0.02) with UV detection at 210 nm and flow rate of 1 mL/min. An improved chiral separation of (*R*)-MBA (26 min), (*S*)-MBA (31 min) and acetophenone (7 min) was achieved with clear baseline separation [Figure 13]. Although a relatively long HPLC run time (40 min), it did enable direct HPLC analysis of the commercially available (\pm)- α -MBA.

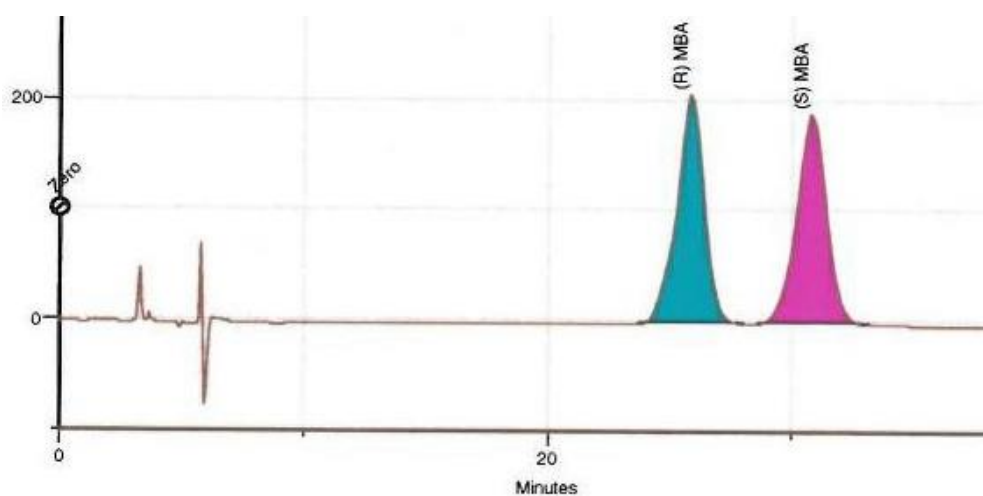


Figure 13: Separation of (\pm)- α -MBA on a ChiralPak AD-H column; (*R*)-MBA (Blue) (*S*)-MBA (Red)

This method however had a major limitation and therefore other protocols had to be investigated. Any attempts to add water to the mobile phase, as little as 0.01 % v/v, caused distortion on the lower upslope of both enantiomer peaks (not shown). This prevented direct injection of the acid-quenched supernatant from the reaction mixture. Nevertheless, dilution of the reaction mixture with organic solvent (acetonitrile) and drying eliminated this distortion, enabling use in some instances.

A CrownPak[®] CR+ (150 mm x 4.6 mm; 5 μ m) column was also tested as an alternative to the ChiralPak[®] AD-H column under a series of conditions. The optimum results were observed using a mobile phase of perchloric acid (pH 1.5)/acetonitrile (85:15) at 210 nm and a flow rate of 0.7 mL/min. Under these conditions (*S*)- α -MBA

eluted at 9 minutes, (*R*)-MBA at 12 minutes with clear baseline separation and acetophenone at 36 minutes [Figure 14].

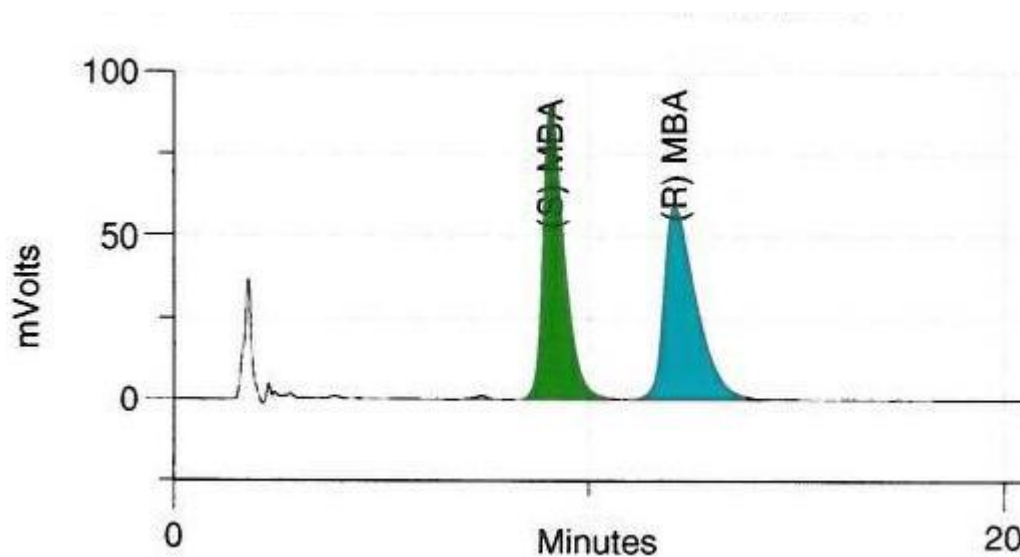
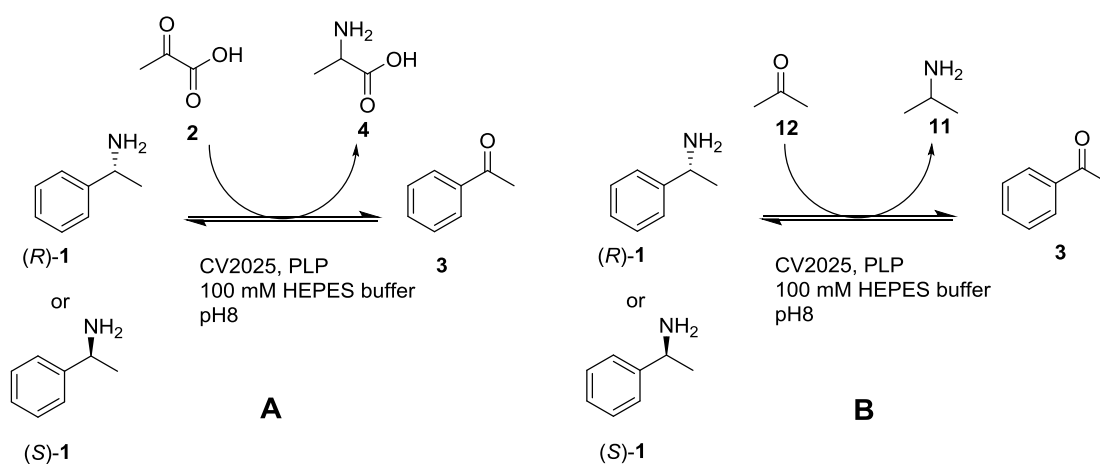


Figure 14: Separation of (\pm)- α -MBA on the CrownPak CR+ column; (*S*)-MBA (Green) (*R*)-MBA (Blue)

This method was preferred as it gave clear chiral separation of the enantiomers in under 15 minutes compared to 31 minutes on the AD-H column. For a full analysis of the reaction mixture however, a 40 minute run was required as the acetophenone peak appears only after 36 minutes.

2.6. Assessment and Optimisation of Conversion Yields For the Formation of (*S*)- α -MBA

In order to better understand the relationship between an amine donor and the stereochemistry of the amine product in a TAM reaction, the procedure in scheme 18 was investigated for CV2025, using enantiopure (*S*)- α -MBA as amine donor. These were performed in a time-course study using pyruvate (**2**) and acetone (**12**) as amine acceptors.



Scheme 18: Reactions to assess the enantiopreference of CV2025 ω-TAm using (A) pyruvate as amine acceptor and (B) acetone as amine acceptor

In accordance with precedent for (*S*)-selectivity, it was expected that the rate of reaction when (*S*)-α-MBA was used in the presence of either amine acceptors, would be higher than for (*R*)-α-MBA. Results from the pyruvate reaction [Scheme 18-A] confirmed the enantiopreference of CV2025 as (*S*)-selective. The results also showed that the reaction reached its optimum conversion after approximately 5 minutes [Figure 15]. The average consumption of (*S*)-α-MBA was 92% while (*R*)-MBA was 6% over a period of 24 h.

Four of the initial panel of 10 novel transaminases (KpN_00799, BSU09260_402, BSU09260_1971 and PP_3718) and VF_JS17, were then selected to be screened against (*S*)- and (*R*)-α-MBA. In keeping with the results from CV2025, these five omega-transaminases also exhibited preference for the consumption of (*S*)-α-MBA [Figure 16-A]. Under the same conditions as the CV2025 reactions [Scheme 18] the novel enzyme PP_3718 had a relatively faster rate of reaction for the consumption of (*S*)-α-MBA (98% conversion) [Figure 16A]. The other enzymes however, with the exception of VF_JS17 (cloned from a synthetic gene), exhibited relatively poor rates and poor overall conversion yields.

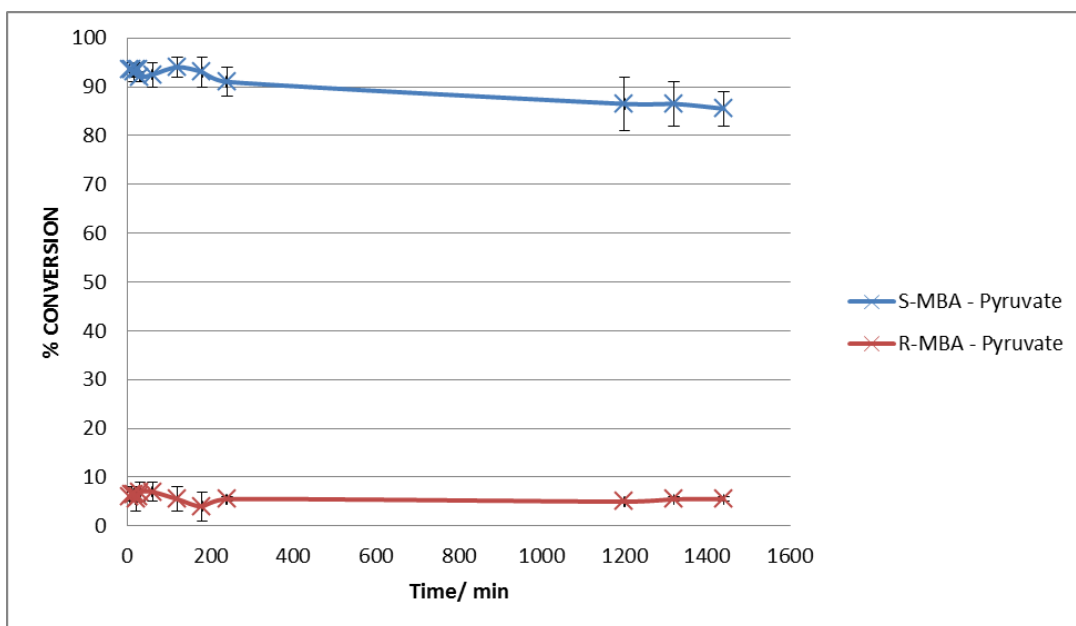


Figure 15: Acetophenone production using CV2025 with (*R*)- and (*S*)- α -MBA, and pyruvate.

This was probably due to poor substrate compatibility and could be optimised, if required, by an adjustment of substrate and enzyme concentrations, however this was not pursued further. When the five enzymes were screened against (*R*)- α -MBA, once again a similar trend to that with CV2025 was observed. All had comparatively lower rates of reaction and lower overall conversion yields. Interestingly however, with the exception of the two *Bacillus subtilis* enzymes, the conversions were much higher than what is observed for CV2025. This implied that VF_JS17, KpN_00799 and PP_3718 accept (*R*)-MBA more readily than the other 3 enzymes and therefore might have poorer enantio-preference. This was therefore expected to translate to lower e.e. values when used in the synthesis of chiral amines.

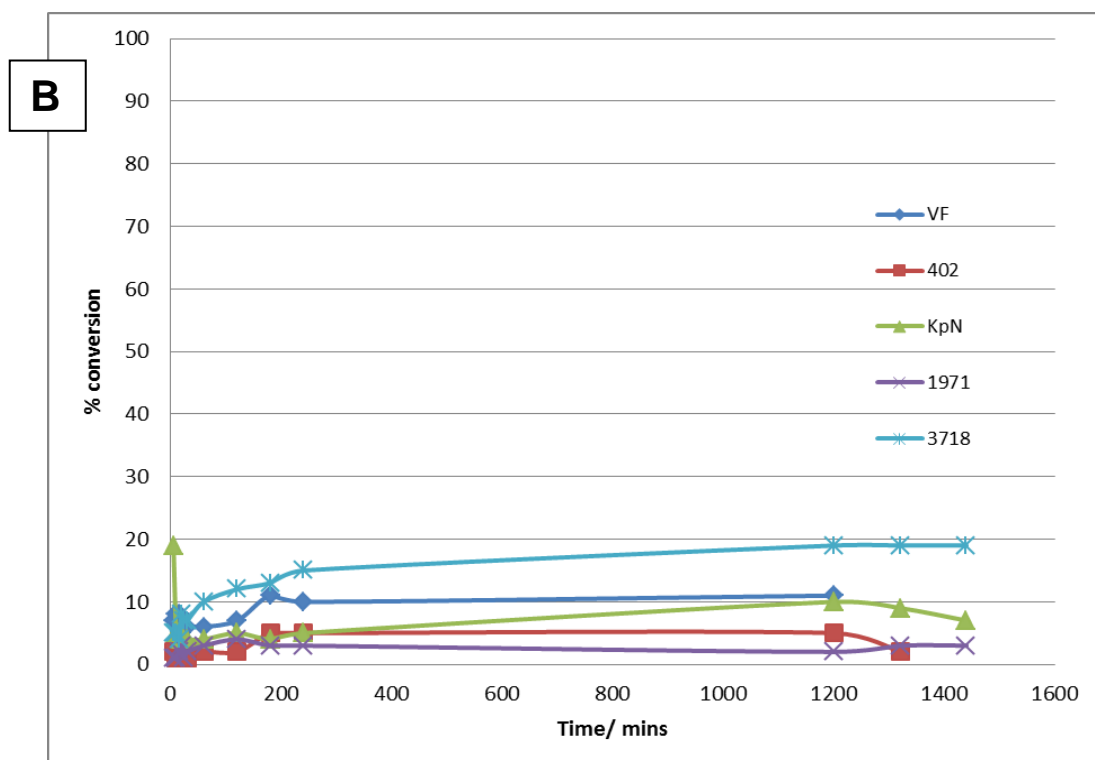
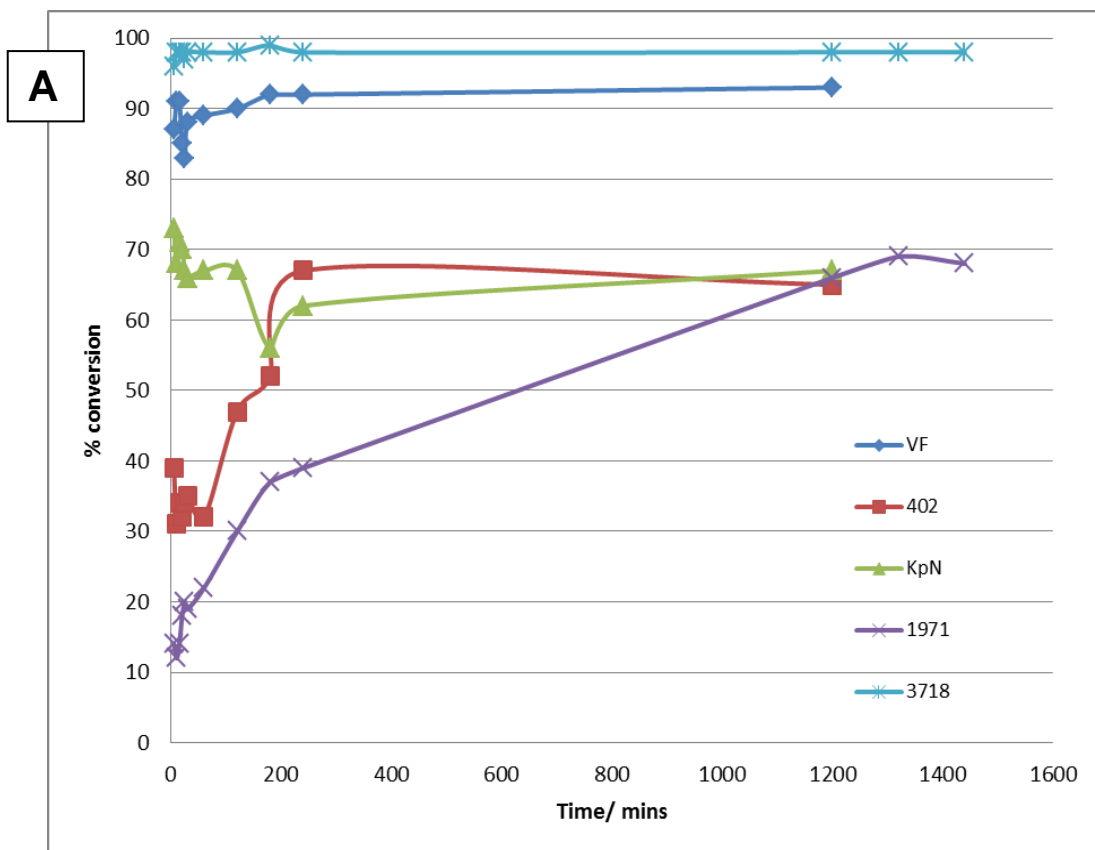


Figure 16: Enantio-preference time-course experiment of 5 ω -TAMs monitoring acetophenone production in (A): (S)- α -MBA/pyruvate reaction and (B): (R)- α -MBA/pyruvate reaction.

In repeating the reaction with acetone as an amine acceptor however [Scheme 18-B], initial results indicated very low conversions [Figure 17]. Under the same conditions as the pyruvate reactions, both (*R*)- and (*S*)- α -MBA produced background levels of acetophenone (<4%) when paired with acetone as amine acceptor. This was significantly lower than anticipated, especially compared to the results from the pyruvate reaction. The results implied that acetone was a poor amine acceptor when paired with either enantiomers of α -MBA. The reaction was then further investigated in an attempt to improve the conversion yield. A number of methods were attempted including the use of a partially sealed vessel (in case of loss of isopropylamine by evaporation), doubling of the enzyme loading (60% v/v), and using freeze-dried cells. Conversion yields in both reactions were not improved by any of these methods however.

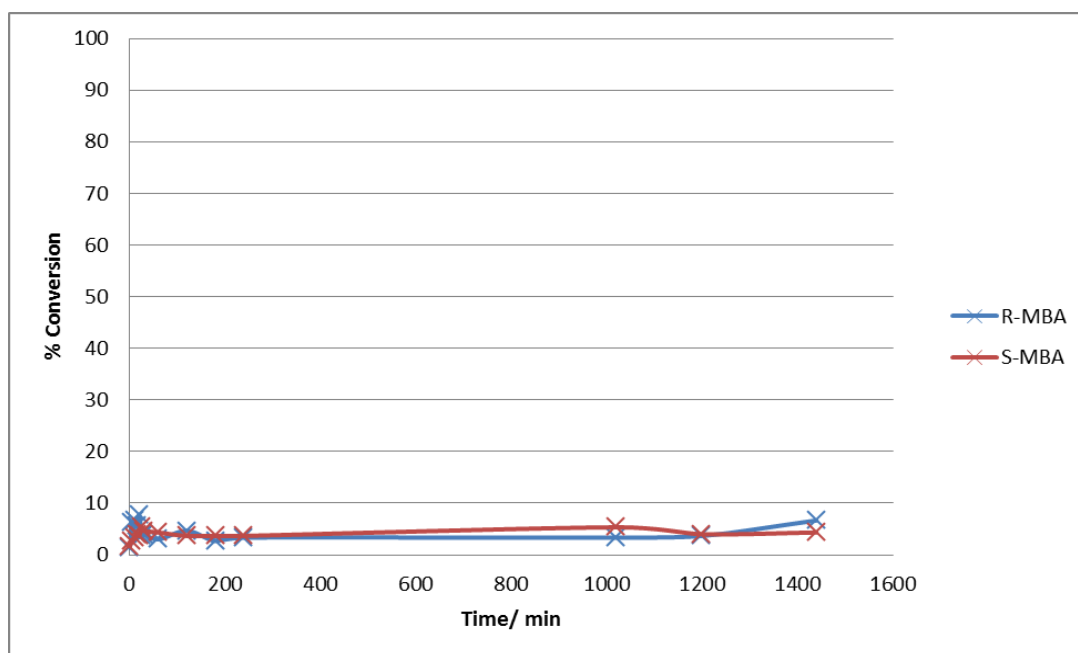


Figure 17: CV2025 biotransformation using (*S*)- and (*R*)-MBA with acetone

Imbalance of pH in the reaction medium was eventually determined to be the problem during a pH profiling experiment. Even though the reactions were buffered at

pH 8 using 100 mM HEPES buffer (based on previous studies to find pH optima), in the case of acetone, the final reaction pH was often 12. The enzymes are easily denatured at such a high pH value which explains the very low conversion yields. The reason behind this pH increase is that the pK_b of the starting amine (**1**) is 4.25 whereas that of the product isopropylamine (**11**) is 3.37. This difference amounts to a significant increase in pH during the reaction as one molecule of amine **1** is consumed and replaced by one molecule of a more basic amine (**11**). A solution to this problem could be to increase the concentration of HEPES buffer in the reaction. Alternatively, the pH of the reactions could be corrected before the enzyme is added to the reaction mixture and maintained throughout the reaction by automation.

A pH profile of CV2025 ω -TAm was therefore investigated in the acetone acceptor reaction in this manner. It was performed using a Metrohm[®] STAT Titrino, a device which monitors the pH of a reaction and adds aliquots of acid or base to correct the pH whenever it rises above a set level. The results [Table 8] showed that when the reaction was started and maintained at pH 10, there was less than 1% acetophenone detected by HPLC. Maintaining the reaction pH at 8 and 7 gave a 66% and a 78% conversion respectively. The highest recorded percentage conversion was found to be at pH 7.5 with 88% conversion.

Table 8: Screening of Biotransformation Reaction pH

pH	Conversion (%)
6	43
7	78
7.5	88
8	66
10	<1

The relationship between reaction pH and conversion yield was not surprising and it confirmed the optimum pH for the enzyme to be about pH 7.5. This investigation did highlight however, the need for automatic pH monitoring and correction when using an amine acceptor that is likely to raise reaction medium pH above safe levels.

2.7. Enantioference Reactions Using CV2025 with Acetone and α -MBA

Having established conditions for the successful biotransformation of α -MBA to acetophenone using CV2025 ω -TAm and acetone, the enantioference of the enzyme in the acetone reaction was further investigated. In separate time-course experiments, using the two enantiomers of α -MBA [Scheme 18-B], a different trend was observed compared to the pyruvate reaction. CV2025 still preferred the (*S*)-enantiomer as an amine donor over the (*R*)-enantiomer as expected. However, a comparison of the conversion yields of the two acetone reactions indicated that (*S*)-MBA consumption was four times faster than that of (*R*)-MBA [Figure 18] whereas a comparison of the two pyruvate reactions [Figures 15] showed a 16-fold preference for (*S*)-MBA over (*R*)-MBA. Overall, the pyruvate/(*S*)-MBA reaction was twice as fast as the equivalent optimised acetone reaction. Conversely however, the acetone/(*R*)-MBA reaction was twice as fast as the corresponding pyruvate reaction. The enzyme therefore appeared to be slower and less selective when a small substrate like acetone was used.

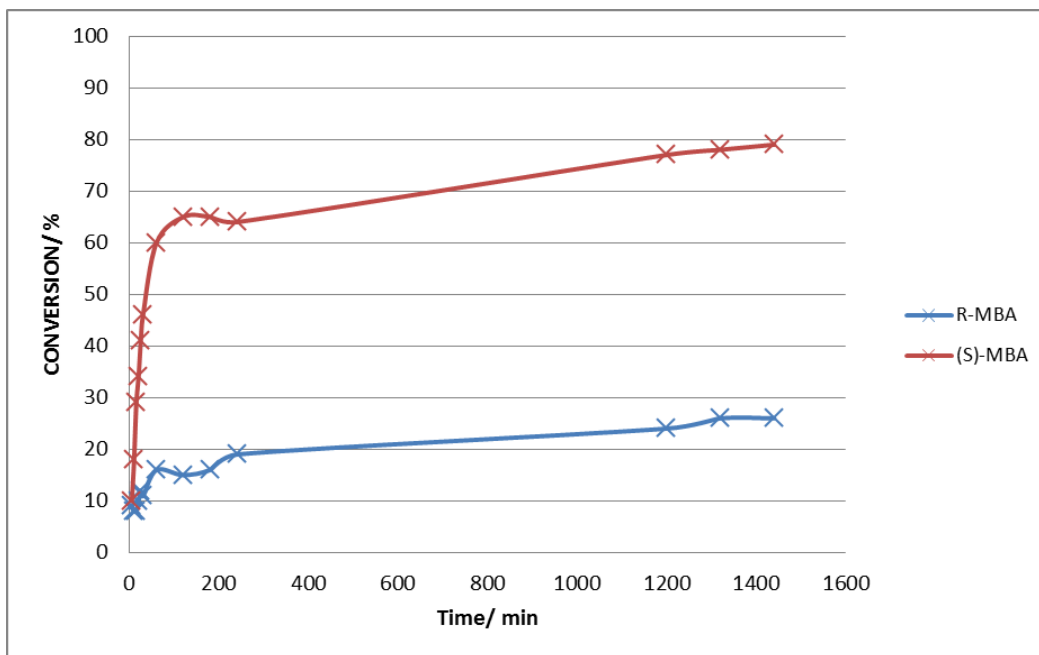


Figure 18: Time-course reaction - Acetophenone production using (R)- and (S)-MBA with acetone at pH 7.5 and CV2025 ω -TAm

Establishing the conditions for an optimised transamination of enantiomerically pure α -MBA (**1**) using acetone, the reverse reaction was investigated under the same conditions to improve conversion yields for the synthesis of (S)- α -MBA. Prior to this point, production of (S)- α -MBA (**1**) had been very poor (< 5%), however a final conversion of 13%, >99% e.e of (S)- α -MBA was achieved with pH correction (pH 7.5). This represented the first time such significant amounts of α -MBA had been isolated in the biotransformation reaction in this study. It did however prove the need for an equilibrium displacement method in TAm reactions in order to improve on conversion yields for the synthesis of chiral amines from prochiral ketones.

2.8. LDH/GDH Coupled enzyme reaction

The LDH/GDH coupled enzyme reaction was subsequently investigated in order to improve reaction turnover in the chiral amine synthesis direction [Scheme 11]. This assay, in the literature, was conducted using the Codexis® ATA-113 (S)-selective and

ATA-117 (*R*)-selective transaminases. In both cases they produced amines in >99% *e.e.*

An experiment to investigate this reaction using CV2025 with D-alanine and again with L-alanine was therefore performed. The two Codexis® enzymes ATA-113 and ATA-117 were used as controls.

Table 9: Results from the LDH/GDH coupled-enzyme experiment

Reaction	% Conversion	% e.e.
CV2025 – D-ala	93	>99 % (<i>S</i>)-MBA
CV2025 – L-ala	96	>99% (<i>S</i>)-MBA
ATA113 – D-ala	29	>99% (<i>S</i>)-MBA
ATA113 – L-ala	44	>99% (<i>S</i>)-MBA
ATA117 – D-ala	94	>99% (<i>R</i>)-MBA
ATA117 – L-ala	90	>99% (<i>R</i>)-MBA

Conditions: Acetophenone (10 mM), alanine (100 mM), pH 8, CV2025 (30% w/v), HEPES buffer (100 mM), 24 h.

The results [Table 9] suggested, first of all, that when pyruvate was removed from the system (*S*)- α -MBA was produced with >99% *e.e.* for both ATA-113 and CV2025 ω -TAm. The opposite was found to be true of the (*R*)-selective ATA-117 transaminase which produced >99% *e.e.* (*R*)- α -MBA as expected. Interestingly, the conversion yields of the reactions suggest that all three enzymes converted both enantiomers of alanine without any preferences. When the assay was extended to the other novel enzymes, the same trend was observed. All produced (*S*)- α -MBA (>99% *e.e.*) albeit with very low conversion in both the D- and L-alanine reactions.

With regards to amine donor enantioselectivity, this is contrary to what was expected. Results from the pyruvate and acetone reactions (Section 2.6) suggest

that the stereochemistry of the amine donor plays a role in the rate and overall yield of the reaction. In all cases (*S*)- α -MBA was more readily accepted than (*R*)- α -MBA irrespective of the amine acceptor. This was reflected in the relative percentages of acetophenone produced in both reactions [Figures 15 and 18]. It is therefore difficult to rationalise this new result in the context of previous results. Substrate docking experiments were later performed to reveal more about the orientation of different amine donors within the active site of ω -TAMs. It was however clear from these experiments that despite the difference in stereochemistry, L- and D-alanine react in the same way with PLP whereas (*S*)- and (*R*)- α -MBA do not. This is discussed further in a later chapter.

Chapter 3. Scale-up/Fermentation of TAm Recombinant *E. coli*

3.1. Acquiring Biomass

In order to test the potential industrial viability of the chosen recombinant cells as expression systems for the production of TAM proteins of interest, medium-scale fermentations were explored. This phase of the work was carried out at the facility of our collaborating company Dr. Reddy's Chirotech Technology Centre in Cambridge, UK under the supervision of Dr. Ian Taylor. The process involved medium-scale fermentation of pre-prepared glycerol stocks of the enzymes using microbiology techniques which were slightly different from what was usually employed for the small scale work. The aim was to produce hundreds of grams of the enzymes being studied, to assess how well the cells grew and how much protein to expect from a larger scale growth. The procedure would also save time in the future and eliminate the need to keep growing new cultures when enzyme stocks were depleted. In addition, this could lead to more consistent results as all the enzymes used in subsequent biotransformations would be from the same batch, providing they can be stored for several months without loss of activity.

Representative trial runs of three 750 mL fermentations of *E. coli* BL21 Star™ (DE3) pLysS cells containing pET29a⁺ vectors with *C. violaceum* 2025 gene inserts were conducted. This was based on a protocol already developed in-house by the biology group at Dr. Reddy's Chirotech Ltd. The process began with the inoculation of 10 mL of LB media (containing 50 µg/mL of kanamycin) with glycerol stocks of the recombinant *E. coli* cells for overnight growth in a 50 mL Falcon® tube in a shaking incubator (35 °C, 200 rpm). A 5% v/v sample of this overnight culture was then used to inoculate seed media (45 mL + 5 mL 20% glycerol) (components in Table 10) in a 250 mL flask and placed in a shaking incubator overnight (30 °C, 200 rpm).

Table 10: Components of Seed, Production, and Feed Media used for *E. coli* fermentation

Seed Medium Components	Amount added (g/L)
Hycase SF (Amisoy)	15
Yeast Extract	5
MgSO ₄ .7H ₂ O	0.5
NaCl	5
KH ₂ PO ₄	5
50% Glucose	20
 <i>Production Medium Components</i>	
Hycase SF (Amisoy)	15
Yeast Extract	15
(NH ₄) ₂ SO ₄	4
KH ₂ PO ₄	8
K ₂ HPO ₄	7
MgSO ₄ .7H ₂ O	1
Trace Elements	1 mL
PPG (antifoam)	2
Glycerol	50
 <i>Feed Medium Components</i>	
Hycase SF (Amisoy)	40
Yeast Extract	20
(NH ₄) ₂ SO ₄	4
MgSO ₄ .7H ₂ O	1
Trace Elements	1.25 mL
Glycerol	208

Trace elements solution:

CuSO ₄ ·5H ₂ O	1.0 mg
ZnSO ₄ ·7H ₂ O	220.0 mg
CoCl ₂ ·6H ₂ O	10.0 mg
MgCl ₂ ·4H ₂ O	180.0 mg
Na ₂ MoO ₄ ·H ₂ O	6.3 mg
Distilled water	1.0 L

The use of amisoy in this media instead of the tryptone, which was used in the small scale over-expressions, is to increase the amount of free amino acids readily available to the growing cells ^[49]. The incorporation of a seed media stage in the fermentation process greatly increases the overall yield of the cell culture. This is partly due to the 20% glucose in the seed medium which serves as an energy reserve to aid rapid growth of the *E. coli* cells.

Freshly prepared production media (700 mL) in a 1 L fermentation vessel [Figure 19] under temperature, pH, and dissolved oxygen control (30 °C, pH 7, 40% DOS) was set up after all components had been sterilised in an autoclave (121°C, 20 mins) . Regulation of pH was achieved by attaching two 250 mL feed bottles to the fermentation set-up containing sodium hydroxide (5 M) and phosphoric acid (5 M). The temperature was controlled by the use of a thermostat with an external re-circulation pump connected to a vessel cooling jacket [Figure 20].



Figure 19: Biostat® B-CDU II fermentor showing the overhead stirrer, cooling jacket, and feed bottle.

*Image taken and annotated from <http://www.sartorius.co.uk/en/products/bioreactors-fermentors/autoclavable-benchtop/biostat-b-dcu-ii/>

The constitution of the production media was chosen primarily to allow for slow growth of the recombinant cells. It contains half as much amisoy (15%) as the seed medium and no glucose. It does however contain 49% glycerol which greatly increases the viscosity of the medium, a condition that facilitates slow cell growth due to relatively poor oxygen mass-transfer ^[50]. Unlike the small-scale over-expressions conducted previously, fermentations at this scale are best conducted over a longer period of time to avoid protein mis-folding and cell lysis. Ensuring a thorough and even distribution of dissolved oxygen therefore is paramount in making this system work efficiently. The increased viscosity due to the amount of glycerol is offset by the highly efficient Biostat® B-CDU II over-head stirrer/agitator and relatively high oxygen transfer rates that can be achieved as a result. Pre-inoculation optical density (OD_{600}) values of the production media from the three fermentors were as follows: A1 = 6.0, A2 = 5.8, A3 = 5.0. Upon inoculation of the fermentors with the overnight seed culture (5 mL), the jacket temperature was manually decreased (25 °C), leading to automatic

drops in dissolved oxygen across all three fermentors and an increase in aeration rates.

After 20 h of fermentation the OD_{600} of all three fermentors were as follows: A1 = 12.2, A2 = 18.4, A3 = 12. Feed bottles containing freshly prepared feed media in 90% glycerol (300 mL) (components in Table 10) was then added at a rate of 0.2 mL/min. After 1 h of feeding, a post-feed OD_{600} was taken to check the progress of the fermentation and the following values were ascertained: A1 = 18.5, A2 = 18.6, A3 = 12. The lack of change of OD_{600} in fermentor A3 was perhaps a result of an error in the over-head agitator which had dropped from 1200 rpm to 730 rpm and an aeration rate of 0.7 L/min (instead of the 1.4 L/min in the other two fermentors). The absence of growth at this stage implied that the cells may have died and so this particular fermentation was void. It was decided to leave the fermentor to continue regardless and check the OD_{600} at a later stage as this may be due to a comparatively slower culture growth. After 4 h of feed media addition, the OD_{600} of the fermentors were as follows: A1 = 23, A2 = 33, A3 = 28. This new observed increase in OD_{600} in fermentor A3 suggested that perhaps the agitator malfunction had not caused any lasting damage to the overall cell culture. All three cell culture fermentations were induced with IPTG (1 mM final concentration) and left to run for 16 h before the next OD_{600} analysis (A1 = 31, A2 = 46, A3 = 24). This final result, showing a decrease in OD_{600} in fermentor A3 compared to 16 h prior, confirmed the likelihood of cellular damage in that culture. Indeed upon harvesting of the cells, the morphology of the resultant cell paste compared to the other two cultures was indicative of cell lysis on a large scale during growth. The wet cell weights from all three fermentors were as follows: A1 = 56 g, A2 = 68 g, A3 = 53 g.

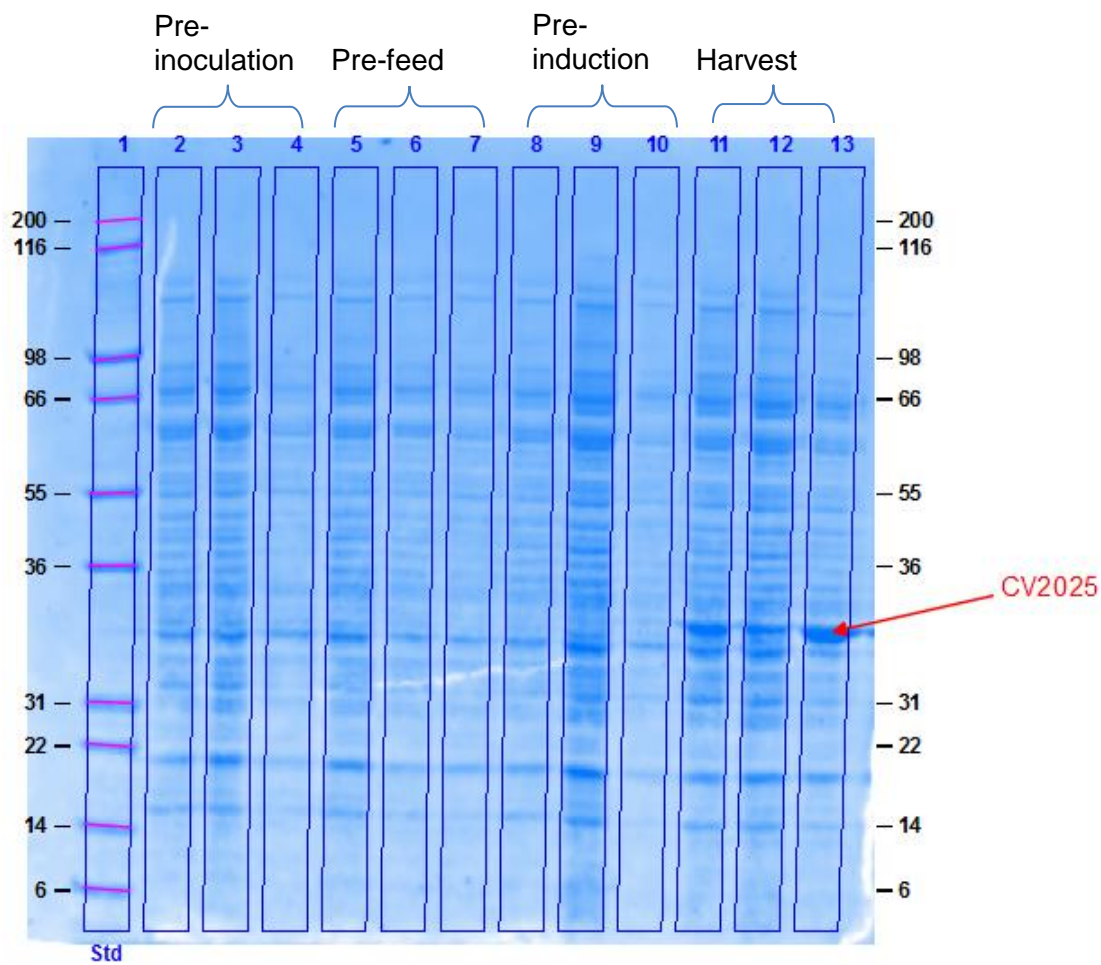


Figure 20: SDS-PAGE gel of samples taken during the fermentation process

In all three fermentors, pre-induction (Lanes 2 – 10) and post-induction/harvest (Lanes 11 – 13). Lane 2 = A1, Lane 3 = A2, Lane 4 = A3, subsequent lanes follow this order
 SDS-PAGE analysis of all three pre-induction OD₆₀₀ samples and one post-induction

sample from the three fermentors [Figure 20] showed the fermentation process was successful in producing protein of the required molecular weight. The CV2025 protein band appeared at the expected molecular weight (45 kDa) with band densities of 21%, 32% and 40% respectively

3.2. Colorimetric Enzyme Activity Assay Screen of CV2025 ω-TAM

The colorimetric assay described in scheme 8 ^[33c] was investigated using the newly harvested crude lysates from the fermentation batches A1, A2, and A3. The assay facilitates detection of the amino acid product (L- or D-alanine) when pyruvate is used

as amine acceptor. In order to investigate the activity and selectivity of a transaminase, the assay requires L- or D-amino acid oxidase (L- or D-AAO) depending on which enantiomer of alanine is produced in the first reaction. If the transamination step produces a particular enantiomer of alanine, the complementary amino acid oxidase oxidises the amine to an imine and reduces a molecule of oxygen to hydrogen peroxide. The resultant H_2O_2 is reduced by horse radish peroxidase (HRP) which then oxidises pyrogallol red to purpurogallin affecting a colour change from red to yellow.

The assay was initially tested using a commercially available (S)-selective transaminase from Codexis® Inc, ATA-113 [Figure 21]. The red to yellow colour change was visible in lane 3 which contains all the components necessary for the colorimetric detection of ω -transaminase activity (pyruvate, (S)- α -MBA, (S)-selective TAm, AAO, pyrogallol red and HRP).

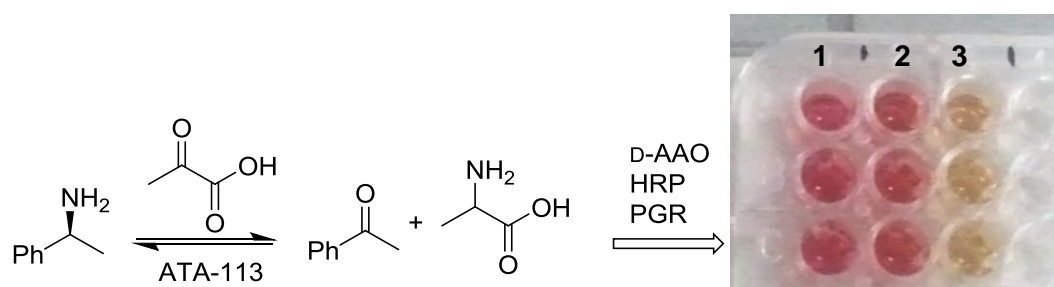


Figure 21: Control colorimetric assay using ATA-113

1 = Negative control (No Horse radish peroxidase), 2 = Negative control (No ATA-113), 3 = Positive control (with ATA-113)

ATA-113 was chosen as it is a known (S)-selective TAm, like CV2025, and in the absence of a TAm there was clearly no activity [Figure 21 lane 2]. Similarly in the absence of HRP [Figure 21 lane 1] there was no activity either. According to the literature, when screening a transaminase like CV2025, L-AAO is required, as the amino acid product of the transamination reaction is L-alanine. However, in the absence of L-AAO (due to the ready availability of D-AAO in the lab and the high cost

of L-AAO) the test assay with ATA-113 and D-AAO gave a positive result. The rate of colour change however, was considerably slower (after 1 h) than what is stated in the literature (after 5 min). This implied that there was a very small amount of D-alanine produced from the transamination step even though the major isomer formed will have been L-alanine ^[33c].

Using the AAO colorimetric assay for a kinetic assessment of the CV2025-TAm harvested from the fermentation batches was deemed impractical due to the high cost of L-AAO (as discussed in chapter 1). In addition, L-AAO is isolated from *Crotalus atox* venom which is difficult to work with due to extreme toxicity. It was therefore decided that it would not be possible to use the colorimetric assay for kinetic analysis of the enzyme batches. Instead it was used in a qualitative assessment of transaminase activity as the test with ATA-113 (above) demonstrated.

When crude lysates from the fermentation of CV2025 were screened in this way, it was clear that not all three fermentations yielded active protein [Figure 22]. CV2025 crude lysate from the third fermentor [Figure 22 lane A3] was shown to be inactive with pyruvate in the colorimetric enzyme activity assay. The other two however showed activity as did the positive control (ATA-113) in lane 4.

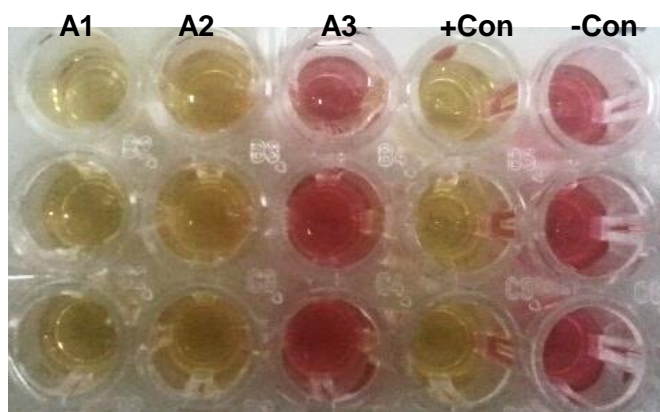


Figure 22 Colorimetric assay using CV2025 from the three fermentations

It was first noted during the batch fermentation process that the OD_{600} of samples in Fermentor A3 did not increase after 1 h post-inoculation [Section 3.1]. It was later noticed during harvesting that its cellular morphology differed distinctly from the other two cell pastes and that it was indicative of cell lysis during growth. In spite of the presence of a CV2025 transaminase band in the subsequent SDS-PAGE analysis [Figure 20], the colorimetric assay [Figure 22], established that active enzymes had not been produced in batch A3. This highlighted the importance of a sufficient and efficient rate of agitation and aeration when using high viscosity growth media. Having established that some of the fermentations had yielded active enzymes, an investigation into the protein concentration of the crude lysates was carried out prior to His-Tag purification of the enzymes.

3.3. Protein Purification

Nickel nitrilotriacetic acid (Ni-NTA) affinity chromatography for the purification of hexa-histidine tagged CV2025 transaminase was then carried out on a semi-preparative scale. Wet cell paste (10 g) was re-suspended in potassium phosphate buffer (100 mM, 40 mL, pH 7.5), sonicated, and filtered. A 5 mL Ni-NTA column was pre-primed using a mixture of nickel sulphate ($NiSO_4$) and ethylenediaminetetraacetic acid (EDTA) before running the crude lysate through the column. Several rounds of

binding of hexa-histidine tagged proteins and washing of the flow-through were followed by elution of the proteins using a buffered solution of 1 M imidazole. A total of 300 mL of eluant was collected for each of the three wet cell paste batches. The total volume was concentrated using desalting spin columns. There were three distinct peaks on the protein detection chromatograms of each of the runs [Figure 23].

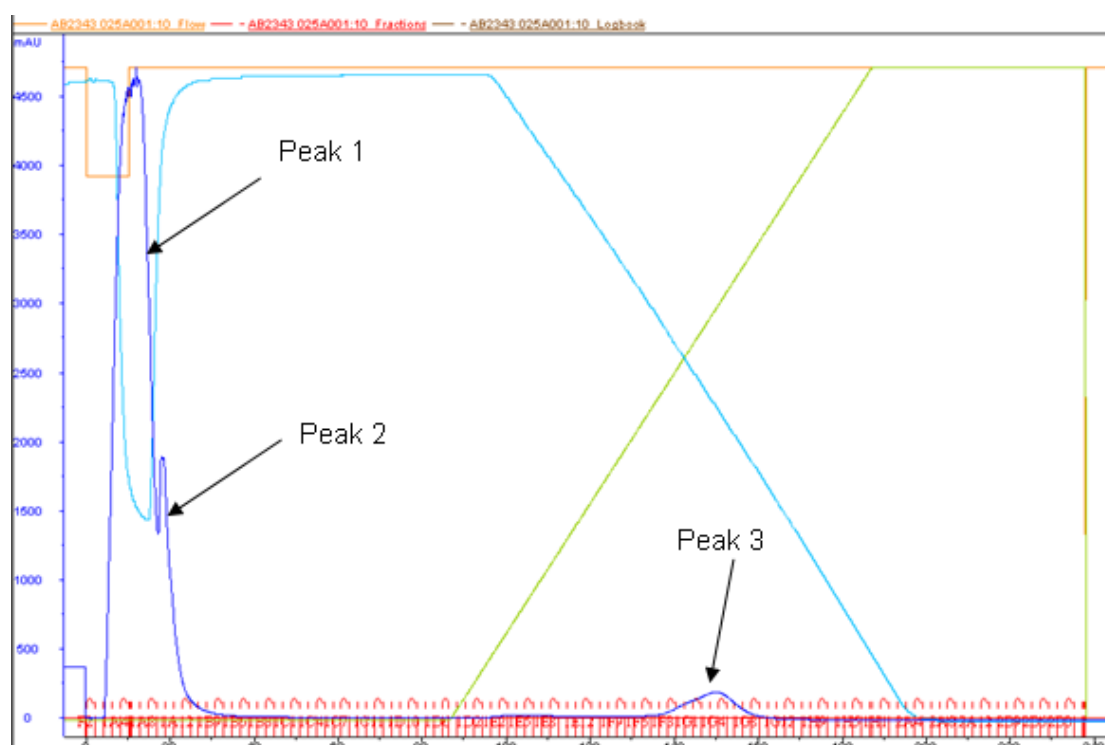


Figure 23: Chromatogram of CV2025 crude lysate purification by nickel affinity chromatography showing the UV peaks (blue) that denote protein concentration.

Although it was believed that the CV2025 TAM would only be present in “peak 3” (the only peak present after elution due to high imidazole concentration in the elution buffer), all three peaks were analysed by SDS-PAGE for confirmation [Figure 24]. Unbound cellular proteins were detected in the first two peak samples. The third peak was detected and collected after the nickel column had been washed with an elution buffer containing 100 mM potassium phosphate buffer, 300 mM sodium chloride, and 1 M imidazole at pH 7.5. The high concentration of imidazole served to displace the

hexa-histidine tag from the nickel coated beads on the column. It was then possible to store purified CV2025 transaminase in 1 mL aliquots at -20 °C for future use.

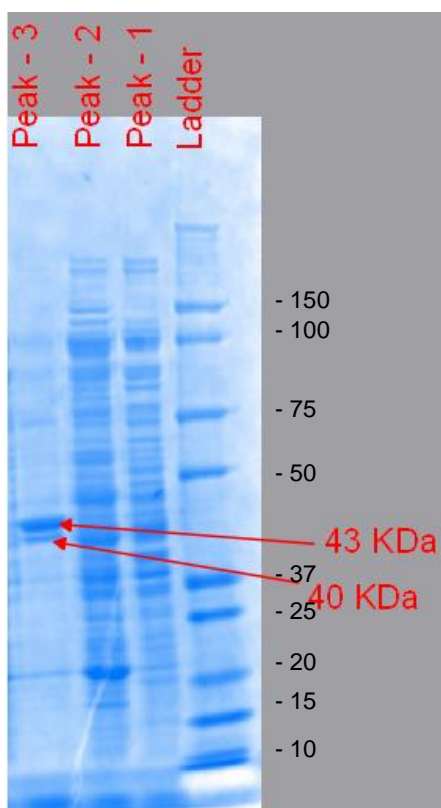


Figure 24: SDS-PAGE analysis of peaks isolated from the flow-through during His-tag purification of CV2025.

In order to fully assess the viability of the enzymes produced from the fermentation process, the total concentration of CV2025 transaminase had to be ascertained in conjunction with an enzyme activity assay to determine units of enzyme harvested per fermentor. Using a standard Bradford assay, a calibration curve was plotted [Figure 25] correlating absorbance at 595 nm with the protein concentration.

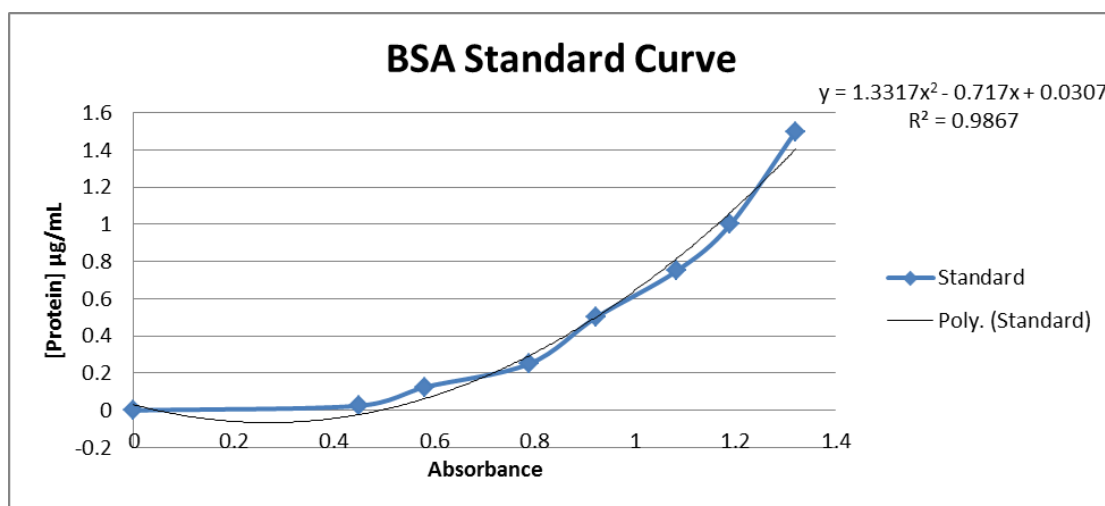


Figure 25: Bovine Serum Albumin (BSA) standard curve to determine protein concentration of CV2025 transaminases.

Using the polynomial equation of the trend in a standard curve for BSA, spectrophotometric data from the analysis of CV2025 samples taken from the three fermentation batches were converted to protein concentration values [Table 11].

Table 11: Bradford Assay Results from all three CV2025 fermentation batches

Fermentation batch	Sample dilutions				Average protein conc./ mg/mL
	2x	3x	5x	10x	
A1	7.7	12.5	14.5	14.5	12.3
A2	12.5	16.6	26.0	39.1	23.6
A3	3.06	2.86	2.73	2.56	2.80

To ensure reliability of the data, four different dilutions of crude lysate were taken (2x, 3x, 5x, and 10x). The sample from fermentor A2 was shown to have the highest total protein content after Ni-NTA purification (23.6 mg/mL) whilst A3 had the lowest (2.8 mg/mL).

Using a Bio-Rad™ gel imaging software, the SDS-PAGE gel of the fermentation process [Figure 24] was analysed to estimate (based on band density) what

percentage of the total protein content of the crude lysate was CV2025 transaminase. The estimated values were 21%, 32%, and 40% of the total protein content of crude lysate. These were lower than observed during the previous small-scale over-expression experiments. It is well known that overly long fermentation times can sometimes cause inclusion bodies to form. That was not found to be the case however, in this experiment as there was no CV2025 observed in the re-suspended cell pellet. The concentrations of CV2025 transaminase from the three fermentation batches were therefore estimated to be: A1 = 2.6 mg/mL, A2 = 7.6 mg/mL, and A3 = 1.1 mg/mL.

3.4. Fermentation of (S)-Specific omega-Transaminases

Having established conditions for the growth, over-expression, purification, and screening of the recombinant *E. coli* for CV2025 ω -TAm, the procedure was applied (with minor changes) to the sub-set of four (from the initial panel of ten novel (S)-specific ω -TAm) previously screened (section 2.7). Narrowing down the initial list of 10 novel enzymes for fermentation was necessary in order to be able to conduct all the fermentations within a reasonable time-frame. The four recombinant *E. coli* cell cultures were chosen based on how well the TAm genes were over-expressed on the small scale [Figure 7]. Recombinant *E. coli* containing KpN_00799 and Pput_3718 were amongst the cell cultures with the highest levels of over-expression (60%) whilst the two *Bacillus subtilis* TAm (BSU_402 and BSU_1971) were amongst the cultures with the lowest levels of over-expression (20%). Medium-scale fermentation of these two sets of cell cultures along with recombinant *E. coli* containing VF-JS17 ω -TAm (for comparison) was conducted following the same procedure as with CV2025 ω -TAm. The two *B.subtilis* TAm were chosen in order to investigate the effect of the fermentation conditions on cells that had poor overexpression profiles under the previous small scale conditions. All the data collected during fermentation

of the five cell cultures was indicative of a normal and healthy culture. As a result, similar growth levels were expected from these fermentation batches. This was reaffirmed by the amounts of wet cell pastes harvested from each batch: VF_JS17 = 105 g, BSU_402 = 92 g, KpN_00799 = 70 g, BSU_1971 = 72 g, PP_3718 = 60 g [Figure 26].

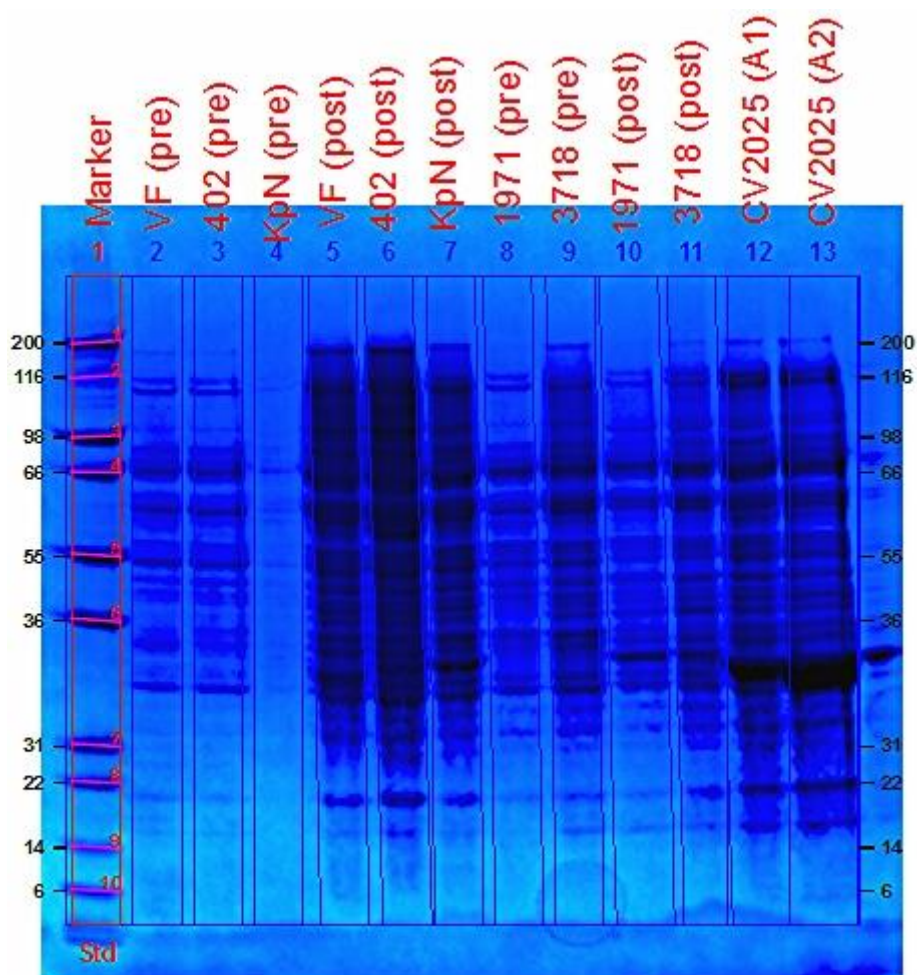


Figure 26: SDS-PAGE gel of samples taken during the fermentation process

Including all five fermentations; pre-induction (Lanes 2 – 4, 8 & 9) and post-induction (Lanes 5 – 7, 10 & 11). Positive Controls (CV2025 A1 & A2)

Across the larger scale fermentation cultures over-expression did not follow the same pattern observed on the smaller scale. Using the BioEdit™ imaging software, again the levels of over-expression were approximated to be as follows: VF_JS17 = 9%, BSU_402 = 7%, KpN_00799 = 13%, BSU_1971 = 20, PP_3718 = 10% compared to

CV2025 (A1) = 21% and CV2025 (A2) = 32%. Although not shown in this thesis, previous small scale over-expression of this panel of enzymes suggested that the transaminases are soluble as there was no protein present in their re-suspended cell pellets.

Table 12: Total protein concentrations of fermentation batches from Figure 26

TAm	Sample dilutions*				Average	%TAm from SDS-PAGE**	TAm conc. mg/mL
	x2	x3	x5	x10			
VF	9.8	10.4	22.6	31.2	18.5	9	1.7
402	11.2	22.1	26.3	34.1	23.4	7	1.6
KpN	12.1	13.4	34.3	54.6	28.6	13	3.7
1971	14.8	15.5	27.2	39.1	24.1	20	4.8
3718	10.4	18.5	14.7	12.9	14.1	10	1.4
CV2025	14.6	1.4	28.9	54.4	24.8	32	7.9

*Calculated from BSA standard. **Calculated using BioEdit™

Notwithstanding the low transaminase over-expression levels in these cell cultures, the total protein concentration values were in the expected regions when compared to the CV2025 fermentation results [Table 11]. In all six 1 litre fermentation cultures, the lysates contained less than 10 mg/mL transaminase [Table 12]; a much lower turnover than expected considering the enzyme yields on the 500 mL scale (>20%) [Figure 7]. This was perhaps due to introduction of the induction agent (IPTG) too early in the growth stage. Another possibility is the difference in components between the small scale over-expression medium (2xTY) and the high viscosity medium of the one litre fermentation (HyCase® amisoy). Although the soy medium is ideal for large scale fermentations, the expression systems used in this work were not designed for such conditions which might have led to uneven growth and low protein expression.

In order to investigate these hypotheses further, a new cell culture medium was tested. Studier auto-induction medium ^[51] was selected to be trialled as it addresses the issue of early induction in the fermentation cultures. It is a ZYP-5052 rich medium designed for growth with very little early induction (in the log phase) and only switching to auto-induction when the culture reaches saturation. This is determined by the cells switching from glucose to lactose as a carbon source and as oxygen levels become limiting.

During a 45 h, 400 mL over-expression of all six recombinant *E. coli* cell cultures under these conditions the observed OD₆₀₀ values [Table 13] showed only modest increases. This, when compared to the values obtained during the large scale fermentation was indicative of even lower over-expression levels than had previously been observed in the amisoy medium. SDS-PAGE analysis of the wet cell pastes showed negligible levels of transaminase over-expression; a result which discredits the possibility of an early over-expression induction being the reason for lower than expected transaminase protein levels in the 1 litre scale fermentation.

Table 13: OD₆₀₀ values of the auto-induction screen of the six TAm *E. coli* cultures

Cell culture	OD ₆₀₀			
	19 h	23 h	43 h	45 h
CV2025	18	28	28	28
VF_JS17	16	15	20	16
BSU_402	12	15	22	19
KpN_00799	13	15	19	17
BSU_1971	12	13	21	16
Pput_3718	12	15	18	17

There are many factors hindering the successful scale-up of recombinant *E. coli* fermentation. They range from uniformity-related barriers such as irregular aeration which leads to the formation of small anoxic regions and later apoptosis, to cell death as a result of pH imbalance. Having eliminated early induction as a possible reason for this low protein over-expression, the limitations of the larger-scale over-expression were accepted as well as the need for further studies in order to address this.

Chapter 4. AAO-Based Screening of Novel Enzymes and Amine Donors

4.1. Screening of Novel TAM Enzymes

Screening of the novel transaminases for enzyme activity followed the same procedure as for CV2025 [Section 3.2]. The amino acid oxidase colorimetric assay was used with (*S*)- or (*R*)- α -MBA as amine donor and either L- or D-amino acid oxidase as the complimentary second enzyme in the assay [Scheme 8]. In spite of the high cost of the AAO enzymes, it was deemed necessary to purchase them for a one-off screening of the batch of novel TAMs. The results confirmed that all the novel transaminases were active against (*S*)- α -MBA. They did however exhibit much lower volumetric enzyme activities when compared to the CV2025 standard with (*S*)- α -MBA [Table 14]. As a further test to investigate the unexpected observation discussed in section 2.9 where CV2025 accepted both D- and L-alanine, the novel transaminases were also tested against (*R*)- α -MBA. The subsequent results showed above-background levels of consumption of (*R*)- α -MBA, between 2% and 50% of the volumetric enzyme activity against (*S*)- α -MBA. This is significant enough activity to suggest, coupled with the previous observation in the LDH/GDH assay, that for some transaminases enantiopreference is likely to be of a kinetic cause. There is however no literature precedent for this observation and further testing would be needed to corroborate and validate these observations.

Table 14: Colorimetric screening of transaminase enzymes against both enantiomers of α -MBA

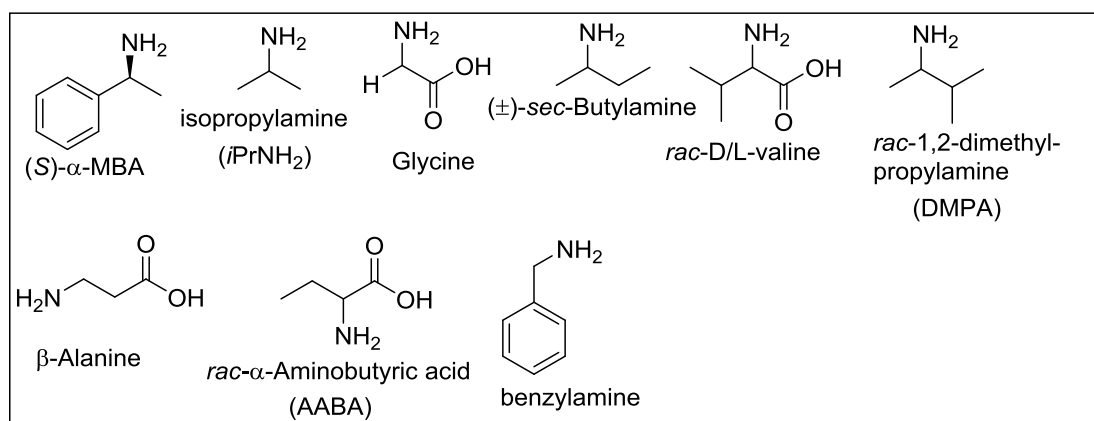
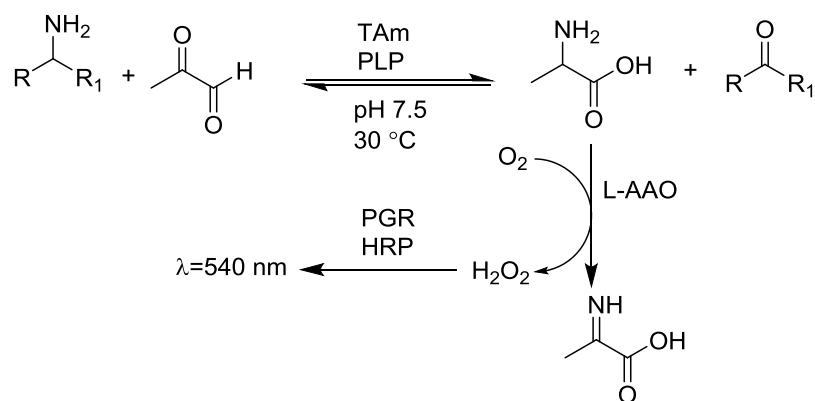
Enzyme	Volumetric Enzyme Activity (U/mL)	
	(S)- α -MBA	(R)- α -MBA
CV2025	0.05	0.005
VF_JS17	0.04	0.008
BSU_402	0.04	0.0007
KpN_00799	0.006	0.001
BSU_1971	0.01	0.005
Pput_3781	0.02	0.008

Conditions: Na⁺ pyruvate (0.2 mg/mL), α -MBA (5 mM), ω -TAm (0.5 mg/mL), PLP (0.1 mg/mL), PGR (0.1 mg/mL), HRP (1 mg/mL), AAO (10 U)

4.2. Screening of Amine Donors using CV2025 and VF_JS17

An important feature of all enzyme-catalysed reactions is substrate specificity. This is a key factor in determining reaction rate and yield. Due to the reaction mechanism of transaminases however there are two substrates to be considered. For the purposes of this study (synthesising valuable chiral amines as pharmaceutical intermediates), the screening of amine donors is necessary. Six new amine compounds were chosen to be screened based on the structure of three previously tested amines (α -methylbenzylamine, isopropylamine, and alanine). The chosen list of new amine donors [Scheme 19] included glycine, valine, α -aminobutyric acid, and β -alanine which were chosen based on their functional group similarity to alanine (as an amino acid). Similarly, *sec*-butylamine and 1,2-dimethylpropylamine were chosen based on their structural similarity to isopropylamine (aliphatic amine). Benzylamine was the

only α -MBA-like amine donor chosen as part of the amine panel. The experiment was designed for a dual purpose: to find viable new amine donors for the transaminases and to explore the active site of the enzymes in a short structure-activity study coupled with *in silico* substrate docking.



Scheme 19: Screening of amine donors against transaminases using the amino acid oxidase colorimetric assay against a panel of 9 amine donors

Studying the seven new amine donors alongside the two previously tested amine compounds in an AAO-based colorimetric assay, the relative enzyme activities were compared in a series of small scale screening experiments over 3 h [Figure 27]. The spectrophotometer at 540 nm detected the change of colour from red to yellow as pyrogallol red is oxidised. As shown, there was a background level of colour change due to oxidation from atmospheric oxygen.

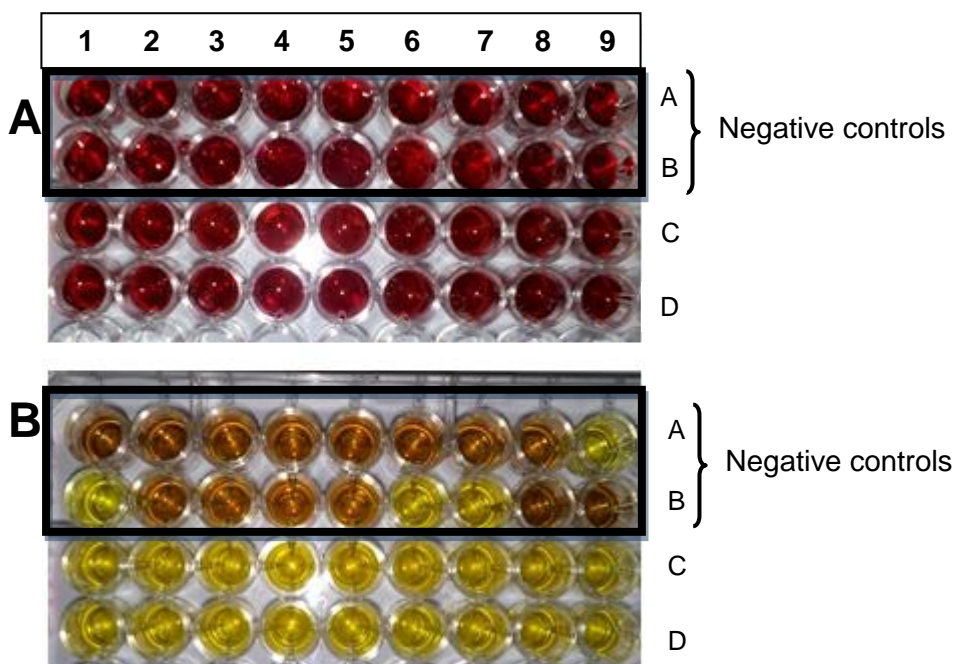


Figure 27: Screening of amine donors against CV2025 – (A): after 1 min and (B): after 180 min.

Negative control: A1-A2 = (S)-MBA, A3-A4 = *i*-PrNH₂, A5-A6 = glycine, A7-A8 = sec-butylamine, A9-B1 = D/L-valine, B2-B3 = DMPA, B4-B5 = β -alanine, B6-B7 = AABA, B8-B9 = benzylamine.

Reaction: Amine donors follow the same order as in the negative controls in duplicates starting from C1-C2 = (S)-MBA.

All the substrates except D/L-valine [Figure 27-B, lanes C9-D1] exhibited above-background levels of enzyme activity with CV2025 [Table 15]. The same was observed when VF_JS17 was used in the assay. The second poorest substrate in both enzyme reactions was α -aminobutyric acid which exhibited volumetric enzyme activity values close to or below the negative control reaction (colorimetric assay without transaminase). These results are indicative of perhaps steric hindrance or unfavourable electrostatic interactions within the active site which impairs one or both half-reactions of the transaminase ping-pong mechanism. CV2025 consistently performed better than VF_JS17 against all the tested substrates in this investigation. Benzylamine was the second best amine donor against CV2025 (0.04 U/mL) and may be preferred over (S)- α -MBA as a cheap achiral amine donor partner for this enzyme.

Table 15: Volumetric enzyme activity of nine amine donors against CV2025 and VF_JS17

Amine Donor	Volumetric Enzyme Activity (U/mL)	
	CV2025	VF_JS17
(S)-MBA	0.05	0.04
<i>i</i> -PrNH ₂	0.02	0.01
glycine	0.02	0.01
sec-butylamine	0.02	0.02
D/L-valine	-0.03	-0.02
1,2-dimethylpropylamine	0.02	0.02
β-alanine	0.03	0.004
α-aminobutyric acid	0.006	-0.001
benzylamine	0.04	0.01

Conditions: Na⁺ pyruvate (0.2 mg/mL), amine donor (5 mM), ω-TAm (0.5 mg/mL), PLP (0.1 mg/mL), PGR (0.1 mg/mL), HRP (1 mg/mL), AAO (10 U)

4.3. Substrate Docking Studies

In silico studies to explore the substrate preferences of CV2025 was conducted using its full crystal structure [23]. The enzyme active site reveals a pyridoxal-5'-phosphate (PLP)-anchoring site and two substrate-binding pockets i.e. a large binding pocket (R_L) and small binding pocket (R_S) [6a, 51]. The PLP phosphate group is anchored by Gly155, Ser121, Gly120, Phe320*, Thr321* and Tyr322* (where the asterisk indicates residues belonging to the other subunit in the dimeric enzyme). The pyridine ring is bound by the two conserved residues Lys288 and Asp256 creating a Schiff base salt bridge and a hydrogen bond to the pyridine nitrogen respectively [Figure 28]. The R_L pocket consists of three main amino acid residues Tyr153, Phe22 and Thr321*. All three amino acid residues were reported to contribute to substrate recognition.

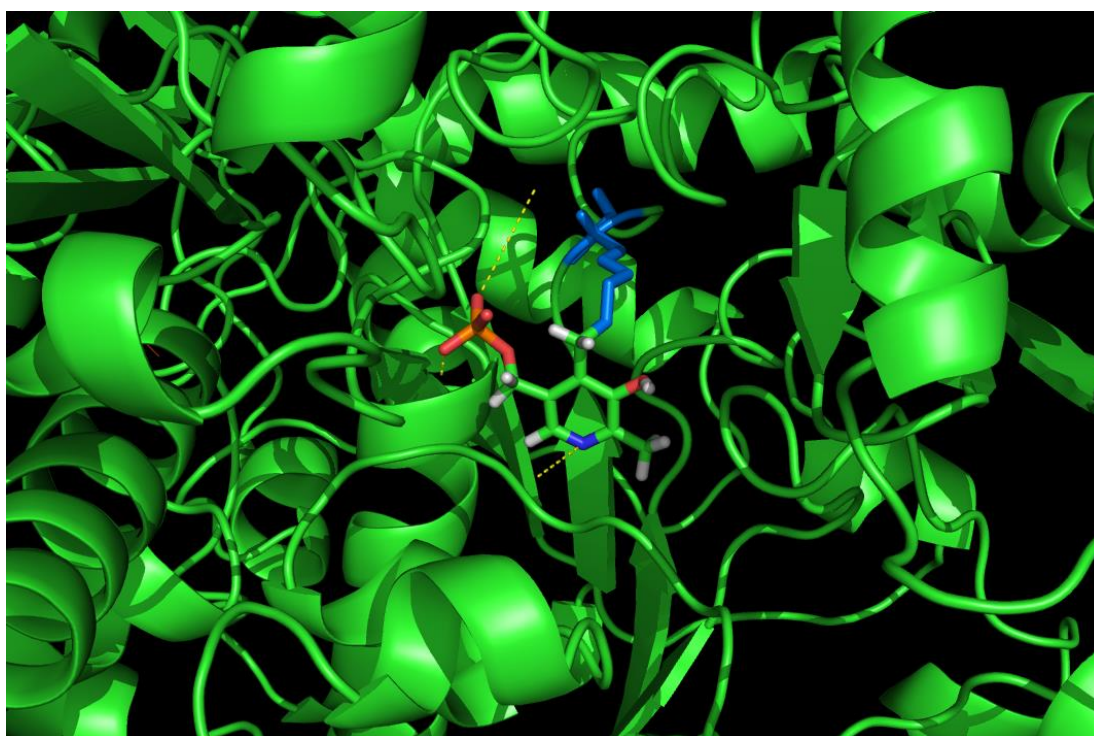


Figure 28: *In silico* docking image of PLP in the active site

Showing the phosphate-binding cup (Thr321 and Tyr322), the Schiff base salt bridge with Lys288 and the pyridine nitrogen hydrogen bond with Asp256

The R_s pocket has interactions with Arg416, Trp60 and Leu59; among these three amino acid residues Arg416 is a well-documented conserved amino acid in transaminases ^[6a]. By binding to both (*S*)- α -MBA (via a hydrogen bond) and pyruvate (via a salt bridge), Arg416 determines the orientation of the amine acceptor substrate relative to the plane of the PLP-amine amine donor. As a result, any potential mutation to that amino acid could result in a decrease in enzyme activity (Liu, 2004; Shin, 2003). Indeed, Arg416 is a well conserved residue in all but one of the ω -transaminases screened. Only the *K. pneumoniae* ω -transaminase (KpN_00799) presents alanine instead of arginine in that position [Figure 29]. It is possible that this naturally occurring mutation results in KpN_00799 ω -TAm having a significantly lower enzyme activity (against α -MBA and pyruvate) [Table 14] due to the absence of an interaction with the carboxylate group of pyruvate.


```

CV_2025      1 MQHQRTTSQWR...ELDAAHHLHPFTDTASLNQAGARVMTRGEGVYLW
PP_3718      1 MATPSKAPAIADHPELVEADKAHYMHCYHVDFDEHREQGALNIVAGEGAYIR
BSU09260     1 MEMMGMENIQQN...QGLKQKDEQFVWHAMKGAHQADSLIAQKAEAWWT
KEN 00799    1 MTLDD.....LAFDRRHIWHPYTSMTSPLFVYP...VVSARGCELS

CV_2025      46 DSEGSKIIDSMAGLWCVNVGYGRHDFAEAARRQMEELPFYNTFFKTHPA
PP_3718      51 DTGHRFLDAVGRWCTNIGLGREEMALAIVDQVRQLAYSNPFSDMANDV
BSU09260     45 DTGHRFLDAMSGLWCVNIGYGRKELAEAAEYQLKELPHY...PLTQSHAP
KEN 00799    50 LAGGEQLVDGMSSWAAIHGYNHFLNAAALNGQIDQMSHVMPGG.IITHPP

CV_2025      96 VVELSSLLAEVTPAGFDRVFTNSSGSESVDTMIRMVRRYNDVQGKPEKKT
PP_3718      101 AIELCQKLAQLAPGDLNHVFLTSGSTAVDTAAYRLIQYYQNCRGRKPHGKH
BSU09260     96 AIQLAEKLNWLGSDY.VIFFSNSGSEANETAFKIAHQYHLQNGDHSRYK
KEN 00799    95 AVALCRQLVAMTPASLECVPLADSGSVAVEVAMMALQYVQAKGEPREFF

CV_2025      146 LIGRWNGYHGSTIGGASLGG.MKYMHEQGDLPIPGMAHIEQPWNY...KHG
PP_3718      151 IIRYMAYHGSTITLMSIGNKAADRVPEFDYHDLIHHVSNPNFY...RAP
BSU09260     145 FISRYRAYHCNTLGALSATG.QAQKRYKYEPLSQGFLHAAFPDIYR....
KEN 00799    135 LTFR.NGYHGDTFGAMSWCDPQNSMHSLNQGYLFDNLFAPAPQSR.....

CV_2025      243 PEIERICRKYDVLVADEVICGPGRTGEWFG.HQHFGFQPDLETAAKGLS
PP_3718      249 QRMNQLCQTYDILFVADEVVTSFGRIGTFASEELFGVTPDIITAKGLT
BSU09260     235 KQVEDICRRHGALLICDEVICGPGRTGEPFG.FMHYGVKFDITMAKGIT
KEN 00799    229 KRVRKMCDRREGILLADEIATGPGRTGKLF.CEHAGITADILCLGKALT

CV_2025      292 SGYLPIGAVFVGRVAEGLI...AGG.DFNHGFTYSGHFVCAVAHANVA
PP_3718      299 SAYLPLGACIPSERINQVIA.EPGWRCFTHGFTYSGHFVCCTAALKNIE
BSU09260     287 SAYLPLSATAVKRDIFEAYQG.EAPYDRFRHVNTFGSPAACALALKNLQ
KEN 00799    275 GGTMTLSAAITTRTVAETIS...NGEAGCFMHGPTFMGNPLACAVASESLR

CV_2025      355 KAKRELFPDFGEIGTLCRDIFF.....BNNLIMRACGDHIVSAPPLVMIR
PP_3718      356 KASKALFADEVNIGERISKAQ.....EKGLLVRPIMHLNVMSPPLIITH
BSU09260     354 KLTKEPADAAMVNVQVAACKEKGLIIGFNGDTVRGYNNVIQLAPPCLTE
KEN 00799    374 .....VNMAALQRFP.....VEQGVVIAPFGRLIYLMFPYIITP

```

Figure 29: Amino acid sequence alignment of the novel TAmS and CV2025 showing the residues of the R_L and R_S binding domains.

Another conserved residue in the R_S pocket is Trp60, which is right below Arg416 in the enzyme quaternary structure. Although manual docking results did not show any potential interaction with pyruvate or (S)- α -MBA, Trp60 was shown to interact with (R)- α -MBA via a hydrogen bond in addition to interactions with all three of the other R_S amino acid residues. Its universal distribution amongst all the enzymes investigated perhaps explains their consumption of (R)- α -MBA, albeit at a slower rate.

Using the molecular docking freeware AutoDock Vina, the amine donors studied [Table 15] were docked within the CV2025 active site. This highlighted that for example, the aryl group of (S)- α -MBA formed a π - π -stacking interaction with Phe22 or Tyr153 allowing the aromatic ring to be stabilised in the active site [Figure 30].

This explains the increased enzyme activity when (*S*)- α -MBA or benzylamine is used as an amine donor compared to the other substrates. In addition, Tyr153, Lys288 and Thr321* form hydrogen bonds with the substrate amine group. The most important amino acid residue in conferring (*S*)- α -MBA affinity was found to be Tyr153 [52]. It forms two strong interactions with the amine donor via a hydrogen bond and a pi-stacking interaction. Lys288 and Thr321* by comparison have weaker interactions with (*S*)- α -MBA as they both have the additional roles of interacting with the phosphate group of PLP.

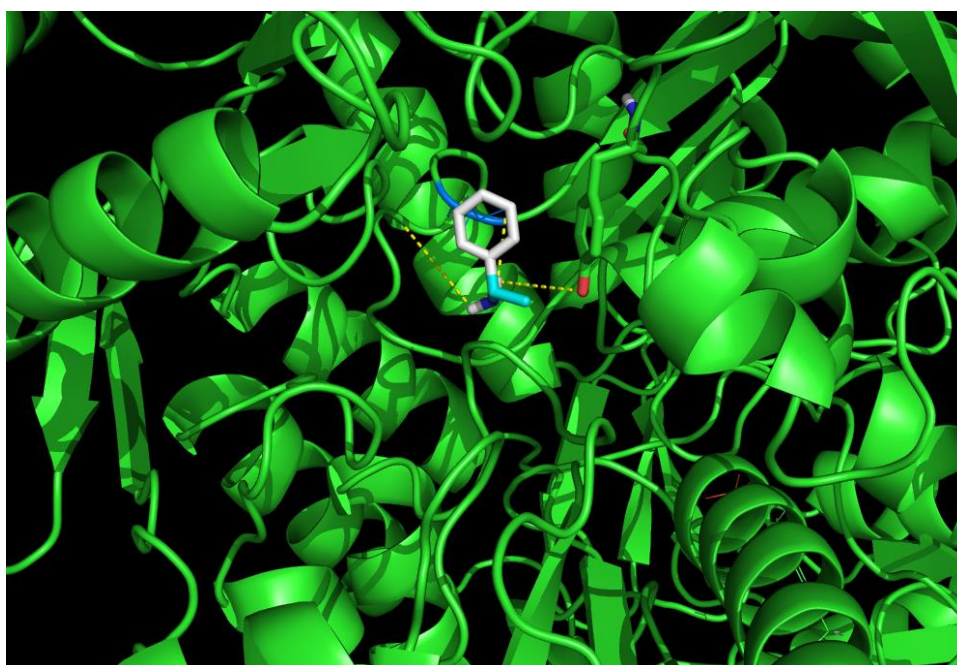


Figure 30: *In silico* docking image of (*S*)-MBA in the R_L

Showing phenyl ring stacking and H-bonding with Tyr153, Thr321 and Lys288

Using the commercial Schrödinger[®] Maestro modelling tool, the lowest energy conformations of each binding interaction between a CV2025 active site residue and the amine donors screened in section 4.2 were determined (not shown). An additional list of eight active site residues (besides the phosphate binding cup and the R_S and R_L binding domain residues) were highlighted to be involved in the

binding of some of the amine donors. These are: Thr23, Phe88, Phe89, Lys90, Asn151, Asp315, Arg405, and Cys418. A correlation between strength of interaction (bond energy) and substrate affinity (based on enzyme activity [Table 15]) was noted and is discussed below.

Isopropylamine was found to have the weakest intermolecular interaction with the active site. Due to its low molecular weight, it has a total of ten possible conformations, twice the average for the full list of amine donors. The absence of any extraneous functional groups on the molecule coupled with its short carbon chain length allows isopropylamine to move with a higher degree of freedom within the active site compared to all the other amine donors. All ten conformers showed interaction with the same active site residue (Asp315) making it the most crucial residue for isopropylamine reactivity in the enzyme.

(S)- α -MBA, with only two conformations, was shown to be the most stable with regards to the energy of its primary conformer. In addition to the conformation shown [Figure 30], the amine donor also interacts with Phe22 and Phe88, a less favourable higher energy conformation. These low energy conformations of (S)- α -MBA and isopropylamine allow for the release of their respective ketone side-products more readily, creating the space for amine acceptor entry into the active site.

At the other end of the scale however, the two amine donors with the lowest volumetric enzyme activity in CV2025 (valine and α -aminobutyric acid) [Table 15] were found to be involved in the most stable intermolecular interactions with Arg416, Tyr168, Arg405, Thr23, and Phe22. These amine donors become, in effect, inhibitors due to the strength and number of their intermolecular interactions with the enzyme active site.

In the case of the amine acceptors, the highly conserved and functionally crucial Tyr153 recognises and interacts with pyruvate via its carboxylic side chain [Figure 31]. In spite of the important role played by Thr321*, interacting with and stabilising both co-factor and substrates, it is not as highly conserved as Tyr153. A tyrosine residue has been identified in the same position and has a similar role to Thr321* in other transaminases [32b, 51]. However, it was also reported that by replacing this residue with Ala, Leu, Val or Phe, the substrate specificity of the enzyme was increased but the activity was reduced considerably. This indicates the major role Thr321* plays in maintaining enzyme activity by strongly interacting with the PLP phosphate moiety. Whether this might be the case for Thr321* in CV2025 is as yet unknown, however site-directed mutagenesis may verify this.

Phe22 is the least well conserved active site residue [Figure 29]. It is only found in CV_2025 and none of the others. Considering its role in π -stacking interactions with aromatic substrates, it is perhaps partly responsible for the observed higher relative activity of CV_2025 against (*S*)- and (*R*)- α -MBA compared to the novel enzymes [Table 15]. Leu59 is also poorly conserved; in spite of this there is no observable trend in activity in the presence or absence of this residue. It appears that this particular active site residue is of no crucial catalytic importance, at least regarding aromatic amine donors.

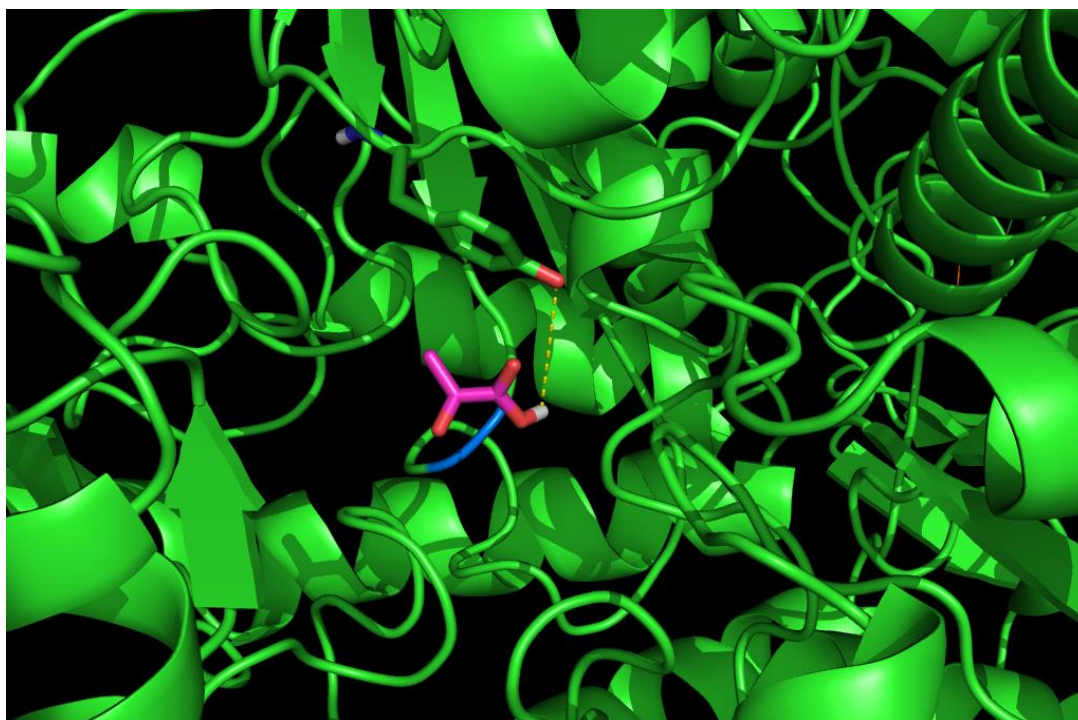


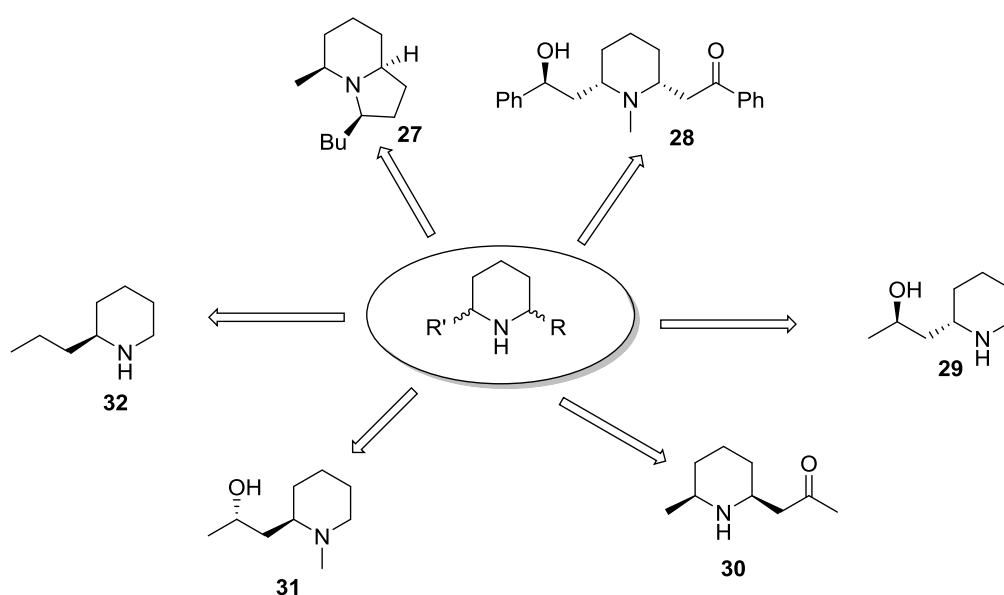
Figure 31: Pyruvate in the R_s H-bonding to the highly conserved residue Tyr153

Phe320 and Tyr322 as part of the triad of residues in the phosphate-binding cup are both poorly conserved with Phe320 being the lesser conserved of the two. Enzymes without one or both of these active site residues have markedly lower activity against (*S*)- and (*R*)- α -MBA compared to those with the full triad (Phe320, Thr321 and Tyr322). The two lowest performing enzymes in the amine donor assays: KpN00799 and BSU09260_1971 [Table 15] do not have phenylalanine and tyrosine in positions 320 and 322 respectively. Their poor activity may be due to the absence of the stabilising effect of Phe320 on the PLP co-factor in the active site.

Chapter 5. Transaminase-mediated Synthesis of Cyclic Amines

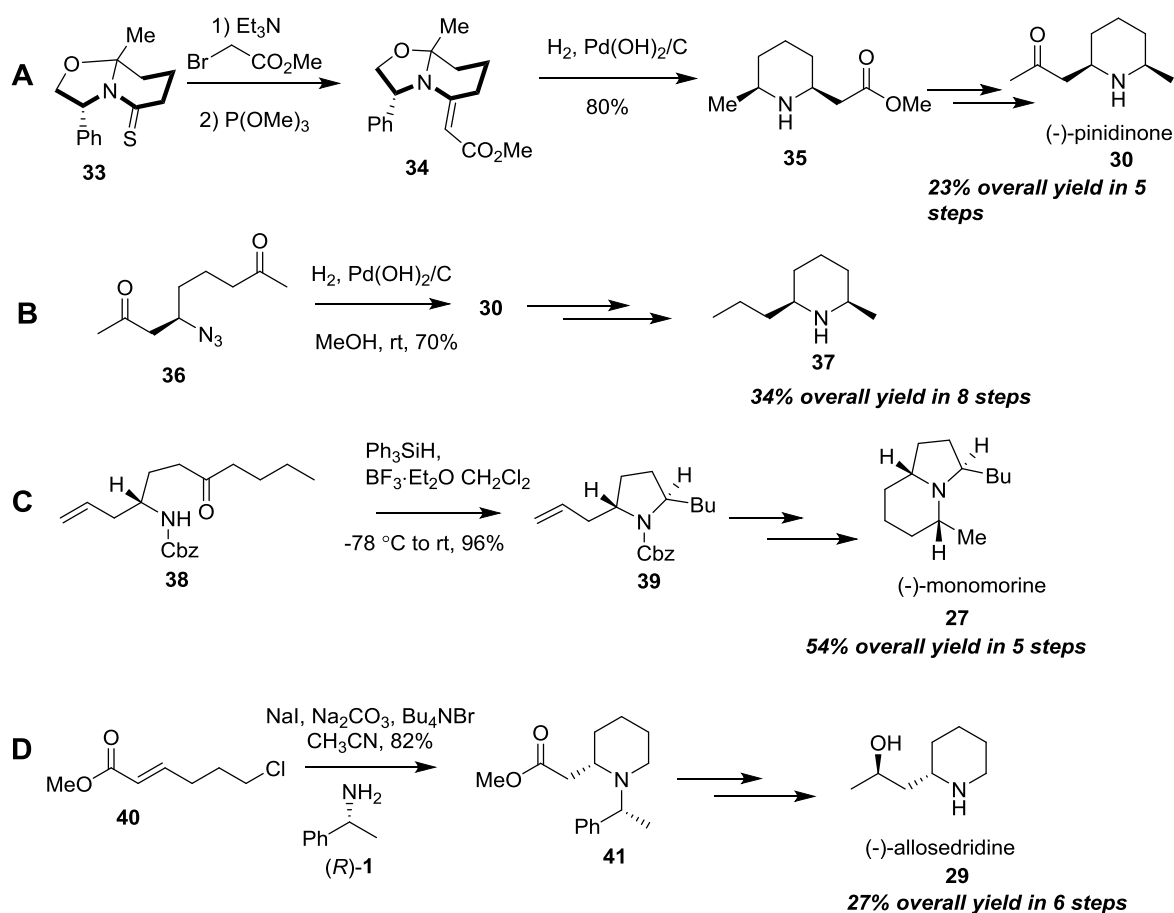
5.1. Introduction

Cyclic amines (piperidines and pyrrolidines) are a class of key structural scaffolds, present in a variety of natural products [Scheme 20]. In addition, the piperidine moiety has been used in a broad spectrum of pharmaceutical agents [53]. The chemical synthesis of these bioactive compounds follow a myriad of strategies most of which involve protecting groups that may complicate and elongate the synthetic process in order to access a particular stereoisomer of interest [54].



Scheme 20: Examples of biologically active piperidine alkaloids

One of the earliest attempts to access 2,6-disubstituted piperidines included synthesis of the anti-feedant agrochemical (+)-pinidinone (**30**) and the ant trail pheromone (+)-monomorphine (**27**) [55]. To achieve this, thioamide (**31**) was transformed, in five steps, into (-)-pinidinone (**30**) and in seven steps into (+)-monomorphine (**27**) using the Eschenmoser contraction to furnish an α,β -unsaturated ester (**34**) [Scheme 21-A]. A subsequent hydrogenation to produce piperidine (**35**) was followed by treatment with a Weinreb reagent followed by methyl-magnesium bromide to furnish (-)-(**30**) in 23% overall yield [55].



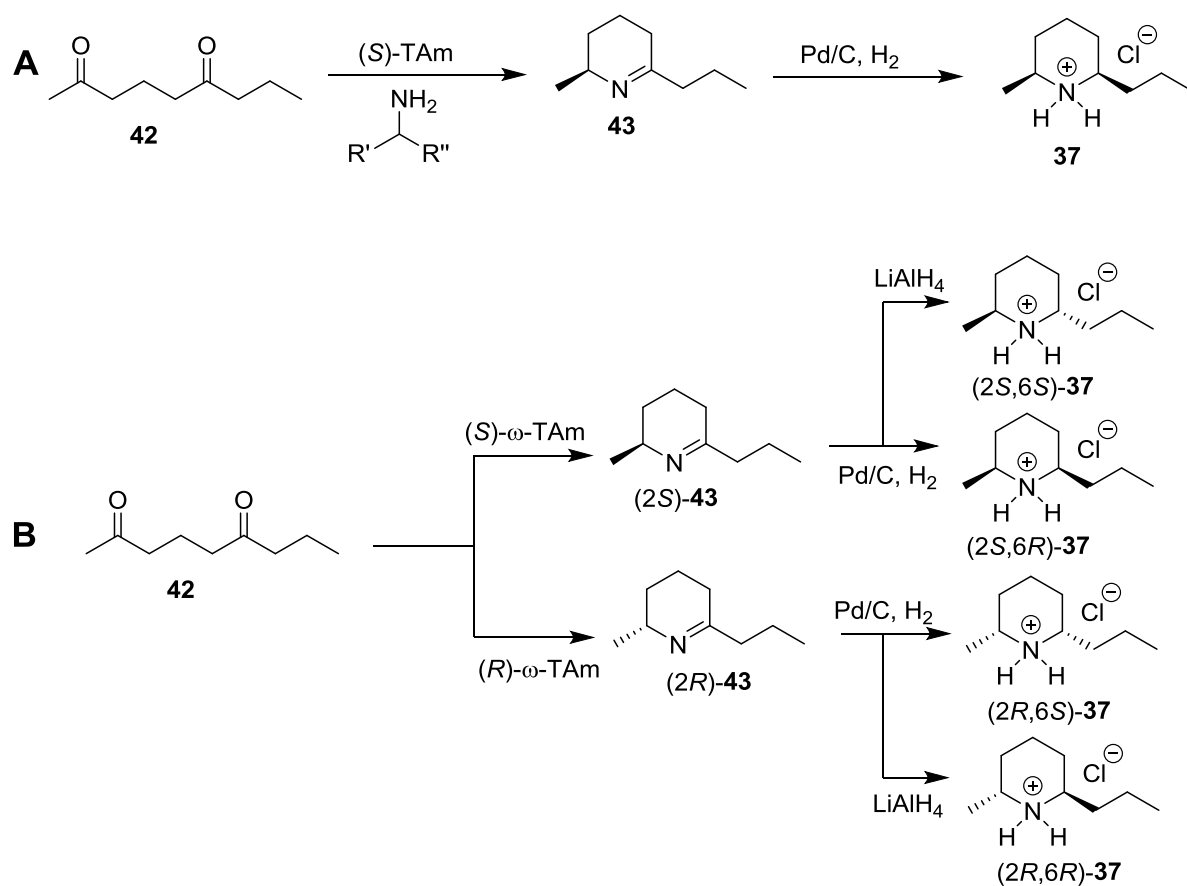
Scheme 21: Chemical synthesis of the piperidine and pyrrolidine cores of a selection of alkaloids.

A more recent approach to this synthesis adopts a different strategy. The Szolcsanyi approach to stereoselective synthesis of the 2,6-disubstituted piperidine of (-)-pinidinone is an elegant sequence which employs an azidodiketone intermediate (**36**) in a one-pot three-step sequence involving azide reduction, amine condensation, and imine reduction [Scheme 21-B] ^[56]. Nemoto and co-workers' approach to the synthesis of the 2,5-disubstituted pyrrolidine section of the bicyclic (-)-monomorine (**27**) involved the spontaneous ring-closure of Cbz-protected amine (**38**) and a stereoselective reduction of the less hindered β -face of the resultant iminium salt with triphenylsilane [Scheme 21-C] ^[57]. Subsequent cross-metathesis and hydrogenation furnished alkaloid **27**.

The most universally applicable approach to the synthesis of a 2,6-disubstituted structure is exemplified in the synthesis of (-)-allosedridine (**29**) [Scheme 21-D] ^[54a]. (*R*)- α -methylbenzylamine (**1**) is used as a chiral auxiliary in an intramolecular aza-Michael addition with α,β -unsaturated ester **40** to furnish both diastereomers of piperidine **41** in a 2:1 ratio. This strategy lends itself to much more straightforward chemical transformations as the amine is introduced immediately prior to ring-closure. The approach directly complements the potential functionality of transaminases with regards to the introduction of an amine functionality that could facilitate spontaneous ring-closure and formation of a disubstituted cyclic amine.

The first example of a transaminase-mediated synthesis of a disubstituted cyclic amine is from the Kroutil laboratory in Graz, Austria ^[58]. A selection of (*R*)- and (*S*)-selective transaminases were used in an asymmetric transamination followed by subsequent chemical reduction of the cyclic imine product to furnish 2,6-disubstituted piperidines in perfect regio- and stereoselectivity [Scheme 22].

Starting from a 2,6-diketone (**42**), an (*S*)- ω -transaminase-mediated biocatalytic reaction furnished regioisomer **37** by installation of an amine at the C6 position. This underwent spontaneous nucleophilic addition under acidic conditions to afford ring closure and the formation of a cyclic imine (**43**). Synthesis of piperidine **37** was completed by a diastereoselective reduction of the imine in a hydrogenation reaction [Scheme 22-A]. This chemoenzymatic route was expanded in order to access all four diastereomers of the piperidine by using a combination of (*R*)- or (*S*)- ω -TAM and imine reduction via hydrogenation or lithium aluminium hydride reduction [Scheme 22-B].

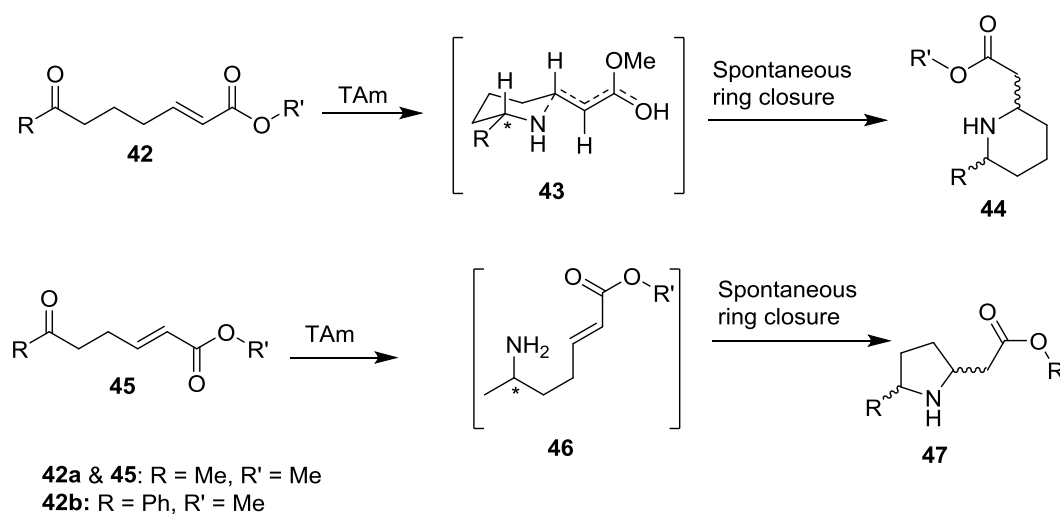


Scheme 22: Transaminase-catalysed synthesis of a 2,6-disubstituted piperidine by reductive amination of a diketone

5.2. Synthetic Plan For Transaminase-Mediated Aza-Michael Reaction

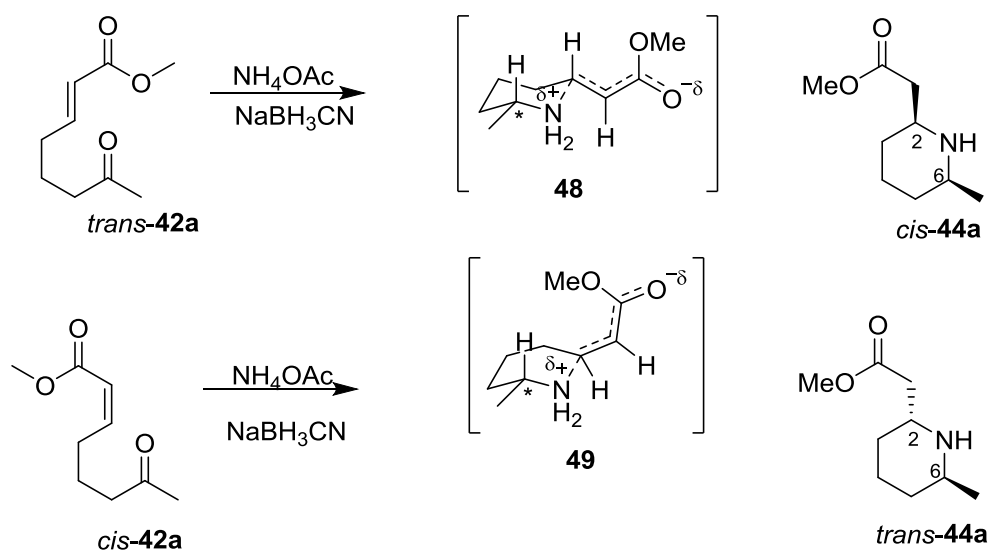
The chemoenzymatic strategy above is useful for the synthesis of dialkylated products such as **41**. However, an approach to access all four diastereomers with a pendant electron withdrawing group is a transaminase-mediated intramolecular aza-Michael cyclisation reaction. Use of an α,β -unsaturated ketoester substrate and spontaneous ring closure would allow for direct access to a myriad of single isomer cyclic amines.

Ketoesters **42** and **45** are examples of substrates where the ketone for transamination 4- or 5-carbon atoms away from the Michael acceptor respectively to facilitate the formation of 5- or 6-membered rings after transamination [Scheme 22]. To our knowledge, there is no literature precedence for a chemoenzymatic intramolecular aza-Michael reaction of this nature. There are examples of chemical reductive amination strategies to access the racemic diastereomers of piperidine **44** [59] but none for pyrrolidine **47**.



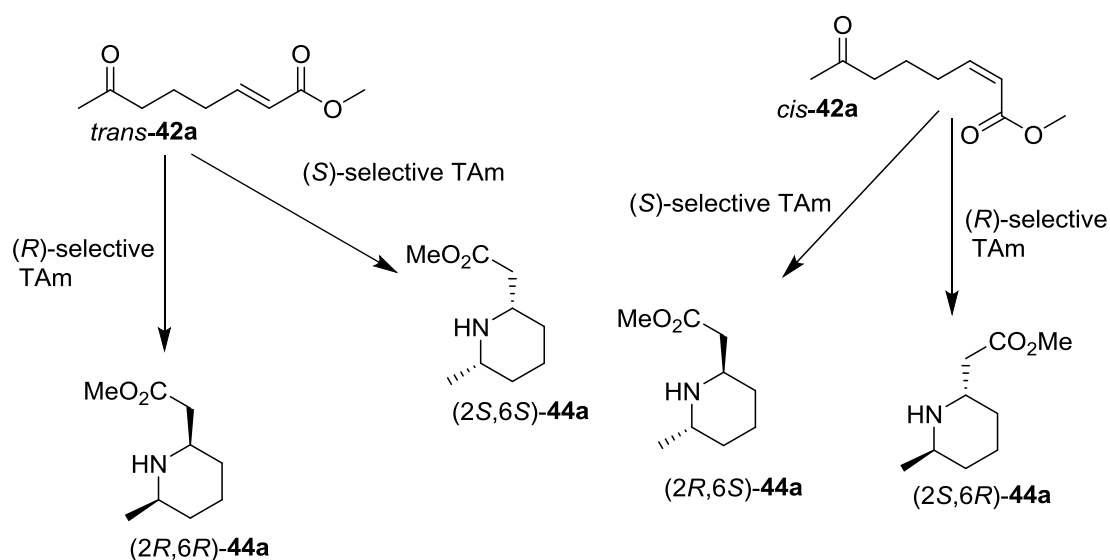
Scheme 22: Proposed transaminase-mediated one-pot synthesis of disubstituted piperidines and pyrrolidines

Banwell and co-workers investigated and confirmed the crucial role of double-bond geometry in controlling the diastereoselectivity of cyclisations in the chemical synthesis of piperidine **44a** [Scheme 22] [59]. They postulated transition state structures **48** and **49** to be the possible reasons for the observed diastereoselectivities as shown in scheme 23. A transaminase-mediated equivalent of this reductive amination offers more potential stereocontrol. By using (*S*)- or (*R*)-TAm, the stereochemistry at C2 can be controlled and after cyclisation will give a single isomer..



Scheme 23: The role of double-bond geometry in the control of diastereoselectivity in an intramolecular aza-Michael reaction ^[59]

The geometry of the substrate ketoester can enable access potentially to all four diastereomers of 2,6-disubstituted piperidines [Scheme 24] as the *trans*-ketoester (**42a**) will give the *cis*-piperidine (**44a**) and the *cis*-ketoester will give the *trans*-piperidine product.



Scheme 24: Transaminase-mediated synthesis of 2,6-disubstituted piperidine 44a may potentially access all four diastereomers

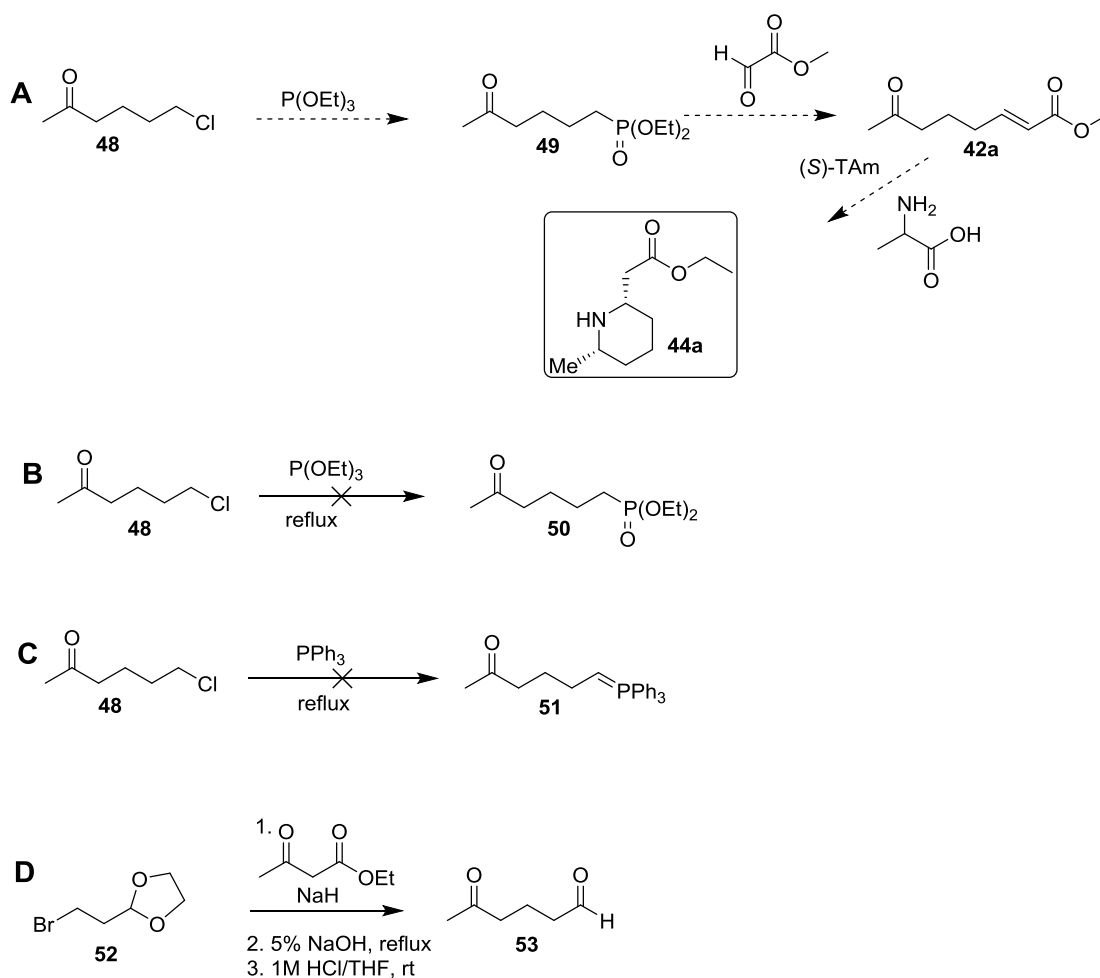
In addition to the possibility of increased control of diastereoselectivity, cyclisation of the transaminase amine product serves to solve one of the major drawbacks in reactions of this type, reaction equilibrium. By constantly cyclising and removing amines from the pool of possible reactants, the reaction becomes irreversible, thereby promoting 100% conversion in theory.

5.3. Synthesis of Methyl-7-oxooct-2-enoate

5.3.1. Michaelis-Arbuzov Reaction Approach

Synthesis of the unsaturated ketoester **42a** for use with transaminases was initially investigated following a Michaelis-Arbuzov reaction to transform alkyl halide **48** to its corresponding phosphonate ester **49** [Scheme 25-A]^[60]. This was in preparation for its use in a Horner-Wadsworth-Emmons olefination reaction to furnish ketoester **42a** in 2 steps. Phosphonate ester **49** was not formed in the reaction perhaps due to the poor reactivity of alkyl chlorides [Scheme 25-B]. A slightly different route was then explored incorporating a Wittig olefination. Synthesis of the requisite phosphorane precursor was attempted using the same alkyl halide **48**. However despite heating

this was unsuccessful again perhaps due to the poor reactivity of the chloride **48**. The corresponding bromide was not commercially available so an alternative approach was investigated.

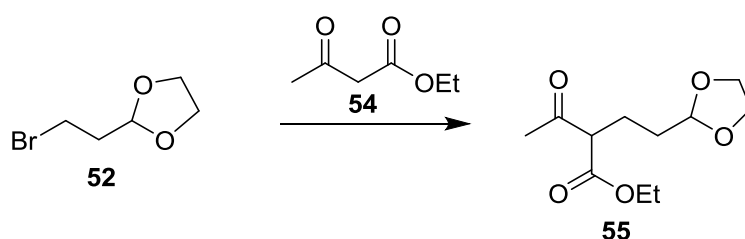


Scheme 25: (A) Initial plan for the synthesis of TAM substrate **42a and (B) Michaelis-Arbuzov reaction (C) Phosphorane synthesis for Wittig approach (D) Alkylation reaction in aldehyde synthesis for Wittig approach**

5.3.2. Optimisation of Alkylation Step

In this approach, bromodioxolane **52** was used in an alkylation reaction with ethyl acetoacetate followed by ester hydrolysis with aqueous sodium hydroxide and decarboxylation under acid conditions to furnish the 5-oxo-hexanal (**53**) [Scheme 25-D] ^[61]. The reaction was further optimised with alternative solvents and longer

reaction times [Table 16]. Three different bases were tested (sodium hydride (60%), sodium ethoxide and caesium carbonate) to find the most favourable reaction conditions based on the isolated yields of **55**. When using sodium hydride several side products were formed possibly due to deprotonation at C4 as well as C2 or the base behaving as a nucleophile ^[62]. Another attempt using the non-nucleophilic base, lithium diisopropylamide (LDA) as described in the literature, was unsuccessful as no product was observed by thin layer chromatography (TLC) due to possible deprotonation at C4.



Scheme 26: Alkylation of bromodioxolane 52

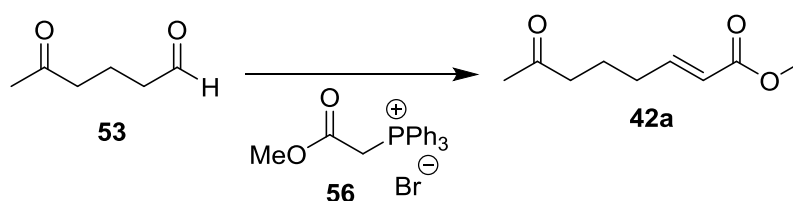
Table 16: Optimisation of Alkylation Reaction

Reaction conditions	Yield/ %
NaH, THF, reflux, 18 h	19
NaH, PhMe, reflux, 18 h	8
NaOEt, THF, reflux, 20 h	21
NaOEt, EtOH, reflux, 72 h	62
CsCO ₃ , MeOH, reflux, 20 h	5
CsCO ₃ , MeCN, reflux, 72 h	65

Sodium ethoxide and caesium carbonate were subsequently screened in different solvents with more success [Table 16]. Ultimately, the use of longer reaction times with either base in anhydrous ethanol or acetonitrile gave the alkylation product **55** in moderate yield (62-65% yield). Ester hydrolysis of **55** under basic conditions then decarboxylation at room temperature yielded 5-oxohexanal (**53**).

5.3.3. Optimisation of Wittig Step

Olefination and installation of the electron withdrawing group that would facilitate the amine-mediated cyclisation was achieved via a Wittig reaction [Scheme 27]. Using a methyl ester Wittig reagent, various reaction conditions were investigated to optimise the yield and stereoselectivity of the reaction to give *cis*- or *trans*-**42a** [Table 17]. To enhance the green chemistry credentials of the project, water-based Wittig reactions were also investigated.



Scheme 27: Wittig olefination reaction

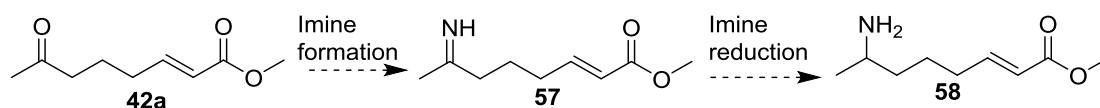
Table 17: Optimisation of Wittig Reaction

Reaction Conditions	% Yield (<i>E/Z</i> ratio)
56 , NaOH, H ₂ O, 80 °C	27 (80:20)
56 , NaOH, THF, reflux	34 (95:5)
56 , NaOH, H ₂ O, 20 °C	65 (80:20)
CH ₂ Cl ₂ , r.t. (phosphonium ylide)	68 (90:10)

Reaction temperature appeared to make a difference to yields when water was used as the reaction medium. The *E/Z* ratio however remained unchanged in both of those reactions. This may be due to a lack of solubility of the Wittig reagent in water preventing complete consumption of the aldehyde substrate. Using dichloromethane as reaction medium at room temperature gave slightly higher yields than water and with a higher *E/Z* ratio. Since the difference in yield was only marginal, the water-based Wittig reaction was chosen to be ideal for the project. An *E/Z* ratio of 80:20 also allowed for a substantial amount of *cis*- and *trans*-ketoester to be produced for the subsequent aza-Michael reaction investigations.

5.4. Chemical Synthesis of Methylpiperidine 44a

Synthetic routes were explored to the non-cyclised primary amine intermediate **58** [Scheme 28] to study the cyclisation to piperidine **44a**. Synthesis of the corresponding imine was therefore attempted under reported reaction conditions ^[63] [Table 18].



Scheme 28: Imine synthesis to facilitate trapping of amine precursor to piperidine 44a

Table 18: Reaction conditions non-cyclised primary amine 58

Reaction Conditions	% Yield
2M NH ₃ in EtOH, Ti(OEt) ₄ , 18 h	No reaction
Zn, NH ₄ OAc, NH ₃ , 18 h	No reaction

When using ammonia and titanium (IV) ethoxide as the reducing agent, neither the amine nor its precursor imine was observed to have formed. The same outcome was observed when ammonium acetate and ammonia was used with zinc powder. It was then decided to not attempt to form the amine but to go directly to the piperidine using the conditions employed by Banwell *et al* (as discussed in section 5.1). These were replicated to furnish both diastereomers of 2,6-disubstituted piperidine **44a** from the pure isomers of their precursors.

5.5. Analytical Methods

Obtaining the target piperidine (**44a**) by chemical synthesis and its spectral analysis (based on data from Banwell *et al* [59]) provided a basis for its subsequent biocatalytic synthesis as the chemical product was used as a standard. Firstly confirmation of the position of the protons at the C α position by ^1H NMR spectroscopy allowed for *cis*- and *trans*-**44a** to be readily identified after extraction of the product from the reaction medium.

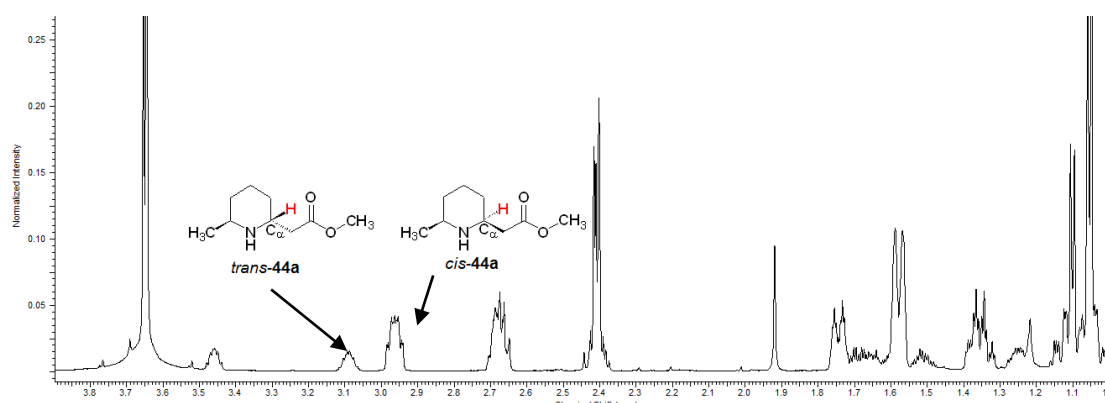


Figure 32: ^1H NMR spectrum of mixed *cis*- and *trans*-**44a**, showing the variation in chemical shifts of the protons at the C α position

For a high-throughput analytical approach however, the retention times of unsaturated ketoester substrates *cis*- and *trans*-**42a** and the product piperidine (**44a**)

were investigated by HPLC. On a standard C18 reverse phase column (250 mm, 4.6 mm, 5 μ m), the retention times of all three analytes were distinct with clear baseline separation [Figure 33]. One major drawback however was the need for relatively long run-times to allow for full separation of the peaks and re-equilibration of the column after each run. Under the conditions employed (35% acetonitrile (0.1% TFA):65% H₂O (0.1% TFA), 1 mL/min, 218 nm) *cis*-**42a** had a retention time of 14.5 min and *trans*-**42a** was 15.6 min, whilst **44a** was detected at 19.2 min. In addition, the limit of detection (LOD) on the HPLC was found to be in the hundred micromolar range (150 μ M) which would prove problematic for a microliter-scale high-throughput screen where analyte concentrations may be as low as 100 μ M due to poor enzyme activity.

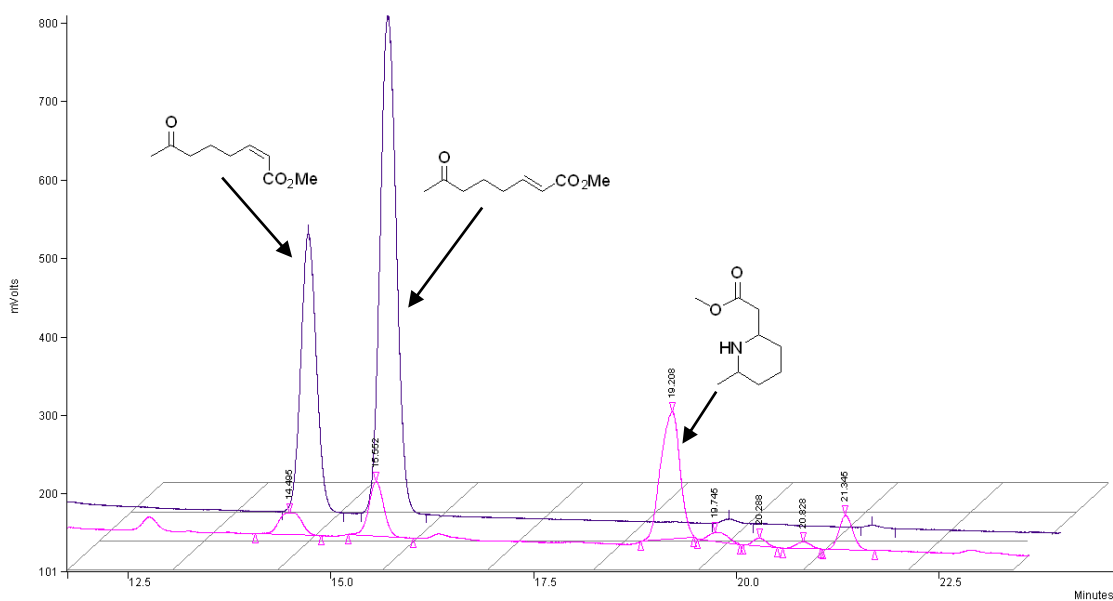


Figure 33: Non-chiral HPLC traces of *cis*- and *trans*-42a (Blue) and methylpiperidine 44a (Red)

In order to improve on these run times and low LODs, other chromatographic methods were also investigated. Gas chromatography-mass spectrometry (GC-MS) was chosen as a suitably fast analytical method with wide applicability in small molecule analysis and an LOD of 100 picomolar. A major benefit in using a gas

mobile phase as opposed to a liquid mobile phase is a significant reduction in run-time, allowing for quicker sample analyses. The additional mass spectrometry functionality provides an extra peak validation. Under the conditions (column: Trace PLOT TG-BOND U, FID: 245 °C, inlet temperature: 200 °C, carrier gas: helium, and 150 °C hold for 12 min) unsaturated ketoesters *cis*- and *trans*-**42a** had retention times of 8.5 min and 9.0 min respectively [Figure 34-A]. Piperidine **44a** however had a retention time of 10.2 min [Figure 34-B].

Each of the peaks at the aforementioned retention times was accompanied by the expected mass value under positive chemical ionisation (CI+) [Figure 34-C&D]. Gas chromatography-mass spectrometry was found to work very well for clean analytes that are isolated and purified pre-injection. The sample preparation steps involved in this approach were more time consuming and labour intensive however compared to reverse phase HPLC. GC-MS required multiple rounds of extraction of the organic analytes from a reaction mixture (chemical or biocatalytic) using organic solvents (CH₂Cl₂, MeOH 9:1). This was then followed by drying of the combined organic layers using MgSO₄ and removal of the organic solvent *in vacuo*. For enhanced sensitivity in some cases the crude product had to be purified by silica flash chromatography.

This approach was therefore not feasible for a high-throughput screen. In addition, the ultra-low LOD of GC-MS made saturation of the detector and blockages of needles and columns a common occurrence when handling multiple aqueous biotransformation reaction samples. In spite of meticulous filtration and organic extraction of samples it was difficult to completely eliminate particulates from injected samples.

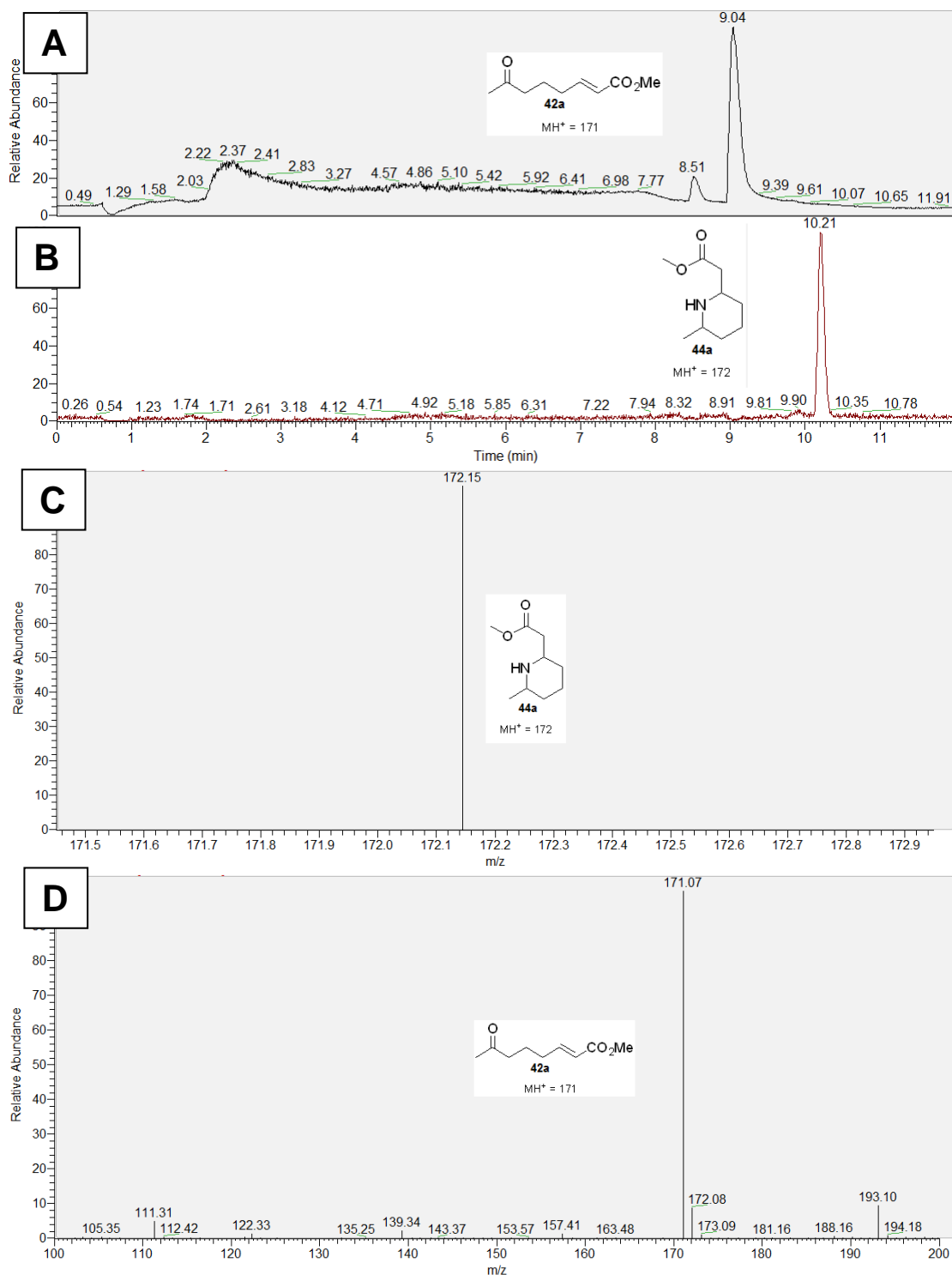


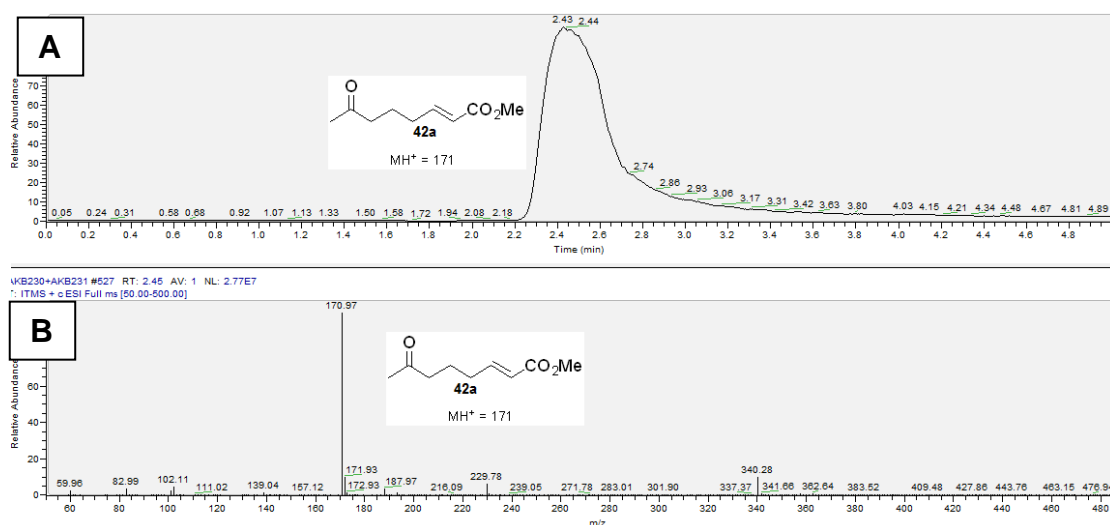
Figure 34: GC-MS traces of (A): chromatogram of *cis*- and *trans*-42a, (B): chromatogram of piperidine 44a, (C) mass peak of piperidine 44a and (D) mass peak of 42a

It was suggested that an ion trap liquid chromatography mass spectrometry (LC-MS) method might provide a solution to the GC-MS problem by shortening the sample preparation time (aqueous samples can be injected and a guard column installed)

whilst still providing the same added level of analytical mass spectrometry data. The LOD of this device was also found to be in the picomolar region which allowed for sample dilutions of up to a 100 times, in order to prevent the accumulation of particulates on the column and in the solvent tubes.

In addition to a reduced sample preparation time, the sample running time was also significantly reduced from 12 minutes on the GC-MS to 5 minutes on the ion trap LC-MS. This finally allowed the sample analysis timescale to approach a high-throughput level of efficiency as it combined a short sample preparation procedure (dilution of reaction sample in methanol (x 50) and then microfiltration) with an even shorter sample run-time (5 min). Under the conditions (Hypersil Gold PFP (150 x 2.1 mm, 5 μ m), 15% MeCN (0.01% formic acid):85% H₂O (0.01% formic acid), 0.3 mL/min) ketoester *trans*-**42a** had a retention time of 2.4 min whilst methylpiperidine *cis*-**44a** had a retention time of 1.8 min [Figure 35].

Having established an analytical method for the rapid detection of both the ketoester substrate **42a** and the piperidine product **44a**, an investigation in to the transaminase-mediated intramolecular aza-Michael synthesis of cyclic amines was conducted.



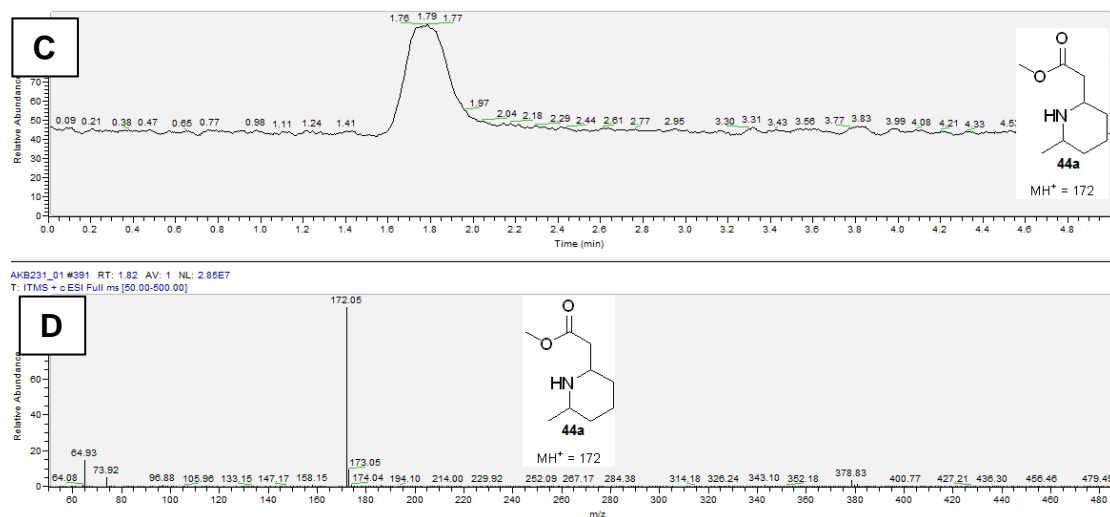
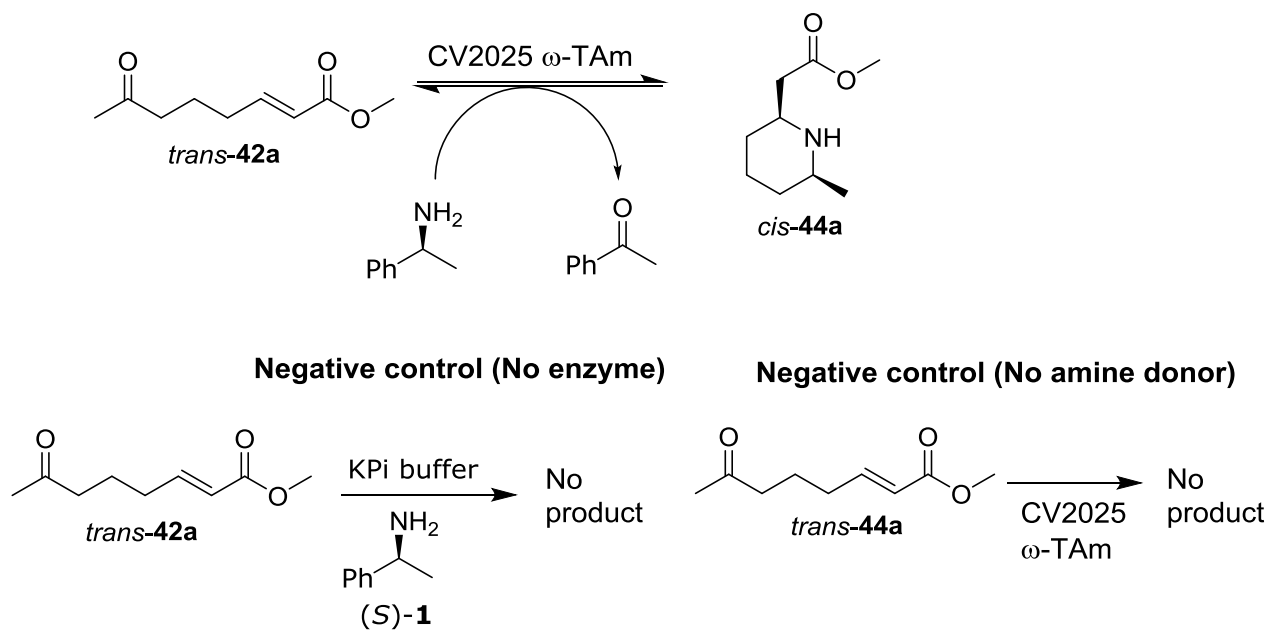


Figure 35: Linear ion trap LC-MS traces showing (A): Chromatogram of ketoester 42a. (B): Mass peak of ketoester 42a. (C): Chromatogram of piperidine 44a. (D): Mass peak of piperidine 44a

5.6. Biocatalytic Synthesis of Methylpiperidine 44a

Initial attempts towards the biocatalytic synthesis of piperidine **44a** employed amine donors (S)-MBA (**1**) and isopropylamine (**11**) with the enzyme CV2025 ω -TAm [Scheme 29]. The amines were used with unsaturated ketoester *trans*-**42a** and the reactions tested in a small-scale time-course experiment, monitoring conversion yields by ion trap LC-MS.



Scheme 29: TAM-mediated synthesis of 2,6-disubstituted piperidine 44a

Following several rounds of method optimisation to allow for the detection of all four components of the transamination reaction, it was necessary to increase the run-time to 16 min. Under the new conditions (10% MeCN (0.01% formic acid):80% H₂O (0.01% formic acid), 0.2 mL/min) ketoester **42a** had a retention time of 13.8 min, and piperidine **44a** at 2.5 min [Figure 36].

A calibration curve of piperidine **44a** was then run on the LC-MS in order to determine the concentration of the cyclic amine produced in the time-course biotransformation reactions [Figure 37].

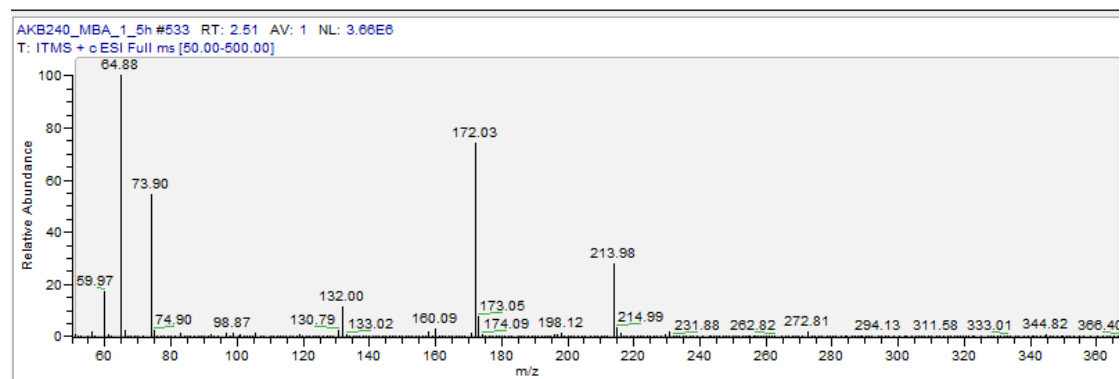
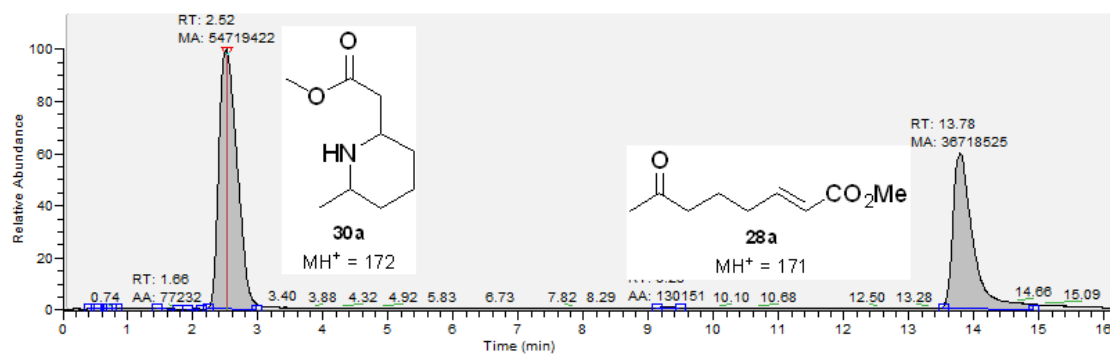


Figure 36: Optimised ion trap LC-MS method for the detection of all components of transaminase reaction in scheme 29

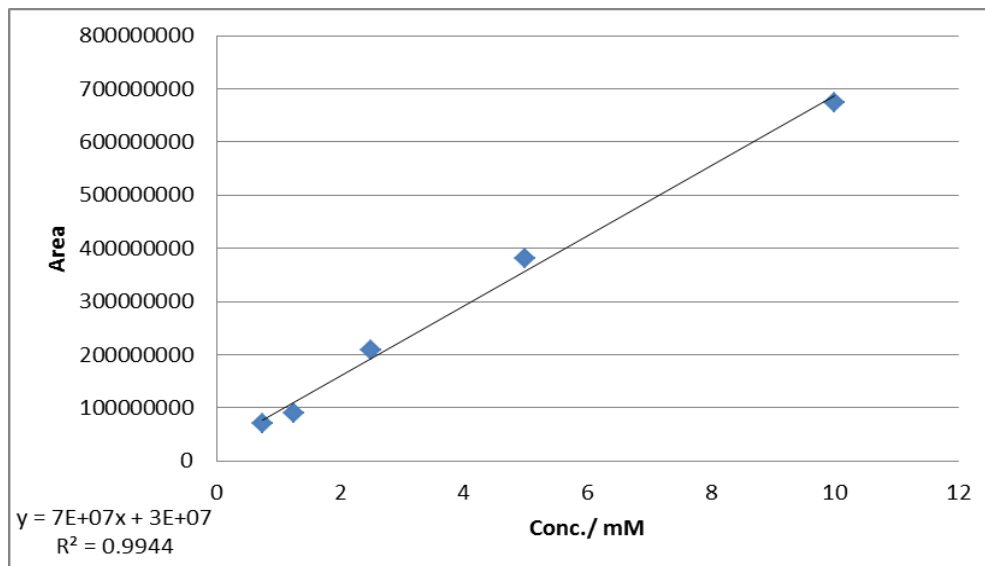


Figure 37: Calibration curve of methylpiperidine 44a on the ion trap LC-MS

Results from comparative time-course studies using the amine donors (S)-1 and 11 revealed small variations in rates of reaction but a similar trend in reaction profile

[Figure 38]. Isopropylamine appeared to be approximately twice as fast as (S)- α -MBA over the first 2 h, after which the two rates levelled off to 44% and 40% conversion yield respectively after 4 h.

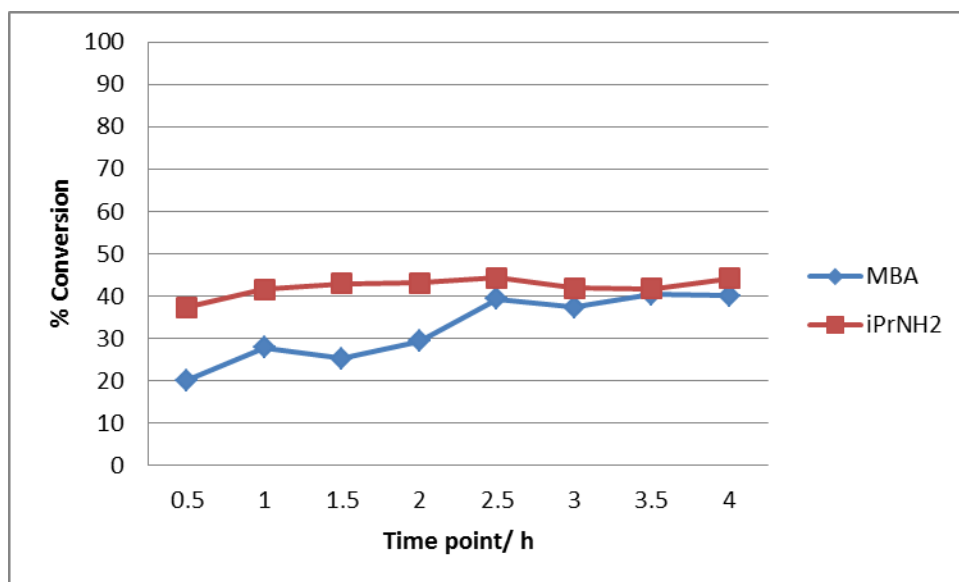


Figure 38: Ion trap LC-MS results from comparative time-course TAm-mediated synthesis of 44a using (S)- α -MBA (Blue) and isopropylamine (Red)

Conditions: CV2025 (0.1 U), PLP (1 mM), potassium phosphate buffer (100 mM, pH 7.5), *trans*-**42a** (10 mM), (S)- α -MBA (100 mM), *i*-PrNH₂ (1000 mM), 30 °C, reaction volume (1 mL), DMSO (5% v/v).

A possible explanation for the comparatively faster rate in the isopropylamine reaction is due to its higher concentration in the reaction medium (1000 mM) compared to that of (S)- α -MBA (100 mM). Increasing the concentration of (S)- α -MBA beyond 100 mM begins to have an inhibitory effect on transaminases [15]. Isopropylamine however has no such inhibitory role but instead a higher concentration improves reaction dynamics and drives the reaction towards amine synthesis. The advantage of higher isopropylamine concentration is however lost over 2 h as both reactions enter a possible steady state.

Later time points show a slow decrease in product (piperidine **44a**) concentration from 43% to 26% in the (S)- α -MBA reaction and 51% to 35% in the isopropylamine

reaction [Figure 39]. This is perhaps due to a change in reaction dynamics allowing for the reverse reaction to take place as the amine product (**44a**) is consumed.

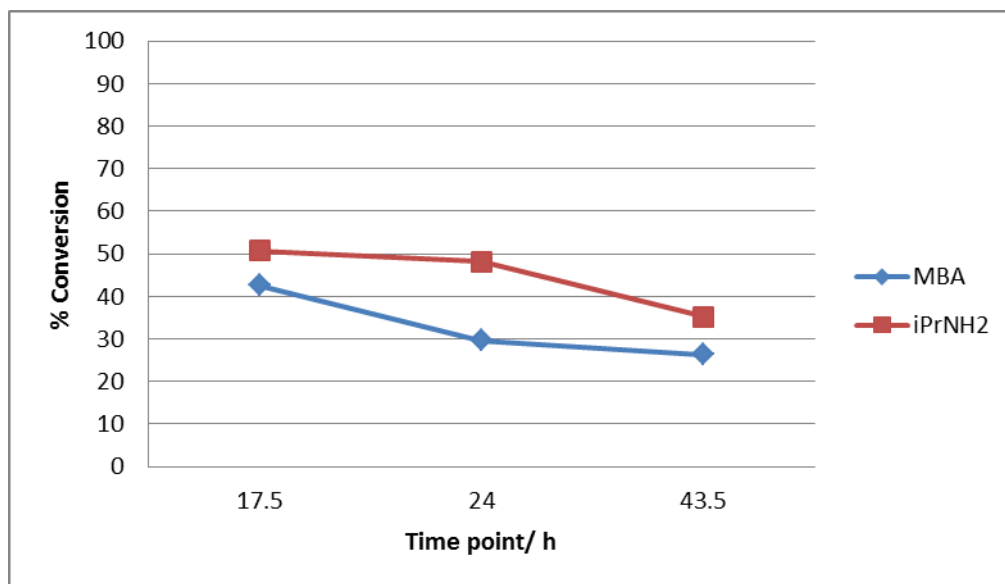


Figure 39: Ion trap LC-MS results from comparative time-course TAm-mediated synthesis of **44a using (S)- α -MBA (Blue) and isopropylamine (Red) after overnight reaction**

This was an unexpected outcome as the cyclisation of the transaminase reaction product (possibly amine **58** although it was never isolated) was expected to occur spontaneously as observed in the chemical synthesis of **44a**. One major advantage of a spontaneous cyclisation is the removal of free amines from the reaction mixture causing an equilibrium shift towards product formation. In theory therefore the forward reaction will be favoured and the reaction will reach completion if the aza-Michael ring closure happens. Observing a decrease in product over time therefore suggested this may not be the case and in fact spontaneous ring-closure does not occur, at least not at a high enough rate to overcome the reverse reaction.

It was speculated that perhaps the high-throughput analytical methods that had been tested were inherently unable to differentiate between cyclised and non-cyclised product as they have the same mass (171 g/mol). Also, without a chemical standard

of amine **58** to determine its chromatographic retention times, it was unclear as to whether there would be a noticeable difference between the two products under any of the screening methods employed thus far.

To confirm piperidine **44a** as the product formed in the transaminase reaction in scheme 29, the reaction was scaled up to 20 mL and the crude product analysed by ^1H NMR spectroscopy [Figure 40]. The requisite protons at $\text{C}\alpha$ were present in the spectrum along with all the other expected peaks for piperidine **44a**. No peaks corresponding to the non-cyclised amine **58** was observed however, suggesting that all the starting material that had been consumed was converted to piperidine **44a** or another hitherto unanticipated adduct.

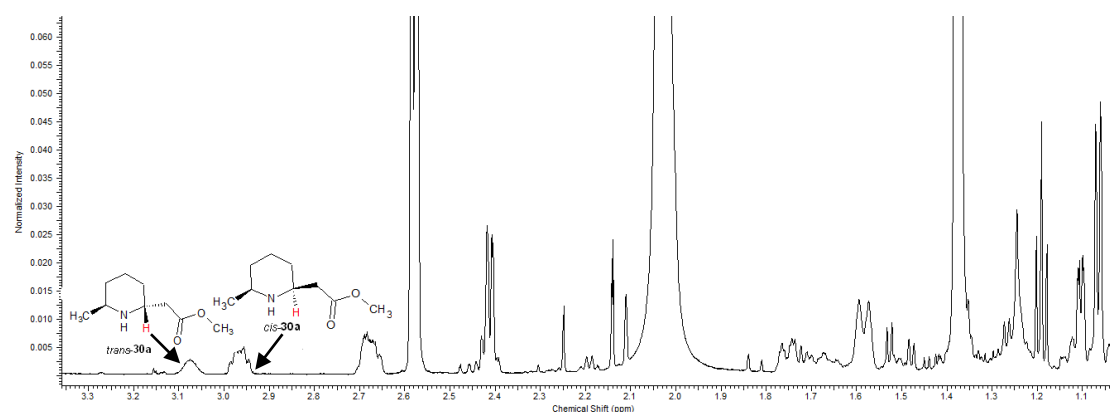


Figure 40: ^1H NMR spectrum of the crude product from TAM-mediated synthesis of piperidine **44a** showing the *cis*- and *trans*- protons at $\text{C}\alpha$ starting from a mixture of *cis*- and *trans*-**42a**

Attempts to purify the biotransformation product (**44a**) proved unsuccessful under the conditions used for the purification of the chemical standard. A combination of the large excess of amine donor used in the TAM reactions, the presence of buffer salts and other components from bacterial cell debris made extraction and purification of the crude product challenging. The difficulty in purifying amines by silica flash

chromatography (due to streaking and a tendency to not elute from the column) ensured that piperidine **44a** was never cleanly isolated from a TAm reaction.

In spite of this, further confirmation of the validity of the TAm reaction product was sought through a repeat of the reactions in scheme 29 and the use of another chromatographic analysis method. Ultra high-performance liquid chromatography (UPLC), an LC device able to reach pressures of up to 100 MPa, combined with a mass spectrometer was able to give similar results to the ion trap LC-MS. The device was set up to conduct selected ion monitoring (SIM) in order to improve sensitivity to the analytes. Methylpiperidine **44a** was found to have a retention time of 0.5 min, confirmed by its mass spectrum [Figure 41].

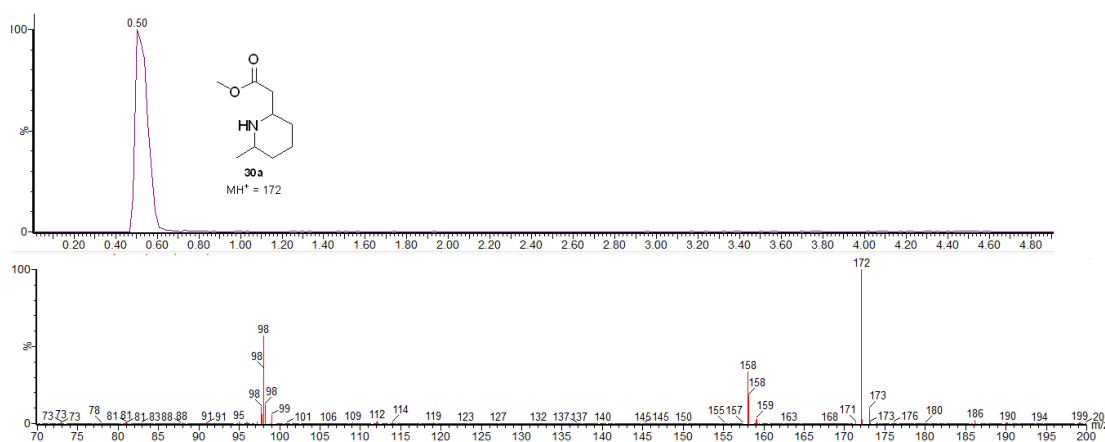


Figure 41: UPLC-MS trace chromatogram of methylpiperidine 44a chemical standard

UPLC-MS analysis of a transaminase-mediated synthesis of piperidine **44a** also showed a peak within the same region as the chemical standard and a mass fragment peak of 172 (MH^+) [Figure 42].

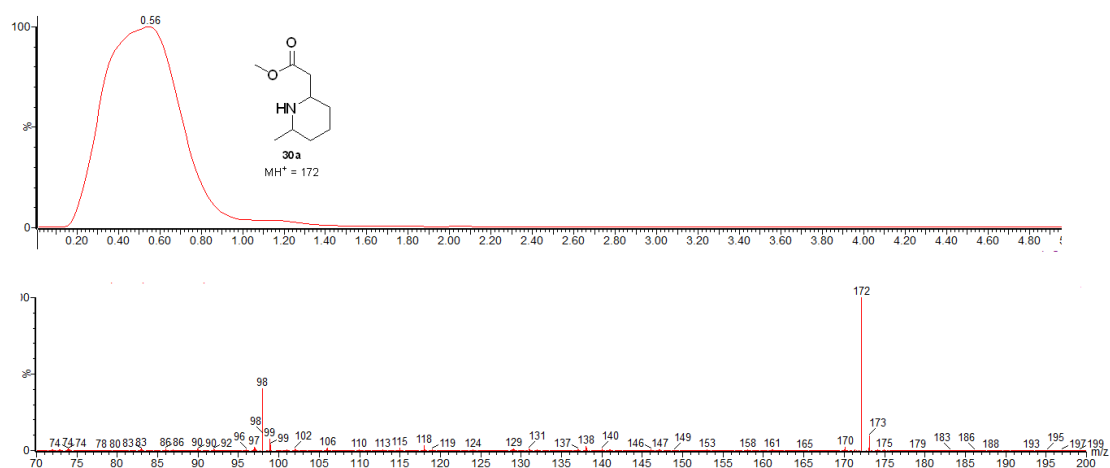


Figure 42: UPLC-MS trace chromatogram of methylpiperidine 44a from a TAM-mediated synthesis

Conditions: CV2025 (0.1 U), PLP (1 mM), potassium phosphate buffer (100 mM, pH 7.5), *trans*-42a (10 mM), *i*-PrNH₂ (1000 mM), 30 °C, reaction volume (1 mL), DMSO (5% v/v).

5.7. Design of Experiment (DoE) Studies

A maximum conversion yield of 51% in the reaction in scheme 29 was below what was envisaged, particularly as the aza-Michael reaction will shift the equilibrium towards formation of the amine. Attempts were therefore made to optimise the reaction. Using a DoE approach, various reaction parameters were investigated in order to ascertain the best possible combination of conditions. A total of five parameters were investigated in parallel with two experimentation levels [Table 19]. Using typical reaction conditions reported in the literature [58] and the previously tested conditions [Figure 42] as a mid-point, new reaction conditions were selected to give lower yields (Low) and others to give higher yields (High) [Table 19]. This was in order to observe decreases as well as increases in conversion yields compared to the previous results obtained [Figure 38] to better understand key reaction parameters. The best performing combination of parameters would then be chosen to go through a second round of DoE.

Table 19: First Round of DoE Studies

Parameters	High	Low
Enzyme	0.12 U	0.07 U
Amine	50 eq	5 eq
pH	8.5	7.5
PLP	1.5 mM	0.5 mM
Temperature	35 °C	25 °C

Conditions: Ketoester **42a** (10 mM), (S)- α -MBA (50 mM or 500 mM).

A calibration curve was run in order to quantify the peak area of a range of concentrations of the product piperidine **44a** [Figure 43]. Based on this calibration, results from the DoE reactions were analysed by UPLC-MS.

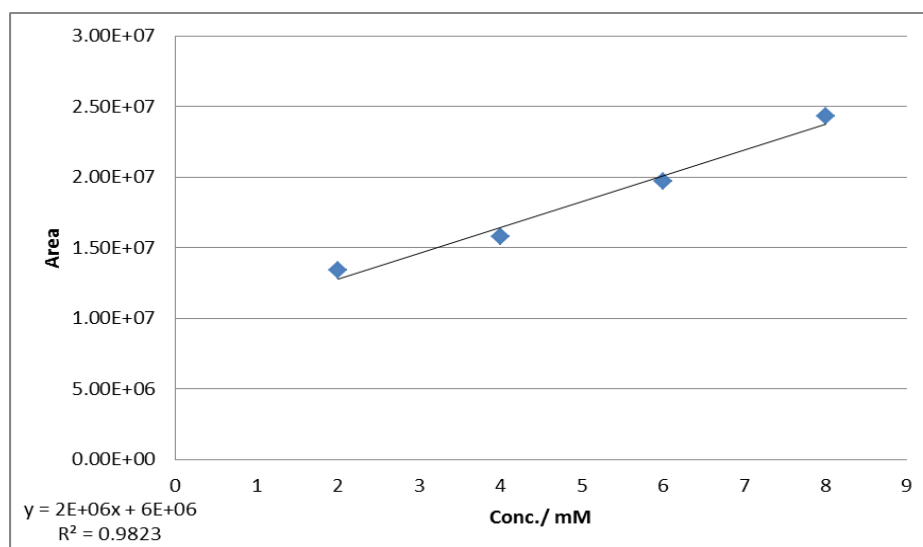
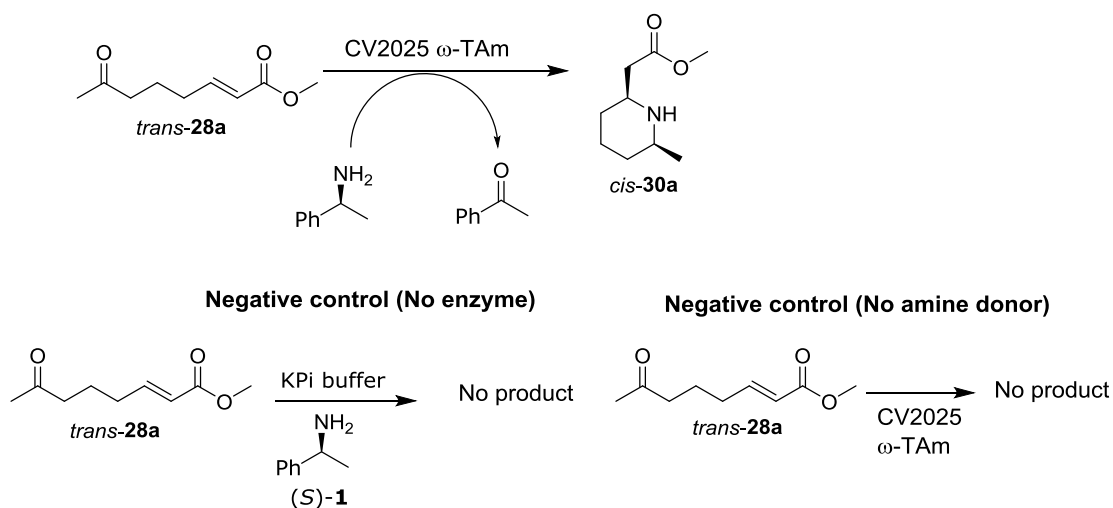


Figure 43: Calibration curve of methylpiperidine **44a** on the UPLC-MS

A total of thirty-two 300 μ L reactions were run over a 24 h period [Scheme 30], quenched with HCl (1 M) and analysed by UPLC-MS. Negative controls for each of the thirty two reactions were also run with no product detected in any of them.



Scheme 30: Reaction scheme used in DoE

Using the freeware programme Design-Expert (V8.0.6.1), the conversion yields were collated and analysed to produce a probability distribution plot [Figure 44] showing a set of eight reactions outside the mean. All the reactions from the first round of DoE experiments showed poor conversion yields (up to 12%) [Table 20] compared to the 51% previously determined [Figure 38]. This was a feature of the DoE study as the reaction conditions were purposely chosen to be sub-optimal so as to observe the impact of changing each parameter separately. The results implied that the parameters had varying degrees of influence on the overall outcome of the reaction [Table 20]. As expected, a higher enzyme loading resulted in better conversion yields. The highest conversion yields also had ten times more amine donor present. Reaction pH and PLP concentration had little impact on conversion yield.

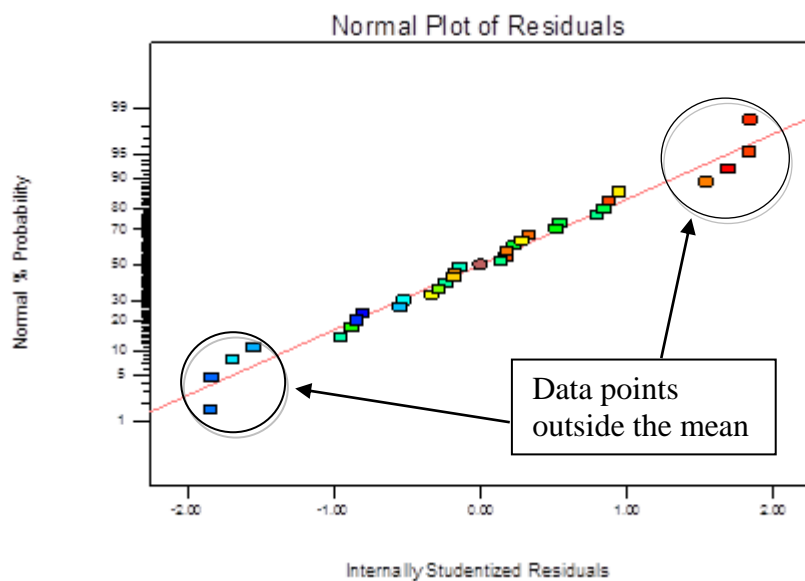


Figure 44: Probability distribution plot of DoE results across 32 reactions

Table 20: “Best” and “Worst” Conditions from the First Round of DoE

Best conditions	Conversion yield/ %
0.12 U, 50 eq, pH 7.5, 1.5 mM PLP, 25 °C	12
0.12 U, 50 eq, pH 8.5, 0.5 mM PLP, 25 °C	12
0.12 U, 50 eq, pH 8.5, 1.5 mM PLP, 25 °C	12
0.12 U, 50 eq, pH 7.5, 0.5 mM PLP, 25 °C	11
Worst Conditions	
0.07 U, 5 eq, pH 7.5, 1.5 mM PLP, 35 °C	0
0.07 U, 5 eq, pH 7.5, 0.5 mM PLP, 25 °C	0
0.07 U, 5 eq, pH 8.5, 1.5 mM PLP, 35 °C	0
0.07 U, 5 eq, pH 7.5, 0.5 mM PLP, 25 °C	0

This was not surprising as TAM already has PLP in its active site. There have however been reports of the inhibitory effects of excess PLP (>3 mM) [16]. As

discussed in section 2.7. Table 8, CV2025 ω -TAm is active across a range of pH values. Its optimum pH is pH 7.5 but it does however remain very active above pH 8.

The effect of temperature on the overall yield in this study also revealed a moderate impact. Overall, 25 °C gave better conversion yields than 35 °C in reactions where enzyme activity and amine donor concentration was already at a preferred level. When paired with enzyme activity and amine donor concentrations that are not conducive to the reaction proceeding however, the temperature made no significant difference.

This first round of DoE investigation highlighted enzyme activity and amine donor concentration to be the most crucial of all the parameters when considering conversion yield after 24 h. These observations were taken in to account in the design of a second round of DoE to investigate increasing conversion yield beyond what had been achieved. The upper levels of two parameters from the first round of DoE (amine equivalence and PLP concentration) were used as mid-point values around which the new “high” and “low” levels were selected for the second round. The upper level of enzyme loading from the first round was chosen to be the lower level in this second round and the new high level was chosen to be 0.15 U/mg. Transaminase enzymes are prone to substrate and/or product inhibition ^[16-17], it is therefore possible that although 5 eq of amine donor was too low to drive the reaction towards the amine product, perhaps 50 eq was so high as to be inhibitory. This made investigating a lower level than the previous round all the more crucial.

Table 21: Second Round of DoE Studies

Parameters	High	Low
-------------------	-------------	------------

Enzyme	0.15 U/mg	0.12 U/mg
Amine	100 eq	25 eq
pH	8.5	7.5
PLP	2 mM	1 mM
Temperature	30 °C	25 °C

Conditions: Ketoester **42a** (10 mM), (S)- α -MBA (250 mM or 1 M).

The upper level of amine donor equivalence was chosen to be 100 eq since this has been reported to be used with other TAMs ^[37b]. The PLP concentrations was chosen to be 1 mM and 2 mM, covering both the typical literature value as well as twice this to further explore what impact, if any, this will have within the new context of reaction parameters. The temperature and pH values remained unchanged due to the fact that their optimal ranges were already covered in the first round of DoE.

Another thirty-two 300 μ L scale reactions were run over a 24 h period, quenched and analysed in the same way as the previous round of experiments. The probability distribution plot [Figure 35] appeared distinctly different from the previous round with regards to the distribution range. It was indicative of a plateauing of outcomes as a number of the parameters appeared to be within their upper limits. The number and degree of outliers were significantly reduced compared to the previous round and there was only one distinctly high yielding reaction.

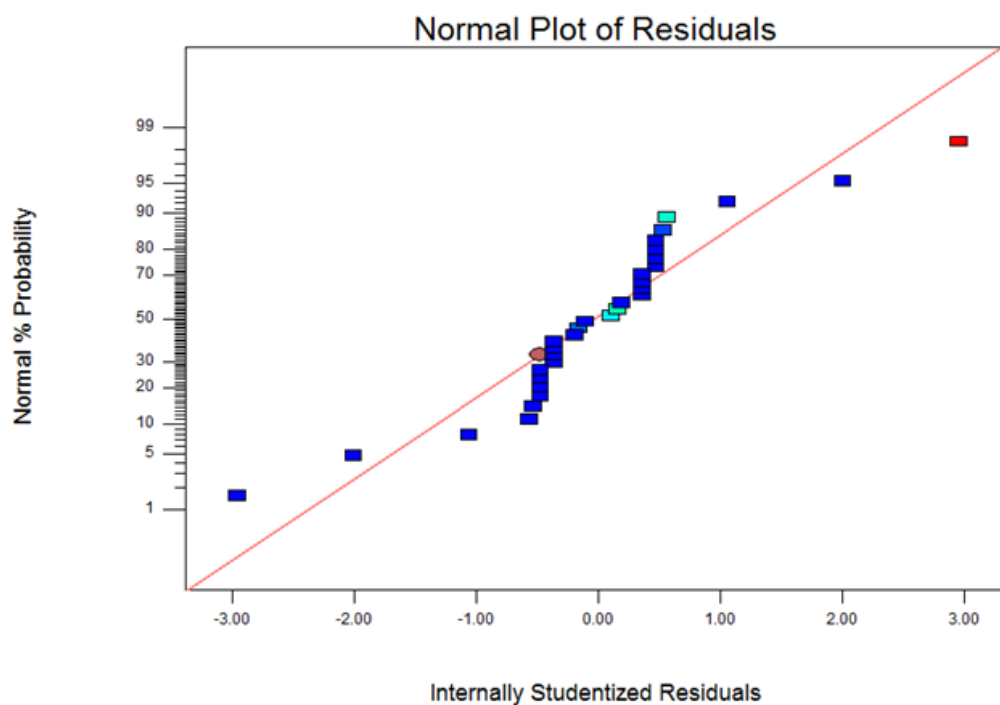


Figure 45: Probability distribution plot of second round of DoE reactions

The conversion yields of all thirty-two experiments and negative controls were calculated from the UPLC-MS retention time peak areas of piperidine **44a** [Figure 42]. These were converted to concentration values using the equation of line of best fit from the calibration curve ($y = 2E+06x + 6E+06$) [Figure 43]. A percentage conversion yield was then calculated based on a starting material (**42a**) concentration of 10 mM [Table 22].

Table 22: The “Best” Conditions from the Second Round of DoE

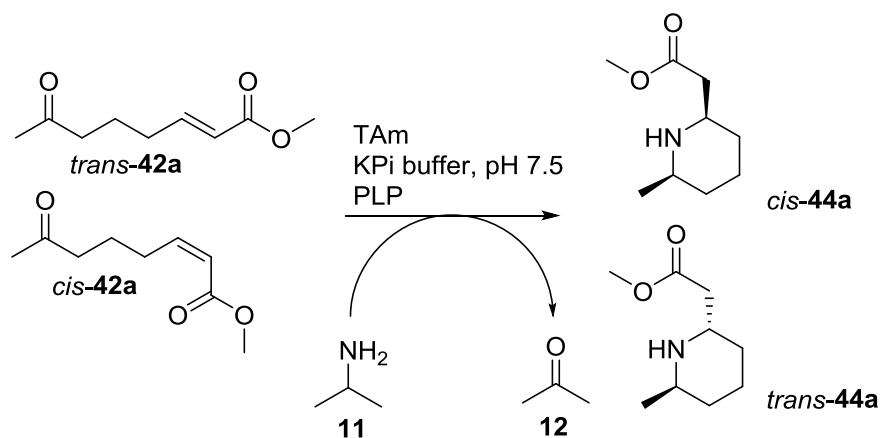
Conditions	Peak Area	[Prod]/mM	Conversion yield/ %
0.15 U, 25 eq, pH 7.5, 2 mM, 30 °C	22881500	8.44	84
0.12 U, 25 eq,, pH 7.5, 1 mM, 30 °C	11347150	2.67	27
0.12 U, 25 eq,, pH 7.5, 2 mM, 25 °C	11015100	2.51	25
0.12 U, 25 eq,, pH 7.5, 2 mM, 30 °C	9955800	1.98	20

Substrate ketoester **42a** concentration: 10 mM

A list of the four highest-yielding reaction parameters suggested that a lowering of the amine donor equivalents from 50 eq [Table 20] to 25 eq [Table 22] when coupled with an increase in enzyme-loading (0.15 U/mg) provide the best conditions for this biotransformation. Along with a pH of 7.5, PLP concentration of 2 mM and a reaction temperature of 30 °C, an 84% conversion yield was obtained. This was the highest observed yield of 2,6-disubstituted piperidine **44a** produced. When taken alongside the first DoE results, it suggests that an (S)- α -MBA equivalence of 50 is perhaps inhibitory over a 24 h period, which allows for only a limited conversion of ketone substrate compared to 25 equivalents. These conditions can now be applied in future to scale-up a TAM-mediated synthesis of piperidine **44a** from its ketoester precursor **42a** using 25 equivalents of (S)- α -MBA as amine donor.

5.8. Screening of Ketoester **42a** Against Novel TAMs

The TAM-mediated synthesis of piperidine **44a** was subsequently extended to include the panel of novel ω -TAMs previously selected for 1 L scale fermentation. These were: BSU_402, KpN_00799, BSU_1971, and PP_3718. Three other previously discovered ω -TAMs were included in the screening, CV2025^[18], VF_JS17^[15], and ArRMut11, the (*R*)-selective *Arthrobacter* sp. mutant used by Merck & Co in the synthesis of Sitagliptin^[37b] [Chapter 1.7.2]. Both *cis*- and *trans*-**42a** were screened against the panel of enzymes [Scheme 31] yielding very interesting results with regards to enzyme preferences towards the two isomers of **42a**. Isopropylamine (**11**) was used as amine donor at pH 7.5 and the product piperidine **44a** was analysed by reverse phase HPLC. Once again, there was no uncyclised amine detected and the background control reactions showed no product.



Scheme 31: Biocatalytic synthesis of *cis*- and *trans*-44a** from their respective ketoester **42a** isomers**

A calibration curve of piperidine **44a** was run on a reverse phase HPLC C18 column [Figure 46] and the data used to interpret the results of the screening. Non-chiral HPLC analysis showed that both *cis*- and *trans*-**44a** had the same retention time (8.9 min). Based on previous ^1H NMR spectroscopy data however [Figure 40] it was assumed that *cis*-**42a** produces *trans*-**44a** and *trans*-**42a** produces *cis*-**44a**. The results show a wide variation in substrate affinity across the six enzymes that were tested [Table 23]. There were small variations in conversion yield of *cis*- and *trans*-**44a** within each enzyme. The majority of the ω -TAmS showed preference for *trans*-**42a** and therefore produced *cis*-**44a** [Figure 47].

The ω -TAmS CV2025, VF_JS17, KpN_00799, and PP_3718 all showed higher affinity for *trans*-**42a**, whilst the two *B.subtilis* ω -TAmS (BSU_402 and BSU_1971) along with the *Arthrobacter* sp. mutant (ArRMut11) showed higher affinity for *cis*-**42a** [Figure 5.16]. BSU_1971 showed the highest level of substrate conversion across the two isomers (93% *trans*-**44a** and 84% *cis*-**44a**) whilst ArRMut11 showed the lowest (25% *trans*-**44a** and 12% *cis*-**44a**).

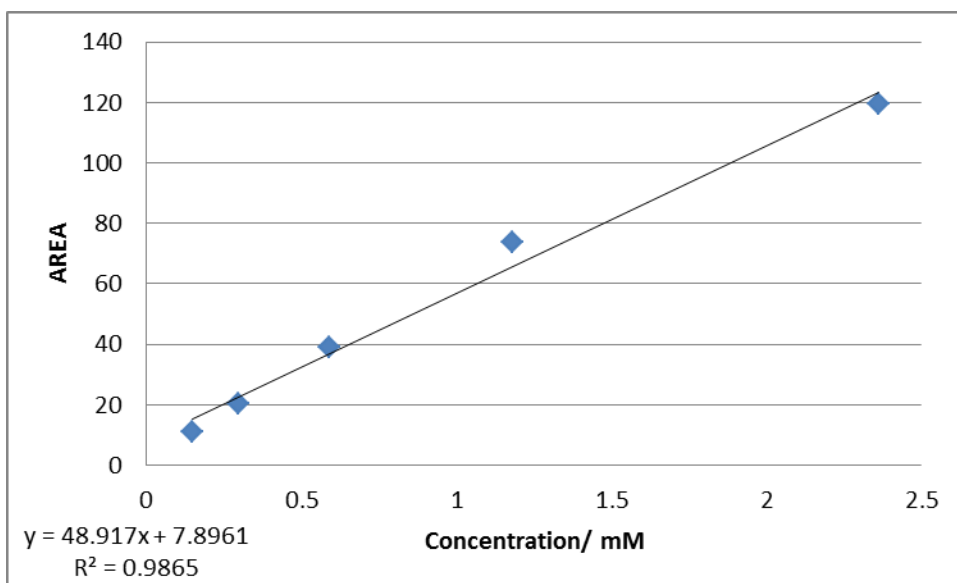


Figure 46: Calibration curve of piperidine 44a on a reverse phase HPLC

VF_JS17 showed only a slight preference for the *trans*-unsaturated ketoester (**42a**) over the *cis*-isomer (4 percentage point's difference). The largest difference in substrate preference however was shown by KpN_00799 with a seventy percentage point difference between the conversion yields of *cis*- and *trans*-**44a** in favour of the *cis*-isomer.

The variations in overall substrate affinity might be explained by the active site geometry of the various enzymes. This was explored through substrate docking studies into the 3D structure of CV2025 ω -TAm. Both unsaturated ketoester substrates *cis*- and *trans*-**42a** were docked in the active site in the presence of pyridoxamine-5'-phosphate and the lowest energy conformations analysed.

Table 23: HPLC analysis of piperidine 44a in TAM screening of *cis-/trans-42a*

Substrate: <i>cis-42a</i>			
Enzyme	Area	[Product]/ mM	Conversion yield/ %
CV2025	1520	6	31
VF_JS17	3153	6	64
KpN_00799	242	0.5	5
BSU_402	3634	7	74
BSU_1971	4569	9	93
PP_3718	2301	5	47
ArRMut11	1208	3	25

Substrate: <i>trans-42a</i>			
Enzyme	Area	[Product]/ mM	Conversion yield/ %
CV2025	2930	3	60
VF_JS17	3343	7	68
KpN_00799	3667	8	75
BSU_402	3186	7	65
BSU_1971	4108	8	84
PP_3718	2856	6	58
ArRMut11	577	1	12

Conditions: *cis-* or *trans-42a* (10 mM), isopropylamine (1000 mM), ω -TAM (60% w/v), KPi buffer (100 mM) pH 7.5, PLP (2 mM), 30 °C, 400 rpm, Reaction volume (1 mL). Reactions were run in duplicate.

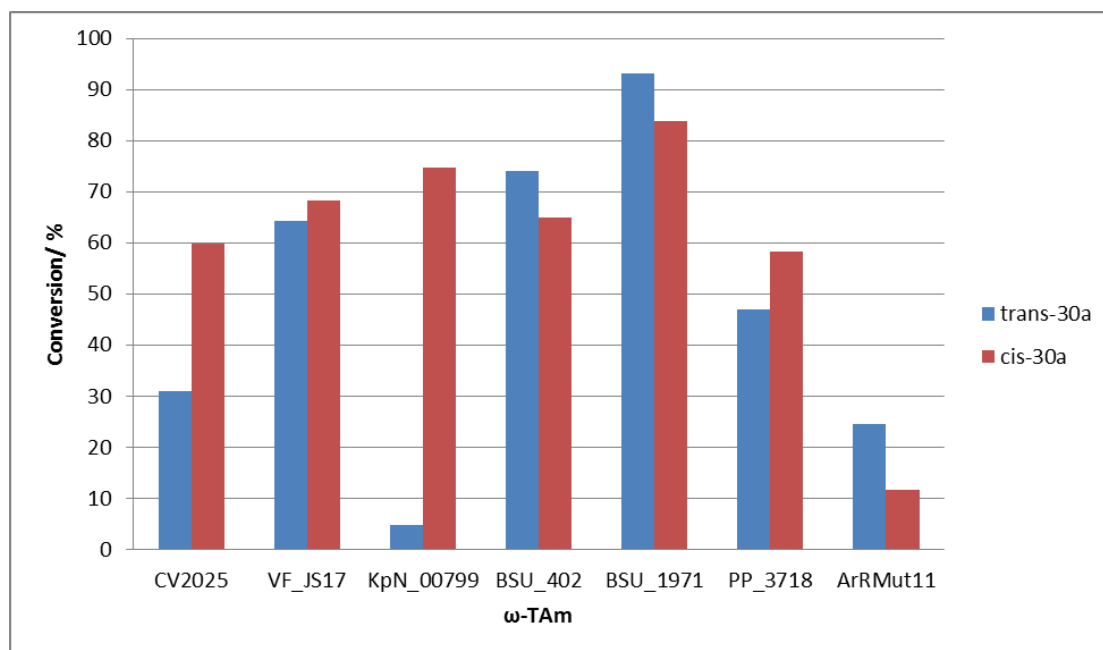


Figure 47: Screening of ketoester substrates *cis*- and *trans*-42a against a panel of ω -TAMs using non-chiral HPLC detection of piperidine 44a

Due to the ping-pong mechanism of transaminase activity, the unsaturated ketoester will only react with PMP in the active site of a TAM. The amino acid sequence from the crystal structure of CV2025 ω -TAM^[23] was therefore manually modified to place PMP in the active site instead of PLP. The lowest energy conformation of *trans*-unsaturated ketoester **42a** was found to be in the correct orientation for nucleophilic attack by the PMP amine [Figure 48A]. The hydroxyl group on the pyridine ring of PMP is involved in a hydrogen bonding interaction with the lone pair of electrons on the carbonyl oxygen. This stabilizes the carbonyl centre in close proximity to the cofactor primary amine which may allow the necessary nucleophilic attack to take place. Whilst this appears to be the most crucial interaction between the two species, there are three other hydrogen bonding interactions between *trans*-**42a** and the CV2025 active site. Amino acid residues Tyr153, Gly319, and Thr321 are all shown to be in hydrogen bonding interaction with the distal methyl ester group of *trans*-**42a**.

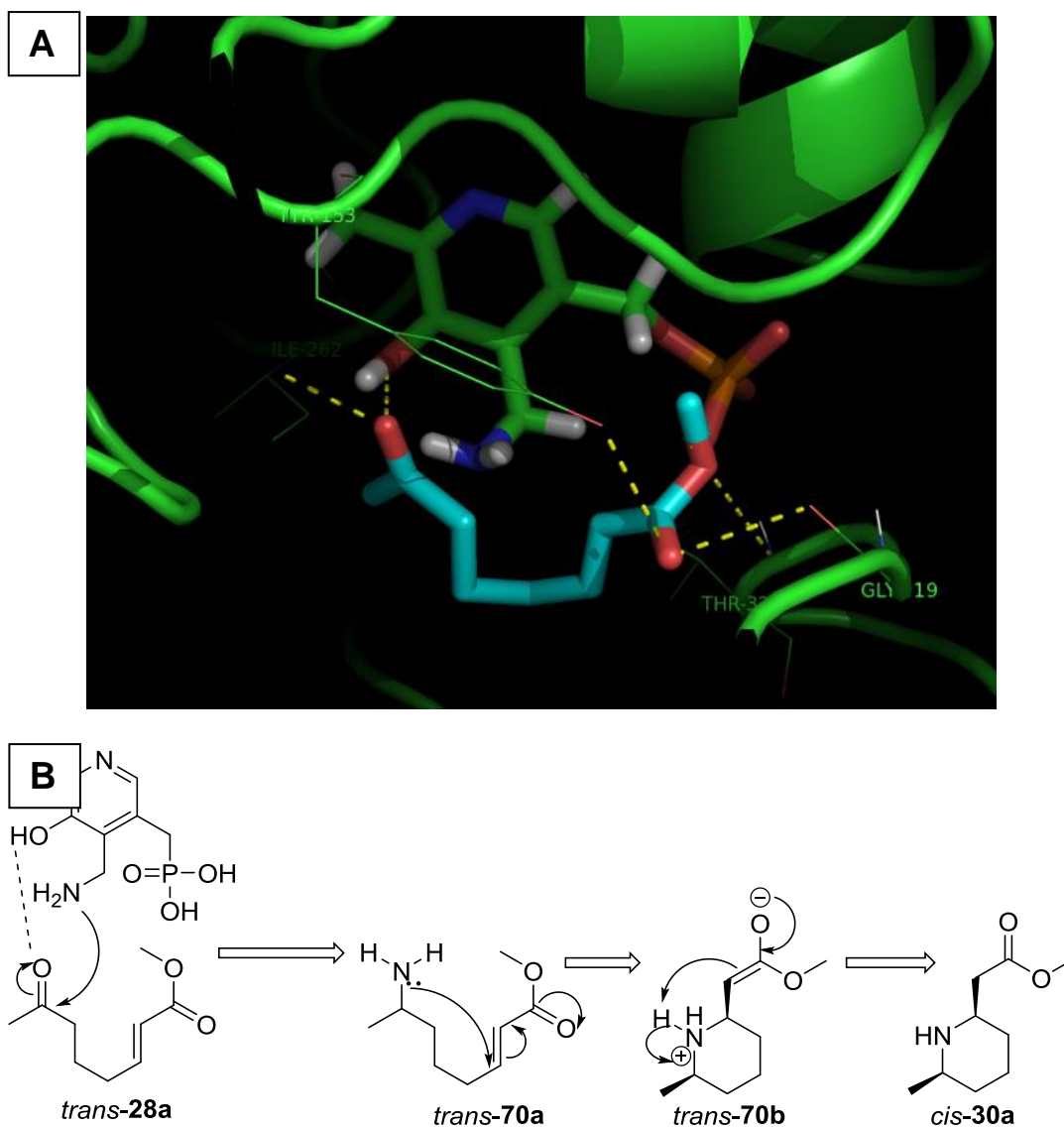


Figure 48: (A): *In silico* docking studies on *trans-42a*

Showing the hydrogen bonding interactions between *trans-42a* (bottom stick model) and PMP (top stick model) along with Tyr153, Thr321, and Gly319 (line models) in the CV2025 active site. (B): A schematic of the possible electron exchanges that may lead to ring-closure and the formation of *cis-44a*

This further stabilises the substrate within the active site to facilitate the formation of *trans-58*. Hydrogen bonding interactions between the active site residues and the methyl ester of *trans-58* may also play a role in facilitating ring closure as it creates a partially formed ring [Figure 48B]. By comparison, substrate docking studies show the lowest energy conformation of *cis-42a* in the active site of CV2025 has a less folded orientation that may not ring-close as readily [Figure 49].

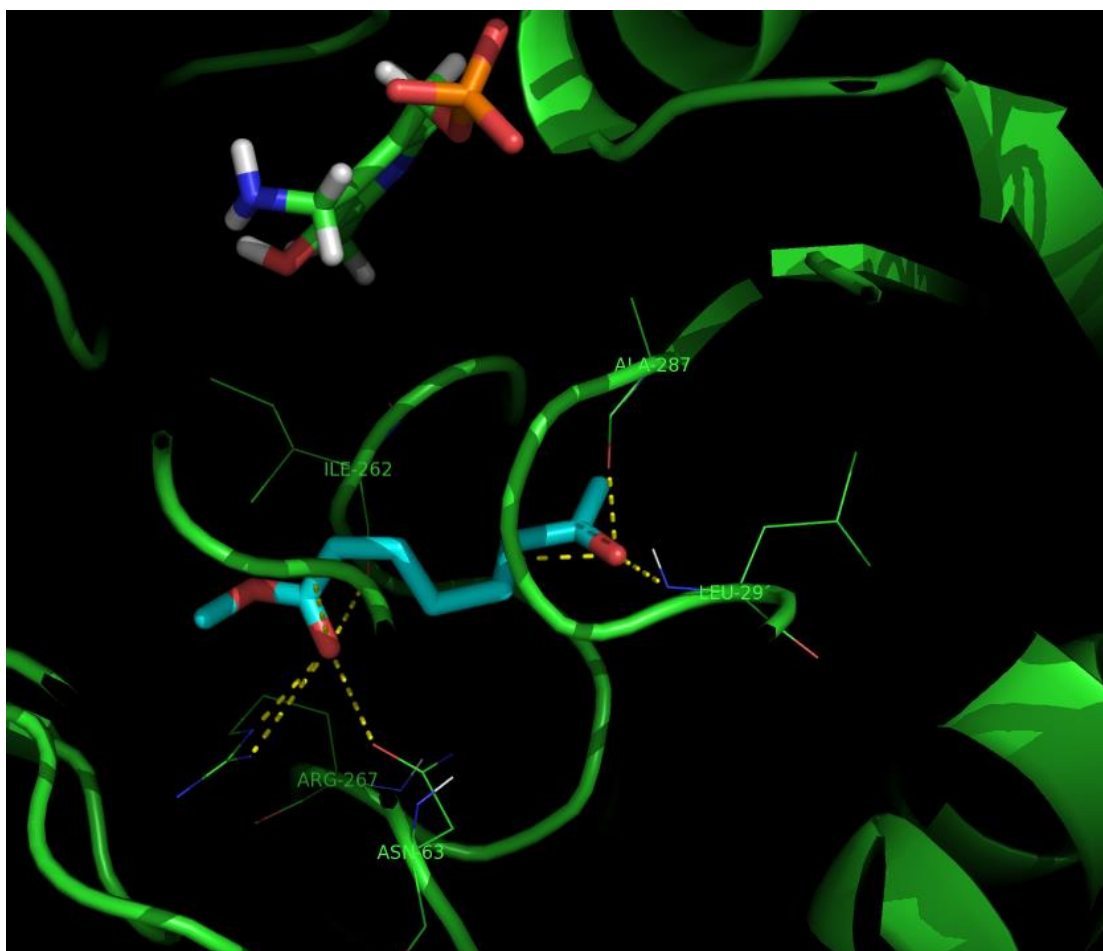


Figure 49: *In silico* docking studies on *cis-42a*

Showing the hydrogen bonding interactions between *cis-42a* (bottom stick model) and the active site residues of CV2025 ω -TAm – R267, N63, L29', A287, I262 (line model)

The ketone functional group of *cis-42a* hydrogen bonds to L29' and A287, far enough away from the primary amine of PMP to suggest the probability of a nucleophilic attack from the nitrogen lone pair is lower compared to in the *trans*-isomer. Three further hydrogen bonding interactions between the methyl ester and R267, N63, and I262 further hold back the substrate from the cofactor.

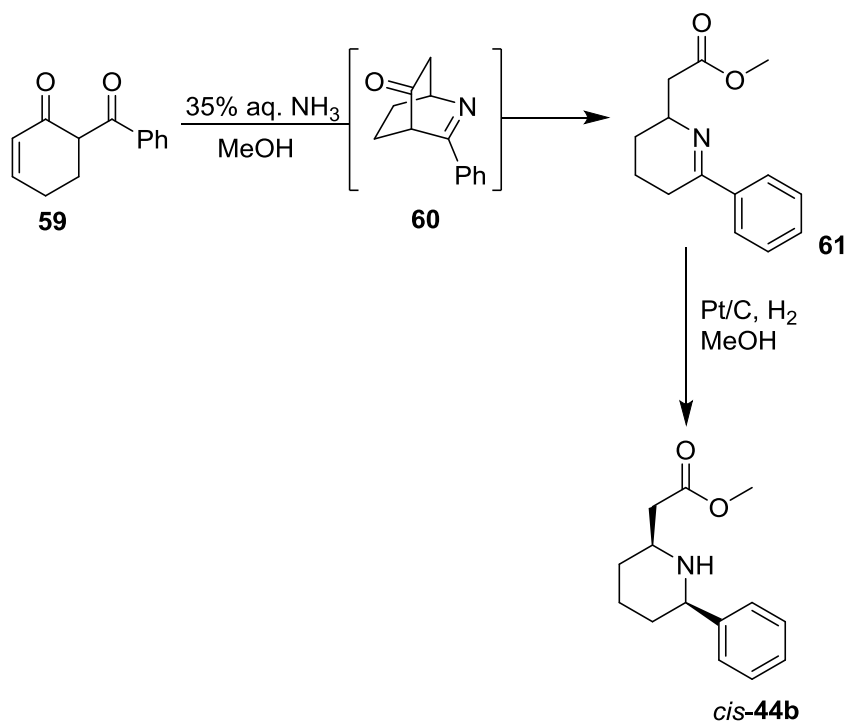
Overall, substrate docking investigations into the lowest energy conformations adopted by the two isomers in the active site of CV2025 suggest a difference in substrate affinity in favour of *trans-42a*. This is primarily down to the hydrogen bonding interactions involved in stabilising the two substrates; in the case of *trans*-

42a the positioning is favourable whereas it is unfavourable for the *cis*-isomer. It is worth noting that these are all approximate conformers and in reality enzyme active sites are much more dynamic and fluid. This perhaps explains why in spite of the lack of interaction between *cis*-**42a** and the PMP cofactor in [Figure 49], in reality, CV2025 still reacts with the substrate to give a moderate yield [Figure 47].

By contrast, ArRMut11, with 27 mutations was designed to accommodate pro-Sitagliptin (**21**) [37b]. It is a very highly specialised enzyme and therefore may have performed poorly in screening against unsaturated ester **42a** as a result of this. Without substrate docking studies on the enzyme and further optimisation however it is impossible to determine the reason for its poor conversion yield. Similarly, the varying preferences for *cis*- or *trans*-**42a** within the other enzymes may be down to similar reasons as CV2025; however that is difficult to determine without available crystal structures and further investigation.

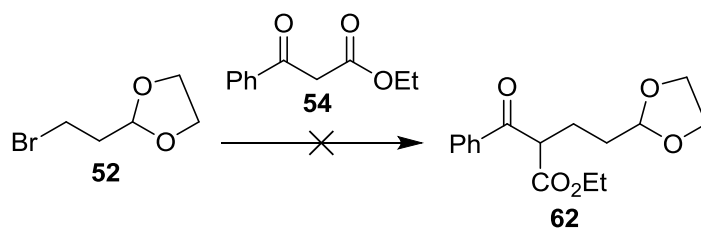
5.9. Synthesis of Phenylpiperidine **44b**

To our knowledge, the only reported chemical synthesis of phenylpiperidine **44b** is that of Taylor and Cuthbertson in their synthesis of (-)-grandisine G, a natural product shown to express binding affinity to human δ -opioid receptors. Starting from the advanced intermediate diketone (**59**), treatment with aqueous ammonia in methanol afforded imine **61** via the bicyclic intermediate **60** in a cyclisation/ring-opening sequence [Scheme 32]. A stereoselective reduction of imine **37** by treatment with Pt/C, H₂ afforded a single diastereomer *cis*-**44b**



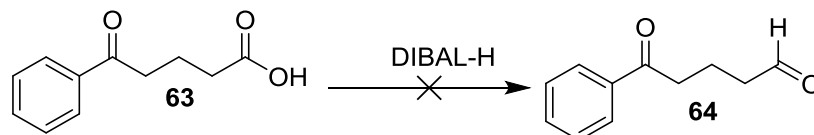
Scheme 32: Rearrangement hydrogenation approach to the synthesis of phenylpiperidine 44b

Applying the same procedure used to synthesise the unsaturated ester **42a** was unsuccessful for the synthesis of phenylpiperidine **44b** [Scheme 33]. The reaction of **54** with bromodioxolane (**52**) in the presence of either caesium carbonate or sodium ethoxide lead to a mixture of products and not dioxolane **62**. The requisite triplet at ~3.7 ppm was never observed by ^1H NMR spectroscopy.



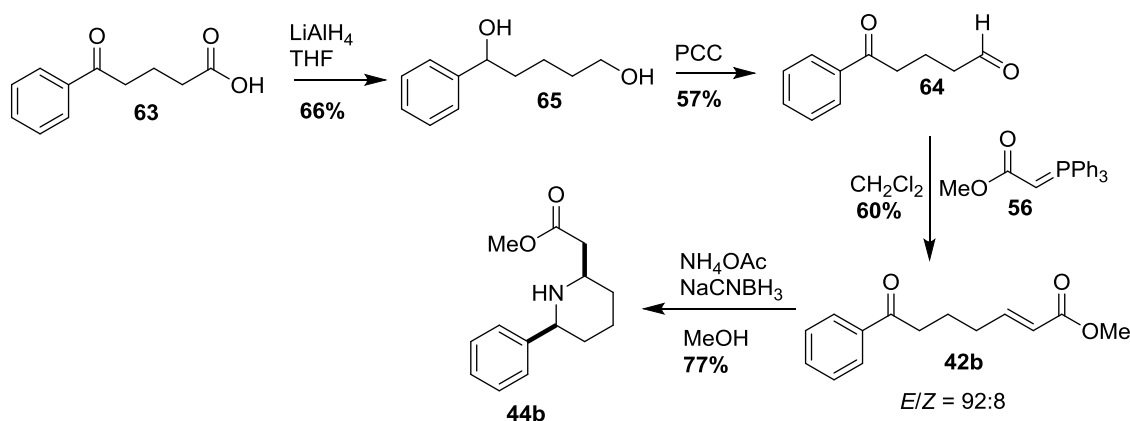
Scheme 33: Unsuccessful alkylation attempt to prepare dioxolane 62

A new approach was subsequently used to access the precursor ketoester **42b**. A diisobutylaluminium hydride reduction of the commercially available ketoacid (**63**) gave no aldehyde peak but a mixture of other products [Scheme 34].



Scheme 34: Attempt at partial reduction of phenyl ketoacid

Reduction of the ketoacid (**63**) using lithium aluminium hydride however, readily gave the corresponding diol (**65**) which was isolated in 82% yield and oxidised back to aldehyde **64** with pyridinium chlorochromate (PCC) in 80% yield. [Scheme 35]. The subsequent Wittig olefination reaction at room temperature afforded the α,β -unsaturated ketoester **42b** in 85% yield and *E/Z* ratio of 92:8 which was directly used in the next step without separation of the *cis*- and *trans*-isomers.



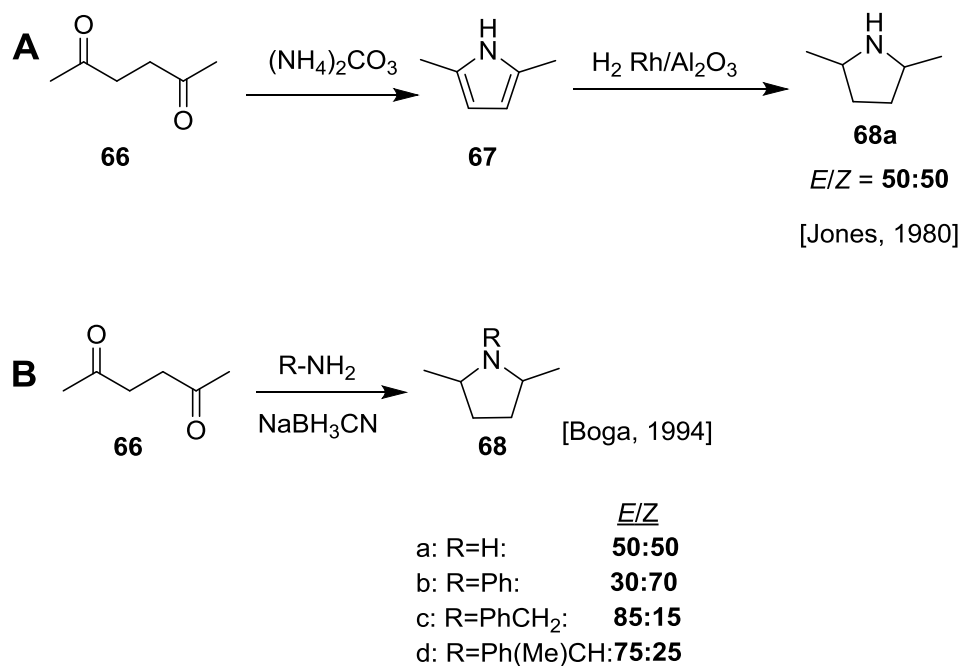
Scheme 35: Synthesis of unsaturated ester 42b and phenylpiperidine 44b

The subsequent reductive amination synthesis of phenylpiperidine **44b** proceeded under the same conditions as methylpiperidine **44a** affording a 70% yield of a single *cis*-diastereomer and no uncyclised amine was detected.

5.10. Synthesis of Methylpyrrolidine 47

Pyrrolidines also form another class of cyclic amine heterocycles of high value. A number of natural products isolated from plants, animals, and microorganisms contain this motif and this class of compounds have found use in the pharmaceutical and agrochemical industries as anticholinergic and haemolytic agents as well as anti-feedants and insecticides ^[64].

There are many chemical transformations able to access this structure from a variety of starting points. The most relevant of these transformations to this project is a reductive amination approach and two examples from Jones ^[65] and Boga ^[66] demonstrate its utility and shortcomings. Amination of a diketone (**66**) with ammonium carbonate formed the non-isolated pyrrole (**67**) which was reduced to give a mixture of *cis*- and *trans*- isomers of dimethyl pyrrolidine **68a** [Scheme 36-A]. The approach is non-stereoselective and gives a 50:50 mixture of the *trans/cis* isomers. Further optimisations of this methodology over the years using ammonium acetate and a hydroxide base, with sodium cyanoborohydride, has improved stereoselectivities for some analogues up to a ratio of 85:15 (*trans/cis*). Investigations by Boga and co-workers explored the different factors affecting these variations in diastereomeric ratio [Scheme 36-B]. It was reported that a combination of conditions such as ring size (piperidine or pyrrolidine), the type of reducing agent used and the nature of the nitrogen substituent all combined to give variations in the final diastereomeric ratio.

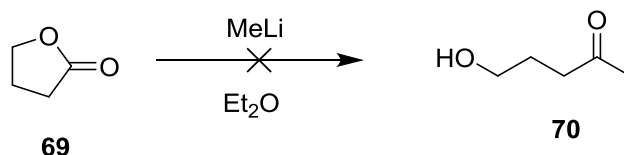


Scheme 36: Reductive amination of diketones to synthesise pyrrolidines

(A): Jones' non-stereoselective approach with pyrrole intermediate. (B): Boga's investigation into factors affecting diastereomeric ratio

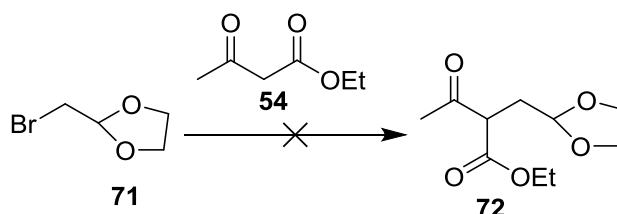
To our knowledge there is no literature precedence for the synthesis of 2,5-disubstituted pyrrolidines via an intramolecular aza-Michael reaction to date. In order to apply this strategy to pyrrolidines, a number of routes were explored to access the α,β -unsaturated ketone precursor.

Initially ring opening of butyrolactone (**69**) by methyl lithium was investigated^[67], but the reaction was not successful [Scheme 37]. Different solvents (DMF, THF) and temperatures (-78 °C) were used, but the alcohol **70** was not formed.



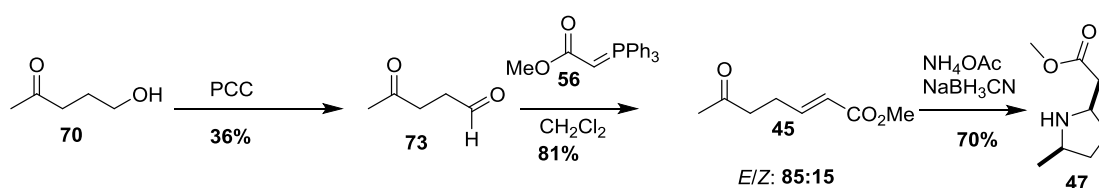
Scheme 37: Ring-opening of butyrolactone to synthesise ketol 70

A return to the previously successful bromodioxolane alkylation approach was again attempted with a shorter chain bromodioxolane substrate (**71**) [Scheme 38]. This was also unsuccessful probably due to the crowded electrophile centre in **71**.



Scheme 38: Unsuccessful alkylation reaction in the synthesis of pyrrolidine 47

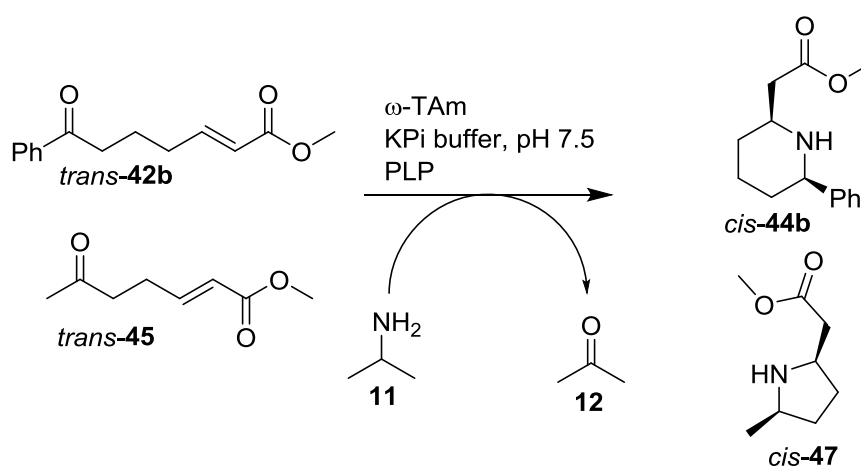
Ketol **70** was found to be commercially available and was then used in a PCC oxidation to give the corresponding aldehyde **73** in 36% yield after purification [Scheme 39]. Subsequent Wittig olefination with **72** yielded unsaturated ketoester **45** in a mixture of isomers (*E/Z* = 85:15) in 81% yield. Amination of **45** using ammonium acetate and the aza-Michael reaction as before was repeated with this analogue to furnish the *cis*-disubstituted pyrrolidine **47** exclusively in 70% yield after purification (presumably the *trans*-isomer was lost during purification).



Scheme 39: Chemical synthesis of 2,5-disubstituted pyrrolidine 47

5.11. Screening of Ketoester Substrates 42b and 45 Against Novel TAmS

The screening of unsaturated ketoester substrates against transaminases was extended to include *trans*-**45** and *trans*-**42b** using isopropylamine (**11**) as amine donor along with the panel of TAmS used in the screening of ketoester **42a** [Table 24].



Scheme 40: Omega-TAm screen of *trans*-42b and *trans*-45 with isopropylamine (11)

The chemically synthesised cyclic amines *cis*-phenylpiperidine **44b** and *cis*-pyrrolidine **47** were first used as standards to determine the retention times of the two cyclic amine products on a reverse phase C8 column (ACE 5 C8-300, 150 x 4.6mm) (9.2 min and 8.8 min respectively). They were also used to calibrate the HPLC and run a calibration curve [Figures 50 and 51].

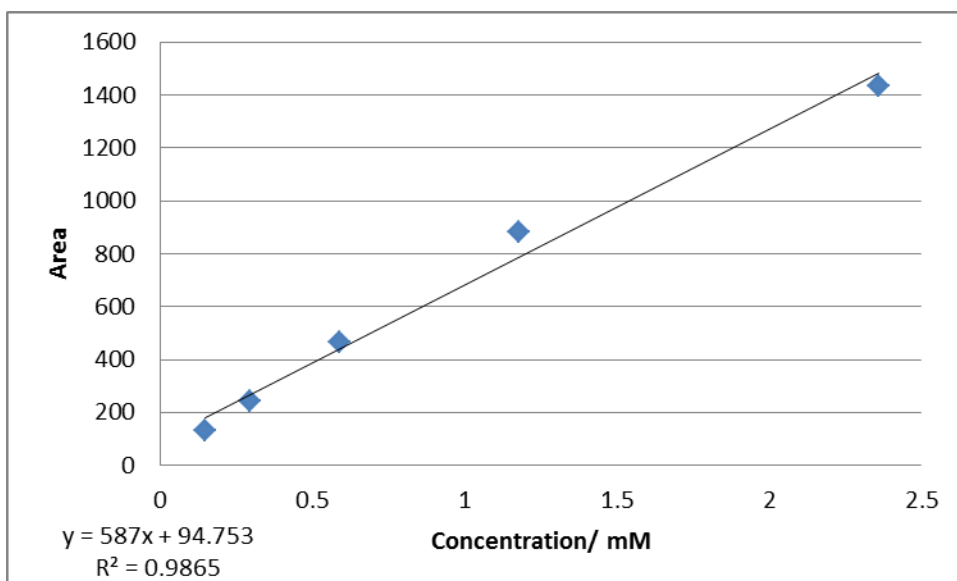


Figure 50: Calibration curve of *cis*-phenylpiperidine **44b** by non-chiral HPLC

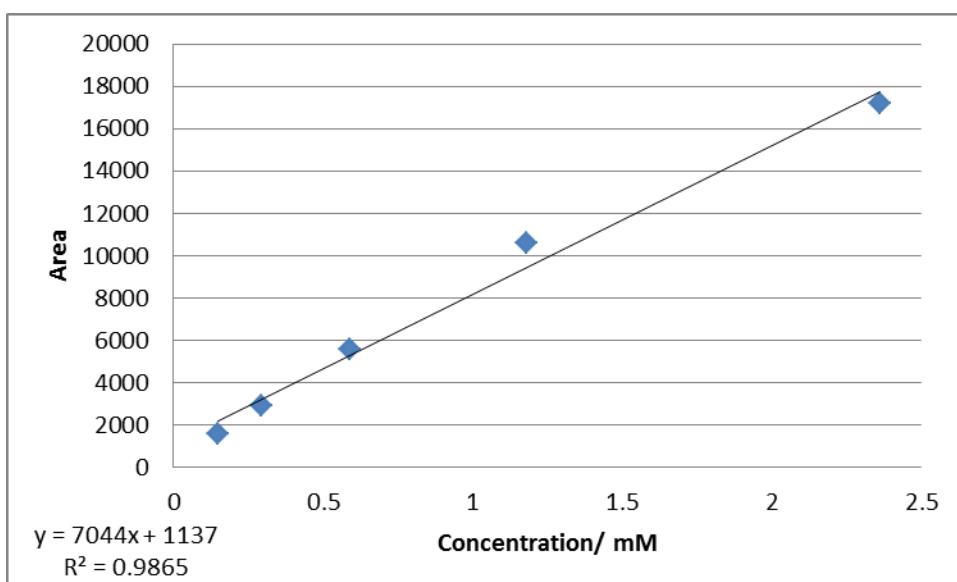


Figure 51: Calibration curve of *cis*-pyrrolidine **47** by non-chiral HPLC

Using the equation of the line of best fit from these two calibration curves, the concentrations of cyclic amines **44b** and **47** were calculated from their respective biotransformation reactions [Table 5.9]. All the enzymes screened exhibited activity towards both ketoester substrates.

Table 24: HPLC analysis of phenylpiperidine 44b and pyrrolidine 47 in TAM screening of their respective precursors

Phenylpiperidine <i>cis</i>-44b			
Enzyme	Area	[Product]/ mM	Conversion yield/ %
CV2025	2026	3.3	33
VF_JS17	2238	3.7	37
KpN_00799	1944	3.2	32
BSU_402	2047	3.3	33
BSU_1971	3076	5.1	51
PP_3718	1656	2.7	27
As-TAm	681	1.0	10
Pyrrolidine <i>cis</i>-47			
Enzyme	Area	Conc./ mM	Conversion yield/ %
CV2025	3718	4.4	44
VF_JS17	2889	3.0	30
KpN_00799	3676	4.0	43
BSU_402	3566	4.1	41
BSU_1971	4483	5.7	57
PP_3718	2851	3.0	29
As-TAm	1957	1.4	14

Conditions: ketoester (10 mM), isopropylamine (1000 mM), PLP (2 mM), potassium phosphate buffer (100 mM) pH 7.5, ω-TAm (60% w/v), 30 °C, 400 rpm, Reaction volume (1 mL)

All except VF_JS17 showed relatively higher affinity for the phenylketoester (*trans*-**42b**) over the pyrrolidine precursor (*trans*-**45**) [Figure 52]. In addition, there were small internal variations within each enzyme for affinity towards the two substrates.

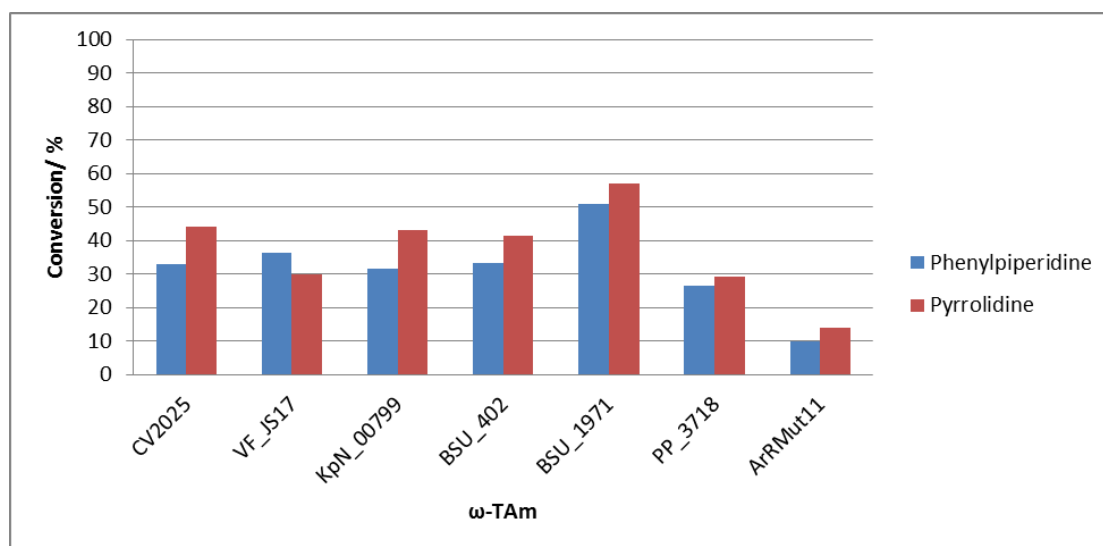


Figure 52: Screening of ketoester substrates *trans*-42b and *trans*-45 against a panel of ω -TAMs using non-chiral HPLC detection of piperidine 44b and pyrrolidine 47

As with the results from the ω -TAM screening of *cis/trans*-methylketoester **42a**, BSU_1971 exhibited the highest substrate conversion under the conditions [Figure 52]. A 3D crystal structure of BSU_1971 may reveal an active site geometry that is favourable to the entry and stabilisation of bulkier substrates compared to CV2025 and the other ω -TAMs. This might therefore be a useful investigation for the future of this project. The mutant ω -TAM ArRMut11 once again showed comparatively lower conversion yields under the conditions than any of the other six TAMs. It showed a small preference for the pyrrolidine precursor (*trans*-**45**) than the phenylketoester (*trans*-**42b**). Further investigations would need to be performed in order to explain this outcome however.

Chapter 6. Conclusions and Future Directions

6.1. Conclusions

A group of ten novel (*S*)-specific omega-transaminases were cloned and over-expressed in this project from the amino acid sequence of a previously characterised ω -TAm from the literature (VF_JS17) [Table 7 and Figure 7]. Starting from a previously characterised (*R*)-TAm from *Arthrobacter aureescence*, three novel (*R*)-specific TAmS were also discovered and cloned but were never screened for activity [Figures 2.5 and 2.6]. Four of the novel ω -TAmS, along with two other previously characterised ones (CV2025 and VF_JS17) were however screened for activity against (*R*)- and (*S*)- α -methylbenzylamine (**1**), confirming their preference for the (*S*)-enantiomer [Figures 2.12 and 2.13] as an amine donor.

CV2025 ω -TAm was successfully used to synthesise (*S*)- α -MBA from acetophenone and isopropylamine in 13% yield and >99% e.e. without an equilibrium displacement strategy in place. This was further improved by employing an equilibrium displacement method involving LDH as a secondary enzyme to remove the ketone product (**2**) [Scheme 11] thereby driving the reaction towards completion (>90% conversion, >99% e.e.) [Table 9]. Interestingly however, CV2025 converted both D- and L-Alanine readily under the reaction conditions.

Screening CV2025 and VF_JS17 ω -TAmS against a diverse panel of amine donors, it was discovered that under the reaction conditions, benzylamine was a suitable amine donor for both transaminases [Table 15]. This was supported by findings of π -stacking interactions between the phenyl ring of (*S*)- α -MBA and those of Phe22 and Tyr153 in docking experiments with CV2025. Fermentation scale-up experiments carried out on the recombinant *E. coli* cells containing the ω -TAmS CV2025, VF_JS17, KpN_00799, BSU_402, BSU_1971, and PP_3718 were successful and yielded ~100 g of wet cell paste in each fermentation.

The second half of this project involved an investigation into the broad utility of transaminases, specifically their use in biocatalytic aza-Michael reactions for the synthesis of cyclic amines. Piperidines and pyrrolidines are common key structural scaffolds in a variety of natural products [Scheme 5.1]. Transaminase-mediated synthesis of cyclic amines from unsaturated ketoester substrates was successfully conducted in this project using four novel (*S*)-selective ω -TAMs, two previously discovered (*S*)-selective ω -TAMs and an (*R*)-selective ω -TAM mutant (ArRMut11) from the literature [Sections 5.2. and 5.11]. The conversion of *trans*-methyl ketoester **42a** by CV2025 was confirmed by ¹H NMR spectroscopy data which was in agreement with literature data. The screening of both isomers of **42a** against the panel of seven TAMs showed differences in substrate preference, based on conversion yield, within the TAMs. CV2025 had a higher conversion yield against *trans*-**42a** (60%) compared to *cis*-**42a** (31%) [Figure 47]. Subsequent substrate docking studies using a published CV2025 crystal structure ^[23] indicated active site residues are perhaps involved in sequestering *trans*-**42a** in close proximity with the primary amine of PMP thereby facilitating the necessary nucleophilic attack to form intermediate amine **58** [Figure 48]. The amine is thus in a favourable orientation for spontaneous ring closure. It is unclear however as to where this cyclisation may take place, inside the active site or outside.

All except BSU_1971 showed this same substrate preference. It was also discovered that BSU_1971, under the reaction conditions, has the highest percentage conversion amongst the TAMs against both substrate isomers. A crystal structure of this enzyme may shed more light on how it is able to achieve this.

Two analogues of unsaturated ketoester **42a** were prepared and screened against the panel of seven transaminases [Table 24]. All except VF_JS17 showed relatively higher affinity for phenylketoester (*trans*-**42b**) over the pyrrolidine precursor (*trans*-**45**) [Figure 52]. The majority of the TAmS in the screen showed higher conversion against the phenyl analogue with BSU_1971 showing the highest conversion (57%).

6.2. Future Directions

Expansion of the initial TAm screen in [Figure 17] to include the six remaining novel ω -TAmS and the three (*R*)-selective branched-chain TAmS will complete that section of the work begun in this project. The possible discovery of a new ω -TAm with improved enzyme activity and a broader substrate spectrum justifies such a course of action.

A further expansion of the unsaturated ketoester screens [Sections 5.8 and 5.11] towards the remaining unscreened novel TAmS is also prudent. The discovery of BSU_1971 as a better TAm for the conversion of unsaturated ketoesters suggests there may be other such TAmS within the initial panel of ten due to their amino acid sequence homology and phylogenetics.

Protein crystallisation and X-Ray crystallography of the BSU_1971 ω -TAm enzyme to provide a 3D structure for substrate docking studies will enable further understanding of the underlying reasons for its higher performance against such substrates. This may prove even more valuable if coupled with directed evolution studies to identify the specific active site residues involved in the TAm-mediated intramolecular aza-Michael cyclisation reaction.

And finally, a total synthesis of the piperidine and pyrrolidine alkaloids [Scheme 5.1] via a TAM-mediated aza-Michael reaction can be undertaken as a proof-of-concept study to demonstrate the utility of this approach.

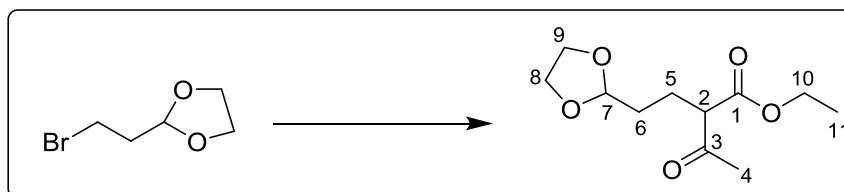
Chapter 7. Experimental

7.1. General Instrumentation

All reagents were obtained from commercial sources and used as received unless otherwise stated. Analytical HPLC was performed on a Varian Prostar instrument equipped with an autosampler, a UV-visible detector and a DiscoveryBIO wide Pore C18-10 Supelco column (250 mm x 4.6 mm, 10 μ m) or an ACE 5 C8-300 column (150 x 4.6 mm). HPLC runs were monitored at 210 nm or 218 nm. Chiral HPLC analyses were performed under reverse phase conditions (85:15 HClO₄/ acetonitrile) on a Crownpak® CR+ column (4.6 mm x 150 mm, 5 μ m) and monitored at 210 nm. Normal phase (80:20 hexane/ isopropanol) chiral HPLC analyses however were performed on a Chiralpak® AD column (4.6 mm x 250 mm, 10 μ m).

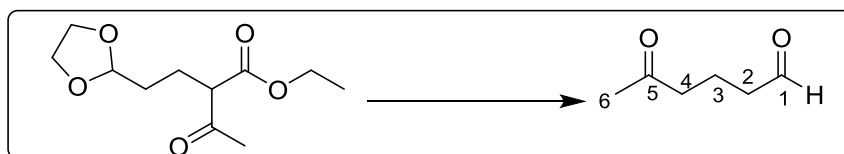
¹H and ¹³C NMR spectra were recorded at 298 K at the field indicated using an Avance 600 machine. Coupling constants were measured in Hertz (Hz) and referenced to the deuterated solvent used. Mass spectra were recorded on Thermo Finnegan MAT 900XP and Micro Mass Quattro LC electrospray mass spectrometers VG ZAB 2SE. Infrared spectra were recorded on a Perkin Elmer Spectrum 100 FTIR spectrophotometer. GC-MS was performed on a Thermo Scientific™ ISQ™ series Quadrupole GC-MS with a TracePLOT TG-BOND U GC column. LC-MS was carried out by a Thermo Scientific™ LTQ XL™ Ion Trap mass spectrometer. UPLC-MS was carried out with a Waters™ Acquity UPLC M-Class system with a C-18 column.

7.2. Synthesis of Ethyl 2-(2-(1,3-dioxolan-2-yl)ethyl)-3-oxobutanoate [55] [68]



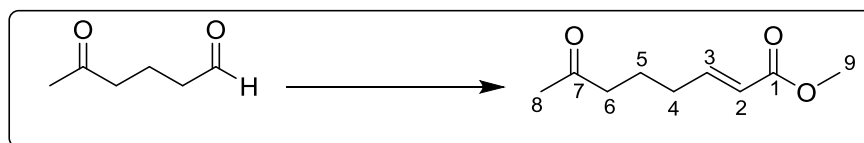
To a suspension of Cs_2CO_3 (9.40 g, 28.8 mmols) in dry acetonitrile (60 mL) was added ethyl acetoacetate (3.20 g, 24.4 mmols) at room temperature. The mixture was then heated and stirred at 50 °C (1 h). 2-(2-Bromoethyl)-1,3-dioxolane was added (4.10 g, 22.1 mmol) and the mixture heated at reflux under argon (48 h). The reaction mixture was then filtered and concentrated followed by purification by silica column chromatography (4:1 petroleum ether/ ethyl acetate) to yield **55** as a pale yellow oil (3.12 g, 62%). ^1H NMR (300 MHz; CDCl_3): δ 1.25 (3H, t, $J = 7.1$ Hz, 11- H_3), 1.68-1.61 (2H, m, 6- H_2), 1.96 (2H, q, $J = 7.5$ Hz, 5- H_2), 2.21 (3H, s, 4- H_3), 3.50 (1H, t, $J = 7.5$ Hz, 2-H), 3.84-3.79 (2H, m, 8- H_H , 9- H_H), 3.96-3.90 (2H, m, 8- H_H , 9- H_H), 4.17 (2H, q, $J = 7.1$ Hz, 10- H_2), 4.84 (1H, t, $J = 4.5$ Hz, 7-H). ^{13}C NMR (75 MHz; CDCl_3): 14.2 (C-11), 22.4 (C-5), 29.1 (C-4), 31.3 (C-6), 59.3 (C-2), 61.5 (C-10), 65.0 (C-8, C-9), 104.0 (C-7), 169.7 (C-1), 203.1 (C-3). IR (film, cm^{-1}): 2887, 1711, 1138. m/z (+ESI) 231.12 (100%, MH^+)

7.3. Synthesis of 5-oxohexanal [53] [69]



A suspension of ethyl 2-(2-(1,3-dioxolan-2-yl)ethyl)-3-oxobutanoate (3.14 g 13.5 mmols) in 5% aqueous sodium hydroxide (20 mL) was heated at reflux (5 h). The mixture was then acidified to pH 2 with HCl (2 M), THF (15 mL) added and the reaction stirred at room temperature (16 h). The organic layer was then extracted and the aqueous layer washed with ethyl acetate (15 mL) twice. The organic layers were then combined, dried (MgSO_4) and concentrated and purified by silica gel chromatography (6:3.9:0.1 petroleum ether, dichloromethane, and acetone) to give **53** as an oil (1.22 g, 76%). ^1H NMR (600 MHz; CDCl_3) δ 1.77 (2H, quintet, $J = 7.1$ Hz, 3- H_2), 2.12 (3H, s, 6- H_3), 2.46-2.50 (4H, m, 4- H_2 , 2- H_2), 9.74 (1H, s, 1-H). ^{13}C NMR (150 MHz; CDCl_3): 16.1 (C-3), 30.0 (C6), 41.8 (C-4), 43.4 (C-2), 202.0 (C-1), 208.8 (C-5), . IR (film, cm^{-1}): 2956, 1713. m/z (+ESI) 114.91 (50%, MH^+), 226.83 (100%).

7.4. Synthesis of Methyl (*E*)-7-oxooct-2-enoate *trans*-[42a]^[68]

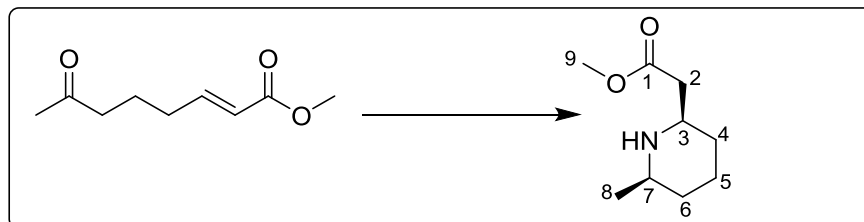


(Methoxycarbonylmethyl) triphenylphosphonium bromide (9.50 g, 23 mmols) in dichloromethane (30 mL) was shaken with aqueous sodium hydroxide (2 M, 20 mL) for 5 min. The organic layer was separated, dried (MgSO₄) and concentrated *in vacuo*. 5-Oxohexanal (1.54 g, 13.2 mmols) dissolved in dichloromethane (20 mL) and the mixture stirred at room temperature (12 h). The reaction was concentrated *in vacuo*, re-suspended in pentane and filtered (3 x 20 mL). The crude product with an 80:20 *E/Z* ratio was then purified over silica (4:1 petroleum ether/ethyl acetate) to yield *trans*-**42a** as a clear oil (1.14 g, 49%). ¹H NMR (600 MHz; CDCl₃): δ 1.70-1.75 (2H, m, 5-H₂), 2.11 (3H, s, 8-H₃), 2.18-2.21 (2H, m, 4-H₂), 2.44 (2H, t, *J* = 7.3 Hz, 6-H₂), 3.70 (3H, s, OMe), 5.81 (1H, d, *J* = 15.6 Hz, 2-H), 6.88-6.92 (1H, m, 3-H). ¹³C NMR (150 MHz; CDCl₃): 21.9 (C-5), 30.1 (C-8), 31.4 (C-4), 42.7 (C-6), 51.6 (C-9), 121.2 (C-2), 148.6 (C-3), 166.1 (C-1), 208.4 (C-7). IR (film, cm⁻¹): 2952, 1714, 1645, 1137; *m/z* (+ESI) 171.10 [MH]⁺; [HRMS (ESI)] calcd. for C₉H₁₄O₃, 171.0977. Found: [MH]⁺ 171.1021

7.5. Methyl (*Z*)-7-oxooct-2-enoate *cis*-[42a] ^[68]

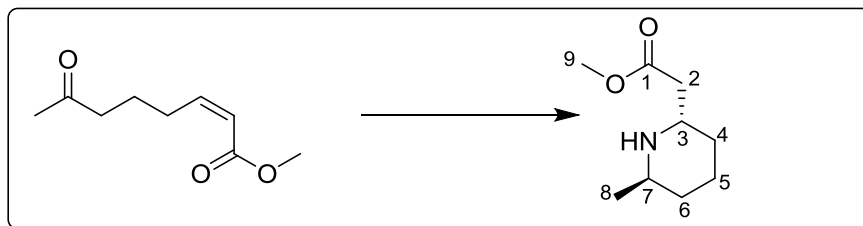
Cis-**42a** was isolated from the crude yield following silica purification (0.28 g, 20%). ¹H NMR (600 MHz; CDCl₃): δ 1.72 (2H, quint, *J* = 7.5 Hz, 5-H₂), 2.13 (3H, s, 8-H₃), 2.46 (2H, t, *J* = 7.5 Hz, 4-H₂), 2.64 (2H, q, *J* = 7.5 Hz, 6-H₂), 3.69 (3H, s, OMe), 5.78-5.80 (1H, d, *J* = 11.0 Hz, 2-H), 6.18 (1H, dt, *J* = 11.0 Hz, 7.5 Hz, 3-H). ¹³C NMR (150 MHz; CDCl₃): δ 22.9 (C-5), 28.3 (C-8), 30.1 (C-4), 43.0 (C-6), 51.2 (C-9), 120.1 (C-2), 149.7 (C-3), 166.9 (C-1), 208.8 (C-7). *m/z* (+ESI) 171.1021 (100%, MH⁺)

7.6. Synthesis of Methyl (\pm)-(cis-6'-methylpiperidin-2'-yl)acetate *cis*-[44a] [59]



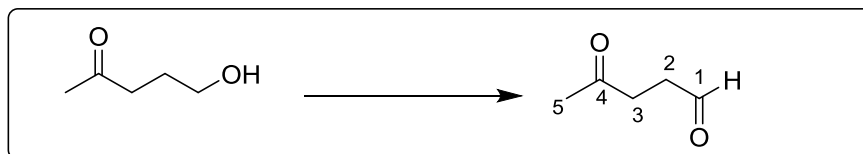
To a solution of methyl (*E*)-7-oxooct-2-enoate (*trans*-**42a**) (0.12 g, 0.71 mmols) in methanol (20 mL) was added ammonium acetate (1.2 g, 15 mmols) and sodium cyanoborohydride (0.06 g, 0.9 mmols). The reaction was stirred at 60 °C for 11 h and then concentrated to dryness. The residue was partitioned between saturated aqueous sodium hydrogen carbonate (10 mL) and dichloromethane/methanol (9:1) (10 mL). The organic layer was extracted and the aqueous layer washed again dichloromethane (3 x 10 mL). The combined organic layer was dried (MgSO₄), concentrated *in vacuo* and purified by silica gel chromatography (dichloromethane/methanol, 19:1) to yield *cis*-**44a** as a clear oil (0.085 g, 70%). ¹H NMR (600 MHz; CDCl₃): δ 1.06 (3H, d, J = 6.2 Hz, 8-H₃), 1.03-1.14 (2H, m, 6-H₂), 1.31-1.38 (1H, m, 5-H_H), 1.57 (2H, m, 4-H₂), 1.74 (1H, m, 5-H_H), 2.42 (2H, m, 2-H₂), 2.66-2.69 (1H, m, 7-H), 2.94-2.98 (1H, m, 3-H), 3.64 (3H, s, OMe). ¹³C NMR (150 MHz; CDCl₃): δ 22.6 (C-8), 24.4 (C-5), 31.5 (C-6), 33.4 (C-4), 40.8 (C-2), 51.6 (C-3), 52.6 (C-9), 53.6 (C-7), 172.8 (C-1). IR (film, cm⁻¹): 1713, 1656, 1437, 1159; m/z (+ESI) 172.13 (100%, MH⁺).

7.7. Methyl (\pm)-(trans-6'-methylpiperidin-2'-yl)acetate *trans*-[44a] [59]



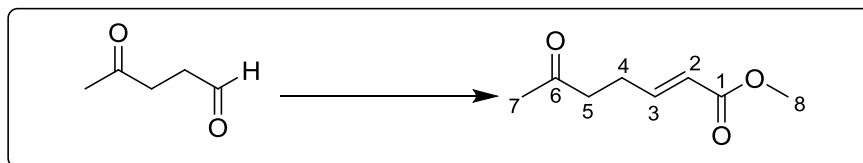
The same procedure as above was used, with methyl (*Z*)-7-oxooct-2-enoate (*cis*-**42a**) (0.12 g, 0.71 mmols). The crude product was purified by silica chromatography to yield *trans*-**44a** as a clear oil (0.080 g, 66%) ^1H NMR (600 MHz; CDCl_3): δ 1.11 (3H, d, $J = 6.2$ Hz, 8- H_3), 1.15-1.20 (2H, m, 6- H_2), 1.35-1.42 (1H, m, 5- H_H), 1.62 (2H, m, 4- H_2), 1.76-1.79 (1H, m, 5- H_H), 2.39-2.52 (2H, m, 2- H_2), 2.70-2.76 (1H, m, 7-H), 2.99-3.04 (1H, m, 3-H), 3.67 (3H, s, OMe). ^{13}C NMR (150 MHz; CDCl_3): δ 22.6 (C-8), 24.4 (C-5), 31.5 (C-6), 33.4 (C-4), 40.8 (C-2), 51.7 (C-3), 52.6 (C-9), 53.6 (C-7), 172.7 (C-1).

7.8. Synthesis of 4-oxo-pentanal [73] [70]



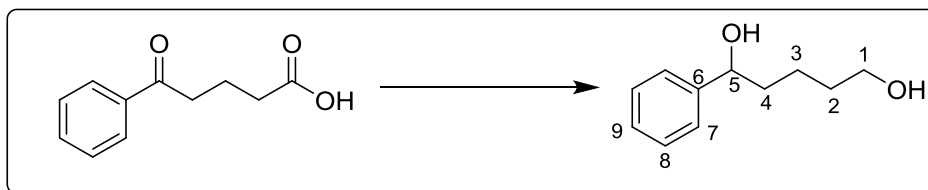
To a suspension of pyridinium chlorochromate (9.50 g, 44.1 mmols) in dichloromethane (50 mL) is added 5-hydroxy-2-pentanone (3.00 g, 29.4 mmols) was added. The reaction mixture was stirred for 6 h at room temperature, filtered over silica and washed with diethyl ether (4 x 25 mL). The organic filtrate was combined, concentrated *in vacuo*, and purified by silica gel chromatography (petroleum ether/ethyl acetate 7:3) to give **73** as a dark oil (1.57 g, 36%). ^1H NMR (600 MHz; CDCl_3): δ 9.75 (1H, s, 1-H), 2.70 (4H, s, 2-H₂, 3-H₂), 2.14 (3H, s, 5-H₃). ^{13}C NMR (150 MHz; CDCl_3): δ 30.1 (C-5), 36.9 (C-3), 38.3 (C-2), 201.5 (C-1), 208.2 (C-4). IR (film, cm^{-1}): 2942, 2831. m/z (+ESI) 101.05 (100%, MH^+).

7.9. Synthesis of Methyl (E)-6-oxohept-2-enoate *trans*-[45] [61]



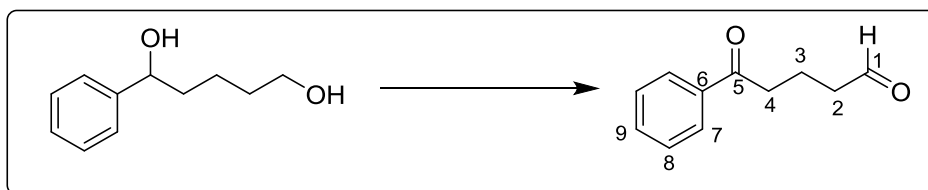
(Methoxycarbonylmethyl) triphenylphosphonium bromide (8.20 g, 20.0 mmols) dissolved in dichloromethane (30 mL) was shaken with aqueous sodium hydroxide (2 M, 20 mL) for 5 min. The organic layer was separated, dried (MgSO₄) and concentrated *in vacuo*. 4-Oxopentanal (**73**) (1.80 g, 18 mmols) in dichloromethane (20 mL) was then added and the mixture stirred at room temperature (12 h). The reaction was concentrated *in vacuo*, re-suspended in pentane and filtered (3 x 20 mL). The crude product was then purified using silica flash chromatography (4:1 petroleum ether/ethyl acetate) to yield **45** as a clear oil (2.30 g, 81%). ¹H NMR (600 MHz; CDCl₃): δ 2.10 (3H, s, 7-H₃), 2.41 (2H, q, *J* = 7.1 Hz, 4-H₂), 2.55 (2H, t, *J* = 7.1 Hz, 5-H₂), 3.65 (3H, s, OMe), 5.75-5.79 (1H, dt, *J* = 15.8 Hz, 1.6 Hz, 2-H), 6.84-6.90 (1H, dt, *J* = 15.8 Hz, 7.1 Hz, 3-H). ¹³C NMR (150 MHz; CDCl₃): δ 26.0 (C-4), 30.0 (C-7), 41.5 (C-5), 51.5 (C-8), 121.7 (C-2), 147.5 (C-3), 166.8 (C-1), 206.7 (C6). IR (film, cm⁻¹): 2952, 1712, 1656, 1155; *m/z* (+ESI) 179.07 [M+Na]⁺; [HRMS (ESI):calcd. for C₈H₁₂O₃, 157.0820 Found: [M+Na]⁺ 179.0682

7.10. Synthesis of 1-phenylpentane-1,5-diol [65] [71]



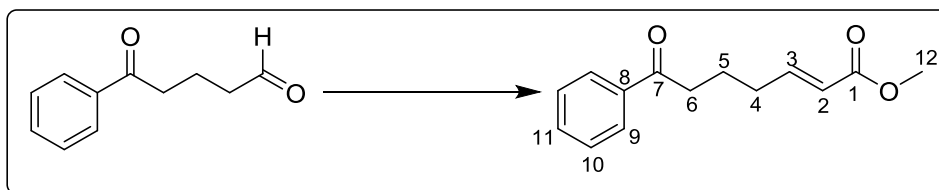
To a solution of commercially available 5-oxo-5-phenylvaleric acid (5.00 g, 26 mmols) in THF (100 mL) was added lithium aluminium hydride (3.00 g, 78 mmols) at 0 °C under argon slowly over 45 min. The reaction was warmed to room temperature over 4 h then cooled to 0 °C and quenched by the slow addition of distilled water (50 mL). The aqueous layer was extracted with ethyl acetate (3 x 100 mL), dried (MgSO₄), and concentrated *in vacuo*. The crude product was purified by silica flash chromatography (petroleum ether/ethyl acetate 3:2) to yield **65** as a clear viscous oil (3.13 g, 66%). ¹H NMR (600 MHz; CDCl₃): δ 1.30-1.75 (6H, m, 2-H₂, 3-H₂, 4-H₂), 3.50 (2H, t, *J* = 6.2 Hz, 1-H₂), 4.58 (1H, t, *J* = 6.5 Hz, 5-H), 7.22-7.31 (5H, m, Ph). ¹³C NMR (150 MHz; CDCl₃): δ 22.1 (C-3), 32.5 (C-2), 38.8 (C-4), 62.8 (C-1), 74.6 (C-5), 125.9 (C-7), 127.7 (C-9), 128.6 (C-8), 144.6 (C-6). IR (film, cm⁻¹): 3317, 2937, 1453, 1024. *m/z* (+ESI) 181.19 (100%, MH⁺).

7.11. Synthesis of 5-oxo-5-phenylpentanal [64] [70-71]



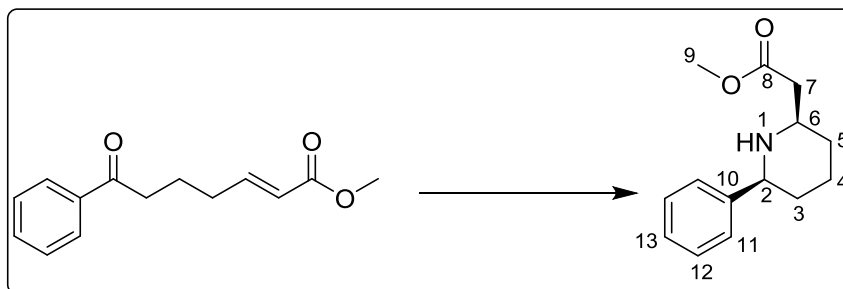
To a suspension of pyridinium chlorochromate (0.40 g, 1.7 mmols) in dichloromethane (10 mL) was added 1-phenylpentane-1,5-diol (**65**) (0.22 g, 1.2 mmols). The reaction mixture was stirred for 2 h at room temperature, filtered over silica and washed with diethyl ether (3 x 10 mL). The organic filtrate was combined, concentrated *in vacuo*, and purified by silica flash chromatography (petroleum ether/ethyl acetate 7:3) to give **64** as a pale yellow oil (0.11 g, 57%). ¹H NMR (600 MHz; CDCl₃): δ 9.75 (1H, s, 1-H), 7.95 (2H, m, 7-H), 7.58-7.41 (3H, m, 8-H, 9-H), 3.02 (2H, t, *J* = 7.5 Hz, 4-H₂), 2.58 (2H, m, 2-H₂), 2.05 (2H, m, 3-H₂). ¹³C NMR (150 MHz; CDCl₃): δ 180.9 (C-1), 179.0 (C-5), 126.6 (C-6), 124.0 (C-9), 120.2 (C-7), 119.5 (C-8), 49.0 (C-2), 43.9 (C-4), 27.0 (C-3). IR (film, cm⁻¹): 3314, 2943, 2831, 1412. *m/z* (+ESI) 177.08 (100%, MH⁺).

7.12. Synthesis of Methyl (E)-7-oxo-7-phenylhept-2-enoate *trans*-[42b]
[68, 72]



(Methoxycarbonylmethyl) triphenylphosphonium bromide (1.20 g, 2.90 mmols) in dichloromethane (10 mL) was shaken with aqueous sodium hydroxide (2 M, 5 mL) for 5 min. The organic layer was separated, dried (MgSO₄), and concentrated *in vacuo*. 5-Oxo-5-phenylpentanal (**64**) (0.45 g, 2.6 mmols) dissolved in dichloromethane (10 mL) was then added and the mixture stirred at room temperature (6 h). The reaction was concentrated *in vacuo*, re-suspended in pentane and filtered (3 x 10 mL). The crude filtrate was then purified by silica flash chromatography (4:1 petroleum ether/ethyl acetate) to yield **42b** as a clear viscous oil (0.41 g, 60%). ¹H NMR (600 MHz; CDCl₃): δ 1.94 (2H, quint, *J* = 7.1, 5-H₂), 2.32 (2H, quartet, *J* = 7.1, 4-H₂), 3.01 (2H, t, *J* = 7.1 Hz, 6-H₂), 3.73 (3H, s, OMe), 5.87 (1H, d, *J* = 15.6 Hz, 2-H), 6.99 (1H, dt, *J* = 15.6 Hz, 7.1 Hz, 3-H), 7.47 (2H, t, *J* = 7.3, Hz, 10-H), 7.57 (1H, t, *J* = 7.3, Hz, 11-H), 7.95 (2H, d, *J* = 7.3 Hz, 9-H). ¹³C NMR (150 MHz; CDCl₃): δ 22.4 (C-5), 31.6 (C-4), 37.6 (C-6), 51.5 (C-12), 121.7 (C-2), 128.1 (C-8), 128.7 (C-9, C-10), 133.2 (C-11), 136.9 (C-3), 148.6, 199.6 (C-7). IR (film, cm⁻¹): 2952, 1716, 1684, 1436, 1199; *m/z* (+ESI) 233.12 [MH]⁺; [HRMS (ESI):calcd. for C₁₄H₁₆O₃, 233.1133. Found: [MH]⁺, 233.1260

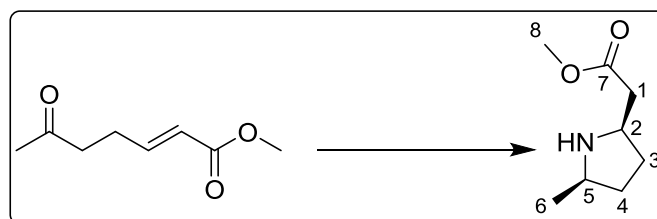
7.13. Synthesis of Methyl 2-((2*R*,6*S*)-6-phenylpiperidin-2-yl)acetate *cis*-[44b] ^[73]



To a solution of methyl (*E*)-7-oxo-7-phenylhept-2-enoate (**42b**) (0.12 g, 0.51 mmols) in methanol (30 mL) was added ammonium acetate (0.33 g, 4.3 mmols) and sodium cyanoborohydride (0.041 g, 0.65 mmols). The reaction was stirred at 60 °C for 11 h and then concentrated to dryness. The residue was partitioned between saturated aqueous sodium hydrogen carbonate (20 mL) and dichloromethane/methanol (9:1) (20 mL). The organic layer was extracted and the aqueous layer washed again with dichloromethane (3 x 20 mL). The combined organic layer was dried (MgSO₄), concentrated *in vacuo* and purified by silica flash chromatography (dichloromethane/methanol 20:1) to yield *cis*-**44b** as a clear oil (0.077 g, 77%). ¹H NMR (600 MHz; CDCl₃): δ 1.26-1.28 (1H, m, 5-H), 1.29-1.34 (2H, m, 3-H, 4-H), 1.53-1.55 (1H, m, 5-H), 1.67-1.69 (1H, m, 3-H), 1.79-1.80 (1H, m, 4-H), 2.50-2.51 (2H, m, 7-H₂), 3.14-3.19 (1H, m, 6-H), 3.66 (3H, s, OMe), 3.70-3.71 (1H, m, 2-H), 7.26 (1H, m, 13-H), 7.32-7.35 (2H, m, Ar-H₂), 7.37-7.41 (2H, m, Ar-H₂). IR (film, cm⁻¹): 3326, 2943, 2831, 1500, 1022; *m/z* (+ESI) 234.14 [MH]⁺; [HRMS (ESI):calcd. for C₁₄H₂₀NO₂, 234.1489. Found: [MH]⁺, 234.1485

Spectroscopic data was in agreement with literature values

7.14. Synthesis of Methyl 2-(5-methylpyrrolidin-2-yl)acetate *cis*-[47]
[74]



To a solution of Methyl (E)-6-oxohept-2-enoate (**45**) (0.1 g, 0.6 mmols) in methanol (20 mL) was added ammonium acetate (1.2 g, 15 mmols) and sodium cyanoborohydride (0.1 g, 0.9 mmols). The reaction was stirred at 60 °C for 11 h and then concentrated to dryness. The residue was partitioned between saturated aqueous sodium hydrogen carbonate (10 mL) and dichloromethane/methanol (9:1) (10 mL). The organic layer was extracted and the aqueous layer washed again (x3). The combined organic layer was dried over magnesium sulfate, concentrated *in vacuo* and purified by silica gel chromatography (dichloromethane/methanol 9.5:0.5) to yield **47** as a clear oil (0.085 g, 0.5 mmols, 83%). ¹H NMR (600 MHz; CDCl₃): δ 1.54 (3H, d, *J* = 6.8 Hz, 6-H₂), 2.24-2.36 (4H, m, 4-H₂, 3-H₂), 2.85-2.88 (1H, m, 1-H), 3.04-3.08 (1H, m, 1-H), 3.75 (3H, s, 8-H₃), 3.83-3.88 (1H, m, 5-H), 4.05-4.08 (1H, m, 2-H). IR (film, cm⁻¹): 3322 (N-H stretch), 2943 (C-H stretch), 1411 (C-H bending), 1022 (C-O stretch). *m/z* (+ESI) 158.11 (100%, MH⁺).

Spectroscopic data was in agreement with literature values

7.2. Biological and Biochemical Methods

7.2.1. Strains and Chemicals

Bacillus subtilis strain 1971, *Bacillus subtilis* strain 402, *Pseudomonas putida* 4475, *Klebsiella pneumoniae* (i.e. strain that produces KpN I restriction enzyme), *Rhodospirillum rubrum* DSM 467, and *Rhodobacter sphaeroides* 17025 and 17029, were obtained from an in-house culture collection (Prof. J. Ward, UCL). *E. coli* TOP10 and BL21 (DE3) PlysS were obtained from Invitrogen (Invitrogen, Paisley, UK). Zero Blunt® TOPO® Cloning Kit vector was purchased from Invitrogen (Invitrogen, Parsley, UK) and pET29a⁺ expression vector from Merck Bioscience (Merck, Darmstadt, Germany). Oligonucleotides were obtained from Operon (Cologne, Germany). Restriction enzymes were purchased from New England Biolabs (NEB, Hertfordshire, UK). Cell cultures (100 mL scale) were incubated in New Brunswick Scientific Innova 44 Incubator Shaker Series. Fermentations (1 L scale) were conducted on a Sartorius Stedim Biostat® Q plus multifermentor. Isopropyl β-D-1-thiogalactopyranoside (IPTG) and pirodoxal 5'-phospahte (PLP) were obtained from Fisher Scientific (Fisher, Loughborough, UK). All chemicals and solvents were analytical grade.

7.2.1.1. Chiral HPLC analysis of α -methylbenzylamine (1) to determine e.e.'s.

AD Column

Commercially available (\pm)- α -MBA (from Sigma-Aldrich, UK) was *N*-benzoylated and analysed using a ChiralPak AD normal phase column (4.6 mm x 250 mm, 10 μ m). An isocratic system of isopropanol:hexane (20:80) was run over 15 min (column temperature not controlled, flow rate 1 mL/min). UV detection was carried out at 254 nm. The retention times under these conditions were: 5.8 min (*R*)-MBA and 7.9 min (*S*)-MBA.

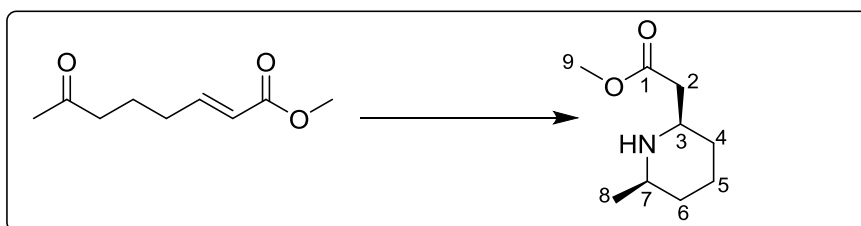
AD-H Column

Commercially available (\pm)- α -MBA (from Sigma-Aldrich, UK) was analysed directly using a ChiralPak® AD-H (4.6 mm x 250 mm, 5 μ m particle size). An isocratic solvent system of heptane:ethanol:formic acid (95:5:0.02) was run for 40 min (column temperature not controlled, flow rate 1 mL/min). UV detection was carried out at 210 nm. The retention times under these conditions were: 26.5 min (*R*)-MBA, 31.2 min (*S*)-MBA and 7.6 min acetophenone.

CrownPak CR+ Column

Commercially available (\pm)- α -MBA (from Sigma-Aldrich, UK) was analysed directly using a CrownPak® CR+ (4.6 mm x 150 mm, 5 μ m). An isocratic solvent system of perchloric acid (pH 1.5):acetonitrile (85:15) was run for 40 min (column temperature not controlled, flow rate 0.7 mL/min). UV detection was carried out at 210 nm. The retention times under these conditions were: 9.2 min (*S*)-MBA, 12.8 min (*R*)-MBA and 36 min acetophenone.

7.2.1.2. Biotransformation of Methyl (\pm)-(cis-6'-methylpiperidin-2'-yl)acetate *cis*-[44a] with (*S*)- α -methylbenzylamine [1]



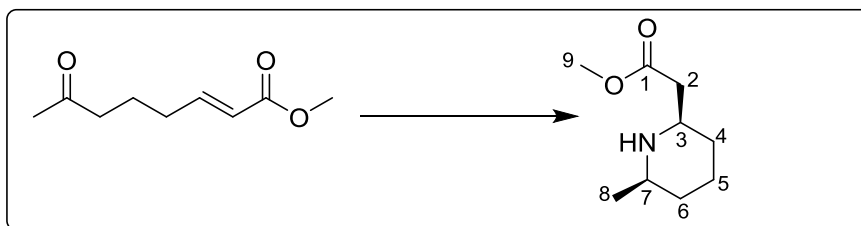
(*S*)- α -methylbenzylamine (0.31 mL, 100 mM) was added to potassium phosphate buffer (100 mM, pH 8.5, 5 mL) and the pH corrected to 7.5 with hydrochloric acid (10 M). Methyl (*E*)-7-oxooct-2-enoate (**42a**) (40 mg, 10 mM) was added to the reaction mixture, sonicated in a sonicating bath (1 min), and the reaction volume made up to 24 mL with more potassium phosphate buffer. Lyophilised CV2025 (0.5 g) and pyridoxal-5'-phosphate (12 mg, 2 mM) were then added and the reaction mixture left shaking (30 °C, 200 rpm, 72 h). The reaction was stopped with saturated aqueous sodium hydrogen carbonate (20 mL) and extracted with ethyl acetate (3 x 15 mL). The combined organic layers were then dried (MgSO₄) and concentrated to an oil. All spectroscopic data was in agreement with the literature ^[59].

Reverse phase HPLC: C18 column (250 mm x 4.6 mm, 10 μ m), (35% acetonitrile (0.1% TFA):65% H₂O (0.1% TFA), 1 mL/min, 218 nm) *cis*-**44a** was detected at 19.2 min.

GC-MS: Column (Hypersil Gold PFP (150 x 2.1 mm, 5 μ m), 15% MeCN (0.01% formic acid):85% H₂O (0.01% formic acid), 0.3 mL/min) *cis*-**44a** had a retention time of 1.8 min

LC-MS: C18 column (150 mm x 4.6 mm; 5 μ m), 10% MeCN (0.01% formic acid):80% H₂O (0.01% formic acid), 0.2 mL/min) *cis*-**44a** had a retention time of 2.5 min.

7.2.1.3. Biotransformation of Methyl (±)-(cis-6'-methylpiperidin-2'-yl)acetate *cis*-[44a] with isopropylamine [11]



Isopropylamine (2.7 mL, 1 M) was added to potassium phosphate buffer (100 mM, pH 8.5, 5 mL) and the pH corrected to 8.5 with hydrochloric acid (10 M). Methyl (E)-7-oxooct-2-enoate (**42a**) (40 mg, 10 mM) was added to the reaction mixture, sonicated in a sonicating bath (1 min), and the reaction volume made up to 24 mL with more potassium phosphate buffer. Lyophilised CV2025 (0.5 g) and pyridoxal-5'-phosphate (12 mg, 2 mM) were then added and the reaction mixture left shaking (30 °C, 200 rpm, 72 h). The reaction was stopped with saturated aqueous sodium hydrogen carbonate (20 mL) and extracted with ethyl acetate (3 x 15 mL). The combined organic layers were dried over magnesium sulfate and concentrated to an oil. All spectroscopic data were in agreement with the literature ^[59].

All chromatographic data were identical to section 7.2.1.2 (above)

7.2.1.4. LDH/GDH Coupled enzyme reaction

In order to ascertain a qualitative assessment of the enzyme activity of the novel enzymes, the LDH/GDH-coupled enzyme reaction was used [Scheme 11]. Two sets of amine donor stock solutions were prepared, containing L- or D-alanine in potassium phosphate buffer (40 mL, pH 7.5) [Table 25].

Table 25: Components of the LDH/GDH-coupled enzyme reaction for the screening of novel TAmS

TAm Reaction Component	Concentration g/mL	Stock Solution g/40mL
Pyridoxal phosphate	0.5	0.02
L-Alanine	45	1.8
D-Alanine	45	1.8
Acetophenone	-	5 mM
Potassium phosphate monobasic	2.15	-
Potassium phosphate dibasic	14.7	-
ATA-113	5	0.025
ATA-117	5	0.025
Novel TAmS (5+CV2025)	5	0.025
Recycling Component		g/32mL
Lactate dehydrogenase	1	0.032
Glucose dehydrogenase	1	0.032
NADH	1	0.032
Glucose	10	0.32

One 8 mL aliquot each was taken from each of the two stock solutions and acetophenone was added (4.7 μ L). One mL aliquots were then taken from each of

these stock solutions to prepare seven negative control experiments with the seven TAmS in this study (CV2025, BSU_402, KpN_00799, BSU1971, PP_3718, ATA-113, ATA-117). In total there were 14 negative control experiments, covering L- and D-alanine, all the novel TAmS (including CV2025) and the two commercially available Codexis® TAmS.

The LDH/GDH recycling components were then added to the remaining alanine-PLP stock solutions (32 mL). These were further split into seven 4 mL aliquots and the various transaminases (0.02 g) added to the separate batches. Acetophenone (2.4 μ L) was then added to each of the fourteen 4 mL samples to start the reaction. The reaction samples were aliquoted out into triplicates of 1 mL reactions in a standard 96-well plate and shaken at 35 °C, 400 rpm for 24 h.

7.2.1.5. Design of experiment (DoE) study

To investigate the optimal conditions required for improving the biocatalytic conversion of methyl (*E*)-7-oxooct-2-enoate (**42a**) using CV2025 ω -TAm and (*S*)-MBA, a design of experiment (DoE) study was conducted. A list of five parameters was chosen to be investigated across two value ranges (high and low) [Table 26]. The low value range for all the parameters was chosen based on literature conditions from various sources [33b, 58]. A freeware programme (Design-Expert V8.0.6.1) was used to generate a reaction list comprising 32 reactions [Table 27].

Table 26: Parameters and value ranges used in the first DoE study

Parameters	High	Low
------------	------	-----

Enzyme	0.12 U	0.07 U
Amine	50 eq	5 eq
pH	8.5	7.5
PLP	1.5 mM	0.5 mM
Temperature	35 °C	25 °C

Table 27: Design of experiment reaction list

	Run #1	Run #2	Run #3	Run #4
Block	Block1	Block 1	Block 1	Block 1
[Enz]/ %	25	25	25	25
[Amine]/ eq	100	100	10	10
pH	8.5	7.5	8.5	7.5
[PLP]/ mM	1	1	3	3
Temp/ °C	35	25	25	35

	Run #5	Run #6	Run #7	Run #8
Block	Block1	Block 1	Block 1	Block 1
[Enz]/ %	25	25	25	25
[Amine]/ eq	10	100	10	10
pH	7.5	7.5	8.5	7.5
[PLP]/ mM	1	3	3	3
Temp/ °C	25	25	35	25

	Run #9	Run #10	Run #11	Run #12
Block	Block1	Block 1	Block 1	Block 1
[Enz]/ %	25	25	25	25
[Amine]/ eq	10	100	10	100
pH	8.5	8.5	7.5	8.5
[PLP]/ mM	1	1	1	3
Temp/ °C	25	25	35	35

	Run #13	Run #14	Run #15	Run #16
Block	Block 1	Block 1	Block 1	Block 1
[Enz]/ %	25	25	25	25
[Amine]/ eq	10	100	100	100

pH	8.5	7.5	7.5	8.5
[PLP]/ mM	1	1	3	3
Temp/ °C	35	35	35	25

	Run #17	Run #18	Run #19	Run #20
Block	Block 1	Block 1	Block 1	Block 1
[Enz]/ %	45	45	45	45
[Amine]/ eq	100	100	100	100
pH	7.5	7.5	7.5	8.5
[PLP]/ mM	3	1	1	1
Temp/ °C	35	25	35	35

	Run #21	Run #22	Run #23	Run #24
Block	Block1	Block 1	Block 1	Block 1
[Enz]/ %	45	45	45	45
[Amine]/ eq	10	100	10	10
pH	8.5	7.5	7.5	8.5
[PLP]/ mM	1	3	3	1
Temp/ °C	25	25	35	35

	Run #25	Run #26	Run #27	Run #28
Block	Block1	Block 1	Block 1	Block 1
[Enz]/ %	45	45	45	45
[Amine]/ eq	10	100	10	100
pH	7.5	8.5	7.5	8.5
[PLP]/ mM	1	3	1	1
Temp/ °C	25	35	35	25

	Run #29	Run #30	Run #31	Run #32
Block	Block1	Block 1	Block 1	Block 1
[Enz]/ %	45	45	45	45
[Amine]/ eq	10	10	100	10
pH	8.5	8.5	8.5	7.5
[PLP]/ mM	3	3	3	3
Temp/ °C	35	25	25	25

Transaminase stock solutions were prepared at twice the required concentration (50% and 90%) in 20 mL of potassium phosphate buffer (100 mM). The two concentrations of amine donor were then prepared also in potassium phosphate buffer and pH-corrected to a final volume of 24 mL. These two sets of stock solutions

were then divided into four groups of 6 mL and the two concentrations of PLP added to the respective groups. Methyl (*E*)-7-oxooct-2-enoate (**42a**) (10 mM) was added to all eight 6 mL reaction mixtures. According to the layout of the reaction list [Table 27] 150 μ L aliquots were taken from each of the eight reaction mixtures and dispensed in their respective wells in two separate 96-well plates. CV2025 ω -TAm lysates (150 μ L) were then added to each well according to the reaction list and the reactions shaken at 25 °C or 35°C on an Eppendorf Thermomixer for 24 h.

7.2.1.6. Cloning of the selected transaminases

7.2.1.6.1. DNA extraction using phenol-chloroform

The extraction of genomic DNA from the five different bacterial strains involved in this work was conducted by a standard phenol-chloroform protocol. A loop of the relevant bacterial strain (from -80 °C storage) was taken and re-suspended in elution buffer (10 mM Tris-HCl, pH 8.5, 200 μ L). This was further diluted with phenol/chloroform/isoamyl alcohol solution (Sigma Aldrich, Haverhill, UK) (200 μ L) and vortexed vigorously (1 min). The mixture was then centrifuged (13,000 x *g*, 5 mins, 4° C) and the aqueous layer of the supernatant removed (180 μ L). Elution buffer (200 μ L) was subsequently added to the remainder of the phenol/chloroform/isoamyl alcohol and cell pellet suspension, vortexed (1 min) and centrifuged (13,000 x *g*, 5 mins, 4 °C). The aqueous layer was once again removed (180 μ L) and combined with the previously extracted aqueous layer in a fresh tube. To this was added equal volumes of the chloroform/isoamyl alcohol solution, vortexed (1 min) and centrifuged (13,000 x *g*, 5 mins 4 °C). The aqueous layer of the supernatant was then removed (330 μ L) and placed in another tube. To this was added NH₄OAc (0.75 M final concentration) and glycogen (1 μ L of 20 mg/mL solution) followed by a thorough mixing. Ethanol was then added (100%, 600 μ L), and the mixture vortexed and incubated (20 °C, 10 mins) before centrifugation

(13,000 x *g*, 20 mins, 4 °C). The supernatant was decanted and the pellet washed with ethanol (80%, 300 µL) by vortexing thoroughly. The mixture was then centrifuged (13,000 x *g*, 15 mins, 4 °C) and supernatant decanted. The wash was repeated once more with ethanol (80%) followed by air drying of the pellet (1 -2 mins) before re-suspending in elution buffer (200 µL) and storing at -80 °C .

7.2.1.6.2. PCR amplification of TAm genes

Using the corresponding primers [Table 7], ten novel omega-transaminase genes were amplified from the chromosomal DNA of their respective microorganisms. PCR amplification was conducted using the corresponding primers and 1 U of Phusion® High-Fidelity DNA Polymerases from Finnzymes (Thermo Scientific, Loughborough, UK). The PCR settings were as follows: heating 98 °C for 2 min (1 cycle); 98 °C for 15 s; 60 °C or 65 °C for 30 s; 72 °C for 15 s (30 cycles); 72 °C for 10 min (1 cycle). The PCR products were then stored at 4 °C for ligation into a cloning vector.

7.2.1.6.3. Ligation into cloning vector

Ligation of the PCR product into a cloning vector was conducted using a pCR™ 4-TOPO® cloning vector (Invitrogen, Paisley, UK) (1 µL) and PCR product (1 µL) mixed in a tube containing a pre-prepared solution of T4 DNA ligase and ATP in ligase buffer. The reaction was incubated (50 mins) before transformation into competent *E. coli* cells and selected on LB plates containing 100 µg/mL ampicillin.

7.2.1.6.4. DNA Miniprep

LB media (3 mL) was inoculated with bacterial clones picked from the appropriate transformation reaction and incubated (37 °C, 200 rpm, 16 h). Aliquots (2 x 750 µL) were taken, centrifuged (10, 000 x *g*, 1 min) and the supernatant removed. The

resultant bacterial pellet was resuspended in buffer (25 mM Tris-HCl, pH 8.0, 10 mM EDTA, and 100 μ L) and vortexed. Lysis buffer (100 μ L) (prepared from equal parts 800 mM NaOH, and 4% SDS solutions) was then added and gently mixed at room temperature (3 mins). Neutralisation buffer (5 M potassium acetate, pH 5.5, 120 μ L) was subsequently added, mixed and incubated at room temperature (3 mins). The solution was then centrifuged (10,000 $\times g$, 2 mins), the supernatant transferred and isopropanol (200 μ L) added to precipitate plasmid DNA. The DNA was collected by centrifugation (10,000 $\times g$, 1 min) and discarded the supernatant isopropanol. Ethanol (70 %, 500 μ L) was added to the DNA pellet, thoroughly mixed and then concentrated (10, 000 $\times g$, 1 min). The supernatant was removed and the pellets air-dried (10 mins) before dissolving the DNA in dionised water (20 μ L).

7.2.1.6.5. Ligation into expression vector

To facilitate the subsequent ligation into the expression vector pET29a⁺ (Merck, Darmstadt, Germany), all oligonucleotide primers were designed to include the restriction cleavage sites *Nde* I and *Xho* I except for those of *Rhodospirillum rubrum* which contain *Nde* I and *Hind* III sites.

Fresh pET29a⁺ expression vector [Figure 53] (50 ng) was linearised using the appropriate restriction enzymes as the PCR products were digested from the TOPO[®] cloning vector in parallel. The digested DNA fragments were electrophoresed on 1% TAE agarose gel (1.5 h, 90 V) and purified using gel DNA extraction kit (Qiagen, UK). The digested PCR fragments and pET29a⁺ were then ligated at a 5:1 molar ratio using a Quick ligase kit (NEB, Hertfordshire, UK) at room temperature. The constructed pET29a⁺ vector with desired insert was confirmed by electrophoresis and designated a pQR code [Table 2.1].

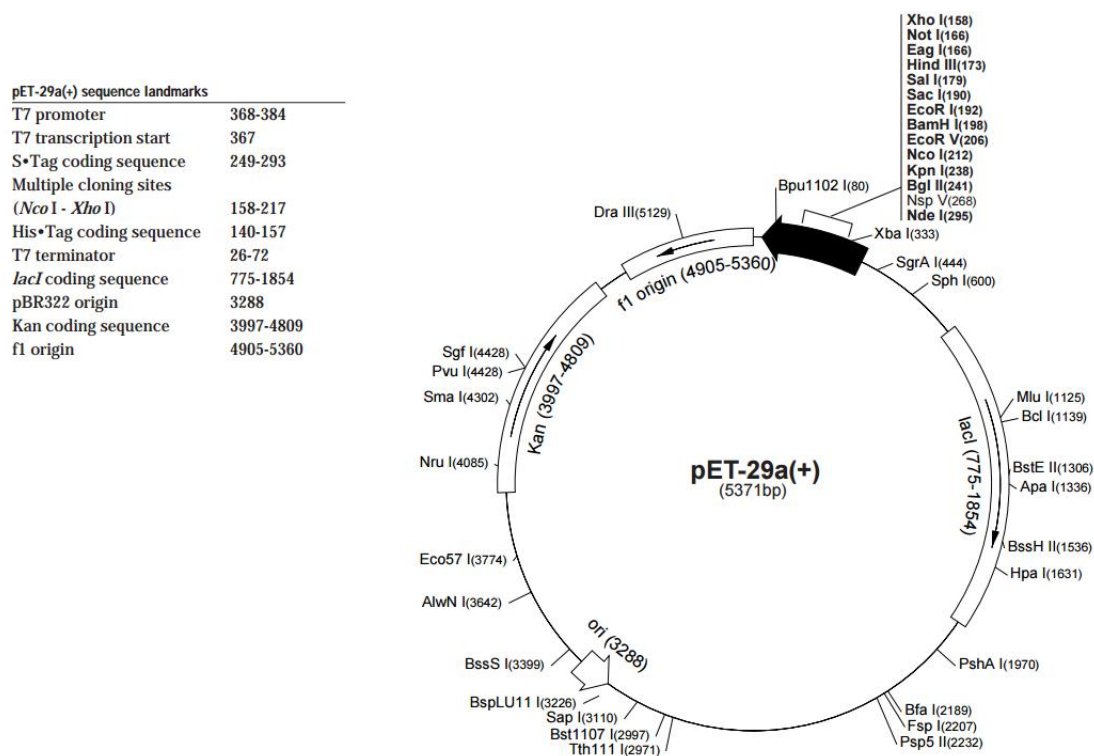


Figure 53: Vector map of pET29a showing the various restriction sites (adapted from <http://www.synthesisgene.com>)

In addition, the previously reported ω -transaminase from *C. violaceum* (Kaulmann et al. 2007) and a synthetic gene version of the TAM from *V. fluvialis* (Shin et al. 2003) were used in this work.

E. coli BL21 StarTM (DE3) pLysS competent cells (Invitrogen, UK) (20 μ l) were transformed with the products of each of the ligation reactions (1 μ l) separately using a short procedure. Competent cells were incubated for 5 min on ice, and heat-shocked by immediate plating on pre-warmed (37 °C) agar plates. Transformed cells were selected on kanamycin (50 μ g/mL) and Chloramphenicol (30 μ g/mL) agar media, and the resulting transformants were cultured in 50 mL 2xTY media (16 g/L tryptone, 10 g/L yeast extract, 5 g/L NaCl) containing 50 μ g/mL kanamycin and 30 μ g/mL chloramphenicol at 37 °C, 220 rpm for 16 h. The culture was diluted 1:100 into 500 mL of fresh 2xTY media containing the same concentration of antibiotics and incubated under the same conditions. When the OD₆₀₀ reached 0.9, IPTG was added

(1 mM final concentration). After 6 h induction at 30 °C, the samples were treated with SDS-loading buffer for SDS-PAGE analysis before cells were pelleted by centrifugation (15,550 g) for 15 min, re-suspended in 0.5% w/v lysis buffer (100 mM HEPES buffer, 0.2 mM PLP, pH 8.0), and centrifuged again to collect cell pellets. These were either stored at -80 °C, freeze dried or sonicated to prepare crude lysates. The lysates were prepared by disrupting the cells by sonication using an MSE Soniprep™ 150 with microprobe tip at a rate of 10 cycles of 15 s on/15 s off. The sonicated suspension was centrifuged at 13,000 × g and 4 °C in an Eppendorf centrifuge for 20 min. The supernatant was used immediately or frozen at -20 °C (clarified lysate) for a maximum of 1 month.

Alternatively, other batches of fermentation were lyophilised using a Cole-Parmer 1 L benchtop freeze dry system at -110 °C. This was conducted by transferring freshly pelleted wet cell paste (0.5 g) into Falcon® tubes (15 mL capacity). The tubes were then placed in a liquid nitrogen bath, fully submerged for 5 min. The frozen tubes were then placed in a long-necked 1 L round bottom flask and attached to the freeze dryer with the vacuum turned on for 16 h. The lyophilised cells were then stored safely at -20 °C for no more than 3 months.

7.2.1.7. *Vibrio fluvialis* transaminase synthetic gene

The *V. fluvialis* aminotranferase wild-type gene (Shin et al. 2003) was codon-optimised, synthesized by MWG Operon (Eurofin MWG Operon, Ebersberg, Germany), and cloned into the pET29a⁺ expression vector (Merck, Darmstadt, Germany). The vector was transformed into the chemically competent BL21 (DE3) pLysS *E. coli* strain (Invitrogen, Paisley, UK).

7.2.2. Fermentation of the Transaminase Gene Recombinant *E. Coli*

Six recombinant *E. coli* cell cultures [Table 28] were grown in a Biostat® Q multifermentor to acquire more biomass. The cell cultures were grown from pre-prepared glycerol stock inoculums in LB media (50 µg/mL) at 37 °C, 200 r.p.m for 16 h. Samples from the overnight LB media cell cultures (5% v/v) were used to inoculate 50 mL of seed media [Table 10] and incubated at 30 °C, 200 rpm for 6 h. 750 mL of production media [Table 10] was sterilised and set up on the fermentor at 30 °C, pH 7 and 40% dissolved oxygen saturation with feed bottles of 5 M NaOH and 5 M H₃PO₄ attached. The recorded pre-inoculation OD₆₀₀ values were as follows: CV2025 (A1) = 6.0, CV2025 (A2) = 5.8, CV2025 (A3) = 5.0, VF_JS17 = 3.1, BSU09269_402 = 3.9, KpN_00799 = 1.7, BSU09269_1971 = N/A, PP_3718 = N/A.

Table 28: OD₆₀₀ Values Recorded During Fermentation of All Six Cultures

Cell culture	OD ₆₀₀			
	Pre-feed	Post-feed	Post-induction	Final
CV2025 (F1)	12.2	18.5	23	31
CV2025 (F2)	18.4	18.6	33	46
CV2025 (F3)	12	N/A	28	24
VF_JS17	17	25	53	58
BSU09269_402	10.7	38	53	55
KpN_00799	1.7	24	38	45
BSU09269_1971	N/A*	N/A	N/A	N/A
PP_3718	N/A	N/A	N/A	N/A

* N/A = Data not recorded

After a 20 h run-time 5 mL of the seed culture was used to inoculate the various primed fermentors. Gradual addition of 300 mL of feed media [Table 10] and subsequent induction of over-expression with IPTG (1 mM) then followed after 3 h and the following OD₆₀₀ values were recorded [Table 28]. All cells were harvested approximately 6 h after induction of over-expression. The following wet weights were recorded: CV2025 (A1) = 56 g, CV2025 (A2) = 68 g, CV2025 (A3) = 53 g, VF_JS17 = 105 g, BSU09269_402 = 92 g, KpN_00799 = 70 g, BSU09269_1971 = 72 g, PP_3718 = 60 g.

7.2.2.1. Purification of recombinant transaminases

Purification of the recombinant transaminases [Table 28] was carried out following standard nickel affinity chromatography of the hexa-histidine-tagged proteins. Binding buffer was prepared by dissolving monobasic potassium phosphate (158 mmols, 2.15 g) and dibasic potassium phosphate (84.1 mmols, 14.7 g) in dH₂O (1 L) to make up 100 mM potassium phosphate buffer (pH 7.5). To this was added imidazole (40 mM) and sodium chloride (300 mM). The resulting solution was degassed and filtered through a pore filter (0.4 µm). The elution buffer was then prepared by dissolving imidazole (1 M) and sodium chloride (300 mM) in potassium phosphate buffer (100 mM, pH 7.5, 1 L), filtering and degassing it as with the binding buffer. A 5 mL nickel column (HisTrap_HP_5 mL, GE Healthcare) attached to a liquid chromatography system was primed following the manufacturer's protocol. Distilled water (10 mL) was flushed through the column (2 mL/min) followed by EDTA (50 mM, 10 mL), a second round of distilled water (10 mL), nickel sulfate solution (100 mM, 5 mL), a third round of distilled water (5 mL), and then the binding buffer solution (15 mL). Transaminase crude lysate (25% w/v, 5 mL) was then loaded on to the column and washed with binding buffer (15 mL). Elution buffer (10 mL) was then pumped through the column and collected (1 mL samples). Another wash with elution buffer (15 mL) was then

followed by distilled water (15 mL) and 20% ethanol (15 mL). Samples were stored for later use at -20°C

7.2.2.2. Amino Acid Oxidase Colorimetric Assay

The amino acid oxidase-based colorimetric assay [33c], was used in this work with minor modifications to screen for enzyme activity in the novel transaminases. Stock solutions of the amine donor (separate solutions for (S)- and (R)-MBA), detection enzymes, and novel TAmS were prepared [Table 29] in potassium phosphate buffer (pH 7.5). All the enzymes were first dispensed (10 µL) in their respective wells in a 400 µL 96-well plate [Table 30]. The reaction was then started by addition of the appropriate substrate cocktail to their corresponding wells. All except “ATA-117 positive control” contained the (S)-MBA substrate cocktail. The plate was incubated in a spectrophotometer at 35 °C with shaking for 30 min.

Table 29: Components of AAO colorimetric assay screening of novel transaminases

Amine Donor Component	Concentration g/mL	Stock solution g/200mL
Pyrogallol Red	0.1	0.02
Sodium pyruvate	0.2	0.04
Pyridoxal phosphate	0.05	0.01
Potassium phosphate dibasic	14.2	2.8
Potassium phosphate monobasic	2.51	0.5
(S)- or (R)-α-MBA	0.61 or 0.65 mL	130 µL

Amine Donor Component	Concentration g/mL	Stock solution g/200mL
Enzyme Component		Stock Solution/ g/2mL
Horseradish peroxidase	1	0.002
(D)- or (L)-amino acid oxidase	10	0.02
Transaminase Component		Stock Solution/ g/mL
ATA-113	0.6	0.006
ATA-117	0.6	0.006
Novel TAmS	0.6	0.006

Table 30: Layout of AAO colorimetric assay screen of novel TAmS

Neg. Control (1)	Neg. Control (2)	Pos. Control ATA- 113	Pos. Control ATA- 117	CV2025	VF_JS17	BSU_402	KpN_00799	PP_3718
No detect.	No TAm	ATA-113 +(S)- MBA	ATA-117 + (R)- MBA	1	1	1	1	1
No detect.	No TAm	ATA-113 +(S)- MBA	ATA-117 + (R)- MBA	2	2	2	2	2
No detect.	No TAm	ATA-113 +(S)- MBA	ATA-117 + (R)- MBA	3	3	3	3	3

*The reaction was carried out in triplicate (1,2,3) and "No detect." refers to the absence of detection enzymes component.

References

- [1] a) A. Braunstein and M. Shemiakin in *Theory on amino acid metabolism processes catalyzed by pyridoxine enzymes*, Vol. 18 Biokhimiia, Russia, 1953, pp. 393-411; b) W. T. Jenkins and M. L. Fonda, *Transaminases*, Wiley, New York, 1985, p.
- [2] J. D. Lueck and H. J. Fromm, *Febs Letters* 1973, 32, 184-186.
- [3] S. J. Okeefe and J. R. Knowles, *Biochemistry* 1986, 25, 6077-6084.
- [4] W. E. Karsten, Z. L. Reyes, K. D. Bobyk, P. F. Cook and L. Chooback, *Archives of Biochemistry and Biophysics* 2011, 516, 67-74.
- [5] P. K. Mehta, T. I. Hale and P. Christen, *European Journal of Biochemistry* 1989, 186, 249-253.
- [6] a) P. K. Mehta, T. I. Hale and P. Christen, *European Journal of Biochemistry* 1993, 214, 549-561; b) J. Ward and R. Wohlgemuth, *Current Organic Chemistry* 2010, 14, 1914-1927.
- [7] B. Y. Hwang, B. K. Cho, H. Yun, K. Koteshwar and B. G. Kim, *Journal of Molecular Catalysis B-Enzymatic* 2005, 37, 47-55.
- [8] a) J. N. Jansonius, *Current Opinion in Structural Biology* 1998, 8, 759-769; b) A. C. Eliot and J. F. Kirsch, *Annual Review of Biochemistry* 2004, 73, 383-415.
- [9] A. M. Delpozo, M. Merola, H. Ueno, J. M. Manning, K. Tanizawa, K. Nishimura, K. Soda and D. Ringe, *Journal of Biological Chemistry* 1989, 264, 17784-17789.
- [10] A. Nedal and S. B. Zotchev, *Applied Microbiology and Biotechnology* 2004, 64, 7-15.
- [11] E. S. Burgie, J. B. Thoden and H. M. Holden, *Protein Science* 2007, 16, 887-896.
- [12] J. Marienhagen, T. Sandalova, H. Sahn, L. Eggeling and G. Schneider, *Acta Crystallographica Section D-Biological Crystallography* 2008, 64, 675-685.
- [13] T. Sehl, H. C. Hailes, J. M. Ward, R. Wardenga, E. von Lieres, H. Offermann, R. Westphal, M. Pohl and D. Rother, *Angewandte Chemie-International Edition* 2013, 52, 6772-6775.
- [14] J. Kim, D. Kyung, H. Yun, B.-K. Cho, J.-H. Seo, M. Cha and B.-G. Kim, *Applied and Environmental Microbiology* 2007, 73, 1772-1782.
- [15] J. S. Shin and B. G. Kim, *Bioscience Biotechnology and Biochemistry* 2001, 65, 1782-1788.
- [16] J. S. Shin, B. G. Kim, A. Liese and C. Wandrey, *Biotechnology and Bioengineering* 2001, 73, 179-187.
- [17] J. S. Shin and B. G. Kim, *Journal of Organic Chemistry* 2002, 67, 2848-2853.
- [18] U. Kaulmann, K. Smithies, M. E. B. Smith, H. C. HaileS and J. M. Ward, *Enzyme and Microbial Technology* 2007, 41, 628-637.
- [19] F. W. Alexander, E. Sandmeier, P. K. Mehta and P. Christen, *European Journal of Biochemistry* 1994, 219, 953-960.
- [20] H. C. Dunathan, *Proceedings of the National Academy of Sciences of the United States of America* 1966, 55, 712-&.
- [21] J. F. Kirsch, G. Eichele, G. C. Ford, M. G. Vincent, J. N. Jansonius, H. Gehring and P. Christen, *Journal of Molecular Biology* 1984, 174, 497-525.
- [22] J. E. Churchich and U. Moses, *Journal of Biological Chemistry* 1981, 256, 1101-1104.
- [23] M. S. Humble, K. E. Cassimjee, M. Hakansson, Y. R. Kimbung, B. Walse, V. Abedi, H.-J. Federsel, P. Berglund and D. T. Logan, *Febs Journal* 2012, 279, 779-792.

- [24] A. I. Denesyuk, K. A. Denessiouk, T. Korpela and M. S. Johnson, *Journal of Molecular Biology* 2002, *316*, 155-172.
- [25] E.-S. Park, M. Kim and J.-S. Shin, *Applied Microbiology and Biotechnology* 2012, *93*, 2425-2435.
- [26] M. Hoehne, S. Schaetzle, H. Jochens, K. Robins and U. T. Bornscheuer, *Nature Chemical Biology* 2010, *6*, 807-813.
- [27] A. Iwasaki, Y. Yamada, N. Kizaki, Y. Ikenaka and J. Hasegawa, *Applied Microbiology and Biotechnology* 2006, *69*, 499-505.
- [28] D. Koszelewski, M. Goeritzer, D. Clay, B. Seisser and W. Kroutil, *Chemcatchem* 2010, *2*, 73-77.
- [29] M. Thomsen, L. Skalden, G. J. Palm, M. Hoehne, U. T. Bornscheuer and W. Hinrichs, *Acta Crystallographica Section D-Biological Crystallography* 2014, *70*, 1086-1093.
- [30] C. Sayer, R. J. Martinez-Torres, N. Richter, M. N. Isupov, H. C. Hailes, J. A. Littlechild and J. M. Ward, *Febs Journal* 2014, *281*, 2240-2253.
- [31] a) H. Kitaguchi, P. A. Fitzpatrick, J. E. Huber and A. M. Klibanov, *Journal of the American Chemical Society* 1989, *111*, 3094-3095; b) A. L. Gutman, E. Meyer, E. Kalerin, F. Polyak and J. Sterling, *Biotechnology and Bioengineering* 1992, *40*, 760-767.
- [32] a) J. S. Shin and B. G. Kim, *Biotechnology and Bioengineering* 1997, *55*, 348-358; b) H. Yun, B. K. Cho and B. G. Kim, *Biotechnology and Bioengineering* 2004, *87*, 772-778; c) M. S. Malik, E.-S. Park and J.-S. Shin, *Green Chemistry* 2012, *14*, 2137-2140.
- [33] a) S. Schaetzle, M. Hoehne, E. Redestad, K. Robins and U. T. Bornscheuer, *Analytical Chemistry* 2009, *81*, 8244-8248; b) M. D. Truppo, J. D. Rozzell, J. C. Moore and N. J. Turner, *Organic & Biomolecular Chemistry* 2009, *7*, 395-398; c) J. Hopwood, M. D. Truppo, N. J. Turner and R. C. Lloyd, *Chemical Communications* 2011, *47*, 773-775; d) M. D. Truppo and N. J. Turner, *Organic & Biomolecular Chemistry* 2010, *8*, 1280-1283; e) M. Bommer and J. M. Ward, *Enzyme and Microbial Technology* 2013, *52*, 218-225; f) E. O'Reilly, C. Iglesias, D. Ghislieri, J. Hopwood, J. L. Galman, R. C. Lloyd and N. J. Turner, *Angewandte Chemie-International Edition* 2014, *53*, 2447-2450.
- [34] a) H. Iloukhani, F. Rajali and A. Zeini, *Physics and Chemistry of Liquids* 2001, *39*, 239-247; b) E. Atala, G. Velasquez, C. Vergara, C. Mardones, J. Reyes, R. A. Tapia, F. Quina, M. A. Mendes, H. Speisky, E. Lissi, M. S. Ureta-Zanartu, A. Aspee and C. Lopez-Alarcon, *Journal of Physical Chemistry B* 2013, *117*, 4870-4879.
- [35] T. Sehl, R. C. Simon, H. C. Hailes, J. M. Ward, U. Schell, M. Pohl and D. Rother, *Journal of Biotechnology* 2012, *159*, 188-194.
- [36] P. P. Taylor, D. P. Pantaleone, R. F. Senkpeil and I. G. Fotheringham, *Trends in Biotechnology* 1998, *16*, 412-418.
- [37] a) K. E. Cassimjee, C. Branneby, V. Abedi, A. Wells and P. Berglund, *Chemical Communications* 2010, *46*, 5569-5571; b) C. K. Savile, J. M. Janey, E. C. Mundorff, J. C. Moore, S. Tam, W. R. Jarvis, J. C. Colbeck, A. Krebber, F. J. Fleitz, J. Brands, P. N. Devine, G. W. Huisman and G. J. Hughes, *Science* 2010, *329*, 305-309; c) N. Richter, R. C. Simon, W. Kroutil, J. M. Ward and H. C. Hailes, *Chemical Communications* 2014, *50*, 6098-6100.
- [38] B. Wang, H. Land and P. Berglund, *Chemical Communications* 2013, *49*, 161-163.
- [39] S. Lalli and A. Albanese, *Expert review of neurotherapeutics* 2008, *8*, 1181-1188.

- [40] M. Fuchs, D. Koszelewski, K. Tauber, W. Kroutil and K. Faber, *Chemical Communications* 2010, *46*, 5500-5502.
- [41] K. B. Hansen, H. Yi, F. Xu, N. Rivera, A. Clausen, M. Kubryk, S. Krska, T. Rosner, B. Simmons, J. Balsells, N. Ikemoto, Y. Sun, F. Spindler, C. Malan, E. J. J. Grabowski and J. D. Armstrong, III, *Journal of the American Chemical Society* 2009, *131*, 8798-8804.
- [42] S. Altschul, W. Gish, W. Miller, E. Myers, D. Lipman, *Journal of Molecular Biology*, 1990, *215*, 403-410
- [43] M. M. Nakano and P. Zuber, *Annual Review of Microbiology* 1998, *52*, 165-190.
- [44] C. Mackenzie, J. M. Eraso, M. Choudhary, J. H. Roh, X. Zeng, P. Bruscella, A. Puskas and S. Kaplan, *Annual Review of Microbiology* 2007, *61*, 283-307.
- [45] S. Kumar, M. Nei, J. Dudley and K. Tamura, *Briefings in Bioinformatics* 2008, *9*, 299-306.
- [46] a) F. G. Mutti, C. S. Fuchs, D. Pressnitz, J. H. Sattler and W. Kroutil, *Advanced Synthesis & Catalysis* 2011, *353*, 3227-3233; b) D. Clay, D. Koszelewski, B. Grischek, J. Gross, I. Lavandera and W. Kroutil, *Tetrahedron-Asymmetry* 2010, *21*, 2005-2009.
- [47] J.-S. Shin and B.-G. Kim, *Biotechnology Letters* 2009, *31*, 1595-1599.
- [48] M. E. B. Smith, B. H. Chen, E. G. Hibbert, U. Kaulmann, K. Smithies, J. L. Galman, F. Baganz, P. A. Dalby, H. C. Hailes, G. J. Lye, J. M. Ward, J. M. Woodley and M. Micheletti, *Organic Process Research & Development* 2010, *14*, 99-107.
- [49] A. Amrane, *Journal of General and Applied Microbiology* 2003, *49*, 21-27.
- [50] F. W. Bai, L. P. Wang, H. J. Huang, J. F. Xu, J. Caesar, D. Ridgway, T. Y. Gu and M. Moo-Young, *Biotechnology Letters* 2001, *23*, 1109-1113.
- [51] F. W. Studier, *Protein Expression and Purification* 2005, *41*, 207-234.
- [52] K. E. Cassimjee, M. S. Humble, H. Land, V. Abedi and P. Berglund, *Organic & Biomolecular Chemistry* 2012, *10*, 5466-5470.
- [53] a) P. J. Gilligan, G. A. Cain, T. E. Christos, L. Cook, S. Drummond, A. L. Johnson, A. A. Kergaye, J. F. McElroy, K. W. Rohrbach, W. K. Schmidt and S. W. Tam, *Journal of Medicinal Chemistry* 1992, *35*, 4344-4361; b) S. S. Yang, G. M. Cragg, D. J. Newman and J. P. Bader, *Journal of Natural Products* 2001, *64*, 265-277; c) S. Mill and C. Hootale, *Journal of Natural Products* 2000, *63*, 762-764.
- [54] a) L.-J. Chen and D.-R. Hou, *Tetrahedron-Asymmetry* 2008, *19*, 715-720; b) C. Zhong, Y. Wang, A. W. Hung, S. L. Schreiber and D. W. Young, *Organic Letters* 2011, *13*, 5556-5559.
- [55] M. J. Munchhof and A. I. Meyers, *Journal of the American Chemical Society* 1995, *117*, 5399-5400.
- [56] M. Kavala, F. Mathia, J. Kozisek and P. Szolcsanyi, *Journal of Natural Products* 2011, *74*, 803-808.
- [57] N. Toyooka, D. Zhou and H. Nemoto, *Journal of Organic Chemistry* 2008, *73*, 4575-4577.
- [58] R. C. Simon, F. Zepeck and W. Kroutil, *Chemistry-a European Journal* 2013, *19*, 2859-2865.
- [59] M. G. Banwell, B. D. Bissett, C. T. Bui, H. T. T. Pham and G. W. Simpson, *Australian Journal of Chemistry* 1998, *51*, 9-18.
- [60] A. K. Bhattacharya and G. Thyagarajan, *Chemical Reviews* 1981, *81*, 415-430.
- [61] P. M. J. Lory, R. C. F. Jones, J. N. Iley, S. J. Coles and M. B. Hursthouse, *Organic & Biomolecular Chemistry* 2006, *4*, 3155-3165.
- [62] D. Heseck, M. Lee, B. C. Noll, J. F. Fisher and S. Mobashery, *Journal of Organic Chemistry* 2009, *74*, 2567-2570.

- [63] a) B. Miriyala, S. Bhattacharyya and J. S. Williamson, *Tetrahedron* 2004, 60, 1463-1471; b) E. M. Dangerfield, C. H. Plunkett, A. L. Win-Mason, B. L. Stocker and M. S. M. Timmer, *Journal of Organic Chemistry* 2010, 75, 5470-5477.
- [64] M. Pichon and B. Figadere, *Tetrahedron-Asymmetry* 1996, 7, 927-964.
- [65] M. S. Blum, T. H. Jones, B. Holldobler, H. M. Fales and T. Jaouni, *Naturwissenschaften* 1980, 67, 144-145.
- [66] C. Boga, F. Manescalchi and D. Savoia, *Tetrahedron* 1994, 50, 4709-4722.
- [67] K. Krohn, M. Riaz and U. Florke, *European Journal of Organic Chemistry* 2004, 1261-1270.
- [68] R. Grigg, J. Markandu, S. Surendrakumar, M. Thorntonpett and W. J. Warnock, *Tetrahedron* 1992, 48, 10399-10422.
- [69] J. P. Guthrie and J. N. Guo, *Journal of the American Chemical Society* 1996, 118, 11472-11487.
- [70] A. Padwa, Y. S. Kulkarni and Z. Zhang, *Journal of Organic Chemistry* 1990, 55, 4144-4153.
- [71] C. Ghobril, C. Sabot, C. Mioskowski and R. Baati, *European Journal of Organic Chemistry* 2008, 4104-4108.
- [72] K. T. Tarantino, P. Liu and R. R. Knowles, *Journal of the American Chemical Society* 2013, 135, 10022-10025.
- [73] J. D. Cuthbertson and R. J. K. Taylor, *Angewandte Chemie-International Edition* 2013, 52, 1490-1493.
- [74] G. V. Thanh, J. P. Celerier, A. Fleurant, C. Grandjean, S. Rosset and G. Lhomme, *Heterocycles* 1996, 43, 1381-1384.